The 70-kDa heat shock protein (Hsp70) chaperone system: linking ATP turnover and complex formation to protein homeostasis

by

Andrea Dooley Thompson

A dissertation submitted in partial fulfillment
of the requirements for the degree of
Doctor of Philosophy
(Chemical Biology)
in The University of Michigan
2012

Doctoral Committee:

Associate Professor Jason Edward Gestwicki, Chair
Professor Henry L. Paulson
Professor John J. Tesmer
Assistant Professor Zaneta Nikolovska-Coleska
Assistant Professor Georgios Skiniotis

Dedication

To my teachers and mentors, past and present,
for your patience and
helping me to realize there is always more to learn.
And to my family,
thank you for bringing so much joy, support,
and perspective into my life

Acknowledgements

I would like to begin by thanking my advisor, Professor Jason E. Gestwicki. He has taught me a great deal about science, leadership, and patience. He has allowed me to make mistakes and learn from them, encouraged me to have an active role in defining and driving my project, and is generous with his time and advice. I couldn't have asked for a better learning environment, than the one Jason has provided for me and for that I am truly grateful. I would also like to thank all the members of the Gestwicki lab, both past and present. You all continue to inspire me with your passion for science, exceptional work ethic, and vibrant personalities. I would especially like to thank Lyra and Ashley, whom made me feel very welcome in lab. You both have unending energy and taught me the true meaning of high-throughput. Also, Srikanth, Paul, and Chris helped me to adjust to graduate school and made coming to lab every day a joy. More recently, Jenny, Victoria, and Sharan have breathed new energy into the lab and have kept this aging graduate student young at heart. I would also like to thank Matt and Yoshi, whose calm approach to science kept me grounded as we grew up in the Gestwicki lab together. I would like to thank Leah and Ashley for your grammar expertise which aided in many writing endeavors. I would also like to thank Leah for her willingness to discuss literature and broad concepts within the field of science, I have learned a great deal from our discussions. Many thanks to Anne for coming to Michigan even after having me as your host, and joining the Gestwicki lab. You have been a joy to work with and I very much appreciate your assistance with the peptide microarrays. I would also like to thank

Tomoko, Atta, Xiaokai, Katie, Sussi, and Gladis. You all were sources of wisdom and experience and I have a learned a great deal from you all. Finally, I would like to thank the undergraduates I had the pleasure of working with; Fanchen Bao, Gelareh Abulwerdi, and Brinae Bain. I likely learned more from you than you did from me and it was a great honor to work with each of you.

I have had the great pleasure to collaborate with a number of exceptional scientists including; Matthew Scaglione, Prof. Paulson, Prof. Jinwal, Prof. Dickey, Min Su, Prof. Skiniotis, and John Prensner. You all were generous with your time and talents and helped to educate me in variety of techniques. I am very greatly for the opportunity to work with you all. I would also like to acknowledge my committee for providing useful insights into my project and helping me develop as a scientist.

On a more personal note I would also like to thank the people who gave me my first opportunities to explore science as a field and a career starting with a few high school teachers, Mr. Kopp and Mr. Boatz, who both opened my eyes to the many opportunities within science. Many thanks to Dr. Chokyua Rah, Dr. Alex Rich, and Dr. Yuan-Ping Pang, whom all allowed me to work in their laboratories as an undergraduate. From each of them I was exposed to different aspects of science and gained real life experience in the lab. Further, their passion for their work made me realize that a career in science is really a career in intellect, discovery, and adventure. I wouldn't be here today if they hadn't taken an interest in my development as an undergraduate. There are many more educators that have helped me along the way, to all of which I am forever grateful.

Finally, my family has provided a constant source of support, love, and joy in my life. My parents and sisters have always supported me. Their unshakable certainty in my abilities has given me the confidence needed to preserve through any challenge. Everything I have done is made possible through this strong foundation of support. Further, my husband Eric and daughter Ava are a source of joy, love, and support in my life daily. It is easy to stay positive through the ups and downs of graduate school when I can return home to you both every night and share your laughter and love. We truly are a team and I couldn't have done this without you.

Preface

This dissertation is a compilation of both published and unpublished work on understanding the functionality of ATP hydrolysis and protein complexes within the heat shock protein 70 (Hsp70) chaperone system. Chapter 1 is primarily based on a review article in preparation for submission to *ACS Chemical Biology* that provides an overview of ways nature modulates protein complexes within the cell. It also highlights ways chemical biologist might be able to leverage these strategies to exert more control over a broad range of protein-protein interactions. Chapter 2 is derived from a manuscript where we explored the relationship of ATPase rate and the molecular chaperone activities of Hsp70. This citation is "Mutagenesis Reveals the Complex Relationships between ATPase Rate and the Chaperone Activities of *Escherichia coli* Heat Shock Protein 70 (Hsp70/DnaK)" **2010** *Journal of Biological Chemistry*. *285*; 21282-21291. Chapter 3 stems from a manuscript that investigates the oligomeric forms of Hsp70. In this work we characterized the presence, architecture, and functionality of Hsp70 oligomers and gained insight into another layer of regulation within the Hsp70 chaperone system. The citation for this paper is "Visualization and functional analysis of the oligomeric states of Escherichia coli heat shock protein 70 (Hsp70/DnaK)." **2012** *Cell Stress and Chaperones.* 17:313-327 doi: 10.1007/s12192-011-0307-1. The original publication is available at www.springerlink.com. Chapter 4 is based on our recent work where we

aimed to define a pathway by which the Hsp70 chaperone system could target a given substrate, tau (MAPT), for degradation. By using a small molecule tool we were able to transiently induce the degradation of tau and uncover discrete changes in protein complex formation which target tau for degradation. A manuscript describing the results of this work is in preparation. Finally, Chapter 5 presents our conclusions and future directions.

Table of Contents

Appendix

A. Chaperones preferentially bind fibril forming peptides.

List of Figures

Figures

List of Tables

Tables

ABSTRACT

The 70-kDa heat shock protein (Hsp70) is a molecular chaperone that binds unfolded proteins and directs them towards a number of divergent pathways, including folding, trafficking, and degradation. This delicate balance is critical for normal protein homeostasis and becomes disrupted in a variety of diseases, including neurodegenerative disorders. However, it isn't yet clear what factors direct Hsp70-bound substrates to adopt a given fate.

Hsp70 is a two-domain protein capable of ATP hydrolysis, substrate binding, and the formation of discrete multi-protein complexes. In this thesis, we aimed to characterize the effect of these different variables on substrate fate. First, using a series of point mutants in the prokaryotic Hsp70, DnaK, we discovered that the ATPase rate is not directly related to molecular chaperone activities, such as protection from heat stress or refolding of denatured model substrates. To further probe how ATP hydrolysis may influence chaperone structure and function, we explored how nucleotide state regulates the oligomerization of DnaK. This work showed that ADP-bound DnaK formed small oligomers that retained some chaperone functions, such as substrate binding. However, these oligomers had reduced refolding activity and they were poorly stimulated by the co-chaperone, DnaJ. These studies suggest that oligomerization might be an important step in Hsp70 chaperone cycling. Finally, we explored how chaperones, including Hsp70, change in their association with the pathologically-relevant substrate, tau (MAPT), during

an acute, small molecule-induced switch to a degradation fate. We hypothesized that this system would, for the first time, provide insight into the early events associated with a change in protein fate. These studies suggested a rapid switch from an Hsp70-bound complex to an Hsp90-bound complex during tau degradation. Further, Hsp70 and Hsp90 seemed to compete for binding to similar regions of tau, suggesting that competition between these chaperones might control tau fate. Taken together these studies improve our understanding of the factors that link Hsp70 to the various fates of its substrates. These studies also suggest previously unanticipated therapeutic strategies to rebalance protein homeostasis.

Chapter 1

Fine-tuning multi-protein complexes using small molecules.

1.1 Abstract

Multi-protein complexes such as the transcriptional machinery, signaling hubs, and protein folding machines are typically comprised of at least one enzyme combined with multiple non-enzymes. Often, the components of these complexes are incorporated in a combinatorial manner, in which the ultimate composition of the system helps dictate the type, location, or duration of cellular activities [1-4]. For example, while the molecular chaperone Hsp70 enzymatically hydrolyzes ATP it also interacts with three distinct classes of co-chaperones and countless substrate proteins. Thus, although drugs and chemical probes have traditionally targeted enzymatic functions, many emerging strategies call for the modulation of protein-protein interactions (PPI) to control the assembly and disassembly of protein complexes [5-7]. However, the challenges of targeting PPIs have been well documented and the diversity of PPIs makes a "one-size-fits-all" solution highly unlikely. These hurdles are particularly daunting for PPIs that encompass large buried surface areas and those with weak affinities. This chapter discusses lessons from natural systems, in which allostery and other mechanisms are used to overcome the challenge of regulating the most difficult PPIs. These systems may provide a blueprint for identifying small molecules that target challenging PPIs and modulate molecular decision-making within multi-protein systems. Finally, how these

concepts impact the development of small molecule modulators for the Hsp70 chaperone system is highlighted.

1.2 Introduction

Protein-protein interactions (PPIs) form the backbone of nearly every facet of cellular function, as illustrated by proteome-wide maps composed of thousands of these contacts [8, 9]. PPI networks are composed of both stable, high affinity contacts and weaker, transient interactions. These weak contacts enable modularity by allowing individual components to serve multiple functions, often by using and re-using the same interfaces. At the core of these networks are a series of multi-protein complexes dedicated to major cellular tasks, including systems involved in transcription, translation, trafficking, energy production, protein folding, cytokinesis, and signaling. These multi-protein complexes are typically composed of at least one enzyme, such as an ATPase, and a series of non-enzymatic factors, such as scaffolding proteins (Figure 1.1). These non-enzyme partners associate either stably or transiently with the complex and help fine-tune activity, subcellular location, and/or selectivity. One traditional goal of drug discovery and chemical biology has been to develop compounds that inhibit the enzyme components of multi-protein complexes [10]. This approach has been fruitful, producing many of the most widely used research reagents and drugs. Yet, PPIs within multi-protein complexes may provide an even greater number of opportunities, especially because there is a growing appreciation of the potential of PPIs as drug targets [11, 12].

1.2.1 Small molecule modulators of PPIs

Although the goal of inhibiting PPIs with small molecules has been recognized for some time, these interactions have been historically challenging to interrupt [10, 13, 14]. Indeed, the majority of PPIs have often been broadly classified as “undruggable” and among the estimated 650,000 PPIs, far less than 0.01% have been targeted with inhibitors [10, 14-16]. Yet there a number of recent success stories, produced by both academic and industrial groups, which highlight that PPIs are not uniformly insurmountable targets [17-19]. A theme in those examples is that a wide range of methodologies and approaches can ultimately be fruitful. Building on these past successes, future efforts to target PPIs moving forward may be aided by understanding the diverse strategies nature employs to modulate PPIs. To support this more optimistic view of PPI modulators, this chapter highlights several representative examples of successful PPI inhibitor programs and discusses potential ways of accelerating their discovery in the future. In particular, this chapter focuses on the most challenging PPIs that are central to many areas of biology yet remain the most difficult to target with small molecules.

1.2.2 The architecture of multi-protein complexes

Given the central role of multi-protein complexes in biology, perturbing the assembly and/or disassembly of these structures has the potential to uncover important insights into their function. In this discussion, a multi-protein complex is defined as a system of proteins that assemble, either permanently or transiently, to perform specific tasks in the cell. Most multi-protein complexes contain at least one enzyme and they typically have multiple non-enzyme components. The role of the non-enzymes is often to provide a

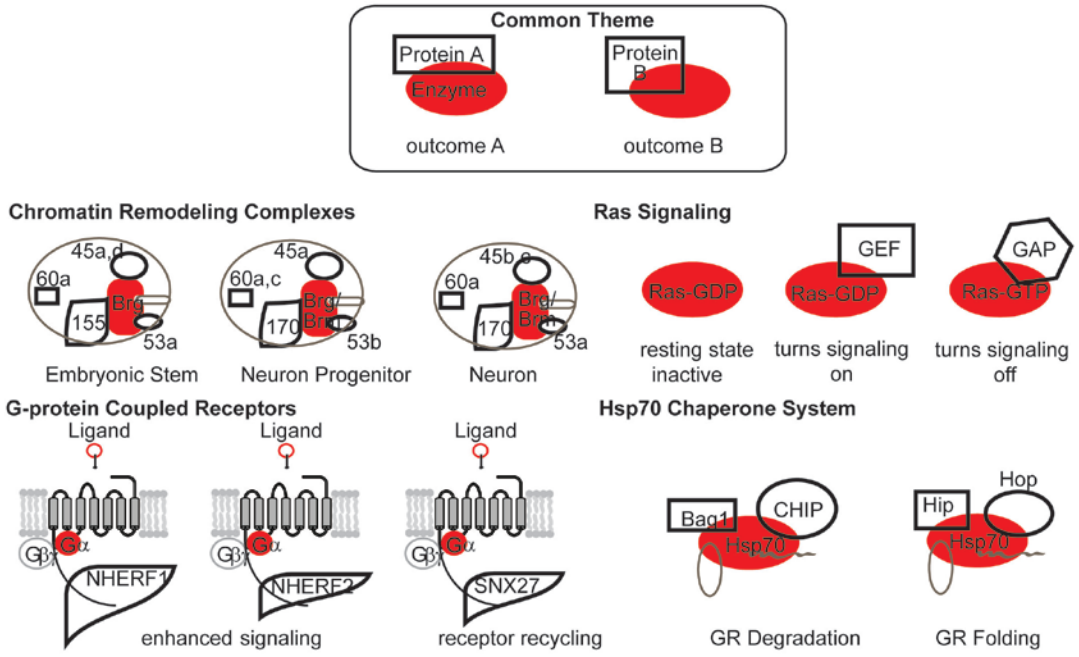

Figure 1.1. Multi-protein complexes are assembled from enzymes or receptors bound to multiple, non-enzyme partners through protein-protein interactions.
The majority of protein complexes in biology share the common features of being assembled from protein-protein interactions (PPIs) between enzymes (red) and non-enzymes (white). These factors assemble into multi-protein systems that have emergent properties (e.g. biology not engendered by any individual component) and essential roles in molecular processes in the cell. To illustrate this idea, a few of the major protein complexes are shown.

scaffolding function, linking proteins together or controlling subcellular localization, as seen in GPCR recycling (Figure 1.1) [20]. Also, the PPIs between the enzyme and non-enzyme can sometimes tune the biochemistry of the enzyme, enhancing K_m or k_{cat}, as seen in the Ras GTPase cycle or the Hsp70 ATPase system (Figure 1.1) [3, 21]. Finally, the protein surfaces used to form PPIs might be shared by multiple components, such that subunits compete for binding. In this way, complexes can be combinatorially assembled. This combinatorial assembly is present within the Hsp70 system (Figure 1.1). As another prime example, BAF-type chromatin remodeling complexes undergo subunit exchange during the transition from a pluripotent stem cell into a neuron progenitor cell and finally into a fully differentiated neuron (Figure 1.1) [22, 23]. In these systems, one appreciates why solely targeting the enzyme component might not be the most informative approach.

Rather, inhibiting (or even promoting) specific PPIs could be of great value for understanding a wide range of essential cellular processes.

1.2.3 Structural and energetic considerations in targeting PPIs

In contrast to protein-ligand interfaces (PLIs), such as those between enzymes and their substrates [13, 24], PPIs are larger and flatter [25] (Figure 1.2A), with an average surface area of 1940 +/- 760 $Å^2$. Sometimes, a disproportionate amount of the binding free energy (ΔG) is found within specific residues, termed "hotspots" [26]. Other times, ΔG is distributed over a larger surface area or in a few regions separated by large distances. Consistent with their wide distribution of contact areas, PPIs exhibit a wide range of affinity values, with examples of pM dissociation constants in more stable complexes and mM values in transient complexes (Figure 1.2) [27-43]. The scope of this diversity is postulated to be even wider than currently appreciated, given the underrepresentation in the Protein Data Bank (PDB) of transient, low affinity, and membrane associated PPIs [29, 44].

1.2.4 Small molecules mainly target high affinity, small surface area PPIs.

To date, the PPIs characterized by high affinities and small surface areas (e.g. most similar to PLIs) have proven to be the most amenable to targeting with small molecules. Often, structure-based approaches have proven successful. For example, pioneering work has been performed on SMAC mimetics (Figure 1.2A) and inhibitors of p53-MDM2 [18, 19, 45-47]. These targets are characterized by binding sites composed of a short peptide interacting with a deep pocket, as in the SMAC interaction with IAPs (Figure 1.2A), or a

single α-helix interacting with a well-defined cleft, as in p53-MDM2. To explore how general these characteristic are for all known PPI inhibitors, the 2P2IDB and TIMBAL databases were queried to sort known PPI inhibitors based on the surface areas and affinities of their targets. It was found that PPIs with smaller surface areas (less than <1,800 $Å^2$) and relatively high affinity (less than 1 μM) are targeted by 68% of reported small molecules (Figure 1.2D) [18, 19]. In contrast, only 10% bind to large surface area PPIs with high affinity binding (Figure 1.2D). One potential explanation for this preference is that concise, high affinity PPIs rely on binding pockets that are best "fit" by low molecular mass (<500 Da) compounds and these compounds are most common in drug discovery libraries [10, 13, 14, 48]. Also, it is relatively straightforward to envision how competitive inhibitors could block these interactions because the ΔG is contributed by a handful (typically less than 5) of tightly clustered residues [17, 49].

1.2.5 Challenges in target low affinity and/or large surface area PPIs

What are the specific challenges to circumvent in successfully modulating the "difficult" PPIs: those with low affinity and/or large surface area PPIs? Large binding surface areas have been particularly difficult to directly (*i.e.* orthosterically) inhibit with small molecules, as the compound must compete with a much larger protein for binding. In some cases, "hotspots" can be used to generate potent inhibitors [26, 50, 51]. Still, accessing hotspots often requires extensive structural knowledge. Another challenge is

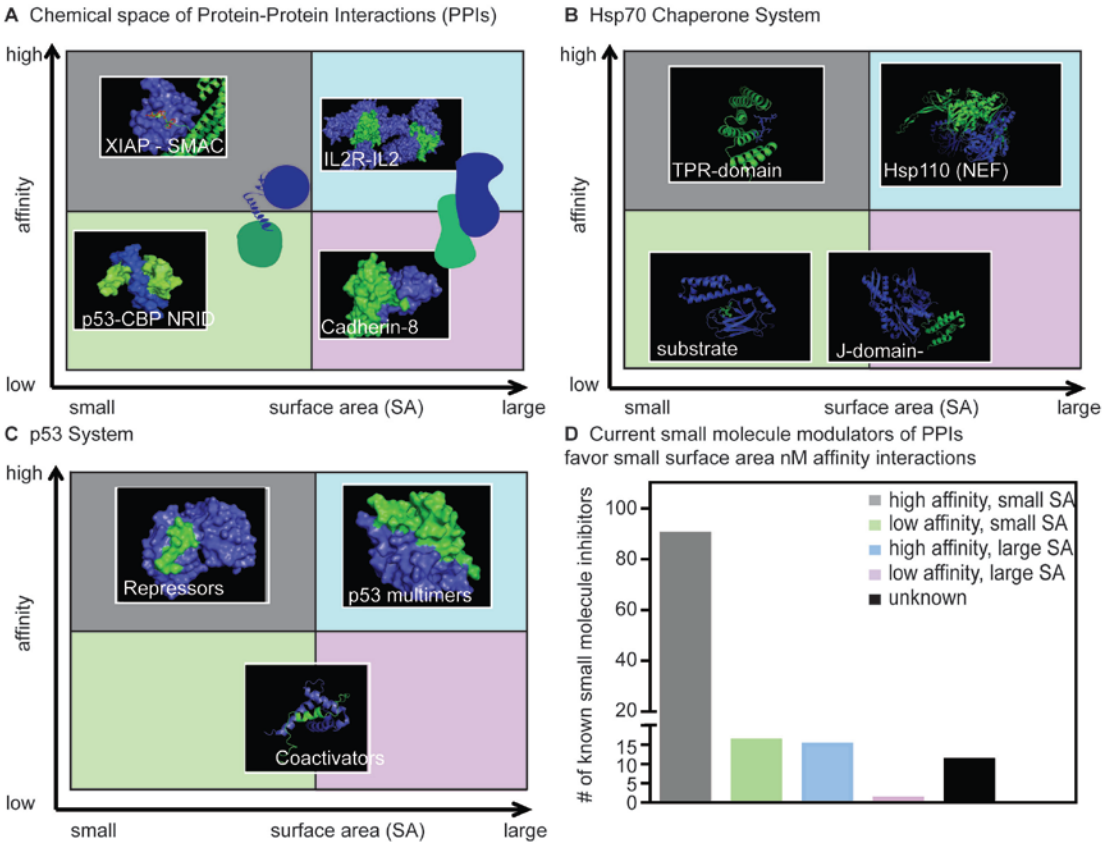

Figure 1.2. Not all protein-protein interactions are created equal: some PPIs are harder to inhibit than others. (A) PPIs can be roughly categorized by their apparent affinity and the buried surface area involved in the contact. This type of analysis creates four major quadrants of interactions: strong and concise, strong and broad, weak and concise, and weak and broad. Examples of each type of interaction from the Protein Data Base (PDB) are shown. Strong and concise: XIAP-SMAC (2JK7, 1G73); strong and broad: IL-2-IL2R (2ERJ); weak and concise: p53-CBP NRID complex (2L14); weak and broad: cadherin-8 homer dimer (1ZXK). (B) Multiple categories of PPIs are often found within a single complex, as illustrated by the Hsp70 system in which the four major types of PPIs are represented in interactions between Hsp70 and its associated partners: substrate (1DKY); TPR-domain protein (3Q49); nucleotide exchange factor (3C7N); J-domain (2QWN). (C) The p53 system is another example of a system in which multiple types of PPIs are found in the same complex. The repressor Mdmx (3DAC); p53 self-association (1PET); transcriptional coactivators (2K8F). (D) PPIs with known inhibitors were acquired from the 2P2IDB and TIMBAL databases and their binding affinities (as reported in the PDBbind 9119) and the surface are of the PPI (as measured by InterProSurf (120)) were determined. Placing these PPIs into categories revealed that small molecules which target PPIs with smaller surface ares (<1,800 $Å^2$) and relatively tight affinities (<1 μM) represent 68% of known PPI inhibitors.

that inhibitors of large surface areas tend to have high molecular weights, often not conforming to the standard Lipinski's Rule of 5 (Ro5) [52, 53]. In fact, many successful PPI inhibitors deviate from the Ro5 [19], potentially creating challenges with pharmacokinetics and oral bioavailability. Another important problem is that many PPIs are of low affinity (Figure 1.2D). Structural information on these weak affinity interactions is often limited [29, 44]. From a practical perspective, these weak systems

are also challenging to study using many typical biophysical methods, such as ITC. These challenges have combined to limit the number of successful inhibitors of the most challenging PPIs. The next section describes how nature has evolved mechanisms to circumvent these issues.

1.3 Lessons from nature

Biology has long developed natural mechanisms by which it modulates PPIs within the cell. Can we as chemical biologists learn some tricks from nature? Protein complexes can be regulated by transcription as well as a variety of regulatory mechanisms which control RNA processing and translation. However, this discussion will focus on dynamic molecular regulation at the protein level, in which, nature invokes a variety of, at times overlapping, mechanisms which include allostery, cellular localization, post-translational modifications, and protein dynamics. Herein these strategies are reviewed to highlight exciting examples of small molecules that have accessed these natural pathways for the modulation of PPIs. By doing so, one gains an appreciation for the properties that govern protein complex formation.

1.3.1 Allostery modulates PPIs

Allostery is one of the most widely used mechanisms to control the assembly and disassembly of multi-protein complexes. Allostery is defined as binding at one site which regulates a function at a distant site [54, 55]. Classic examples include cooperative oxygen binding to hemoglobin or feedback inhibition within metabolic pathways [54]. However, allostery is also frequently utilized to regulate protein complex formation [56-

58]. For example, binding of NotchIC to CSL promotes the binding of Mastermind at a site 40 Å away from its binding site to regulate transcriptional activation [59]. In receptor biology, allosteric networks often translate extracellular ligand binding into changes in PPIs in the cytosol [60-63]. These mechanisms also apply to small molecule binding. In an example of this idea, galactose promotes the formation of a stable complex between Gal3p and Gal80p, which subsequently activates the transcription of galactose metabolizing enzymes in yeast [64].

1.3.2 The advantages of allostery

The use of allostery to control protein complex formation is not surprising given several advantages of this strategy. First, allosteric sites are often distinct from reactive centers in enzymes. Thus, the features of these allosteric binding regions are not constrained by active site chemistry. Further, in the context of PPIs, targeting allosteric sites can sometimes be used to reshape the topology of a PPI even if the small molecule binding site is far from the actual interface [65]. Moreover, these allosteric sites, in some cases, may be deeper and more amenable to binding than the PPI itself. Finally, orthosteric compounds compete for binding at a given interface and, as such, cannot discriminate between two different proteins binding at a single interface. Thus, a compound binding directly at a PPI would block two possible partners equally. In contrast, the outcome of binding to an allosteric regulator can depend on the composition of the complex [66]. Thus, allosteric compounds can sometimes differentiate between the effects of different proteins at the same interface.

1.3.3 Small modulators of PPI leverage allostery

Natural examples may point the way to synthetic ways of controlling the assembly and disassembly of PPIs, especially in systems that are particularly challenging for direct inhibition [54]. As such, a very active area of research is currently focused on defining interactions between metabolites and proteins [67-69]. These efforts have the potential to greatly improve our ability to rationally target PPIs. For example, porphobilinogen synthetase (PBGS) regulates its activity via a dynamic equilibrium between two alternative and functionally distinct conformations: an active octamer and a low activity hexamer. Only the active octamer binds to Mg^{2+}, which enforces the conformational change. Appreciating this natural conformation equilibrium and the ability of the magnesium ion to influence the system, Lawrence and colleagues identified a small molecule, Morphlock 1 (Figure 1.3E), which favors the low activity hexamer by binding to an interface only accessible in the conformation unique to hexamer assembly [70, 71]. Perhaps similar lessons from nature will be useful in providing paths towards small molecules that target the most challenging of PPIs.

Illustrating the advantages of this approach, a number of synthetic molecules with allosteric mechanisms have been reported [72-75]. For example, a compound which binds the inducible nitric oxide synthase (iNOS) leads to disruption of a distant dimerization interface, inactivating the protein by blocking dimer formation [76]. In another example, Conn and colleagues have applied allosteric regulators to target G-protein coupled receptors (GPCRs), finding molecules which activate or inhibit discrete

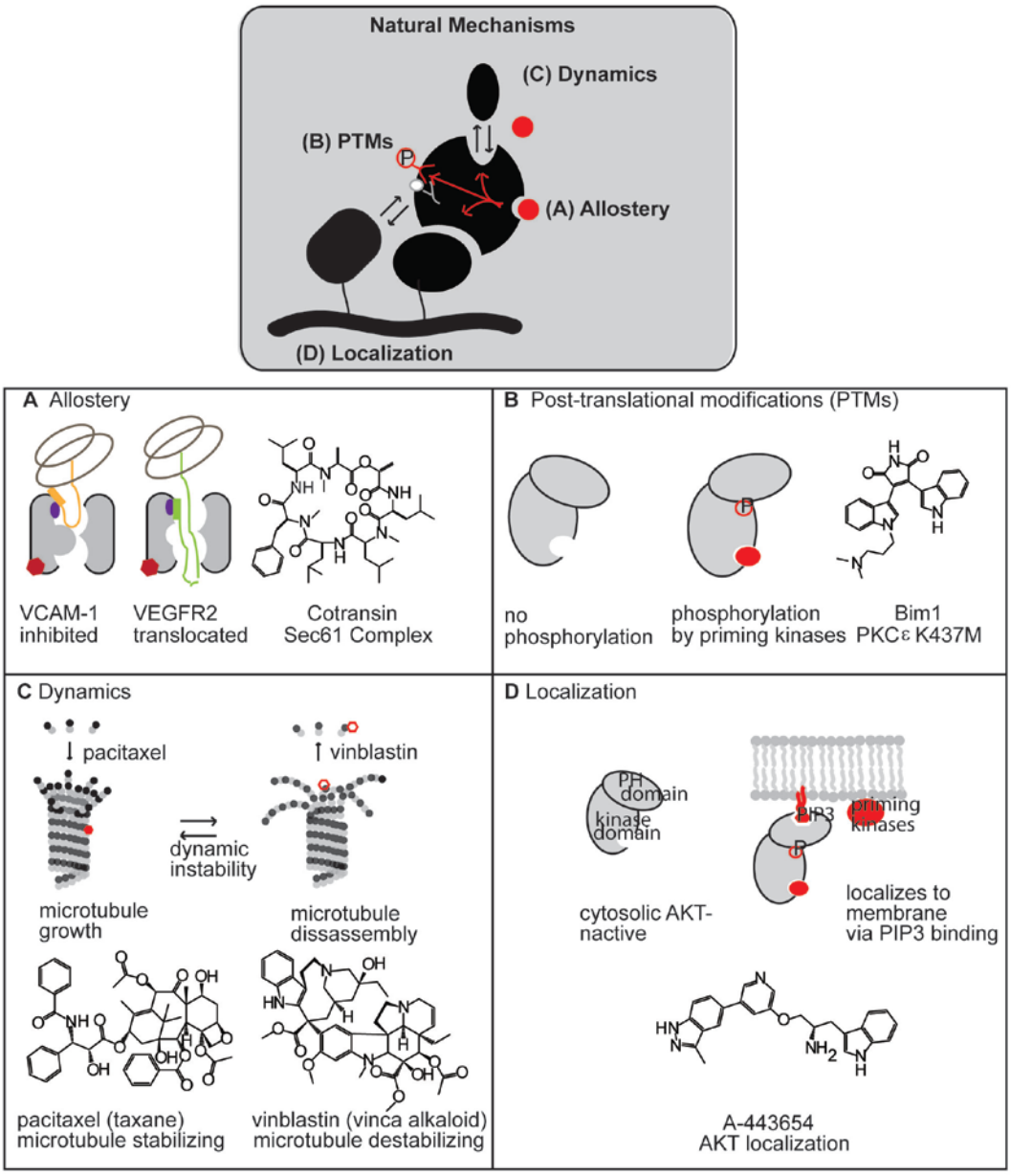

Figure 1.3. Nature-inspired strategies for modulating difficult PPIs.
Natural multi-protein systems use mechanisms such as allostery, PTMs, dynamics, and subcellular localization to control their assembly and disassembly. Small molecules have been found to access similar mechanisms, such as; (A) allosteric regulation of the Sec61 translocon by cotransin, with blocks translocation of VCAM-1 without affective VEGFR2. (B) conformational change in PKCe caused by Bim1, which allows binding to priming kinases, (C) altering microtubule dynamics with pacitaxel and vinblastin, and (D) membrane localization of Akt induced by the kinase inhibitor A-443654.

subsets of downstream pathways by changing the PPIs that occur between the GPCRs and their effector proteins [77, 78]. Another example is found in the allosteric modulation of the Sec61 translocon (Figure 1.3A). The Sec61 translocon is responsible for

transporting nascent polypeptides across the ER membrane [79, 80]. As a nascent polypeptide is synthesized, a signal sequence in its N-terminus binds directly to the Sec61 complex [81, 82], which triggers an allosteric conformational change to open the channel to the ER.[80] Recently both Besmer and Garrison identified small molecules that modulate the Sec61 translocon complex in an interesting way. These compounds, such as cotransin (CT), cause a selective decrease in translocation of vascular cell adhesion molecule 1 (VCAM1) without affecting the levels of other membrane proteins (Figure 1.3A) [83, 84]. CT appears to block the interaction between VCAM-1 and Sec61α by favoring binding to Sec61β, an unexpected and interesting mechanism that provides insight into the biology of the Sec61 complex and its regulation. These examples and others illustrate how allostery can be used to impact seemingly intractable PPIs.

1.3.4 Localization

Protein complex formation can also be regulated by controlling localization of key subunits. An example of this form of control is seen in the signaling of the T-cell receptor (TCR) complex [85, 86], in which multivalent contacts made during the binding of the antigen-MHC complex induces oligomerization to initiate signal transduction. Localization regulates PPI guided by three simple principles [86]. First, the probability of an interaction between two molecules is a third order function of the distance between them, thus localization greatly increases the probability of an interaction between two proteins. Secondly, the importance of localization is further amplified in the cell due to the high viscosity of the cytosol which limits the rate of diffusion. Finally, bringing proteins close together in an organized complex also promotes binding by placing two

proteins in favorable orientations. This is often referred to in chemistry as increasing the effective molarity.

Given the utility of altering protein localization in modulating PPIs, small molecules may be able to modulate PPIs using the same strategy. Perhaps a clear way this could be achieved is through the design of multivalent compounds. Yet another way would be via an allosteric approach. For example, an Akt kinase inhibitor was shown to activate Akt signaling by inducing a conformational change, increasing affinity for phosphatidylinositol (3,4,5)-triphosphate (PIP3) in the membrane, thus facilitating membrane localization and interaction with priming kinases (Figure 1.3D) [87]. This example highlights how taking advantage of natural conformational changes can be used to alter localization and complex formation.

1.3.5 Post-translational modifications

Another widely used mechanism to regulate complex assembly is post-translational modifications (PTMs) including phosphorylation, glycosylation, acetylation, ubiquitination, neddylation, sumoylation, among others [88]. PTMs occur at many PPI interfaces to promote or inhibit binding (*e.g.* SH2 domain binding to phosphorylated tyrosine residues). However, PTMs can also occur far from PPI surfaces, changing protein stability, folding, or conformation and regulating complex formation [88]. There are several ways small molecules could use PTM-like mechanisms to bring about changes in PPIs. One dramatic way is through direct covalent modification by the drug itself via the formation of drug-protein adducts. Often the formation of drug-protein

adducts is avoided due to warranted concerns regarding the unwanted toxicity that can emerge due to lack of specificity and the potential for immunogenicity of the covalent drug-protein adduct, among others [89, 90]. However, despite these potential pitfalls, several examples of covalent drugs with good toxicity profiles are known, including aspirin, proteasome inhibitors, and acetaminophen [89]. Although these classic examples are all enzyme inhibitors, similar mechanisms appear to operate at PPIs, such as those used by compounds that target the NRF2-KEAP1 complex [91, 92]. Another inventive mechanism, by which small molecules can promote PTMs, is exemplified by the paradoxical activation observed with a PKCε kinase inhibitor [93]. A K437M mutant of PKCε has been shown to be overcome by binding of an ATP active site inhibitor, which promotes a conformational change that promotes interaction with and phosphorylation by priming kinases, effectively activating this signaling pathway (Figure 1.3B). These studies demonstrate how small molecules can promote PTMs (and regulate PPIs) by inducing conformational changes.

1.3.6 Protein complex dynamics

Another “nature-inspired” way to develop PPI modulators may be to alter protein dynamics. Like many other cellular processes and signaling pathways, both the ribosome and microtubules rely on the dynamic interchange of subunits to function. In microtubules, dynamics allow for rapid reorganization, efficient sampling of cellular space, and enable mechanical work [94]. For ribosomes, the dynamic nature of EF-Tu interaction with the ribosome is essential for recycling key machinery to perform the iterative process of amino acid chain elongation [95, 96]. One way dynamics can be

regulated is by modulating the affinity of PPIs in either direction. For example, it has been shown that altering the affinity of EF-Tu and ribosome interaction inhibits not only the dynamics but the ability of the ribosome to function [97, 98]. Thus, in these dynamic systems affinities of dynamic PPIs are constrained to ensure they are strong enough to form ternary complexes yet weak enough to release the PPI and allow for timely cycling. These examples highlight that in modulating PPIs within highly dynamic systems small perturbations in protein binding can lead to large changes in cellular function. Thus, success is not dependent on the ability to fully inhibit or promote a given PPI but instead by perturbations in the dynamic equilibrium of complex formation within biological systems of the cell. Widely used therapeutics, such as antibiotics and microtubule stabilizing or destabilizing drugs, demonstrate that disrupting dynamics can target even structurally large and challenging drug targets such as the ribosome and microtubules (Figure 1.3C) [94, 99].

1.4 Identifying compounds that can inhibit/promote complex formation

Although the small molecules discussed above are excellent examples of successful ways one may fine-tune protein complex formation and biological activity, strategies that best facilitate the future discovery of small molecules with similar capabilities are not obvious. How can we take these lessons from nature and develop ways of identifying compounds that target PPIs? Towards these goals there are a variety of screening platforms and assays that can be utilized.

1.4.1 Techniques for the identification of allosteric modulators of PPIs

Many of the compounds discussed earlier act allosterically. Thus, techniques that identify small molecule allosteric binding sites should have broad utility in the search for PPI modulators. One of the first major techniques for finding PPI inhibitors, disulfide tethering, which focused PPI inhibitor discovery on hotspot residues using covalent coupling [100], also has the potential to focus discovery efforts on allosteric sites. For example, disulfide tethering has been utilized to successfully identify a novel allosteric inhibitor of caspase-1/7 that traps it in an inactive conformation [101]. Another related approach to this problem is fragment based screening (FBS) [102, 103]. FBS searches for weak binding (mM) small molecule "fragments" of less than 300 Da, with high ligand efficiency. These chemical libraries are screened using techniques sensitive enough to measure low-affinity interactions, such as NMR [104]. These initial hits are then developed further by either linking or growing fragments to improve affinity and/or activity. This method has proven to be particularly powerful for PPIs because it can identify unanticipated allosteric and adaptive protein binding sites [105]. Further this technique has been applied to find inhibitors of larger PPIs, such as the Bcl-XL/Bcl-2-BAD/BAX interaction, by linking fragments found to bind distinct subpockets within the PPI binding site [106].

Computational approaches offer a complementary approach to predict allosteric binding sites suitable for regulating PPIs [13]. Some techniques use "statistical coupling" of amino acid residues throughout evolution [107, 108]. This technique is based on the theory that if two positions are functionally coupled, their amino acid identities should be

constrained through evolution. Other computational methods simulate mutations and map structural perturbations, or perform computational alanine scanning [109, 110]. Another approach, called anisotropic thermal diffusion, tracks the propagation of kinetic energy emanating from a heated target location [111]. Finally, the protein structure can be searched using van der Waals probes to identify potential ligand sites in allosteric locations [112-115]. This list is not meant to be inclusive but rather to illustrate that computational efforts towards this goal have been extensive, suggesting the possibility of rationally designing allosteric PPI regulators. For example, the previously mentioned, Morphlock-1, was identified through *in silico* screening of an allosteric site [70].

1.4.2 Techniques which monitor small molecule modulation of protein dynamics

Small alterations in binding conformational equilibriums can have dramatic effects on PPIs dynamics and cellular functions. A technique that may allow one to identify such small molecules is Förster resonance energy transfer (FRET), which remains a workhorse method to monitor protein dynamics both *in vivo* and *in vitro*. This approach has been successfully used to identify small molecules which alter a protein's conformational dynamics as well as the dynamics of a PPI [116-118]. Another approach is to employ isotopically labeled amino acids and NMR spectroscopy [119] to measure conformational changes in the presence of small molecules. An advantage of this approach is that it simplifies the NMR spectra, making it suitable for larger proteins. This approach was used to study the binding of a small molecule to the thioesterase domain of fatty acid synthase (FAS-TE), a protein of therapeutic interest in the treatment of cancer and obesity [119]. These spectroscopic methods provide valuable information regarding

conformational transitions and are particularly well suited for discovery of PPI inhibitors that alter dynamics. The goal in many of these discovery efforts is to screen for compounds that shift an ensemble and stabilize specific, active or inactive conformers [120].

1.4.3 High-throughput screening: the continuum from white- to black- box screening.

The techniques discussed thus far largely involve biochemically purified proteins, often truncated to include only the protein domain of interest. In addition to the techniques discussed to identify allosteric small molecules, high-throughput screens which directly monitor PPIs such FRET, fluorescence polarization (FP), capillary electrophoresis, and flow cytometry are often utilized [74, 121, 122]. A major advantage of these approaches is that by targeting a specific PPI, identifying the target and mechanisms of action of active small molecules is straightforward. Further, several groups have explored ways of adjusting direct binding assays to favor the discovery of allosteric molecule [123, 124], such as using high concentrations of an interacting partner to disfavor binding to orthosteric sites.

However, in some cases the approaches discussed thus far may miss or overlook small molecules with interesting activities. A major advantage of allosteric modulation is the ability of small molecules to target PPIs in a context dependent manner, with the functional outcome of binding by an allosteric regulator dependent on the composition of the protein complex. This concept is illustrated by the substrate specific modulation of Sec61 translocon and selective modulation of specific downstream pathways by targeting

GPCRs by small molecules highlighted herein [77, 78, 83, 84]. However, analyzing PPI domains alone remove a given PPI from its cellular context, including the effector proteins and regulatory mechanisms that are central to *in vivo* function. Further, many of the compounds discussed above target PPIs by altering protein localization or the dynamics of a given PPI. In the absence of their cellular context, the utility and capabilities of these small molecules are not fully realized. For these reasons one may wish to go back to the basics to think of ways to effectively carry out functional high throughput screens (HTS).

Functional HTS screening strategies usually utilize cell-based or tissue-based assays to screen small molecules for a given function. This approach is often referred to as chemical genetic screens [125] and allow for the identification of small molecules that achieve the desired function by a multitude of different pathways or molecular targets. As such, this approach has shown great potential for the identification of molecules capable of "fine tuning" protein function and altering complex formation, even among PPIs one would not necessarily predicted to be "druggable" targets [83, 84, 126-128]. For example, ubistatins, which stabilize cyclin B by blocking ubiquitin PPIs, were identified using Xenopus extracts [129]. Further, cellular screens can be specially designed to favor the identification of PPI inhibitors or activators by utilizing techniques like chemoproteomic profiling which measures drug-induced changes in protein complex formation [130, 131]. Finally, although it remains a challenge to perform target identification and analyze mechanism for compounds identified using functional HTS, recently emerging techniques may have the potential to greatly improve our ability to do so [132, 133].

These approaches include the evaluation of chemical genetic synthetic lethal interactions [134], activity based protein profiling technologies, and engineering specificity through the coupling of binding site mutations with chemical alterations in the small molecule of interest [135]. These techniques may make functional based screens more attractive going forward.

Still, despite the utility of *in vitro* and functional based screens, perhaps there may be a middle ground between these very simplified and very complex screening strategies. A promising approach towards this goal may be "grey-box" screening, in which multi-protein complexes are re-constituted *in vitro* and then an HTS method is used to find molecules that impact the biochemical properties of the complex. Whereas *in vitro* binding studies often treat a single protein or PPI as a "white-box" devoid of cellular context and functional studies treat the cell as a "black-box" probing a function without regard to a specific PPI target, "grey-box" screening attempts to screen a specific PPI without removing it from its disease-relevant protein complexes or native regulatory mechanisms. For example, in a screen for inhibitors of the p21-activated kinase (Pak1), Deacon and colleagues chose to use the full-length protein, including its non-catalytic domain, in complex with an activator protein, Cdc42, and a substrate, maltose binding protein [136]. By including this full complex, they identified a non-competitive inhibitor IPA-3 that binds the autoregulatory non-catalytic domain and blocks activation by Cdc42. In another example, the prokaryotic Hsp70 system, composed of DnaK and DnaJ, was reconstituted and screened [75]. DnaK is an ATPase that is stimulated by the non-enzyme DnaJ. An HTS method using a DnaK-DnaJ mixture identified molecules that blocked

ATPase activity by selectively disrupting the weak interactions between these two proteins [75, 137, 138]. These examples suggest that “grey-box” screening has the potential to identify small molecules enriched in their ability to “fine-tune” complex formation.

1.4.4 Lest we forget transient PPIs

As highlighted, a powerful way to uncover inhibitors of PPIs is to directly measure the binding between protein partners and screen for compounds that disrupt this contact. However, one of the challenges imposed by difficult PPIs is that most HTS platforms for measuring binding affinities are less suitable for the characterization of transient, lower affinity interactions [139, 140]. Towards that goal, several methods have proven useful in identifying transiently interacting protein partners in cells, including yeast-2-hybrid (Y2H) systems, bimolecular fluorescence complementation (BiFC), and *in vivo* crosslinking strategies [141-144]. Although there are caveats to each of these methods, their proper implementation provides the ability to measure transient, moderate affinity PPIs in cells. *In vivo* crosslinking using unnatural amino acid mutagenesis has also recently been identified as a powerful tool for covalently capturing both high affinity and transient, lower affinity protein-protein interactions in yeast [142, 145]. Combined with mass spectrometric methods, this technique creates a powerful platform for characterizing weak PPIs. Being able to characterize weak PPIs may subsequently allow one to screen for, develop, and characterize modulators of these contacts.

1.4.5 Towards compound libraries enriched for PPI modulators

Compounds that target PPIs tend to be higher molecular mass, which is expected based on the more complex topology of these interactions [19]. In addition, many successful modulators of PPIs are natural products. These observations have led many groups to suggest that typical commercial chemical libraries may not be the most appropriate for finding PPI modulators, owing to the tendency of these collections to be composed of low molecular weight and low complexity molecules. Accordingly, many new methods such as DNA encoded combinatorial libraries (DELs), and improved diversity-oriented synthesis strategies (DOS) have been developed to produce more complex compounds [146-149]. Similarly, secondary structure mimetics [150], aptamers [151], and antibody-like molecules [152] have been developed in an attempt to better match the topology of PPIs. Finally, natural products, metabolites and natural product-like collections are finding renewed use as sources of PPI modulators [153, 154]. Unfortunately, these concepts have still not been widely adapted by public screening facilities; as of 2010, only 1% of the NIH Molecular Libraries Small Molecule Repository was natural product-like [147]. However, a greater focus on the biology of PPIs may drive the development of additional commercial collections that cater to the particular needs of these systems.

1.5 Summary

PPIs are emerging as promising drug targets and reports of PPI inhibitors have become increasing widespread. The next frontier in PPI research is to go beyond the concise, high affinity PPIs, which have constituted a majority of the published success stories thus far. The next phase is to understand how to target the PPIs with large and complex surface

topologies and those with weak, transient contacts. Because these “challenging” PPIs are the least amenable to classic orthosteric inhibitors, it seems likely that new strategies will be needed. Herein, the varied ways in which the cell naturally regulates and modulates PPIs have been discussed. From these observations, the themes of allosteric inhibition and PTMs become readily apparent and a few synthetic small molecules have already accessed these natural regulatory mechanisms to fine-tune protein complex formation. Deployment of new HTS methodologies and carefully designed chemical libraries may further accelerate discovery of molecules with activity on these difficult systems. By continuing to look to nature for inspiration, chemical biologists have the potential to expand the number of “druggable” PPIs.

1.6 Applying lessons to Hsp70: towards a treatment strategy for tauopathies

Thus far, the varied ways by which the cell regulates and modulates PPIs have been discussed. Further, small molecules which have accessed these naturally regulatory mechanisms to fine-tune protein complex formation in novel ways have been highlighted. Of central importance is the ability of these small molecules modulators of PPIs to uncover biological insight into cellular pathways. Through an iterative process of identifying novel small molecules and mechanistic studies, chemical biology has the potential to understand and control the biology of the cell. The work summarized in this thesis illustrates work aimed towards this iterative process within the context of the Hsp70 chaperone system and a class of neurodegenerative diseases known as tauopathies.

1.6.1 Tauopathies: A class of neurodegenerative disease involving the microtubule associated protein tau (MAPT/tau).

The microtubule binding protein tau is a natively unfolded protein that is primarily expressed in neurons and binds to microtubules promoting stability and assembly [155-158]. Intracellular aggregates formed by tau are a characteristic pathologic feature in approximately fifteen neurodegenerative disease classified as tauopathies [159-166]. Alzheimer's Disease (AD) is the most common tauopathy and affects more than 5 million Americans, incurring a large emotional and financial burden totally more than $148 billion dollars annually [167]. As our population ages, AD prevalence is expected to rise dramatically. Further, there is currently no cure for AD, or any tauopathy for that matter. Whereas acetylcholinesterase inhibitors and NMDA antagonists have been approved for clinical use, they are only able to mildly slow the rate of cognitive decline in patients with AD [168]. Thus, there is a great need for new therapeutic strategies.

The direct pathophysiology which underlies the clinical symptoms within a given tauopathy, is not yet fully understood. Yet, a multitude of studies have highlighted that the aggregation and accumulation of tau significantly contributes to disease. For example, causative mutations within tau have been found in some patients with the tauopathy Frontotemporal Dementia with Parkinsonism linked to chromosome 17 [169-171]. These mutant forms of tau are more prone to aggregation and can recapitulate disease symptoms within mouse models. Finally, and importantly, reductions of tau levels have been shown to reverse clinical symptoms in a variety of mouse models for tauopathies, including mice genetically designed to exhibit amyloid beta pathology [172-176]. Thus, reductions in tau

levels and clearance of tau from neuronal cells could prove to be a viable therapeutic strategy for the treatment of tauopathies.

1.6.2 The Hsp70 chaperone system regulates tau homeostasis

One proposed method by which tau could be targeted for clearance is through the use of molecular chaperones, a natural mechanism within the cell that handles misfolded proteins [177, 178]. Genetic over-expression of the molecular chaperone heat shock protein 70 (Hsp70) has been shown to be cytoprotective, inhibiting aggregation, and/or clearing pathologic aggregates in many cellular and animal models of neurodegenerative diseases, including AD [179-188]. In regards to tau, several studies have shown that Hsp70 plays a central role in regulating tau clearance [182, 187, 189-194]. Hsp70s can facilitate the rebinding of tau to microtubules and have also been implicated in blocking tau aggregation and promoting its degradation [182, 187, 195]. Further, studies have highlighted the important role Hsp70 co-chaperones play in determining tau fate [196]. However, these genetic studies do not clarify the mechanism by which Hsp70 controls the cellular fate of client proteins such as tau [3, 197]. Nor do they clarify the role Hsp70 may play in disease states or how one would go about developing small molecule modulators which would alter Hsp70 activity in such a way to achieve a desired cellular outcome. Towards these goals, a deeper understanding of the variables within the Hsp70 chaperone system is required.

1.6.3 The molecular chaperone Hsp70.

Hsp70 is best known for its ability to prevent aggregation and promote refolding of partially unfolded proteins [198, 199]. Further, the Hsp70 chaperone system plays a central role in the maintenance of cellular protein homeostasis by participating in a variety of multi-protein complexes involved in divergent pathways which include trafficking, complex remodeling, folding, and degradation (Figure 1.1) [3]. At the center of this complex is Hsp70 itself, which is composed of a nucleotide binding domain (NBD) and a substrate binding domain (SBD) (Figure 1.4).

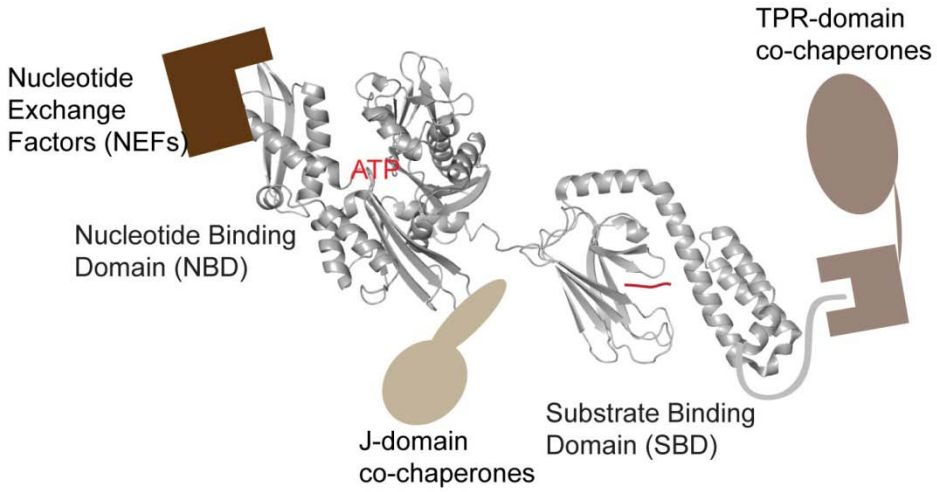

Figure 1.4. The Hsp70 chaperone system.
The molecular chaperone Hsp70 has both a nucleotide binding domain (NBD) and substrate binding domain (SBD) (shown in the grey cartoon). The NBD can bind and hydrolyze ATP while the SBD binds exposed polypeptides within misfolded substrate proteins (both shown in red). Hsp70 also interacts with three classes of co-chaperones; J-domain proteins, nucleotide exchange factors, and TPR domain proteins (all shown in brown).

Within the NBD, Hsp70 carries out a catalytic ATPase cycle, meanwhile within the SBD a wide variety of client proteins interact with Hsp70 via a substrate binding pocket [200]. Although it is appreciated that Hsp70 interacts with extended hydrophobic polypeptides, this binding pocket is promiscuous and Hsp70 has a multitude of client proteins [34, 201]. Further, both the ATPase cycle and the chaperone activities of Hsp70 are

modulated by interactions with three classes of co-chaperones; J-domain proteins, nucleotide exchange factors (NEFs), and tetratricopeptide repeat (TPR) domain proteins [Figure 1.4]. In humans, approximately 40 J-domain proteins and 13 NEFs can modulate the catalytic ATPase cycle of Hsp70. J-domain proteins stimulate ATP hydrolysis and may bind client proteins, delivering them to Hsp70 [202]. Meanwhile, NEFs promote release of ADP and subsequent nucleotide exchange [203, 204]. Many J-proteins and NEFs are multi-domain proteins and may also play a role in determining client fate via outside domains which include ubiquitin-like domains or substrate binding domains [205-207]. For example, over-expression of NEF BAG1 increases tau levels and inhibits proteasomal degradation [192]. Also, a BAG2-mediated ubiquitin-independent degradation pathway for tau has been identified [189]. The final class of co-chaperones, TPR domain proteins, potentially includes hundreds of TPR domain proteins in the human genome which exhibit extensive diversity outside of their conserved TPR domain; the two best characterized as Hsp70 co-chaperones are Hop (the Hsp70 Hsp90 organizing protein) and CHIP (the Carboxy terminal Heat shock conjugate Interaction Protein) [208-210]. Hop can simultaneously bind the molecular chaperones Hsp90 and Hsp70 and functions to coordinate these two chaperone systems frequently to promote proper folding [211, 212]. In contrast to Hop, CHIP is an ubiquitin E3 ligase with an effector Ubox domain [213] and functions to ubiquitinate chaperone client proteins and target them for degradation [214, 215]. Consistent with this, several groups have shown that CHIP mediates the ubiquitination and degradation of tau [187, 190, 191, 193, 194, 216]. Thus, Hsp70 is a multi-component system, in which ATP hydrolysis, structural

transitions, and multiple PPIs likely contribute in various ways to alter the chaperone activities of Hsp70.

1.6.4 "Grey-box" screening uncovers multiple chemical modulators of Hsp70 chaperone system.

Given the central role Hsp70 plays in protein homeostasis within cells, the Gestwicki lab, aims to develop chemical modulators of Hsp70 that can be used to study chaperone biology and understand the potential of Hsp70 as a therapeutic target. Yet, in developing chemical modulators to Hsp70, the field has faced many of the challenges discussed within this chapter. Indeed, as highlighted in Figure 1.1, this system consists of a combinatorial assembly of co-chaperones, thought to dictate client fate [3]. These PPIs cover a range of physicochemical space as discussed in Figure 1.2. Which PPI surface should be targeted to achieve a desired therapeutic outcome, or how to gain selectivity for one co-chaperone over another which bind at overlapping sites is not yet clear. Thus, to develop the first generation of Hsp70 small molecule probes, former members of the Gestwicki lab have utilized a "grey-box" screening approach. Previous work utilized a J-protein to stimulate the ATPase rate of Hsp70 and screen for compounds which either inhibited or stimulated this J-stimulated ATPase activity of Hsp70 [75, 137, 138, 217]. This approach resulted in several different small molecules which could be utilized to gain an improved mechanistic understanding of the Hsp70 chaperone system. The compounds identified included myricetin; a flavonoid which allosterically inhibits J-protein binding to Hsp70 [75]. Further, methylene blue (MB) was found to alter PTMs on Hsp70 via the oxidation of specific cysteine residues [Yoshi Miyata and Jenny Rauch unpublished data]. Finally, additional scaffolds including dihydropyrimidines, MKT-077

derivatives, and spergualins have been shown to nucleate J-protein binding, stabilize the ADP bound state of Hsp70, and function as inhibitors of TPR co-chaperone interactions respectively [138, 218] [Matthew Smith unpublished data]. Thus, available Hsp70 modulators alter Hsp70 activity in a variety of ways. As such, these small molecules may be utilized as chemical probes to improve our understanding of the Hsp70 chaperone system. Consistent with this idea, it was observed that Hsp70 ATPase inhibitors myricetin and MB result in reductions in tau levels, while the ATPase stimulators of the dihydropyrimidine class result in accumulation of tau in multiple cellular models [219].

1.7 Future perspectives

These initial results importantly show that small molecule modulators of Hsp70 are capable of targeting tau for clearance. Next, this thesis aims to utilize these chemical probes to understand what molecular changes within Hsp70 or Hsp70 multi-protein complexes are able to acutely trigger tau for degradation. Further, whether changes in ATP turnover or nucleotide state are indicative of changes in central Hsp70 chaperone functions will be explored. These studies may be able to not only improve our understanding of protein quality control within the Hsp70 chaperone system, but also enable future discovery of improved Hsp70 modulators by uncovering novel screening strategies or enabling “grey-box” screening utilizing more “disease-relevant” complexes.

In this dissertation some of these key questions are addressed. In Chapter 2, the relationship between ATP turnover and Hsp70 chaperone function is evaluated. In Chapter 3, the function and architecture of oligomeric Hsp70 which is preferentially

formed in the ADP-bound state is explored. In Chapter 4, a chemical tool, MB, is utilized to transiently induce tau degradation and monitor changes in protein complex formation in response to this acute pro-degradation trigger. Finally, in Chapter 5, the implications of these studies are discussed as well as potential future strategies for the improved treatment of tauopathies.

Notes

This work will be in part be submitted as a review to ACS Chemical Biology entitled "Fine tuning multi-protein complexes using small molecules." Andrea D. Thompson, Amanda Dugan, Jason E. Gestwicki, and Anna Mapp contributed intellectually to this review.

1.8 References

1. Danielpour, D. and K. Song, *Cross-talk between IGF-I and TGF-beta signaling pathways.* Cytokine Growth Factor Rev, 2006. **17**(1-2): p. 59-74.
2. Papa, S., et al., *Mechanisms of liver disease: cross-talk between the NF-kappaB and JNK pathways.* Biol Chem, 2009. **390**(10): p. 965-76.
3. Hohfeld, J., D.M. Cyr, and C. Patterson, *From the cradle to the grave: molecular chaperones that may choose between folding and degradation.* EMBO Rep, 2001. **2**(10): p. 885-90.
4. Lessard, J.A. and G.R. Crabtree, *Chromatin regulatory mechanisms in pluripotency.* Annu Rev Cell Dev Biol, 2010. **26**: p. 503-32.
5. Dekker, F.J. and H.J. Haisma, *Histone acetyl transferases as emerging drug targets.* Drug Discov Today, 2009. **14**(19-20): p. 942-8.
6. Keskin, O., et al., *Towards drugs targeting multiple proteins in a systems biology approach.* Curr Top Med Chem, 2007. **7**(10): p. 943-51.
7. Mimeault, M. and S.K. Batra, *New promising drug targets in cancer- and metastasis-initiating cells.* Drug Discov Today, 2010. **15**(9-10): p. 354-64.
8. Rual, J.F., et al., *Towards a proteome-scale map of the human protein-protein interaction network.* Nature, 2005. **437**(7062): p. 1173-8.
9. Vidal, M., M.E. Cusick, and A.L. Barabasi, *Interactome networks and human disease.* Cell, 2011. **144**(6): p. 986-98.
10. Hopkins, A.L. and C.R. Groom, *The druggable genome.* Nat Rev Drug Discov, 2002. **1**(9): p. 727-30.
11. Cravatt, B.F., G.M. Simon, and J.R. Yates, 3rd, *The biological impact of mass-spectrometry-based proteomics.* Nature, 2007. **450**(7172): p. 991-1000.
12. Powers, E.T., et al., *Biological and chemical approaches to diseases of proteostasis deficiency.* Annu Rev Biochem, 2009. **78**: p. 959-91.
13. Surade, S. and T.L. Blundell, *Structural biology and drug discovery of difficult targets: the limits of ligandability.* Chem Biol, 2012. **19**(1): p. 42-50.
14. Overington, J.P., B. Al-Lazikani, and A.L. Hopkins, *How many drug targets are there?* Nat Rev Drug Discov, 2006. **5**(12): p. 993-6.
15. Drews, J., *Drug discovery: a historical perspective.* Science, 2000. **287**(5460): p. 1960-4.
16. Stumpf, M.P., et al., *Estimating the size of the human interactome.* Proc Natl Acad Sci U S A, 2008. **105**(19): p. 6959-64.
17. Wells, J.A. and C.L. McClendon, *Reaching for high-hanging fruit in drug discovery at protein-protein interfaces.* Nature, 2007. **450**(7172): p. 1001-9.
18. Bourgeas, R., et al., *Atomic analysis of protein-protein interfaces with known inhibitors: the 2P2I database.* PLoS One, 2010. **5**(3): p. e9598.
19. Higueruelo, A.P., et al., *Atomic interactions and profile of small molecules disrupting protein-protein interfaces: the TIMBAL database.* Chem Biol Drug Des, 2009. **74**(5): p. 457-67.
20. Romero, G., M. von Zastrow, and P.A. Friedman, *Role of PDZ proteins in regulating trafficking, signaling, and function of GPCRs: means, motif, and opportunity.* Adv Pharmacol, 2011. **62**: p. 279-314.
21. Young, A., et al., *Ras signaling and therapies.* Adv Cancer Res, 2009. **102**: p. 1-17.
22. Lessard, J., et al., *An essential switch in subunit composition of a chromatin remodeling complex during neural development.* Neuron, 2007. **55**(2): p. 201-15.

23. Yoo, A.S. and G.R. Crabtree, *ATP-dependent chromatin remodeling in neural development.* Curr Opin Neurobiol, 2009. **19**(2): p. 120-6.
24. Perot, S., et al., *Druggable pockets and binding site centric chemical space: a paradigm shift in drug discovery.* Drug Discov Today, 2010. **15**(15-16): p. 656-67.
25. Fuller, J.C., N.J. Burgoyne, and R.M. Jackson, *Predicting druggable binding sites at the protein-protein interface.* Drug Discov Today, 2009. **14**(3-4): p. 155-61.
26. DeLano, W.L., *Unraveling hot spots in binding interfaces: progress and challenges.* Curr Opin Struct Biol, 2002. **12**(1): p. 14-20.
27. Lo Conte, L., C. Chothia, and J. Janin, *The atomic structure of protein-protein recognition sites.* J Mol Biol, 1999. **285**(5): p. 2177-98.
28. Nooren, I.M. and J.M. Thornton, *Diversity of protein-protein interactions.* EMBO J, 2003. **22**(14): p. 3486-92.
29. Nooren, I.M. and J.M. Thornton, *Structural characterisation and functional significance of transient protein-protein interactions.* J Mol Biol, 2003. **325**(5): p. 991-1018.
30. Wang, L., et al., *Molecular mechanism of the negative regulation of Smad1/5 protein by carboxyl terminus of Hsc70-interacting protein (CHIP).* J Biol Chem, 2011. **286**(18): p. 15883-94.
31. Jiang, J., et al., *Structural basis of J cochaperone binding and regulation of Hsp70.* Mol Cell, 2007. **28**(3): p. 422-33.
32. Schuermann, J.P., et al., *Structure of the Hsp110:Hsc70 nucleotide exchange machine.* Mol Cell, 2008. **31**(2): p. 232-43.
33. Ahmad, A., et al., *Heat shock protein 70 kDa chaperone/DnaJ cochaperone complex employs an unusual dynamic interface.* Proc Natl Acad Sci U S A, 2011. **108**(47): p. 18966-71.
34. Zhu, X., et al., *Structural analysis of substrate binding by the molecular chaperone DnaK.* Science, 1996. **272**(5268): p. 1606-14.
35. Scheufler, C., et al., *Structure of TPR domain-peptide complexes: critical elements in the assembly of the Hsp70-Hsp90 multichaperone machine.* Cell, 2000. **101**(2): p. 199-210.
36. Feng, H., et al., *Structural basis for p300 Taz2-p53 TAD1 binding and modulation by phosphorylation.* Structure, 2009. **17**(2): p. 202-10.
37. Lee, W., et al., *Solution structure of the tetrameric minimum transforming domain of p53.* Nat Struct Biol, 1994. **1**(12): p. 877-90.
38. Popowicz, G.M., A. Czarna, and T.A. Holak, *Structure of the human Mdmx protein bound to the p53 tumor suppressor transactivation domain.* Cell Cycle, 2008. **7**(15): p. 2441-3.
39. Lee, C.W., et al., *Structure of the p53 transactivation domain in complex with the nuclear receptor coactivator binding domain of CREB binding protein.* Biochemistry, 2010. **49**(46): p. 9964-71.
40. Patel, S.D., et al., *Type II cadherin ectodomain structures: implications for classical cadherin specificity.* Cell, 2006. **124**(6): p. 1255-68.
41. Stauber, D.J., et al., *Crystal structure of the IL-2 signaling complex: paradigm for a heterotrimeric cytokine receptor.* Proc Natl Acad Sci U S A, 2006. **103**(8): p. 2788-93.
42. Sun, H., et al., *Structure-based design of potent, conformationally constrained Smac mimetics.* J Am Chem Soc, 2004. **126**(51): p. 16686-7.
43. Wu, G., et al., *Structural basis of IAP recognition by Smac/DIABLO.* Nature, 2000. **408**(6815): p. 1008-12.
44. Vaynberg, J., et al., *Structure of an ultraweak protein-protein complex and its crucial role in regulation of cell morphology and motility.* Mol Cell, 2005. **17**(4): p. 513-23.

45. Whitty, A. and G. Kumaravel, *Between a rock and a hard place?* Nat Chem Biol, 2006. **2**(3): p. 112-8.
46. Wang, S., *Design of Small-Molecule Smac Mimetics as IAP Antagonists.* Curr Top Microbiol Immunol, 2010.
47. Chen, D.J. and S. Huerta, *Smac mimetics as new cancer therapeutics.* Anticancer Drugs, 2009. **20**(8): p. 646-58.
48. Russ, A.P. and S. Lampel, *The druggable genome: an update.* Drug Discov Today, 2005. **10**(23-24): p. 1607-10.
49. Arkin, M.R. and J.A. Wells, *Small-molecule inhibitors of protein-protein interactions: progressing towards the dream.* Nat Rev Drug Discov, 2004. **3**(4): p. 301-17.
50. Thanos, C.D., W.L. DeLano, and J.A. Wells, *Hot-spot mimicry of a cytokine receptor by a small molecule.* Proc Natl Acad Sci U S A, 2006. **103**(42): p. 15422-7.
51. Thanos, C.D., M. Randal, and J.A. Wells, *Potent small-molecule binding to a dynamic hot spot on IL-2.* J Am Chem Soc, 2003. **125**(50): p. 15280-1.
52. Lipinski, C. and A. Hopkins, *Navigating chemical space for biology and medicine.* Nature, 2004. **432**(7019): p. 855-61.
53. Lipinski, C.A., *Drug-like properties and the causes of poor solubility and poor permeability.* J Pharmacol Toxicol Methods, 2000. **44**(1): p. 235-49.
54. Lindsley, J.E. and J. Rutter, *Whence cometh the allosterome?* Proc Natl Acad Sci U S A, 2006. **103**(28): p. 10533-5.
55. Gunasekaran, K., B. Ma, and R. Nussinov, *Is allostery an intrinsic property of all dynamic proteins?* Proteins, 2004. **57**(3): p. 433-43.
56. Lewis, B.A., *Understanding large multiprotein complexes: applying a multiple allosteric networks model to explain the function of the Mediator transcription complex.* J Cell Sci, 2010. **123**(Pt 2): p. 159-63.
57. Li, J., D.J. Callaway, and Z. Bu, *Ezrin induces long-range interdomain allostery in the scaffolding protein NHERF1.* J Mol Biol, 2009. **392**(1): p. 166-80.
58. Meyer, K.D., et al., *p53 activates transcription by directing structural shifts in Mediator.* Nat Struct Mol Biol, 2010. **17**(6): p. 753-60.
59. Friedmann, D.R., J.J. Wilson, and R.A. Kovall, *RAM-induced allostery facilitates assembly of a notch pathway active transcription complex.* J Biol Chem, 2008. **283**(21): p. 14781-91.
60. Doweyko, A.M., *Steroid nuclear hormone receptors: The allosteric conversation.* Drug Development Research, 2007. **68**(3): p. 95-106.
61. Bertrand, D. and J.P. Changeux, *Nicotinic receptor: a prototype of allosteric ligand-gated ion channels and its possible implications in epilepsy.* Adv Neurol, 1999. **79**: p. 171-88.
62. Zhang, X., et al., *An allosteric mechanism for activation of the kinase domain of epidermal growth factor receptor.* Cell, 2006. **125**(6): p. 1137-49.
63. Gronemeyer, H., J.A. Gustafsson, and V. Laudet, *Principles for modulation of the nuclear receptor superfamily.* Nat Rev Drug Discov, 2004. **3**(11): p. 950-64.
64. Yano, K. and T. Fukasawa, *Galactose-dependent reversible interaction of Gal3p with Gal80p in the induction pathway of Gal4p-activated genes of Saccharomyces cerevisiae.* Proc Natl Acad Sci U S A, 1997. **94**(5): p. 1721-6.
65. Weinkam, P., J. Pons, and A. Sali, *Structure-based model of allostery predicts coupling between distant sites.* Proceedings of the National Academy of Sciences, 2012.
66. Kenakin, T.P., *Ligand detection in the allosteric world.* J Biomol Screen, 2010. **15**(2): p. 119-30.

67. Li, X., et al., *Extensive in vivo metabolite-protein interactions revealed by large-scale systematic analyses.* Cell, 2010. **143**(4): p. 639-50.
68. Orsak, T., et al., *Revealing the allosterome: systematic identification of metabolite-protein interactions.* Biochemistry, 2012. **51**(1): p. 225-32.
69. Tagore, R., et al., *A global metabolite profiling approach to identify protein-metabolite interactions.* J Am Chem Soc, 2008. **130**(43): p. 14111-3.
70. Lawrence, S.H., et al., *Shape shifting leads to small-molecule allosteric drug discovery.* Chem Biol, 2008. **15**(6): p. 586-96.
71. Lawrence, S.H., et al., *Allosteric inhibition of human porphobilinogen synthase.* J Biol Chem, 2009. **284**(51): p. 35807-17.
72. Roman, D.L., et al., *Allosteric inhibition of the regulator of G protein signaling-Galpha protein-protein interaction by CCG-4986.* Mol Pharmacol, 2010. **78**(3): p. 360-5.
73. Mallya, M., et al., *Small molecules block the polymerization of Z alpha1-antitrypsin and increase the clearance of intracellular aggregates.* J Med Chem, 2007. **50**(22): p. 5357-63.
74. Blazer, L.L., et al., *Reversible, allosteric small-molecule inhibitors of regulator of G protein signaling proteins.* Mol Pharmacol, 2010. **78**(3): p. 524-33.
75. Chang, L., et al., *Chemical screens against a reconstituted multiprotein complex: myricetin blocks DnaJ regulation of DnaK through an allosteric mechanism.* Chem Biol, 2011. **18**(2): p. 210-21.
76. McMillan, K., et al., *Allosteric inhibitors of inducible nitric oxide synthase dimerization discovered via combinatorial chemistry.* Proc Natl Acad Sci U S A, 2000. **97**(4): p. 1506-11.
77. Conn, P.J., A. Christopoulos, and C.W. Lindsley, *Allosteric modulators of GPCRs: a novel approach for the treatment of CNS disorders.* Nat Rev Drug Discov, 2009. **8**(1): p. 41-54.
78. Leach, K., P.M. Sexton, and A. Christopoulos, *Allosteric GPCR modulators: taking advantage of permissive receptor pharmacology.* Trends Pharmacol Sci, 2007. **28**(8): p. 382-9.
79. Johnson, A.E. and M.A. van Waes, *The translocon: a dynamic gateway at the ER membrane.* Annu Rev Cell Dev Biol, 1999. **15**: p. 799-842.
80. Osborne, A.R., T.A. Rapoport, and B. van den Berg, *Protein translocation by the Sec61/SecY channel.* Annu Rev Cell Dev Biol, 2005. **21**: p. 529-50.
81. Kim, S.J., et al., *Signal sequences control gating of the protein translocation channel in a substrate-specific manner.* Dev Cell, 2002. **2**(2): p. 207-17.
82. Rutkowski, D.T., V.R. Lingappa, and R.S. Hegde, *Substrate-specific regulation of the ribosome- translocon junction by N-terminal signal sequences.* Proc Natl Acad Sci U S A, 2001. **98**(14): p. 7823-8.
83. Garrison, J.L., et al., *A substrate-specific inhibitor of protein translocation into the endoplasmic reticulum.* Nature, 2005. **436**(7048): p. 285-9.
84. Besemer, J., et al., *Selective inhibition of cotranslational translocation of vascular cell adhesion molecule 1.* Nature, 2005. **436**(7048): p. 290-3.
85. Krogsgaard, M., et al., *Linking molecular and cellular events in T-cell activation and synapse formation.* Semin Immunol, 2003. **15**(6): p. 307-15.
86. Klemm, J.D., S.L. Schreiber, and G.R. Crabtree, *Dimerization as a regulatory mechanism in signal transduction.* Annu Rev Immunol, 1998. **16**: p. 569-92.
87. Okuzumi, T., et al., *Inhibitor hijacking of Akt activation.* Nat Chem Biol, 2009. **5**(7): p. 484-93.

88. Deribe, Y.L., T. Pawson, and I. Dikic, *Post-translational modifications in signal integration.* Nat Struct Mol Biol, 2010. **17**(6): p. 666-72.
89. Potashman, M.H. and M.E. Duggan, *Covalent modifiers: an orthogonal approach to drug design.* J Med Chem, 2009. **52**(5): p. 1231-46.
90. Stepan, A.F., et al., *Structural alert/reactive metabolite concept as applied in medicinal chemistry to mitigate the risk of idiosyncratic drug toxicity: a perspective based on the critical examination of trends in the top 200 drugs marketed in the United States.* Chem Res Toxicol, 2011. **24**(9): p. 1345-410.
91. Ahn, Y.H., et al., *Electrophilic tuning of the chemoprotective natural product sulforaphane.* Proc Natl Acad Sci U S A, 2010. **107**(21): p. 9590-5.
92. Zhang, Y., et al., *HSF1-dependent upregulation of Hsp70 by sulfhydryl-reactive inducers of the KEAP1/NRF2/ARE pathway.* Chem Biol, 2011. **18**(11): p. 1355-61.
93. Cameron, A.J., et al., *PKC maturation is promoted by nucleotide pocket occupation independently of intrinsic kinase activity.* Nat Struct Mol Biol, 2009. **16**(6): p. 624-30.
94. Desai, A. and T.J. Mitchison, *Microtubule polymerization dynamics.* Annu Rev Cell Dev Biol, 1997. **13**: p. 83-117.
95. Schmeing, T.M. and V. Ramakrishnan, *What recent ribosome structures have revealed about the mechanism of translation.* Nature, 2009. **461**(7268): p. 1234-42.
96. Steitz, T.A., *A structural understanding of the dynamic ribosome machine.* Nat Rev Mol Cell Biol, 2008. **9**(3): p. 242-53.
97. LaRiviere, F.J., A.D. Wolfson, and O.C. Uhlenbeck, *Uniform binding of aminoacyl-tRNAs to elongation factor Tu by thermodynamic compensation.* Science, 2001. **294**(5540): p. 165-8.
98. Schrader, J.M., S.J. Chapman, and O.C. Uhlenbeck, *Tuning the affinity of aminoacyl-tRNA to elongation factor Tu for optimal decoding.* Proc Natl Acad Sci U S A, 2011. **108**(13): p. 5215-20.
99. Yonath, A., *Antibiotics targeting ribosomes: resistance, selectivity, synergism and cellular regulation.* Annu Rev Biochem, 2005. **74**: p. 649-79.
100. Erlanson, D.A., et al., *Site-directed ligand discovery.* Proc Natl Acad Sci U S A, 2000. **97**(17): p. 9367-72.
101. Scheer, J.M., M.J. Romanowski, and J.A. Wells, *A common allosteric site and mechanism in caspases.* Proc Natl Acad Sci U S A, 2006. **103**(20): p. 7595-600.
102. Coyne, A.G., D.E. Scott, and C. Abell, *Drugging challenging targets using fragment-based approaches.* Curr Opin Chem Biol, 2010. **14**(3): p. 299-307.
103. Hajduk, P.J. and J. Greer, *A decade of fragment-based drug design: strategic advances and lessons learned.* Nat Rev Drug Discov, 2007. **6**(3): p. 211-9.
104. Murray, C.W. and D.C. Rees, *The rise of fragment-based drug discovery.* Nat Chem, 2009. **1**(3): p. 187-92.
105. Jahnke, W., et al., *Allosteric non-bisphosphonate FPPS inhibitors identified by fragment-based discovery.* Nat Chem Biol, 2010. **6**(9): p. 660-6.
106. Oltersdorf, T., et al., *An inhibitor of Bcl-2 family proteins induces regression of solid tumours.* Nature, 2005. **435**(7042): p. 677-81.
107. Lockless, S.W. and R. Ranganathan, *Evolutionarily conserved pathways of energetic connectivity in protein families.* Science, 1999. **286**(5438): p. 295-9.
108. Suel, G.M., et al., *Evolutionarily conserved networks of residues mediate allosteric communication in proteins.* Nat Struct Biol, 2003. **10**(1): p. 59-69.
109. Massova, I. and S. Mobashery, *Structural and mechanistic aspects of evolution of beta-lactamases and penicillin-binding proteins.* Curr Pharm Des, 1999. **5**(11): p. 929-37.

110. Schuyler, A.D., H.A. Carlson, and E.L. Feldman, *Computational methods for identifying a layered allosteric regulatory mechanism for ALS-causing mutations of Cu-Zn superoxide dismutase 1.* Proteins, 2010.
111. Ota, N. and D.A. Agard, *Intramolecular signaling pathways revealed by modeling anisotropic thermal diffusion.* J Mol Biol, 2005. **351**(2): p. 345-54.
112. Hendlich, M., F. Rippmann, and G. Barnickel, *LIGSITE: automatic and efficient detection of potential small molecule-binding sites in proteins.* J Mol Graph Model, 1997. **15**(6): p. 359-63, 389.
113. Kalidas, Y. and N. Chandra, *PocketDepth: a new depth based algorithm for identification of ligand binding sites in proteins.* J Struct Biol, 2008. **161**(1): p. 31-42.
114. Lexa, K.W. and H.A. Carlson, *Full Protein Flexibility Is Essential for Proper Hot-Spot Mapping.* J Am Chem Soc, 2010.
115. Morita, M., S. Nakamura, and K. Shimizu, *Highly accurate method for ligand-binding site prediction in unbound state (apo) protein structures.* Proteins, 2008. **73**(2): p. 468-79.
116. Bill, A., et al., *A homogeneous fluorescence resonance energy transfer system for monitoring the activation of a protein switch in real time.* J Am Chem Soc, 2011. **133**(21): p. 8372-9.
117. Coward, P., et al., *Application of an allosteric model to describe the interactions among retinol binding protein 4, transthyretin, and small molecule retinol binding protein 4 ligands.* Anal Biochem, 2009. **384**(2): p. 312-20.
118. Soderholm, J.F., et al., *Importazole, a small molecule inhibitor of the transport receptor importin-beta.* ACS Chem Biol, 2011. **6**(7): p. 700-8.
119. Cellitti, S.E., et al., *In vivo incorporation of unnatural amino acids to probe structure, dynamics, and ligand binding in a large protein by nuclear magnetic resonance spectroscopy.* J Am Chem Soc, 2008. **130**(29): p. 9268-81.
120. Al-Hashimi, H.M., *Biochemistry. Exciting structures.* Science, 2010. **329**(5997): p. 1295-6.
121. Moerke, N.J., et al., *Small-molecule inhibition of the interaction between the translation initiation factors eIF4E and eIF4G.* Cell, 2007. **128**(2): p. 257-67.
122. Sun, H., et al., *Design, synthesis, and characterization of a potent, nonpeptide, cell-permeable, bivalent Smac mimetic that concurrently targets both the BIR2 and BIR3 domains in XIAP.* J Am Chem Soc, 2007. **129**(49): p. 15279-94.
123. Bobkova, E.V., et al., *Discovery of PDK1 kinase inhibitors with a novel mechanism of action by ultrahigh throughput screening.* J Biol Chem, 2010. **285**(24): p. 18838-46.
124. Converso, A., et al., *Development of thioquinazolinones, allosteric Chk1 kinase inhibitors.* Bioorg Med Chem Lett, 2009. **19**(4): p. 1240-4.
125. Stockwell, B.R., *Chemical genetics: ligand-based discovery of gene function.* Nat Rev Genet, 2000. **1**(2): p. 116-25.
126. Foster, C.A., et al., *Pharmacological modulation of endothelial cell-associated adhesion molecule expression: implications for future treatment of dermatological diseases.* J Dermatol, 1994. **21**(11): p. 847-54.
127. Aghajan, M., et al., *Chemical genetics screen for enhancers of rapamycin identifies a specific inhibitor of an SCF family E3 ubiquitin ligase.* Nat Biotechnol, 2010. **28**(7): p. 738-42.
128. Orlicky, S., et al., *An allosteric inhibitor of substrate recognition by the SCF(Cdc4) ubiquitin ligase.* Nat Biotechnol, 2010. **28**(7): p. 733-7.
129. Verma, R., et al., *Ubistatins inhibit proteasome-dependent degradation by binding the ubiquitin chain.* Science, 2004. **306**(5693): p. 117-20.

130. Erlbruch, A., et al., *Uncoupling of bait-protein expression from the prey protein environment adds versatility for cell and tissue interaction proteomics and reveals a complex of CARP-1 and the PKA Cbeta1 subunit.* Proteomics, 2010. **10**(16): p. 2890-900.
131. Moulick, K., et al., *Affinity-based proteomics reveal cancer-specific networks coordinated by Hsp90.* Nat Chem Biol, 2011. **7**(11): p. 818-26.
132. Moellering, R.E. and B.F. Cravatt, *How chemoproteomics can enable drug discovery and development.* Chem Biol, 2012. **19**(1): p. 11-22.
133. Schirle, M., M. Bantscheff, and B. Kuster, *Mass spectrometry-based proteomics in preclinical drug discovery.* Chem Biol, 2012. **19**(1): p. 72-84.
134. Tong, A.H., et al., *Global mapping of the yeast genetic interaction network.* Science, 2004. **303**(5659): p. 808-13.
135. Alaimo, P.J., M.A. Shogren-Knaak, and K.M. Shokat, *Chemical genetic approaches for the elucidation of signaling pathways.* Curr Opin Chem Biol, 2001. **5**(4): p. 360-7.
136. Deacon, S.W., et al., *An isoform-selective, small-molecule inhibitor targets the autoregulatory mechanism of p21-activated kinase.* Chem Biol, 2008. **15**(4): p. 322-31.
137. Miyata, Y., et al., *High-throughput screen for Escherichia coli heat shock protein 70 (Hsp70/DnaK): ATPase assay in low volume by exploiting energy transfer.* J Biomol Screen, 2010. **15**(10): p. 1211-9.
138. Wisen, S., et al., *Binding of a small molecule at a protein-protein interface regulates the chaperone activity of hsp70-hsp40.* ACS Chem Biol, 2010. **5**(6): p. 611-22.
139. Berggard, T., S. Linse, and P. James, *Methods for the detection and analysis of protein-protein interactions.* Proteomics, 2007. **7**(16): p. 2833-42.
140. Perkins, J.R., et al., *Transient protein-protein interactions: structural, functional, and network properties.* Structure, 2010. **18**(10): p. 1233-43.
141. Kerppola, T.K., *Bimolecular fluorescence complementation (BiFC) analysis as a probe of protein interactions in living cells.* Annu Rev Biophys, 2008. **37**: p. 465-87.
142. Krishnamurthy, M., et al., *Caught in the act: covalent cross-linking captures activator-coactivator interactions in vivo.* ACS Chem Biol, 2011. **6**(12): p. 1321-6.
143. Pellegrini, M., *Defining interacting partners for drug discovery.* Expert Opin Ther Targets, 2003. **7**(2): p. 287-97.
144. Tanaka, Y., M.R. Bond, and J.J. Kohler, *Photocrosslinkers illuminate interactions in living cells.* Mol Biosyst, 2008. **4**(6): p. 473-80.
145. Majmudar, C.Y., et al., *Impact of nonnatural amino acid mutagenesis on the in vivo function and binding modes of a transcriptional activator.* J Am Chem Soc, 2009. **131**(40): p. 14240-2.
146. Clark, M.A., *Selecting chemicals: the emerging utility of DNA-encoded libraries.* Curr Opin Chem Biol, 2010. **14**(3): p. 396-403.
147. Dandapani, S. and L.A. Marcaurelle, *Grand challenge commentary: Accessing new chemical space for 'undruggable' targets.* Nat Chem Biol, 2010. **6**(12): p. 861-3.
148. Dandapani, S. and L.A. Marcaurelle, *Current strategies for diversity-oriented synthesis.* Curr Opin Chem Biol, 2010. **14**(3): p. 362-70.
149. Goldman, S., *Genetic chemistry: production of non-native compounds in yeast.* Curr Opin Chem Biol, 2010. **14**(3): p. 390-5.
150. Fletcher, S. and A.D. Hamilton, *Protein surface recognition and proteomimetics: mimics of protein surface structure and function.* Curr Opin Chem Biol, 2005. **9**(6): p. 632-8.
151. Buerger, C. and B. Groner, *Bifunctional recombinant proteins in cancer therapy: cell penetrating peptide aptamers as inhibitors of growth factor signaling.* J Cancer Res Clin Oncol, 2003. **129**(12): p. 669-75.

152. Traczewski, P. and L. Rudnicka, *Treatment of systemic lupus erythematosus with epratuzumab.* Br J Clin Pharmacol, 2011. **71**(2): p. 175-82.
153. Drewry, D.H. and R. Macarron, *Enhancements of screening collections to address areas of unmet medical need: an industry perspective.* Curr Opin Chem Biol, 2010. **14**(3): p. 289-98.
154. Renner, S., et al., *Recent trends and observations in the design of high-quality screening collections.* Future Med Chem, 2011. **3**(6): p. 751-66.
155. Drechsel, D.N., et al., *Modulation of the dynamic instability of tubulin assembly by the microtubule-associated protein tau.* Mol Biol Cell, 1992. **3**(10): p. 1141-54.
156. Drubin, D.G., et al., *Nerve growth factor-induced neurite outgrowth in PC12 cells involves the coordinate induction of microtubule assembly and assembly-promoting factors.* J Cell Biol, 1985. **101**(5 Pt 1): p. 1799-807.
157. Kempf, M., et al., *Tau binds to the distal axon early in development of polarity in a microtubule- and microfilament-dependent manner.* J Neurosci, 1996. **16**(18): p. 5583-92.
158. Uversky, V.N., C.J. Oldfield, and A.K. Dunker, *Intrinsically disordered proteins in human diseases: introducing the D2 concept.* Annu Rev Biophys, 2008. **37**: p. 215-46.
159. D'Souza, I., et al., *Missense and silent tau gene mutations cause frontotemporal dementia with parkinsonism-chromosome 17 type, by affecting multiple alternative RNA splicing regulatory elements.* Proc Natl Acad Sci U S A, 1999. **96**(10): p. 5598-603.
160. Yasuda, M., et al., *A mutation in the microtubule-associated protein tau in pallido-nigro-luysian degeneration.* Neurology, 1999. **53**(4): p. 864-8.
161. D'Souza, I. and G.D. Schellenberg, *Regulation of tau isoform expression and dementia.* Biochim Biophys Acta, 2005. **1739**(2-3): p. 104-15.
162. Furukawa, K., et al., *Pro-apoptotic effects of tau mutations in chromosome 17 frontotemporal dementia and parkinsonism.* Neuroreport, 2000. **11**(1): p. 57-60.
163. Goedert, M., M.G. Spillantini, and S.W. Davies, *Filamentous nerve cell inclusions in neurodegenerative diseases.* Curr Opin Neurobiol, 1998. **8**(5): p. 619-32.
164. Kidd, M., *Paired helical filaments in electron microscopy of Alzheimer's disease.* Nature, 1963. **197**: p. 192-193.
165. Spillantini, M.G., T.D. Bird, and B. Ghetti, *Frontotemporal dementia and Parkinsonism linked to chromosome 17: a new group of tauopathies.* Brain Pathol, 1998. **8**(2): p. 387-402.
166. Williams, D.R. and A.J. Lees, *Progressive supranuclear palsy: clinicopathological concepts and diagnostic challenges.* Lancet Neurol, 2009. **8**(3): p. 270-9.
167. Alzheimer's_Association, *2008 Alzheimer's Disease Facts and Figures.* Alzheimer's & Dementia, 2008. **4**(2).
168. Lleo, A., S.M. Greenberg, and J.H. Growdon, *Current pharmacotherapy for Alzheimer's disease.* Annu Rev Med, 2006. **57**: p. 513-33.
169. Goedert, M., R. Jakes, and R.A. Crowther, *Effects of frontotemporal dementia FTDP-17 mutations on heparin-induced assembly of tau filaments.* FEBS Lett, 1999. **450**(3): p. 306-11.
170. Hutton, M., et al., *Association of missense and 5'-splice-site mutations in tau with the inherited dementia FTDP-17.* Nature, 1998. **393**(6686): p. 702-5.
171. Murrell, J.R., et al., *Tau gene mutation G389R causes a tauopathy with abundant pick body-like inclusions and axonal deposits.* J Neuropathol Exp Neurol, 1999. **58**(12): p. 1207-26.

172. Roberson, E.D., et al., *Amyloid-beta/Fyn-induced synaptic, network, and cognitive impairments depend on tau levels in multiple mouse models of Alzheimer's disease.* J Neurosci, 2011. **31**(2): p. 700-11.
173. Roberson, E.D., et al., *Reducing endogenous tau ameliorates amyloid beta-induced deficits in an Alzheimer's disease mouse model.* Science, 2007. **316**(5825): p. 750-4.
174. Santacruz, K., et al., *Tau suppression in a neurodegenerative mouse model improves memory function.* Science, 2005. **309**(5733): p. 476-81.
175. Sydow, A., et al., *Tau-induced defects in synaptic plasticity, learning, and memory are reversible in transgenic mice after switching off the toxic Tau mutant.* J Neurosci, 2011. **31**(7): p. 2511-25.
176. Vossel, K.A., et al., *Tau reduction prevents Abeta-induced defects in axonal transport.* Science, 2010. **330**(6001): p. 198.
177. Barral, J.M., et al., *Roles of molecular chaperones in protein misfolding diseases.* Semin Cell Dev Biol, 2004. **15**(1): p. 17-29.
178. Muchowski, P.J. and J.L. Wacker, *Modulation of neurodegeneration by molecular chaperones.* Nat Rev Neurosci, 2005. **6**(1): p. 11-22.
179. Auluck, P.K., et al., *Chaperone suppression of alpha-synuclein toxicity in a Drosophila model for Parkinson's disease.* Science, 2002. **295**(5556): p. 865-8.
180. Chan, H.Y., et al., *Mechanisms of chaperone suppression of polyglutamine disease: selectivity, synergy and modulation of protein solubility in Drosophila.* Hum Mol Genet, 2000. **9**(19): p. 2811-20.
181. Cummings, C.J., et al., *Over-expression of inducible HSP70 chaperone suppresses neuropathology and improves motor function in SCA1 mice.* Hum Mol Genet, 2001. **10**(14): p. 1511-8.
182. Dou, F., et al., *Chaperones increase association of tau protein with microtubules.* Proc Natl Acad Sci U S A, 2003. **100**(2): p. 721-6.
183. Fonte, V., et al., *Interaction of intracellular beta amyloid peptide with chaperone proteins.* Proc Natl Acad Sci U S A, 2002. **99**(14): p. 9439-44.
184. Jana, N.R., et al., *Co-chaperone CHIP associates with expanded polyglutamine protein and promotes their degradation by proteasomes.* J Biol Chem, 2005. **280**(12): p. 11635-40.
185. Klucken, J., et al., *Hsp70 Reduces alpha-Synuclein Aggregation and Toxicity.* J Biol Chem, 2004. **279**(24): p. 25497-502.
186. Krobitsch, S. and S. Lindquist, *Aggregation of huntingtin in yeast varies with the length of the polyglutamine expansion and the expression of chaperone proteins.* Proc Natl Acad Sci U S A, 2000. **97**(4): p. 1589-94.
187. Petrucelli, L., et al., *CHIP and Hsp70 regulate tau ubiquitination, degradation and aggregation.* Hum Mol Genet, 2004. **13**(7): p. 703-14.
188. Warrick, J.M., et al., *Suppression of polyglutamine-mediated neurodegeneration in Drosophila by the molecular chaperone HSP70.* Nat Genet, 1999. **23**(4): p. 425-8.
189. Carrettiero, D.C., et al., *The cochaperone BAG2 sweeps paired helical filament- insoluble tau from the microtubule.* J Neurosci, 2009. **29**(7): p. 2151-61.
190. Dickey, C.A., et al., *The high-affinity HSP90-CHIP complex recognizes and selectively degrades phosphorylated tau client proteins.* J Clin Invest, 2007. **117**(3): p. 648-58.
191. Dickey, C.A., et al., *Deletion of the ubiquitin ligase CHIP leads to the accumulation, but not the aggregation, of both endogenous phospho- and caspase-3-cleaved tau species.* J Neurosci, 2006. **26**(26): p. 6985-96.

192. Elliott, E., P. Tsvetkov, and I. Ginzburg, *BAG-1 associates with Hsc70.Tau complex and regulates the proteasomal degradation of Tau protein.* J Biol Chem, 2007. **282**(51): p. 37276-84.
193. Shimura, H., et al., *CHIP-Hsc70 complex ubiquitinates phosphorylated tau and enhances cell survival.* J Biol Chem, 2004. **279**(6): p. 4869-76.
194. Zhang, Y.J., et al., *Carboxyl terminus of heat-shock cognate 70-interacting protein degrades tau regardless its phosphorylation status without affecting the spatial memory of the rats.* J Neural Transm, 2008. **115**(3): p. 483-91.
195. Jinwal, U.K., et al., *Hsc70 rapidly engages tau after microtubule destabilization.* J Biol Chem, 2010. **285**(22): p. 16798-805.
196. Miyata, Y., et al., *Molecular chaperones and regulation of tau quality control: strategies for drug discovery in tauopathies.* Future Med Chem, 2011. **3**(12): p. 1523-37.
197. Vos, M.J., et al., *Structural and functional diversities between members of the human HSPB, HSPH, HSPA, and DNAJ chaperone families.* Biochemistry, 2008. **47**(27): p. 7001-11.
198. Bukau, B., J. Weissman, and A. Horwich, *Molecular chaperones and protein quality control.* Cell, 2006. **125**(3): p. 443-51.
199. Feder, M.E. and G.E. Hofmann, *Heat-shock proteins, molecular chaperones, and the stress response: evolutionary and ecological physiology.* Annu Rev Physiol, 1999. **61**: p. 243-82.
200. Bertelsen, E.B., et al., *Solution conformation of wild-type E. coli Hsp70 (DnaK) chaperone complexed with ADP and substrate.* Proc Natl Acad Sci U S A, 2009. **106**(21): p. 8471-6.
201. Rudiger, S., et al., *Substrate specificity of the DnaK chaperone determined by screening cellulose-bound peptide libraries.* EMBO J, 1997. **16**(7): p. 1501-7.
202. Zhao, X., A.P. Braun, and J.E. Braun, *Biological roles of neural J proteins.* Cell Mol Life Sci, 2008. **65**(15): p. 2385-96.
203. Kabbage, M. and M.B. Dickman, *The BAG proteins: a ubiquitous family of chaperone regulators.* Cell Mol Life Sci, 2008. **65**(9): p. 1390-402.
204. Dragovic, Z., et al., *Molecular chaperones of the Hsp110 family act as nucleotide exchange factors of Hsp70s.* Embo J, 2006. **25**(11): p. 2519-28.
205. Demand, J., et al., *Cooperation of a ubiquitin domain protein and an E3 ubiquitin ligase during chaperone/proteasome coupling.* Curr Biol, 2001. **11**(20): p. 1569-77.
206. Luders, J., J. Demand, and J. Hohfeld, *The ubiquitin-related BAG-1 provides a link between the molecular chaperones Hsc70/Hsp70 and the proteasome.* J Biol Chem, 2000. **275**(7): p. 4613-7.
207. Abisambra, J.F., et al., *DnaJA1 Antagonizes Constitutive Hsp70-Mediated Stabilization of Tau.* J Mol Biol, 2012.
208. Ballinger, C.A., et al., *Identification of CHIP, a novel tetratricopeptide repeat-containing protein that interacts with heat shock proteins and negatively regulates chaperone functions.* Mol Cell Biol, 1999. **19**(6): p. 4535-45.
209. Nicolet, C.M. and E.A. Craig, *Isolation and characterization of STI1, a stress-inducible gene from Saccharomyces cerevisiae.* Mol Cell Biol, 1989. **9**(9): p. 3638-46.
210. Smith, D.F., et al., *Identification of a 60-kilodalton stress-related protein, p60, which interacts with hsp90 and hsp70.* Mol Cell Biol, 1993. **13**(2): p. 869-76.
211. Chen, S. and D.F. Smith, *Hop as an adaptor in the heat shock protein 70 (Hsp70) and hsp90 chaperone machinery.* J Biol Chem, 1998. **273**(52): p. 35194-200.
212. Morishima, Y., et al., *Stepwise assembly of a glucocorticoid receptor.hsp90 heterocomplex resolves two sequential ATP-dependent events involving first hsp70 and*

then hsp90 in opening of the steroid binding pocket. J Biol Chem, 2000. **275**(24): p. 18054-60.
213. Zhang, M., et al., *Chaperoned ubiquitylation--crystal structures of the CHIP U box E3 ubiquitin ligase and a CHIP-Ubc13-Uev1a complex.* Mol Cell, 2005. **20**(4): p. 525-38.
214. Connell, P., et al., *The co-chaperone CHIP regulates protein triage decisions mediated by heat-shock proteins.* Nat Cell Biol, 2001. **3**(1): p. 93-6.
215. Qian, S.B., et al., *CHIP-mediated stress recovery by sequential ubiquitination of substrates and Hsp70.* Nature, 2006. **440**(7083): p. 551-5.
216. Sahara, N., et al., *In vivo evidence of CHIP up-regulation attenuating tau aggregation.* J Neurochem, 2005. **94**(5): p. 1254-63.
217. Chang, L., et al., *High-throughput screen for small molecules that modulate the ATPase activity of the molecular chaperone DnaK.* Anal Biochem, 2008. **372**(2): p. 167-76.
218. Rousaki, A., et al., *Allosteric drugs: the interaction of antitumor compound MKT-077 with human Hsp70 chaperones.* J Mol Biol, 2011. **411**(3): p. 614-32.
219. Jinwal, U.K., et al., *Chemical manipulation of hsp70 ATPase activity regulates tau stability.* J Neurosci, 2009. **29**(39): p. 12079-88.

Chapter 2

Mutagenesis reveals that ATPase rates are not predictive of the chaperone activities of *Escherichia coli* heat shock protein 70 (Hsp70/DnaK).

2.1 Abstract

As was described in Chapter 1, the 70-kDa heat shock protein, Hsp70, is a molecular chaperone that plays important roles in facilitating protein folding and preventing protein aggregation. The *Escherichia coli* Hsp70, DnaK, is composed of an ATPase domain and a substrate-binding domain that binds to unfolded proteins. Nucleotide turnover in DnaK appears to allosterically control the affinity for substrates. In addition, DnaK interacts with the co-chaperones DnaJ and GrpE, which stimulate ATP hydrolysis and nucleotide exchange, respectively. Because this multi-protein system is highly dynamic, it serves as an ideal model in which to understand protein-protein interactions and allostery, especially in relation to molecular chaperone functions. In this study, mutagenesis throughout the nucleotide-binding domain of DnaK was performed to generate a collection of mutants in which the stimulated ATPase rates varied from 0.7 to 13.6 pmol/ μg/ min^{-1}. Next, the correlation between ATPase rate and the ability of DnaK to refold denatured luciferase *in vitro* was examined. Interestingly, these two activities were poorly correlated, with several mutants retaining normal refolding activity in the absence of significant ATP turnover. Further, the ability of these DnaK mutants to complement growth of Δ*dnaK E. coli* cells under heat shock was probed. It was found that the *in vitro*

molecular chaperone activity of refolding was more predictive of *in vivo* activity than ATPase rate. This study suggests that co-chaperone interactions and other factors are more important than ATP turnover in regulating some molecular chaperone activities of Hsp70.

2.2 Introduction

2.2.1 DnaK structure and function

Escherichia coli DnaK is a member of the highly conserved heat shock protein 70 (Hsp70) family, and it is involved in a variety of cellular pathways, including protein folding, transport, and degradation [1, 2]. As a central player in protein quality control and homeostasis, Hsp70 has also been implicated in the pathogenesis of a variety of diseases [3-5]. These observations have led to an interest in understanding how the various activities of Hsp70 are correlated. One of the main roles of DnaK is to enable the folding of nascent or otherwise unfolded proteins [6]. In this role DnaK is thought to limit aggregation and facilitate folding by binding to the hydrophobic regions exposed in these substrates. Briefly, DnaK, like all the Hsp70 family members, consists of a substrate-binding domain (SBD) and a nucleotide-binding domain (NBD) connected by a hydrophobic linker [7-9]. The NBD of DnaK is further divided into four subdomains as follows: IA/IIA, which forms the base, and IB/IIB which form the upper walls of the nucleotide binding cleft (Figure 2.1a). The binding of ATP to DnaK results in an “open” conformation with low substrate affinity. Upon hydrolysis, the ADP-bound form assumes a “closed” conformation that binds substrate with higher affinity [10-16]. Thus, allosteric

communication between the two domains is thought to link nucleotide turnover to substrate binding and release.

2.2.2 Co-chaperones regulate the ATPase rate and substrate binding of DnaK

DnaK alone has a low intrinsic ATPase rate, which facilitates regulation by the important co-chaperones, DnaJ and GrpE. DnaJ specifically stimulates ATP hydrolysis and thus favors high affinity substrate binding [6, 17]. In addition, DnaJ independently binds to substrates via C-terminal domains and is thought to help these proteins bind to DnaK [18, 19]. GrpE, on the other hand, induces nucleotide exchange and leads to substrate release [20]. These co-chaperone activities appear to be required for the cellular functions of DnaK because deletion of either DnaJ or GrpE causes defects in growth at elevated temperatures, similar to what is seen in Δ*dnaK* strains [4, 21, 22]. Thus, as discussed in Chapter 1, this multi-protein system provides a model in which to understand how protein-protein interactions and allostery are regulated and how proteins within larger complexes work together to make important cellular decisions.

2.2.3 The role of co-chaperones and nucleotide hydrolysis in protein folding

One of the major chaperone functions of the DnaK-DnaJ-GrpE system appears to be the refolding of denatured proteins. Many of the key insights into chaperone function have emerged from *in vitro* studies on the refolding of the model substrate firefly luciferase. For example, it was found that DnaK requires DnaJ and GrpE to refold denatured luciferase [6]. Importantly for the work described in this Chapter, this experimental platform has been used to explore the roles of ATP hydrolysis in controlling substrate

folding. For example, this process was found to require multiple cycles of ATP hydrolysis [6]. Also, ATPγS blocks refolding, further suggesting an important role for nucleotide cycling [23-25]. However, truncated forms of DnaJ, which are able to stimulate ATP hydrolysis normally but cannot interact with substrates, are unable to stimulate luciferase refolding [26]. Together, these results suggest that ATPase activity is necessary but not sufficient to achieve luciferase folding.

2.2.4 Mutations which abolish ATPase activity in DnaK are unable to sustain growth at elevated temperatures

The chaperone function of DnaK can also be assayed *in vivo* by monitoring the ability of DnaK mutants to complement growth of Δ*dnaK E. coli* cells under heat shock (called heat shock rescue) [27]. At elevated temperatures, many proteins in *E. coli* become prone to unfolding and aggregation. One of the roles of DnaK is to bind these substrates, protecting them from aggregation [3, 28, 29]. Following return to normal temperature, DnaK also participates in active refolding [30, 31]. Similar to what was observed in the *in vitro* luciferase refolding experiments, the ATPase activity of DnaK appears to be required during heat shock, because active site mutations that abolish nucleotide turnover are unable to rescue heat shock [23-25].

2.2.5 The link between DnaK ATPase rate and chaperone functions is not clear

Taken together, these data suggest that ATPase rate may be an important modulator of chaperone activities. However, previous studies largely relied on either a single mutation of an essential catalytic residue or the use of nucleotide mimics [23-25]. Thus, it remains

unknown if changes in the rate of ATP hydrolysis lead to predictable changes in chaperone functions, such as luciferase folding and heat shock rescue. This question is particularly important when one considers that DnaK and its co-chaperones are highly allosteric. However, insights into the relationships between ATP turnover and chaperone functions have been complicated by several factors. First, the DnaK chaperone system is impacted by a number of variables. For example, several studies have highlighted substrate binding kinetics, interdomain communication, and the stimulation of the DnaK ATPase rate as important variables for refolding or cellular growth under heat shock [18, 32-39]. Second, the interdependence of these variables presents important challenges. For example, a mutation that disrupts interdomain communication might also interfere with substrate binding and DnaJ-mediated ATPase stimulation [40, 41]. Perhaps individual point mutations in catalytic residues would not be sufficient to deconvolute this complex system. Accordingly, a series of point mutations in the nucleotide-binding domain of DnaK was generated to better probe the relationships between ATP turnover, allostery, and measurable chaperone functions. Using a battery of biochemical and cell-based assays, it was found that ATPase rate does not directly correlate with chaperone functions. Rather, this result suggests that co-chaperone interactions and other factors may more closely regulate DnaK function.

2.3 Results

2.3.1 The design of DnaK mutants with varied ATPase rates

The aim of this study was to assess whether changes in the ATPase rate of DnaK lead to predictable changes in chaperone function. Toward this goal available mutational and

structural data was employed to select ~30 novel or established mutations in the NBD of DnaK [8, 41-44]. Mutating the SBD was avoided to minimize direct disruption of substrate binding. Rather, these mutations were specifically designed to impact ATP turnover by four potential mechanisms (Figure 2.1b). Known DnaK mutations, E171S and T199A, which alter residues in the ATP-binding pocket, made up class I. Class II included L177A and I373A, which were predicted to disrupt DnaJ-mediated ATPase stimulation based on homology to mutations made in other Hsp70 family members [10, 40, 41]. Two mutants, V192A and Y193A, which are located near the proposed DnaJ-binding site, were also included in class II. Class III included K55A and R56A, which are known to disrupt binding to GrpE [8, 45], and 10 additional mutants in the IB and IIB subdomains that were hypothesized to impact nucleotide exchange, based on their proximal location to known nucleotide exchange factor binding sites. Finally, class IV mutations included residues around the proposed hinge region (residue 225-230) at the IIA/IIB subdomain interface. This region is proposed to undergo an ATP-induced structural change [42, 44]. Together, this collection of DnaK mutants was intended to provide an analysis of contributions from multiple allosteric pathways.

To characterize these mutants, whether the mutants could bind to nucleotide was tested by measuring their retention on an ATP affinity column. All the mutants were found to retain ATP binding activity qualitatively similar to that of WT DnaK. Next, whether the mutants exhibited WT-like secondary structure was confirmed, as measured by circular dichroism (Appendix 2.1). Finally, each mutant was verified to bind luciferase using a "holdase" assay. In this assay, the ability of DnaK to protect luciferase from heat denaturation was measured. It was found that all the mutants were able to limit unfolding; demonstrating

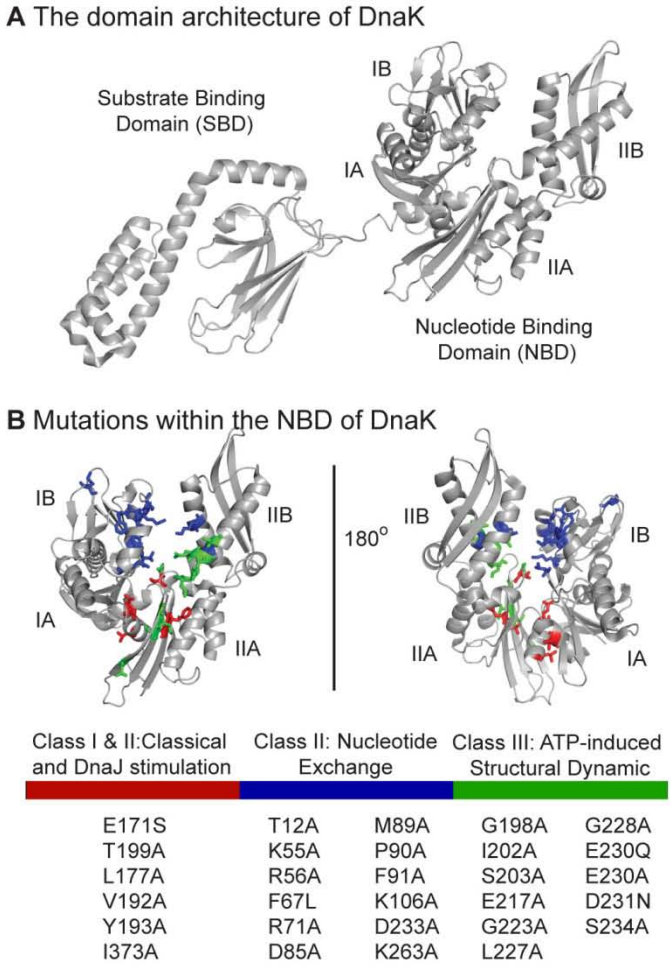

Figure 2.1. The design and location of 29 DnaK mutants. (A) Shown is a cartoon representation of full length DnaK defining domains and subdomains. (B) The location of mutations in the nucleotide binding domain (NBD) of DnaK is shown by stick representations. These mutations, reported above, are both novel and established mutations, designed based on existing structural and mutational studies to alter ATPase rate in a variety of distinct ways (4,36-39). Namely; class I and II mutations (red) were designed to disrupt ATP hydrolysis (E171S, T199A) and DnaJ-mediated stimulation of ATPase rate (L177A, V192A, Y193A, I373A), respectively. Class II mutations (blue) were designed to disrupt GrpE-mediated stimulation of ATPase rate. Finally, Class III mutations (green) were designed to disrupt dynamics within the NBD suggested to be important for nucleotide-dependent conformational changes.

that binding to substrates was intact (Appendix 2.2). During these characterization steps, three mutations were identified that resulted in unstable variants of DnaK (Appendix 2.3). These mutants were removed from further analysis. This design and selection process yielded a collection of 29 DnaK mutants for further investigation (Figure 2.1b).

Table 2.1 The ATPase activity of DnaK mutants

DnaK	Intrinsic ATPase rate	DnaJ Stimulation[b]		GrpE Stimulation[c]		Substrate Stimulation		
	$pmolP_i/\mu g/min$	$Vmax_{,J}$[d] $pmolP_i/\mu g/min$	$Km_{,J}$ μM	$Vmax_{,E}$ $pmolP_i/\mu g/min$	$Km_{,E}$ nM	$Vmax_{,sub}$ $pmolP_i/\mu g/min$	$Km_{,sub}$ μM	
WT	**1.7 ± 0.2**	**10.2 ± 0.5**	**0.58 ± 0.12**	**47.2 ± 4.0**	**108.3 ± 29.0**	**6.0 ± 0.9**	**90 ± 28**	
E171S	1.2 ± 0.1	NF[a]	NF	NF	NF	NF	NF	**Class I**
T199A	0.6 ± 0.2	NF	NF	NF	NF	NF	NF	
L177A	3.1 ± 0.3	8.8 ± 1.1	1.25 ± 0.50	19.5 ± 1.7	47.8 ± 16.2	5.4 ± 0.2	103.1 ± 6.5	
V192A	3.8 ± 1.0	6.7 ± 0.4	0.53 ± 0.13	84.2 ± 5.6	114.3 ± 23.5	5.0 ± 0.1	30.1 ± 1.4	**Class II**
Y193A	5.0 ± 0.3	13.4 ± 0.5	0.81 ± 0.12	57.0 ± 3.2	94.3 ± 17.4	7.0 ± 0.6	73.4 ± 12.2	
I373A	3.7 ± 1.2	NF	NF	26.4 ± 4.7	188.8 ± 82.9	NF	NF	
T12A	2.9 ± 0.4	40.5 ± 2.7	2.57 ± 0.39	11.7 ± 1.9	53.7 ± 34.6	7.1 ± 0.1	65.6 ± 2.8	
K55A	2.5 ± 0.4	30.4 ± 2.5	3.25 ± 0.54	NF	NF	NF	NF	
R56A	3.2 ± 0.3	19.5 ± 1.2	3.53 ± 0.42	64.2 ± 15.5	544.4 ± 210.2	13.3 ± 0.4	47.3 ± 3.9	
F67L	1.4 ± 0.3	NF	NF	NF	NF	NF	NF	
R71A	2.4 ± 0.3	NF	NF	NF	NF	NF	NF	
D85A	3.0 ± 0.3	14.1 ± 1.1	0.82 ± 0.22	17.4 ± 2.6	35.8 ± 21.5	NF	NF	**Class III**
M89A	3.5 ± 0.2	12.7 ± 0.9	0.56 ± 0.14	44.7 ± 17.4	364.6 ± 263.8	8.2 ± 0.2	39.6 ± 2.0	
P90A	1.8 ± 0.4	13.8 ± 4.4	4.3 ± 2.5	15.4 ± 1.9	5.2 ± 2.2	NF	NF	
F91A	1.6 ± 0.4	NF	NF	NF	NF	NF	NF	
K106A	5.0 ± 0.4	14.9 ± 0.6	0.96 ± 0.14	46.4 ± 4.6	64.5 ± 23.6	6.3 ± 0.1	8.4 ± 0.4	
D233A	5.7 ± 0.4	41.6 ± 1.4	1.15 ± 0.13	NF	NF	NF	NF	
K263A	3.4 ± 1.0	NF	NF	NF	NF	NF	NF	
G198A	2.2 ± 0.1	10.4 ± 0.6	0.50 ± 0.11	NF	NF	NF	NF	
I202A	1.5 ± 0.1	13.2 ± 0.8	0.67 ± 0.14	NF	NF	NF	NF	
S203A	3.9 ± 0.1	NF	NF	29.7 ± 0.7	6.9 ± 0.6	2.1 ± 0.2	17.5 ± 5.4	
E217A	1.2 ± 0.1	NF	NF	NF	NF	NF	NF	
G223A	0.5 ± 0.1	NF	NF	NF	NF	NF	NF	**Class IV**
L227A	1.0 ± 0.1	NF	NF	NF	NF	NF	NF	
G228A	2.5 ± 0.1	NF	NF	NF	NF	NF	NF	
E230Q	0.6 ± 0.4	19.1 ± 2.0	3.38 ± 0.70	NF	NF	NF	NF	
E230A	3.2 ± 0.4	14.3 ± 1.8	1.95 ± 0.65	12.5 ± 1.5	37.8 ± 18.3	NF	NF	
D231N	0.6 ± 0.1	NF	NF	NF	NF	NF	NF	
S234A	0.5 ± 0.1	9.9 ± 0.7	0.32 ± 0.09	NF	NF	NF	NF	

[a]The gray boxes (NF) indicate that either ATPase rate was not stimulated, as defined by a mutant in which the SEM of K_m or V_{max} encompassed zero, or when a non-linear fit could not be obtained. [b]DnaJ stimulation was tested in the presence of NR substrate (100 μM). [c]GrpE stimulation was tested in the presence of both DnaJ (1 μM) and NR substrate (100 μM). [d]The V_{max} value (calculated by the equation in the Materials and Methods) represents the increase in ATPase rate compared to solvent control. Raw data can be found in Supplemental Figure 2. Error is standard error of the mean.

As mentioned above, the ATPase rate of DnaK is stimulated by three main factors as follows: DnaJ, GrpE, and substrate. Thus, it was important to measure the ability of these factors to stimulate each of the DnaK mutants. Toward this goal, the K_m and V_{max} values

for DnaJ, GrpE, and a model DnaK substrate NRLLLTG was calculated (Table 1 and Appendix 2.4). From these experiments, it was found that the mutants varied in their responses to these stimuli. Using K_m to estimate binding to DnaK, it was found that most mutants varied in their affinity for DnaJ by ~10-fold (0.32 to 4 μM). In addition a few mutants, such as E217A and L227A, had very weak stimulation, which precluded fitting of the curves (Table 2.1 and Appendix 2.4). Similarly, the K_m value of GrpE stimulation varied over a range of almost 100-fold, with multiple mutants unable to be stimulated. Further, maximum stimulation (V_{max}) varied by ~ 6-fold for DnaJ, 7-fold for GrpE, and 6-fold for substrate. Finally, known mutations exhibited the expected activity, confirming the results reported previously in the literature [8, 10, 40, 41, 45]. Thus, this collection had the desired wide range of K_m and V_{max} values for co-chaperone and substrate-mediated ATPase stimulation. Based on these findings, perhaps these mutants could be used to probe the correlation between ATPase rate and luciferase folding.

2.3.2 ATPase rate and refolding activity of DnaK mutants are weakly correlated

One of the functions of DnaK is to refold damaged proteins, and this activity can be measured *in vitro* by luciferase refolding assays. In this experiment, chemically denatured firefly luciferase is diluted in the presence of DnaK, ATP, DnaJ, and GrpE. This chaperone system gradually restores the misfolded luciferase, and the refolding process can be monitored by an increase in luminescence. To directly explore the correlation between stimulated ATPase activity and chaperone-mediated refolding, both activities for each DnaK mutant at the same concentrations of DnaK, DnaJ, GrpE, luciferase, and ATP were recorded (Appendix 2.5). To explore potential correlations in these two activities of

DnaK, refolding activity was plotted against ATPase rate for each mutant (Figure 2.2A). This analysis revealed poor correlation (R^2 = 0.22), between the activities. A closer inspection of these results revealed some additional trends. For example, many mutants such as T12A, had a higher ATPase rate than WT, but this enhanced turnover did not lead to correspondingly higher refolding activity. Furthermore, some mutants, such as R56A, had the same ATPase rate as WT but decreased refolding activity. Curiously, there were also mutants such as F67L, P90A, F91A, E230Q, D231N, and K263A, which had significantly lower ATP hydrolysis rates than WT DnaK, but they retained normal luciferase refolding activity. These DnaK mutants were named "decoupling mutants."

To explore the observation that many of the DnaK mutants had altered rates of intrinsic ATPase activity further, the correlations between these values and luciferase refolding was also analyzed. Consistent with the previous findings, the intrinsic ATPase rates had almost no correlation with luciferase refolding activities (R^2 = 0.007; Appendix 2.6). Similarly, the ATPase rates of the mutants stimulated by DnaJ alone (i.e. no GrpE or substrate) also failed to correlate (R^2 = 0.071; Appendix 2.7). Interestingly, when the mutants were classified based on their locations, the decoupling mutants clustered on the IB and IIB subdomains. Most mutations in the IB and IIB subdomains had normal refolding activity regardless of ATPase rate (R^2 = 0.04; Figure 2.2C). Correspondingly, when only the IA/IIA subdomain mutants were examined, the overall ATPase rates became more positively associated with refolding activities (R^2 = 0.55; Figure 2.2B).

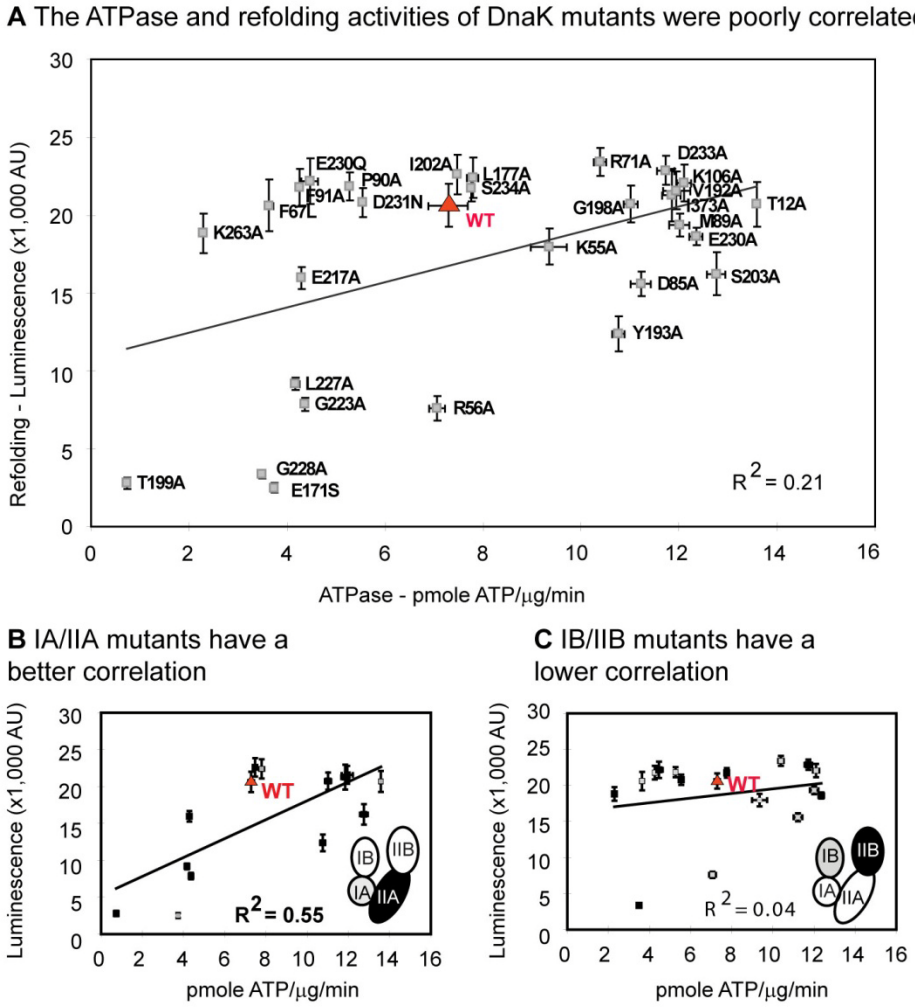

Figure 2.2. The ATPase and luciferase refolding activities of DnaK mutants were poorly correlated. (A) For wild-type (WT) DnaK and each mutant, the luciferase refolding activity and ATPase rate are shown. Each reaction used a final concentration of DnaK (1 μM), DnaJ (0.25 μM), GrpE (0.125 μM), denatured luciferase (8 nM), and ATP (1 mM). (B) & (C) Analysis was also perfrmed on subsets of mutations based on their locations. Mutations in the IA/IIA subdomains (B) have a higher correlation (R^2 = 0.55) than those in the IB/IIB subdomains (C, R^2 = 0.04). In (B) and (C), IA/IB-subdomain mutants are shown as gray squares, IIA/IIB-subdomain mutants as black squares and WT as red triangles. Although WT activity is shown in B and C, it was not included for the calculation of R^2 value. Each data point is the average of triplicates and the error bars represent the standard error of the mean (SEM).

2.3.3 Decoupling mutants of the IB subdomain make DnaK more flexible

Further analysis revealed that the decoupling mutants in the IB subdomains, F67L, P90A, and F91A, were co-localized in a hydrophobic patch adjacent to an adjacent helix and loop (residues: 74-96) (Figure 2.3A). Residues$_{74-96}$ have been shown to be crucial for cooperation with DnaJ and GrpE during both refolding and heat shock rescue [43]. Consistent with this important role, residues$_{74-96}$ are connected to a small helix containing K70, a residue that is essential for ATP hydrolysis [46]. Based on this analysis, it was hypothesized that mutations to the hydrophobic triad of F67, P90, F91 might destabilize residues$_{74-96}$. In turn, this increased flexibility might disrupt positioning of K70, which would explain the low ATPase rates. In support of this hypothesis, it was found that the three decoupling mutants were more sensitive to trypsin digestion and, furthermore, that they exhibited a different digestion pattern than WT or other IB subdomain mutations (Figure 2.3B and Appendix 2.7). This result suggests that, through increased flexibility, the IB subdomain decoupling mutants may allow for productive interactions with misfolded luciferase without relying on the structural transitions normally linked to ATP hydrolysis.

Because residues$_{74-96}$ were reported to be involved in interactions with DnaJ [43], the ability of the decoupling mutants to be stimulated by this co-chaperone was tested, in the presence of denatured luciferase. In ATPase assays, the concentration of DnaJ was varied and it was found that F67L, P90A, and F91A had increased K_m values (2.4, 0.8, and 1.7 μM respectively) compared to WT (0.3 μM) (Figure 2.3C). Despite these higher K_m values, the refolding activity of the three mutants in response to DnaJ remained similar to

WT (Figure 2.3D). Thus, ATPase rate and refolding activity responded differently to DnaJ-mediated stimulation in these mutants, suggesting that these processes are separable.

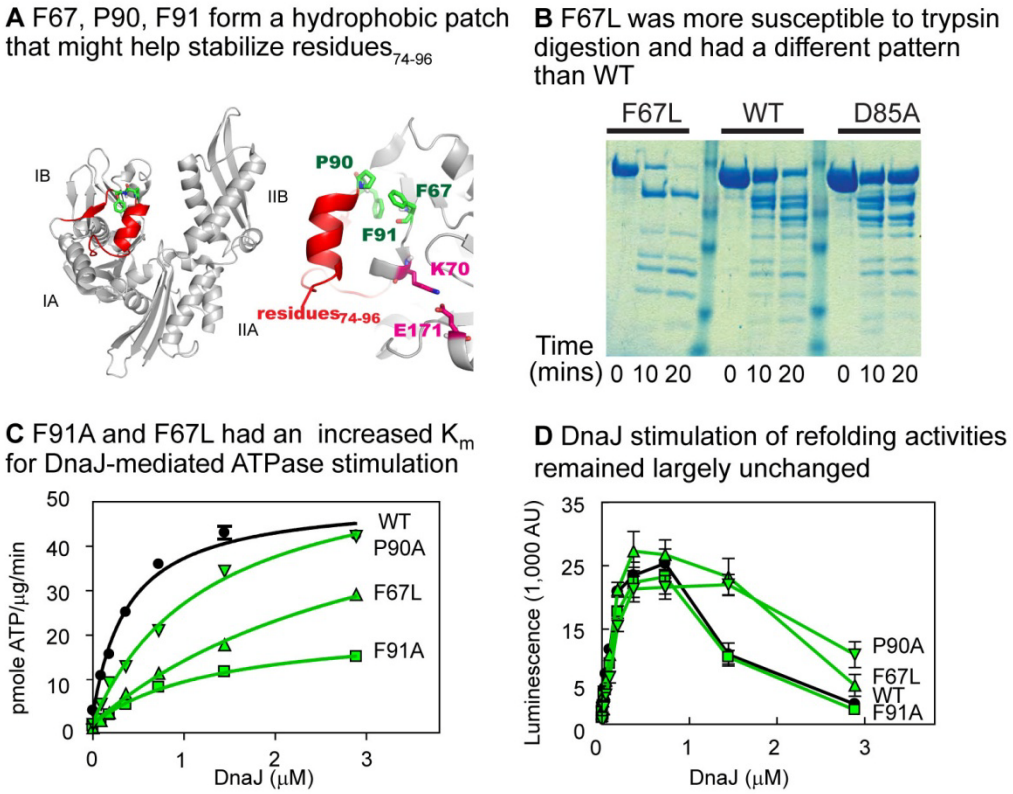

Figure 2.3. IB decoupling mutations increased DnaK flexibility and decreased DnaJ-mediated ATPase stimulation without impacting luciferase refolding activity. (A) The NBD of DnaK is shown with a close-up on the region around residue P90, F91 and F67 (green). These three residues appear to stabilize the helix and loop formed by 74-96 (red), which is connected to the critical catalytic residue, K70 (magenta). (B) Mutant F67L was more susceptible to trypsin digestion and demonstrated a different digestion pattern than WT-DnaK or a representative IB mutant, D85A. (C) For decoupling mutants F91A and F67L, the Km for DnaJ-mediated ATPase stimulation was significantly increased. (D) However, the decoupling mutants did not impact DnaJ-stimulated luciferase refolding.The final concentrations were: DnaK (1 μM), GrpE (0.125 μM), denatured luciferase (8 nM), and ATP (1 mM) in both (C) and (D). Each data point is the average of triplicates and the error bars represent the standard error of the mean (SEM).

2.3.4 IIB subdomain decoupling mutants are located near a hinge region

Another class of decoupling mutations was interesting because the residues, E230 and D231 were located adjacent to each other in the IIB subdomain (Figure 4A). This region is at the interface of the IIB and IIA subdomains, where a hinge region (residue 225 to 230 in DnaK) is thought to rotate the IIB subdomain away from the IB subdomain upon ATP hydrolysis (47). This conformational change has been observed in GrpE-bound DnaK, and it was previously proposed to be important for nucleotide release [8]. To explore the basis for the observed decoupling by mutations E230Q and D231N, the stimulation of these mutants by DnaJ and GrpE was measured. In ATPase assays, the decoupling mutants E230Q and D231N were tested for their ability to be stimulated by DnaJ and GrpE. It was found that the decoupling mutants E230Q and D231N had normal responses to DnaJ (Figure 2.4B). However, unlike WT DnaK, the ATPase activities of these mutants were not stimulated by GrpE and rather, were significantly inhibited by a low concentration of this co-chaperone (~0.1 μM) (Figure 2.4C).

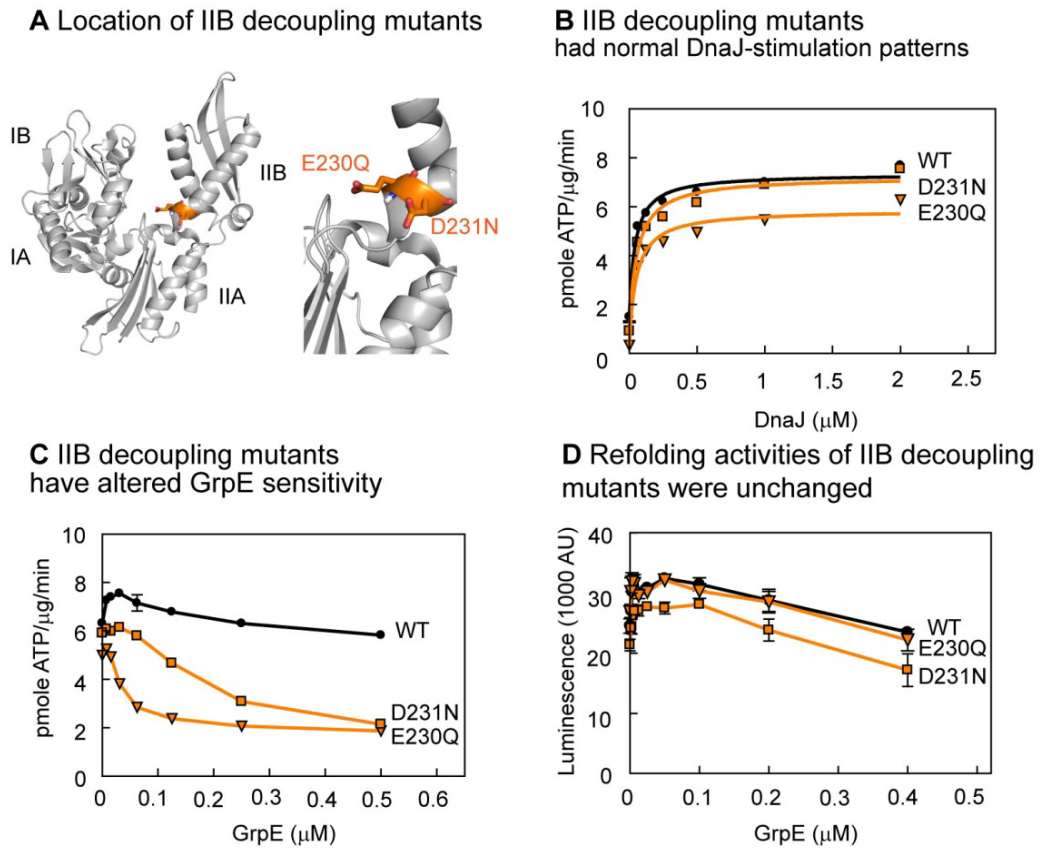

Figure 2.4. The ATPase activities of IIB decoupling mutants were inhibited by a low concentration of GrpE while retaining normal refolding activity.
(A) The NBD of DnaK is shown with the inset focused on the location of the IIB decoupling mutants, E230Q and D231N (orange sticks). (B) Mutants E230Q and D231Q had WT-like, DnaJ-mediated ATPase stimulation in the presence of 8 nM of denatured luciferase. (C) IIB decoupling mutants, E230Q and D231Q, interacted with GrpE, but unlike WT (black circle), their ATPase rate was inhibited by a low concentration of GrpE. Notably, GrpE inhibited the ATPase activities of these mutants around the concentration used in the experiments shown in Figure 2.2 (0.1 μM). (D) The refolding activities of E230Q and D231N responded to GrpE in a manner similar to WT DnaK. For both C and D, the final concentrations were; DnaK (1 μM), DnaJ (0.25 μM), denatured luciferase (8 nM), and ATP (1 mM). Each data point is the average of triplicates and the error bars represent the standard error of the mean (SEM).

2.3.5 Refolding activity of DnaK mutants is more predictive of *in vivo* function

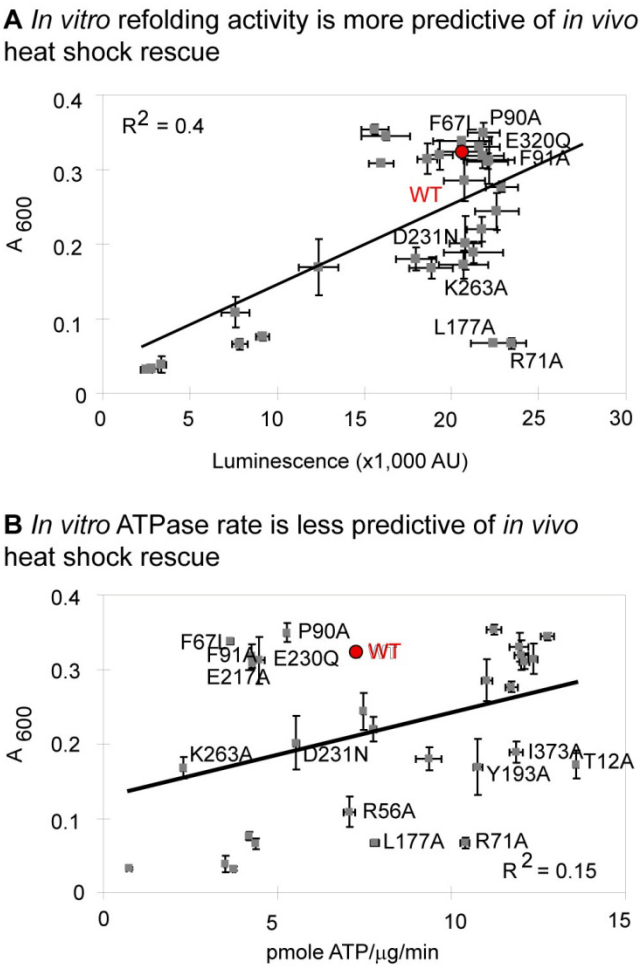

Figure 2.5. *In vitro* refolding activities of DnaK mutants were more predictive of their *in vivo* functions. (A) The luciferase refolding activities (R^2 = 0.4) of DnaK mutants were more predictive than (B) ATPase rate (R^2 = 0.15) for their abilities to complement the growth of ΔdnaK (DE3) *E. coli* cells under heat shock. The growth of ΔdnaK (DE3) *E. coli* cells, transformed with each dnaK mutant, was measured using A_{600} after a 6-hour incubation at 43 °C. WT is highlighted (red circle). Each data point was measured in triplicate, and error bars represent the standard error of the mean (SEM).

Because this collection of DnaK mutants had revealed that ATPase rate and luciferase refolding activity were only weakly correlated, the next aim of this study was to explore which activity, if any, would be most predictive of a cellular function of DnaK. Toward this goal, the ability of the DnaK mutants to protect against heat shock in Δ*dnaK* (DE3) cells was explored. *E. coli* strains lacking dnaK (Δ*dnaK*) are temperature-sensitive and unable to grow after exposure to elevated temperature. As expected, WT DnaK, expressed from an inducible plasmid, could complement growth of Δ*dnaK E. coli* at 43 °C (Figure 2.5, Appendix 2.8A). Using the same procedure, each of the DnaK mutants were subsequently tested. First, plasmids for each mutant were transformed into Δ*dnaK*

(DE3) *E. coli* cells, and protein expression was confirmed (Appendix 2.8B). Following heat shock at 43°C, the absorbance at 600 nm (A_{600}) was measured, and these results were plotted against the ATPase or refolding activity of each mutant (Figure 2.5, *A* and *B*). From this analysis, a strikingly poor correlation between ATPase rate and heat shock rescue (R^2 = 0.15) was found. However, refolding activity was relatively better correlated (R^2=0.40). Interestingly, the decoupling mutants of the IB and IIB subdomains, F67L, P90A, F91A, E230Q, and D231N, were able to complement growth at 43°C. This result demonstrated for the first time that mutants with a severe deficiency in their ATPase activity could rescue heat shock *in vivo*. Still, it is important to note that luciferase refolding was not fully predictive of heat shock rescue. Several mutants, such as L177A and R71A, were potent in the refolding assay yet failed to mediate heat shock rescue. These results suggest that these relationships are complex, and other factors are likely important for heat shock rescue.

2.4 Discussion

2.4.1 Relationship between ATPase and refolding activity of DnaK

As an isolated domain, the SBD of DnaK binds to substrate with the same affinity as ADP-bound DnaK and can slowly refold luciferase [47]. Thus, one major role of the NBD seems to be to power the transition of the SBD between open and closed states, which accelerates binding-and-release of substrates and increases refolding activity [10, 40, 48, 49]. Based on these findings, refolding and ATP turnover are thought to be closely linked functions of DnaK. Consistent with this idea, the co-chaperones DnaJ and GrpE stimulate both the ATPase rate and refolding activity of DnaK [45, 50, 51].

Previous data have suggested that ATP hydrolysis is necessary but not sufficient for luciferase refolding [14, 21, 22, 25]. To explore this finding more deeply, whether the ATPase rate of DnaK could predict its luciferase refolding activity was evaluated using a series of mutants. In the 29 DnaK mutants tested, it was found that the two activities were poorly correlated. This result suggests that additional factors might contribute to refolding.

To explore what some of these contributing factors might be, how the mutants were stimulated by co-chaperones and substrate was specifically investigated (see Table 2.1 and Figure 2.2). This analysis showed that mutants unable to refold luciferase, such as E171S, T199A, and G228A, were also defective in their ability to be stimulated by DnaJ, GrpE, and substrate in the ATPase assay. However, the converse was not necessarily true. For example, there were several mutants whose ATPase rate could not be stimulated, yet they still had the same refolding activity as WT DnaK. These results demonstrated that the relationship between ATPase and luciferase refolding activity is complex. More specifically, these results suggested that the ability of DnaK to be stimulated by DnaJ, GrpE, or peptide substrate is not necessarily predictive of its activity in the refolding assay. This conclusion is illustrated by several mutants in which drastic changes in both the V_{max} and K_m values of DnaJ-mediated ATPase stimulation were observed without a significant impact on refolding activity (see Table 2.1 and Figure 2.3). Most notably, the IB subdomain decoupling mutants, F67L, P90A, and F91A, exhibited WT-like dependence on DnaJ for refolding, but had increased K_m values for DnaJ-mediated stimulation of ATP hydrolysis. This observation suggests that DnaJ might

promote ATPase and refolding activities by different mechanisms. In support of this model, DnaJ mutants that stimulate the ATPase rate of DnaK, but not its refolding activity, have been reported [17, 26, 52-54].

The structure of DnaJ might provide a clue into how these two activities can be separated. Residues 1–104 of DnaJ are essential for interactions with the NBD of DnaK. This region is composed of the J-domain and a glycine- and phenylalanine- rich region. The C-terminal half of DnaJ contains two zinc-binding sites and a domain important for binding to substrate [18, 19, 26]. Although the 1–104-residue fragment of DnaJ can fully stimulate ATP hydrolysis, it cannot stimulate the refolding activity of DnaK [18]. More strikingly, Karzai and McMacken [17] found that DnaJ lacking its second zinc-binding site had normal affinity for denatured luciferase and actively stimulated ATP hydrolysis by DnaK, but this mutant was unable to transfer substrate to DnaK or support luciferase refolding. Those previous reports and our studies suggest that a secondary event, perhaps substrate presentation, may be important for refolding in the DnaK-DnaJ pair. Perhaps the decoupling mutations might interrupt ATPase activity without affecting DnaJ-mediated substrate presentation. However, this model lacks structural support, and the detailed mechanisms await further analysis. It is important to note that other factors may also help to account for the lack of correlation between ATPase rate and refolding activity. These factors might include substrate-binding kinetics, nucleotide-dependent conformational changes, and co-chaperone complex formation [55-58].

2.4.2 Mechanisms of the IB and IIB decoupling mutants

This study was particularly interested in understanding the mechanisms of the "decoupling" mutants, because this is, to our knowledge, the first report of DnaK mutants that have greatly decreased ATPase rates but normal refolding activities. Three of the decoupling mutants were mapped to a hydrophobic patch on the IB subdomain that appears to stabilize residues$_{74–96}$ and therefore regulate the position of K70, a key residue for ATP hydrolysis. These decoupling mutants had low ATPase rates, yet they retained both normal refolding activities and the ability to restore growth under heat shock in *E. coli*. We hypothesize that the unusual properties of these mutants might arise from their increased flexibility, as measured by trypsin susceptibility. Specifically, this flexibility might allow the mutants to sample the open and closed conformational states that facilitate refolding. To date, there is no structure of open ATP-bound full-length Hsp70, but based on the structure of Hsp110, a member of the Hsp70 superfamily, the α-helical lid of the SBD interacts with IA and IB subdomains [59, 60]. Therefore, it is tempting to speculate that the same interactions stabilize the open structure in DnaK. Moreover, this interaction of the SBD with subdomains IA and IB might create a barrier for switching between open and closed conformations. In this model, F67L, P90A, and F91A mutants, by destabilizing or otherwise repositioning residues$_{74–96}$, might reduce the barrier to conformational flexibility in the SBD, essentially mimicking the activity normally reserved for nucleotide hydrolysis. The net effect of this change might be to partially decouple ATP turnover from refolding activities. Further structural investigations of WT DnaK and these mutants may provide additional insight. Interestingly, residues$_{74–96}$ is not

present in Gram-positive bacteria. Moreover, the DnaK from *Tetragenococcus halophilus*, a Gram-positive bacterium, has excellent holdase activity, but its refolding and ATPase activities are not stimulated by *T. halophilus* DnaJ or GrpE [61]. Furthermore, deletion of these residues from *E. coli* DnaK renders it unable to cooperate with cochaperones in both ATP hydrolysis and luciferase refolding [43]. These results further suggest that residues$_{74–96}$ may play a role in the allosteric regulation of DnaK.

The mutations in the IIB subdomain, E230Q and D231N, also appear to decouple ATPase and refolding activities but by a mechanism that is distinct from that used by the IB subdomain decoupling mutations. The IIB residues are co-localized at the interface between the IIA and IIB subdomains. This interface is proposed to contain a hinge region that controls the rotation of the IIB subdomain away from the IB subdomain upon ATP hydrolysis [42, 44]. Decoupling mutations, E230Q and D231N, which are located on an α-helix adjacent to this flexible hinge, exhibited normal refolding and DnaJ-stimulated ATPase activities. However, these mutants had an altered response to GrpE. Specifically, GrpE failed to stimulate the ATPase activity of these mutants; moreover, it inhibited turnover at concentrations greater than ~0.1 μM. Because GrpE binding also induces rotation of the IIB subdomain away from the IB (8), it is possible that E230Q and D231N interfere with the proper movement or positioning of the α-helix in response to interaction with GrpE. However, this change does not appear to prevent the conformational changes required for refolding, because the GrpE-stimulated folding activity was unchanged. Together, our findings with both the IB and IIB decoupling mutants suggest that alterations in co-chaperone-mediated stimulation of ATP turnover

do not uniformly lead to changes in luciferase refolding. Based on published reports, it appears that ATP hydrolysis normally regulates structural transitions in DnaK that allow sampling of the open and closed conformers [62]. Thus, in some of the decoupling mutants, these conformers are likely sampled independent of nucleotide transitions. Although ATP hydrolysis is clearly required for WT DnaK to fold luciferase, as shown in previous studies with non-hydrolysable nucleotide analogs [6], this enzymatic activity is not intrinsically or directly linked to substrate folding. Rather, the relationship between these activities may be driven by structural transitions in the two-domain chaperone and interactions with the co chaperones DnaJ and GrpE.

2.4.3 Luciferase refolding is more predictive of cellular heat shock rescue than ATPase rate

Using this series of DnaK mutants, it was found that luciferase refolding activity was more predictive ($R^2 = 0.40$) than ATPase rate ($R^2 = 0.15$) of heat shock rescue. Although ATPase rate clearly did not predict heat shock rescue in this system, it might be more predictive of other cellular functions of DnaK, such as lambda phage replication. On the other hand, a mild correlation between luciferase folding activity and heat shock rescue was observed. However, it is important to note that this correlation is not sufficient to describe the factors that control the roles of DnaK during heat shock. This model is exemplified by the existence of outliers that were fully active in the luciferase-refolding assay but showed a decreased ability to rescue growth at 43 °C, such as R71A and L177A. Thus, there are likely additional factors that are important for heat shock rescue.

For example, some of the outliers may be caused by the ability of DnaK mutants to work in cooperation with other protein quality control systems involved in heat shock rescue.

Together, these results highlight fundamental aspects of the Hsp70 chaperone system. Members of the Hsp70 family, including DnaK, have many measurable *in vitro* activities (*e.g.* ATP turnover, substrate binding, and folding) that could potentially be used to understand *in vivo* functions (*e.g.* heat shock rescue, anti-apoptotic activity in cancer cells, and modulation of protein aggregation) [5, 63]. Yet, it is not readily obvious which *in vitro* activity of Hsp70 is most predictive of a given *in vivo* function or whether all *in vivo* functions are equally dependent on a given measurable activity. Future work in this area may improve our ability to understand the connection between *in vitro* and *in vivo* functions of Hsp70 and thereby lead to a deeper mechanistic understanding of the Hsp70 chaperone system.

As will be described in Chapter 4, one *in vivo* function I was are particularly interested in exploring is the ability of the Hsp70 chaperone system to promote the clearance of the microtubule associate protein tau (MAPT/tau). It has been shown that clearance of tau in a class of neurodegenerative diseases, termed tauopathies, alleviates some of the functional deficits associated with disease [64-66]. It has already observed that several inhibitors of the ATPase rate of Hsp70 promote the degradation of tau while stimulators promote its stabilization [67]. These results suggest that targeting tau for degradation may be an *in vivo* activity of Hsp70 that is regulated by ATPase rate. To further evaluate this hypothesis, other members of Gestwicki group, in collaboration with Chad Dickey's

laboratory, are using the results presented in this Chapter to generate corresponding mutations in human Hsp70s, tune its ATPase activity and test the effects of these mutants on the stability of tau. One goal of these efforts is to guide our chemical screening strategies to identify novel Hsp70 modulators.

2.5 Experimental procedures

2.5.1 Materials

Reagents were obtained from the following sources: Platinum *Pfx* DNA polymerase (Invitrogen); pMCSG7 plasmid (Midwest Center for Structural Genomics, Bethesda); ATP-agarose column (Sigma); NRLLLTG peptide (University of Michigan Peptide Core) [11]; luciferase and SteadyGlo Reagent (Promega, Madison, WI); and Δ*dnaK E. coli* cells (a generous gift from Dr. Ursula Jacob). Furthermore, all absorbance (A) and luminescence measurements were performed using a SpectraMax M5 (Molecular Devices, Sunnyvale, CA).

2.5.2 Plasmids and protein purification

The *E. coli dnaK* and *grpE* genes were amplified by PCR using Platinum *Pfx* DNA polymerase and inserted into the pMCSG7 plasmid through ligation-independent cloning, as described previously [68]. The partial overlapping site-directed mutagenesis primers for *dnaK* were designed based on the report of Zheng *et al.[69]*, and mutagenesis of the *dnak* gene was carried out following the user manual for the QuikChange site-directed mutagenesis kit (Stratagene, La Jolla, CA). Twenty nine *dnaK* mutants were made as follows: T12A, K55A, R56A, F67L, R71A, D85A, M89A, P90A, F91A, K106A, E171S,

L177A, V192A, Y193A, G198A, T199A, I202A, S203A, E217A, G223A, L227A, G228A, E230A, E230Q, D231N, D233A, S234A, K263A, and I373A. The wild type (WT) His-tagged DnaK and its mutants were expressed in BL21(DE3) cells and first purified by batch purification with nickel-nitrilotriacetic acid His-Bind resin (Novagen, Darmstadt, Germany) following the user manual. The His tag of eluted DnaK was then removed by His-tagged tobacco etch virus protease (1 mM DTT, 4 °C, overnight incubation). After adjusting the $MgCl_2$ and KCl concentration to 10mM, the sample was further purified by ATP-agarose column using previously established protocols [70]. Finally, the remaining cleaved His tag was removed by nickel-nitrilotriacetic acid column. The purification of GrpE followed the same strategy except that the ATP-agarose column was excluded. DnaJ was purified as described previously [70] with the exclusion of hydroxyapatite and Q-Sepharose fast-flow column purification steps and the addition of a Superdex 200 gel filtration column (GE Healthcare) to remove contaminating ATPase activity. Finally, N-terminal His-tagged J-domain 2–108 was purified by nickel-nitrilotriacetic acid column as described above without cleaving the His tag. All proteins were concentrated and exchanged into 25mM Tris buffer (10mM KCl (150mM KCl for DnaJ), 5 mM $MgCl_2$, pH 7.5) and stored at -80 °C until use.

2.5.3 Circular Dichroism

WT DnaK and mutants were prepared in 10 mM sodium phosphate buffer (100 mM sodium fluoride, pH7.4) and spectra collected at 0.1 mg/ml in a 0.1-cm cuvette at room temperature. CD spectra were recorded on a Jasco J-715 spectropolarimeter (Jasco, Easton, MD) at 1-nm intervals from 190 to 260 nm at a scanning speed of 50 nm/min and

a 5.0 nm bandwidth. Each spectrum reported is the average of 15 scans after the subtraction of the base-line spectrum (buffer without the addition of DnaK) and normalization (millidegree cm^2 $dmol^{-1}$).

2.5.4 ATPase activity

This procedure was adapted from a previously described protocol [70]. Briefly, samples were prepared with the addition of DnaK, DnaJ, GrpE, NR substrate (NRLLLTG), and/or denatured luciferase to a total volume of 15 μl in each well. Next, 10 μl of 2.5mM ATP was added to start the reaction. The final concentrations were as follows: ATP (1 mM), DnaK (0.5 μM), and NR substrate (100 μM), unless otherwise noted. Intrinsic ATPase rate was measured with DnaK (0.6 μM) in the absence of co-chaperones or substrate. When ATPase rate was tested as a comparison to refolding activity (see Figures 2.2–2.4), guanidine hydrochloride-denatured luciferaseat 8 nM and DnaK at 1 μM were used to match the conditions described in the luciferase refolding assay (see below). The final concentrations of DnaJ, GrpE, are reported for each experiment under "Results." For steady state conditions, samples were incubated at 37 °C for 1–3 h, and then 80 μl of malachite green reagent was added to each well, immediately followed by 10 μl of 32% (w/v) sodium citrate. Samples were mixed thoroughly and incubated at 37 °C for 15 min. Finally, A_{620} was measured. All experiments were performed in triplicate, and the signal from nonspecific ATP hydrolysis in controls lacking DnaK was subtracted. A phosphate standard curve (using potassium dibasic phosphate) was generated each day and used to

convert the units to pmol of Pi/μg of DnaK/min. Stimulation curves were evaluated by fitting the data using a hyperbolic fit with a non-zero intercept;

$$y = V_{max}*x / (K_m + x) + b$$

The nonlinear fit was performed using GraphPad Prism version 4.0 for Windows (GraphPad Software, San Diego).

2.4.5 Luciferase refolding

The luciferase refolding activity of DnaK WT and mutants was evaluated as described with minor changes [25]. Briefly, denatured firefly luciferase was prepared by beginning with a concentrated stock (8.2 μM) of luciferase with 6 M guanidine hydrochloride in 25 mM HEPES buffer (50 mM potassium acetate, 5 mM DTT, pH 7.2). This stock was incubated at room temperature for 1 h and then diluted to 0.2 μM with the same HEPES buffer without guanidine hydrochloride. This preparation was used as the stock solution for final sample preparation. Enzyme mix (10 μl) containing DnaK, DnaJ, GrpE, and denatured firefly luciferase in 39 mM HEPES (170 mM potassium acetate, 1.7 mM magnesium acetate, 3 mM DTT, 12 mM creatine phosphate, 50 units/ml creatine kinase, pH 7.6) was first added into each well, and then 4 μl of 3.5 mM ATP, dissolved in water, was added to start the reaction. The final concentration of DnaK was 1 μM; denatured luciferase was 8 nM, and ATP was 1 mM unless otherwise noted. The concentration of DnaJ and GrpE is reported for each experiment under "Results." After 1 h of incubation at 37 °C, equilibrium was reached, and 14 μl of 0.5 or 2% (v/v) SteadyGlo reagent in 50 mM glycine buffer (30mM $MgSO_4$, 10mM ATP, and 4mM DTT, pH 7.8) was added into

each well, and the luminescence was measured. For each experiment, the signal from a negative control containing everything but DnaK was subtracted.

2.5.6 Holdase activity

Native luciferase was diluted to 0.032 μM in 50mM HEPES (10mM $MgSO_4$, 300mM KCl, 20mM DTT, pH 7.5) and loaded into a 96-well PCR plate (ThermoFisher) (5 μl/well). Next, 5 μl of 2 μM DnaK was added in triplicate into the wells containing luciferase. The reaction mixtures were heated to 39.5 °C for 8 min, and the samples were transferred into a 96-well, opaque, white microtiter plate (ThermoFisher). Next, 10 μl of 0.5% v/v SteadyGlo reagent, as described above, was added to each well, and the luminescence was measured.

2.5.7 Partial proteolysis

The partial proteolysis protocol was adapted from a previously described method [10]. Briefly, samples were prepared with 6 μM DnaK in 40mM HEPES buffer (20mM NaCl, 8 mM $MgCl_2$, 20 mM KCl, 0.3 mM EDTA, pH 8.0) with 1 mM nucleotide (ADP or ATP). Additives such as J-domain (residues 2–108, 4-fold molar equivalents) were noted when included. Samples were incubated at room temperature for 30 min. Trypsin (Sigma, EC 3.4.2.1.4) was added at a 1:4 (trypsin: DnaK) molar ratio to bring the final volume to 50 μl. Proteolysis was carried out at room temperature for 20 min, unless otherwise noted. The reaction was quenched with the addition of 25 μl of SDS loading buffer (240mM Tris, 6% (w/v) SDS, 30% (v/v) glycerol, and 16% (v/v) β-mercaptoethanol, 0.6

mg/ml bromphenol blue, pH 6.8) and heated to 95 °C for 3 min. Samples were analyzed using a 12% SDS-polyacrylamide electrophoresis gel and stained with Coomassie Blue.

2.5.8 Complementation of the heat shock phenotype in a Δ*dnaK* strain

Thermosensitive *E. coli* Δ*dnaK* (DE3) cells that expressed target genes under the T7 promoter were generated using λDE3 lysogenization kit (Novagen) based on the reported method of Sugimoto *et al*. [61]. pMCSG7 plasmids containing *dnaK* WT and mutant genes were transformed into Δ*dnaK* (DE3) *E. coli* cells, and transformation with an empty pMCSG7 vector served as a negative control. For the complementation assay, a single colony of each *dnaK* mutant was inoculated into 5 ml of LB with 50 μg/ml ampicillin and grown with shaking overnight at 30 °C. The next day, all the overnight cultures were diluted to A_{600} = 0.055 by LB containing 50 μg/ml ampicillin and 4 μM isopropyl 1-thio-β-D-galactopyranoside. From the diluted culture, a 100-μl aliquot was loaded onto a transparent 96-well flat bottom plate (Corning Glass) in triplicate. These samples were incubated at 43 °C with shaking for 6 h, and the *A*600 value for each well was measured. The expression of DnaK protein in each clone was verified by adding 4 μM isopropyl 1-thio-β-D-galactopyranoside to the undiluted overnight culture, incubating at 37 °C for 5 h, lysing the cultures, normalizing the protein content, and then separating proteins by SDS-PAGE.

Notes

This work was published as “Mutagenesis Reveals the Complex Relationships between ATPase Rate and the Chaperone Activities of *Escherichia coli* Heat Shock Protein 70 (Hsp70/DnaK)” **2010** Journal of Biological Chemistry. *285*; 21282-21291. Andrea Thompson, Lyra Chang, and Jason Gestwicki designed the experiments. Andrea Thompson and Lyra Chang conducted the experiments. Peter Ung helped design and purify ten DnaK mutants. The pMCSG7 vector was a generous gift from Clay Brown in the Center for Structural Biology (University of Michigan). We also thank Dr. Erik R. P. Zuiderweg for the original vectors containing J-domain, DnaJ, DnaK, and GrpE and Dr. Ursula Jakob for the orginal Δ*dnak* strain. Finally, we thank Drs. Ari Gafni and Zhaohui Xu for the use of the circular dichroism spectrophotometer and Superdex 200 gel filtration column, respectively.

2.6 Appendix

2.6.1 Circular dichroism (CD) spectra of WT DnaK and mutants.

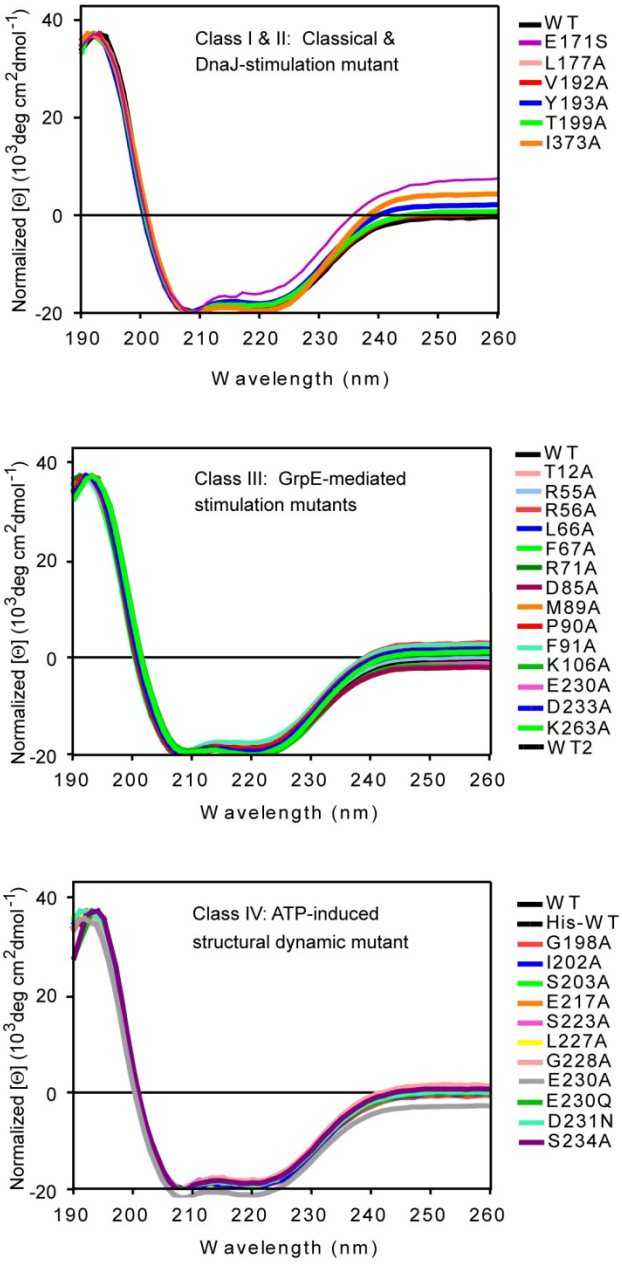

Appendix 2.1. Circular Dichroism (CD) spectra of DnaK WT and mutants. CD spectra (wavelengths 190- 260) are shown for WT DnaK and DnaK mutants. Spectra are normalized (deg $cm^2 dmol^{-1}$) for comparison. The mutant proteins show a spectra similar to the spectra observed for WT DnaK, indicating similar secondary structures within the folded proteins.

2.6.2 Holdase activity

	Holdase activity lum. $x10^3$	error stdev
no DnaK	**2.8**	**0.8**
WT	12.9	0.1
E171S	11.3	1.0
V192A	15.0	0.4
Y193A	13.3	0.8
T199A	14.8	0.7
L177A	21.4	0.8
I373A	17.5	0.8
T12A	29.3	0.7
K55A	21.0	1.1
R56A	25.1	1.3
F67L	22.1	1.4
R71A	20.4	2.2
D85A	17.5	1.4
M89A	25.4	0.7
P90A	20.6	1.6
F91A	21.8	1.5
K106A	26.1	1.6
D233A	22.5	1.0
K263A	18.8	1.1
G198A	16.2	1.0
I202A	15.5	1.0
S203A	16.7	1.1
E217A	15.8	1.3
G223A	15.9	0.5
L227A	17.7	0.4
G228A	17.4	0.4
E230Q	13.2	0.8
E230A	26.3	1.5
D231N	8.4	0.6
S234A	7.7	0.8

All mutants were tested at 1 μM
Abbreviations are as follows;
luminescence (lum.), standard deviation (stdev), and wild type (WT).

2.6.3 Some mutations of DnaK create unstable proteins.

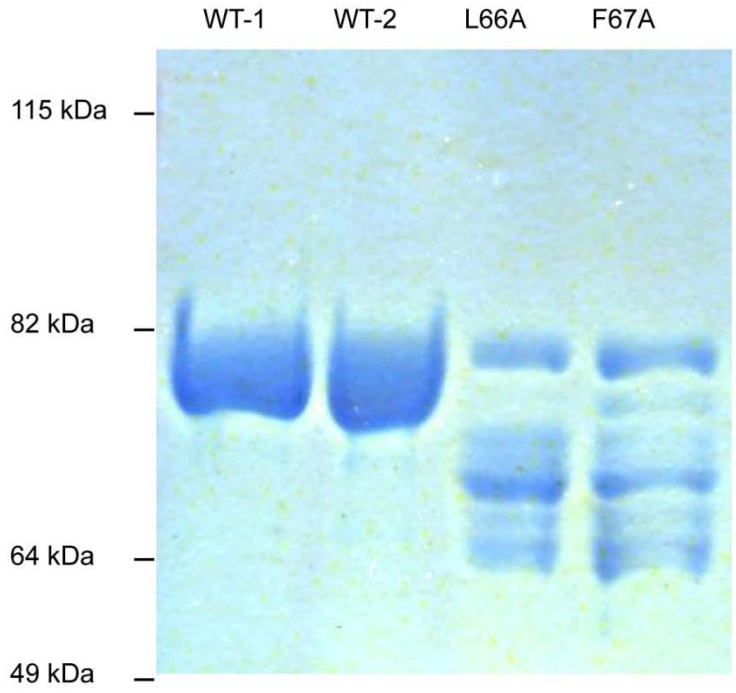

Appendix 2.3. Some mutations of DnaK create unstable proteins, which were removed from the study. During the purification of the DnaK mutants, L66A and F67A were found to have poor stability durign storage. We were not able to express L227P. The gel shown is an 8% SDS PAGE gel with 4 μM protein loaded into each lane.

2.6.4 Co-chaperone mediated stimulation of ATPase turnover in DnaK wild type (WT) and mutants.

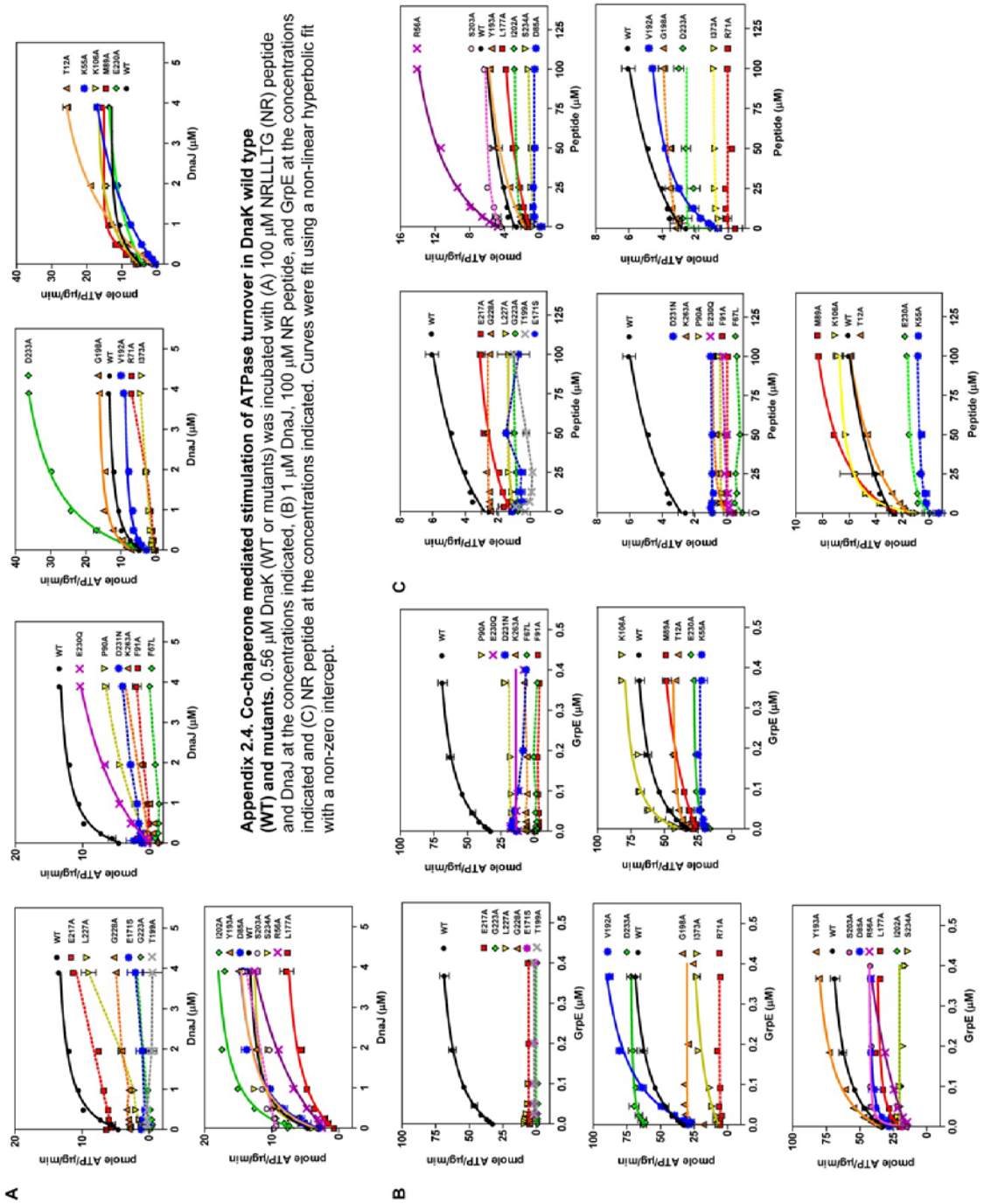

Appendix 2.4. Co-chaperone mediated stimulation of ATPase turnover in DnaK wild type (WT) and mutants. 0.56 µM DnaK (WT or mutants) was incubated with (A) 100 µM NRLLLTG (NR) peptide and DnaJ at the concentrations indicated, (B) 1 µM DnaJ, 100 µM NR peptide, and GrpE at the concentrations indicated and (C) NR peptide at the concentrations indicated. Curves were fit using a non-linear hyperbolic fit with a non-zero intercept.

2.6.5 Surface topology plots for the co-chaperone dependence of wild type (WT) DnaK's luciferase refolding activity and ATPase activity.

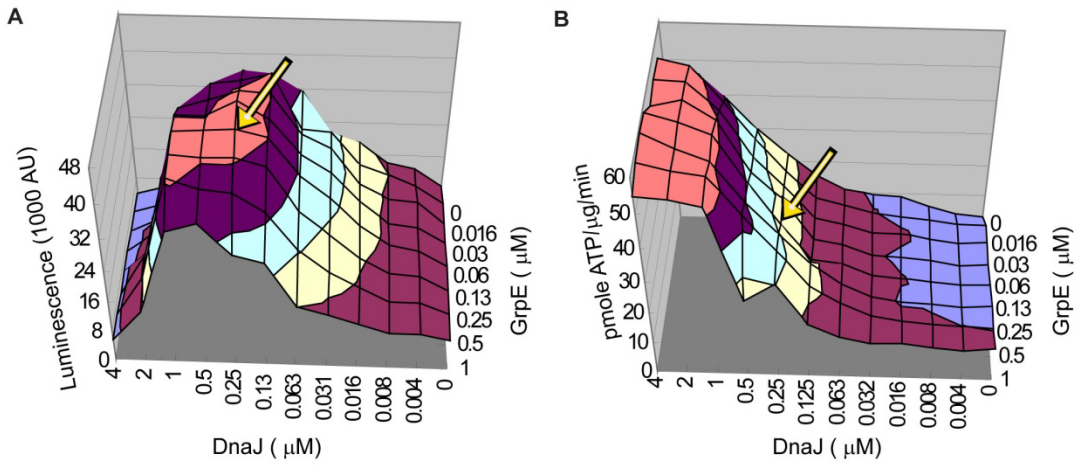

Appendix 2.5. The co-chaperone dependence of wild type (WT) DnaK's lucifrease refolding acitvity and ATPase activity. The co-chaperone dose dependencies of the luciferase refolding (A) and ATPase activity (B) of WT DnaK are shown. In both A and B, the final concentrations were: DnaK (1 μM), denatured luciferase (8nM), and ATP (1μM). The reaction temperature was 37°C for both experiments. We observe that for both DnaJ and GrpE stimulation that eventually reaches a maximum is observed in the ATPase assay. However, in refolding there is an optimal concentration of DnaJ and GrpE for stimulation, above which these co-chaperones begin to inhibit refolding. This phenomenon is believed to be due to competition for binding to luciferase between the co-chaperones and DnaK at these high concentrations. The optimal concentration of DnaJ and GrpE (0.25 μM and 0.125 μM, respectively) for luciferase refolding (pointed to by an arrow in A and B) was used in future experiments, including those shown in figure 2.2,2.3, and 2.4.

2.6.6 The intrinsic and DnaJ-stimulated ATPase rates of DnaK mutants were not well correlated with their luciferase refolding activities.

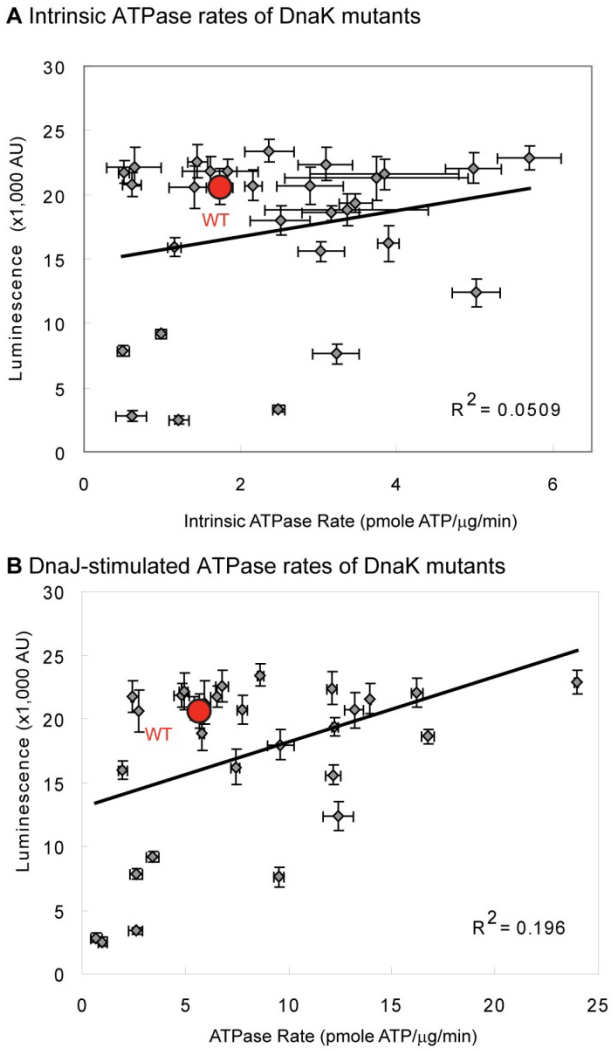

Appendix 2.6. The intrinsic and DnaJ-stimulated ATPase rates of DnaK mutants were not correlated with their luciferase refolding activities. (A) The luciferase refolding activity (in luminescence) is plotted against the intrinsic ATPase rate of each DnaK mutant. (B) The luciferase refolding activity (in luminescence) is plotted against the DnaJ-stimulated ATPase rate of each DnaK mutant. The luciferase refolding activities were measured using 1 μM DnaK, 0.25 μM DnaJ, 0.125 μM GrpE, and 8nM luciferase. The intrinsic ATPase rates were measured using 0.6 μM DnaK. Finally, the DnaJ-stimulated ATPase rate was measured using 0.6 μM DnaK and 0.5 μM DnaJ. 1 mM ATP was used in all experiments. Each data point is the average of triplicates and the error bars represent the standard error.

2.6.7 Partial Proteolysis of DnaK IB subdomain mutants.

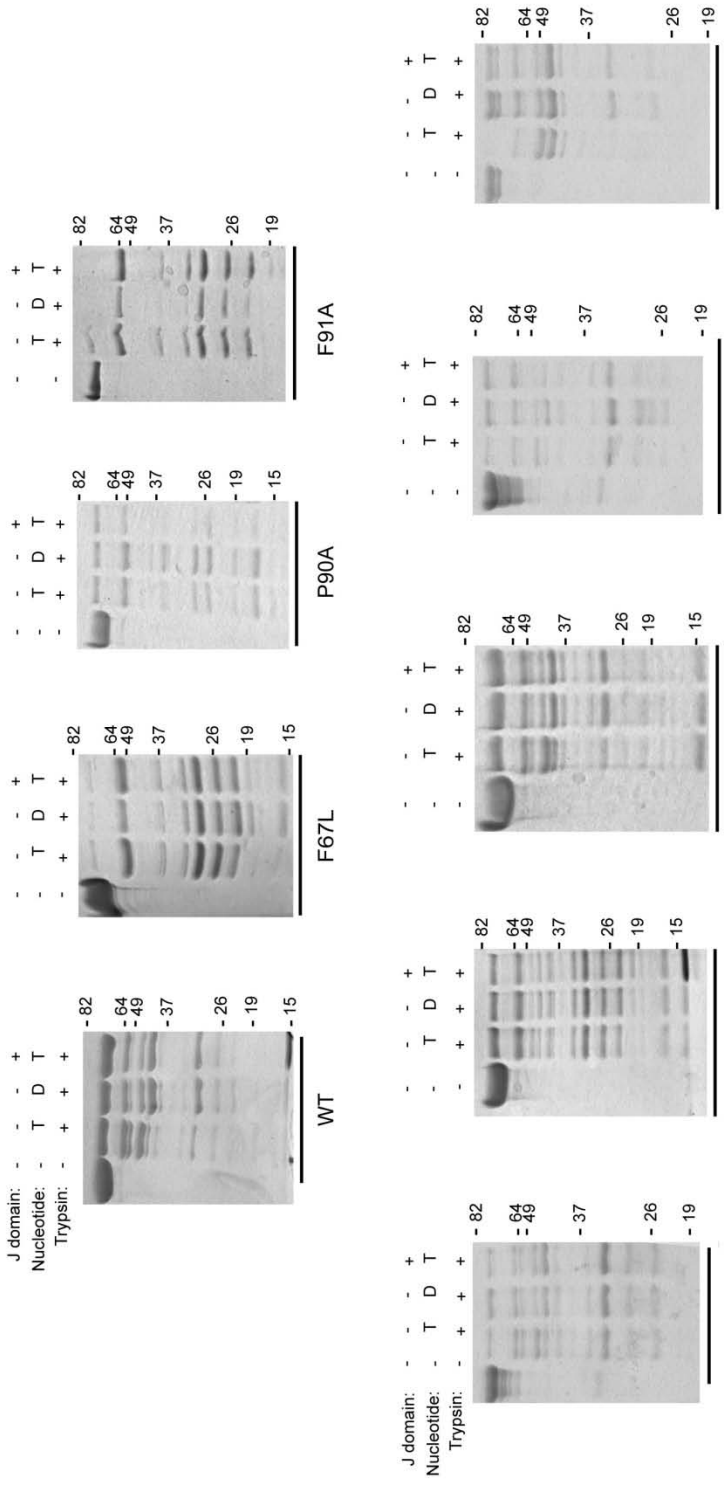

Appendix 2.7. Partial Proteolysis of DnaK IB subdomain mutants. Trypsin digestion was carried out in a 1:4 trypsin:DnaK molar ratio, in the presence of either ATP (T) or ADP (D). Further, we tested in presence of 4 molar equivalents of J-domain (2-108 of DnaJ), as indicated. Trypsinization took place for 20 minutes. We observed that IB decoupling mutants, F67L, P90A, and F91A, had a different clevage pattern than WT and did not undergo nucleotide-state dependent conformational changes as observed in wild type DnaK (WT). Finally, the IB decoupling mutatns were more susceptible to clevage than WT, suggesting increased protein flexibility. Meanwhile, other IB subdomain mutants R56A, R71A, D85A, M89A, and K106A, were more WT-like in their partial proteolysis pattern.

2.6.8 Control experiments for testing the ability of DnaK mutants to complement the growth of Δ*dnak* (DE3) *E. coli* cells under heat shock.

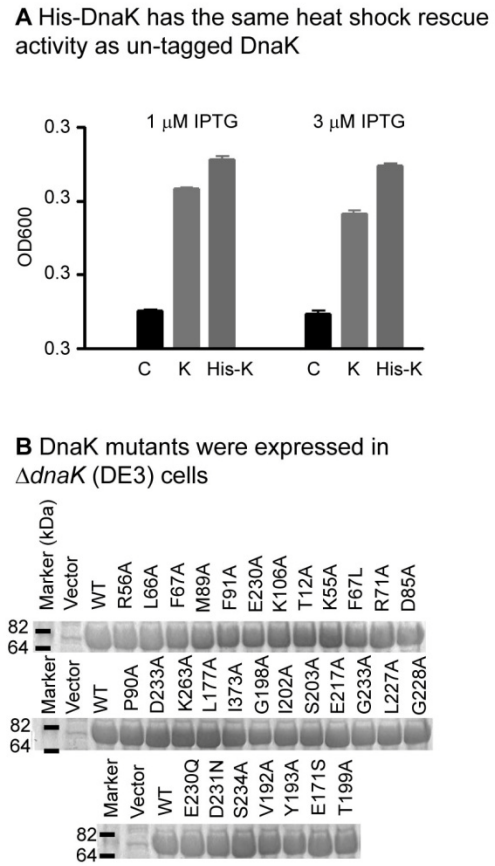

Appendix 2.8. Control experiments for testing the ability of DnaK mutants to complement the growth of Δ*dnaK* (DE3) *E. coli* cells under heat shock. (A) DnaK with an uncleaved N-terminal His-tag (His-K) could rescue the growth of Δ*dnaK* (DE3) *E. coli* cells at 43 deg. C as well as DnaK lacking the N-terminal His-tag (K). An empty vector was tested as a negative control (C). (B) Prior to testing the heat shock rescue activities of all 29 mutants (with N-terminal His-tags), we confirmed they all expressed in Δ*dnaK* (DE3) *E. coli* cells upon addition of 4 μM IPTG by SDS-PAGE electrophoresis followed by staining with coomassie blue.

2.7 References

1. Parsell, D.A. and S. Lindquist, *The function of heat-shock proteins in stress tolerance: degradation and reactivation of damaged proteins.* Annu Rev Genet, 1993. **27**: p. 437-96.
2. Rensing, S.A. and U.G. Maier, *Phylogenetic analysis of the stress-70 protein family.* J Mol Evol, 1994. **39**(1): p. 80-6.
3. Hesterkamp, T. and B. Bukau, *Role of the DnaK and HscA homologs of Hsp70 chaperones in protein folding in E.coli.* EMBO J, 1998. **17**(16): p. 4818-28.
4. Paek, K.H. and G.C. Walker, *Escherichia coli dnaK null mutants are inviable at high temperature.* J Bacteriol, 1987. **169**(1): p. 283-90.
5. Patury, S., Y. Miyata, and J.E. Gestwicki, *Pharmacological targeting of the Hsp70 chaperone.* Curr Top Med Chem, 2009. **9**(15): p. 1337-51.
6. Szabo, A., et al., *The ATP hydrolysis-dependent reaction cycle of the Escherichia coli Hsp70 system DnaK, DnaJ, and GrpE.* Proc Natl Acad Sci U S A, 1994. **91**(22): p. 10345-9.
7. Bertelsen, E.B., et al., *Solution conformation of wild-type E. coli Hsp70 (DnaK) chaperone complexed with ADP and substrate.* Proc Natl Acad Sci U S A, 2009. **106**(21): p. 8471-6.
8. Harrison, C.J., et al., *Crystal structure of the nucleotide exchange factor GrpE bound to the ATPase domain of the molecular chaperone DnaK.* Science, 1997. **276**(5311): p. 431-5.
9. Stevens, S.Y., et al., *The solution structure of the bacterial HSP70 chaperone protein domain DnaK(393-507) in complex with the peptide NRLLLTG.* Protein Sci, 2003. **12**(11): p. 2588-96.
10. Buchberger, A., et al., *Nucleotide-induced conformational changes in the ATPase and substrate binding domains of the DnaK chaperone provide evidence for interdomain communication.* J Biol Chem, 1995. **270**(28): p. 16903-10.
11. Buczynski, G., et al., *Characterization of a lidless form of the molecular chaperone DnaK: deletion of the lid increases peptide on- and off-rate constants.* J Biol Chem, 2001. **276**(29): p. 27231-6.
12. Flynn, G.C., T.G. Chappell, and J.E. Rothman, *Peptide binding and release by proteins implicated as catalysts of protein assembly.* Science, 1989. **245**(4916): p. 385-90.
13. Liberek, K., et al., *The Escherichia coli DnaK chaperone, the 70-kDa heat shock protein eukaryotic equivalent, changes conformation upon ATP hydrolysis, thus triggering its dissociation from a bound target protein.* J Biol Chem, 1991. **266**(22): p. 14491-6.
14. Pierpaoli, E.V., et al., *The power stroke of the DnaK/DnaJ/GrpE molecular chaperone system.* J Mol Biol, 1997. **269**(5): p. 757-68.
15. Schmid, D., et al., *Kinetics of molecular chaperone action.* Science, 1994. **263**(5149): p. 971-3.
16. Slepenkov, S.V. and S.N. Witt, *Detection of a concerted conformational change in the ATPase domain of DnaK triggered by peptide binding.* FEBS Lett, 2003. **539**(1-3): p. 100-4.
17. Karzai, A.W. and R. McMacken, *A bipartite signaling mechanism involved in DnaJ-mediated activation of the Escherichia coli DnaK protein.* J Biol Chem, 1996. **271**(19): p. 11236-46.
18. Goffin, L. and C. Georgopoulos, *Genetic and biochemical characterization of mutations affecting the carboxy-terminal domain of the Escherichia coli molecular chaperone DnaJ.* Mol Microbiol, 1998. **30**(2): p. 329-40.

19. Johnson, J.L. and E.A. Craig, *An essential role for the substrate-binding region of Hsp40s in Saccharomyces cerevisiae.* J Cell Biol, 2001. **152**(4): p. 851-6.
20. Liberek, K., et al., *Escherichia coli DnaJ and GrpE heat shock proteins jointly stimulate ATPase activity of DnaK.* Proc Natl Acad Sci U S A, 1991. **88**(7): p. 2874-8.
21. Ang, D. and C. Georgopoulos, *The heat-shock-regulated grpE gene of Escherichia coli is required for bacterial growth at all temperatures but is dispensable in certain mutant backgrounds.* J Bacteriol, 1989. **171**(5): p. 2748-55.
22. Sell, S.M., et al., *Isolation and characterization of dnaJ null mutants of Escherichia coli.* J Bacteriol, 1990. **172**(9): p. 4827-35.
23. Barthel, T.K., J. Zhang, and G.C. Walker, *ATPase-defective derivatives of Escherichia coli DnaK that behave differently with respect to ATP-induced conformational change and peptide release.* J Bacteriol, 2001. **183**(19): p. 5482-90.
24. Klucken, J., et al., *A single amino acid substitution differentiates Hsp70-dependent effects on alpha-synuclein degradation and toxicity.* Biochem Biophys Res Commun, 2004. **325**(1): p. 367-73.
25. Wisen, S. and J.E. Gestwicki, *Identification of small molecules that modify the protein folding activity of heat shock protein 70.* Anal Biochem, 2008. **374**(2): p. 371-7.
26. Szabo, A., et al., *A zinc finger-like domain of the molecular chaperone DnaJ is involved in binding to denatured protein substrates.* EMBO J, 1996. **15**(2): p. 408-17.
27. Bardwell, J.C. and E.A. Craig, *Major heat shock gene of Drosophila and the Escherichia coli heat-inducible dnaK gene are homologous.* Proc Natl Acad Sci U S A, 1984. **81**(3): p. 848-52.
28. Gragerov, A., et al., *Cooperation of GroEL/GroES and DnaK/DnaJ heat shock proteins in preventing protein misfolding in Escherichia coli.* Proc Natl Acad Sci U S A, 1992. **89**(21): p. 10341-4.
29. Mogk, A., et al., *Identification of thermolabile Escherichia coli proteins: prevention and reversion of aggregation by DnaK and ClpB.* EMBO J, 1999. **18**(24): p. 6934-49.
30. Grimshaw, J.P., et al., *Thermosensor action of GrpE. The DnaK chaperone system at heat shock temperatures.* J Biol Chem, 2003. **278**(21): p. 19048-53.
31. Groemping, Y. and J. Reinstein, *Folding properties of the nucleotide exchange factor GrpE from Thermus thermophilus: GrpE is a thermosensor that mediates heat shock response.* J Mol Biol, 2001. **314**(1): p. 167-78.
32. Buchberger, A., et al., *Functional defects of the DnaK756 mutant chaperone of Escherichia coli indicate distinct roles for amino- and carboxyl-terminal residues in substrate and co-chaperone interaction and interdomain communication.* J Biol Chem, 1999. **274**(53): p. 38017-26.
33. Chang, T.C., et al., *The effect of mutating arginine-469 on the substrate binding and refolding activities of 70-kDa heat shock cognate protein.* Arch Biochem Biophys, 2001. **386**(1): p. 30-6.
34. Davis, J.E., C. Voisine, and E.A. Craig, *Intragenic suppressors of Hsp70 mutants: interplay between the ATPase- and peptide-binding domains.* Proc Natl Acad Sci U S A, 1999. **96**(16): p. 9269-76.
35. Hu, S.M., et al., *Characterization of the L399P and R447G mutants of hsc70: the decrease in refolding activity is correlated with an increase in the rate of substrate dissociation.* Arch Biochem Biophys, 2002. **407**(1): p. 135-41.

36. Kamath-Loeb, A.S., et al., *Analysis of three DnaK mutant proteins suggests that progression through the ATPase cycle requires conformational changes.* J Biol Chem, 1995. **270**(50): p. 30051-9.
37. McClellan, A.J. and J.L. Brodsky, *Mutation of the ATP-binding pocket of SSA1 indicates that a functional interaction between Ssa1p and Ydj1p is required for post-translational translocation into the yeast endoplasmic reticulum.* Genetics, 2000. **156**(2): p. 501-12.
38. Montgomery, D.L., R.I. Morimoto, and L.M. Gierasch, *Mutations in the substrate binding domain of the Escherichia coli 70 kDa molecular chaperone, DnaK, which alter substrate affinity or interdomain coupling.* J Mol Biol, 1999. **286**(3): p. 915-32.
39. Grimshaw, J.P., et al., *The heat-sensitive Escherichia coli grpE280 phenotype: impaired interaction of GrpE(G122D) with DnaK.* J Mol Biol, 2005. **353**(4): p. 888-96.
40. Buchberger, A., et al., *The chaperone function of DnaK requires the coupling of ATPase activity with substrate binding through residue E171.* EMBO J, 1994. **13**(7): p. 1687-95.
41. Jiang, J., et al., *Structural basis of J cochaperone binding and regulation of Hsp70.* Mol Cell, 2007. **28**(3): p. 422-33.
42. Bhattacharya, A., et al., *Allostery in Hsp70 chaperones is transduced by subdomain rotations.* J Mol Biol, 2009. **388**(3): p. 475-90.
43. Sugimoto, S., et al., *A gram-negative characteristic segment in Escherichia coli DnaK is essential for the ATP-dependent cooperative function with the co-chaperones DnaJ and GrpE.* FEBS Lett, 2007. **581**(16): p. 2993-9.
44. Woo, H.J., et al., *ATP-induced conformational changes in Hsp70: molecular dynamics and experimental validation of an in silico predicted conformation.* Biochemistry, 2009. **48**(48): p. 11470-7.
45. Brehmer, D., et al., *Tuning of chaperone activity of Hsp70 proteins by modulation of nucleotide exchange.* Nat Struct Biol, 2001. **8**(5): p. 427-32.
46. O'Brien, M.C., K.M. Flaherty, and D.B. McKay, *Lysine 71 of the chaperone protein Hsc70 Is essential for ATP hydrolysis.* J Biol Chem, 1996. **271**(27): p. 15874-8.
47. Tanaka, N., et al., *The substrate binding domain of DnaK facilitates slow protein refolding.* Proc Natl Acad Sci U S A, 2002. **99**(24): p. 15398-403.
48. McCarty, J.S., et al., *The role of ATP in the functional cycle of the DnaK chaperone system.* J Mol Biol, 1995. **249**(1): p. 126-37.
49. Theyssen, H., et al., *The second step of ATP binding to DnaK induces peptide release.* J Mol Biol, 1996. **263**(5): p. 657-70.
50. Brehmer, D., et al., *Influence of GrpE on DnaK-substrate interactions.* J Biol Chem, 2004. **279**(27): p. 27957-64.
51. Laufen, T., et al., *Mechanism of regulation of hsp70 chaperones by DnaJ cochaperones.* Proc Natl Acad Sci U S A, 1999. **96**(10): p. 5452-7.
52. Cajo, G.C., et al., *The role of the DIF motif of the DnaJ (Hsp40) co-chaperone in the regulation of the DnaK (Hsp70) chaperone cycle.* J Biol Chem, 2006. **281**(18): p. 12436-44.
53. Linke, K., et al., *The roles of the two zinc binding sites in DnaJ.* J Biol Chem, 2003. **278**(45): p. 44457-66.
54. Wall, D., M. Zylicz, and C. Georgopoulos, *The conserved G/F motif of the DnaJ chaperone is necessary for the activation of the substrate binding properties of the DnaK chaperone.* J Biol Chem, 1995. **270**(5): p. 2139-44.

55. Gamer, J., et al., *A cycle of binding and release of the DnaK, DnaJ and GrpE chaperones regulates activity of the Escherichia coli heat shock transcription factor sigma32.* EMBO J, 1996. **15**(3): p. 607-17.
56. Han, W. and P. Christen, *Mechanism of the targeting action of DnaJ in the DnaK molecular chaperone system.* J Biol Chem, 2003. **278**(21): p. 19038-43.
57. Liberek, K., D. Wall, and C. Georgopoulos, *The DnaJ chaperone catalytically activates the DnaK chaperone to preferentially bind the sigma 32 heat shock transcriptional regulator.* Proc Natl Acad Sci U S A, 1995. **92**(14): p. 6224-8.
58. Mayer, M.P., et al., *Multistep mechanism of substrate binding determines chaperone activity of Hsp70.* Nat Struct Biol, 2000. **7**(7): p. 586-93.
59. Schuermann, J.P., et al., *Structure of the Hsp110:Hsc70 nucleotide exchange machine.* Mol Cell, 2008. **31**(2): p. 232-43.
60. Shaner, L., R. Sousa, and K.A. Morano, *Characterization of Hsp70 binding and nucleotide exchange by the yeast Hsp110 chaperone Sse1.* Biochemistry, 2006. **45**(50): p. 15075-84.
61. Sugimoto, S., et al., *In vivo and in vitro complementation study comparing the function of DnaK chaperone systems from halophilic lactic acid bacterium Tetragenococcus halophilus and Escherichia coli.* Biosci Biotechnol Biochem, 2008. **72**(3): p. 811-22.
62. De Los Rios, P., et al., *Hsp70 chaperones accelerate protein translocation and the unfolding of stable protein aggregates by entropic pulling.* Proc Natl Acad Sci U S A, 2006. **103**(16): p. 6166-71.
63. Barral, J.M., et al., *Roles of molecular chaperones in protein misfolding diseases.* Semin Cell Dev Biol, 2004. **15**(1): p. 17-29.
64. Santacruz, K., et al., *Tau suppression in a neurodegenerative mouse model improves memory function.* Science, 2005. **309**(5733): p. 476-81.
65. Sydow, A., et al., *Reversibility of Tau-related cognitive defects in a regulatable FTD mouse model.* J Mol Neurosci, 2011. **45**(3): p. 432-7.
66. Sydow, A., et al., *Tau-induced defects in synaptic plasticity, learning, and memory are reversible in transgenic mice after switching off the toxic Tau mutant.* J Neurosci, 2011. **31**(7): p. 2511-25.
67. Jinwal, U.K., et al., *Chemical manipulation of hsp70 ATPase activity regulates tau stability.* J Neurosci, 2009. **29**(39): p. 12079-88.
68. Stols, L., et al., *A new vector for high-throughput, ligation-independent cloning encoding a tobacco etch virus protease cleavage site.* Protein Expr Purif, 2002. **25**(1): p. 8-15.
69. Zheng, L., U. Baumann, and J.L. Reymond, *An efficient one-step site-directed and site-saturation mutagenesis protocol.* Nucleic Acids Res, 2004. **32**(14): p. e115.
70. Chang, L., et al., *High-throughput screen for small molecules that modulate the ATPase activity of the molecular chaperone DnaK.* Anal Biochem, 2008. **372**(2): p. 167-76.

Chapter 3

Visualization and functional analysis of the oligomeric states of *Escherichia coli* heat shock protein 70 (Hsp70/DnaK).

3.1 Abstract

For the *Escherichia coli* Hsp70, DnaK, it is well known that substrate binding is allosterically regulated by ATP hydrolysis, which drives conformational changes within the interdomain linker and the substrate-binding domain. In addition, a few groups have reported that nucleotide state also influences the homo-oligomerization of DnaK. However, the architecture of oligomeric DnaK and its roles in the chaperone cycle remain undefined. Towards this goal, either monomeric or oligomeric forms of DnaK were stabilized using point mutants, nucleotide analogs, and cross-linking. By negative stain electron microscopy, an ensemble of monomers, dimers, and other small, defined multimers were observed. Interestingly, oligomeric DnaK retained ATPase activity and it protected a model substrate from denaturation, but these structures had greatly reduced ability to refold substrate and they did not respond to DnaJ stimulation. Finally, it was observed that oligomeric DnaK is present in *E. coli* lysates and that these structures become more prevalent when the cells are exposed to heat shock. Together these studies suggest that DnaK oligomers are composed of ordered multimers that are functionally distinct from monomeric DnaK. Thus, oligomerization of DnaK might be an important step in the chaperone cycle by favoring "holdase" activity and minimizing ATP turnover during acute heat shock.

3.2 Introduction

3.2.1 Nucleotide regulates substrate binding by Hsp70s.

As discussed in Chapters 1 and 2, heat shock protein 70 (Hsp70) belongs to a family of highly conserved molecular chaperones that plays central roles in protein homeostasis [1-3]. Hsp70s have been found to be essential in the cellular response to a variety of stressors, including heat shock and oxidation [4-6]. In addition, they have been proposed as a promising drug target in a variety of diseases including cancer and neurodegeneration [7, 8]. Thus, understanding the structure and function of Hsp70 family members is expected to enhance our understanding of cellular proteostasis, while also advancing our ability to design new disease treatments.

Towards those goals, extensive studies have focused on the prokaryotic Hsp70, DnaK. Like other Hsp70s, *E. coli* DnaK is a 70-kDa chaperone composed of a nucleotide binding domain (NBD) and a substrate binding domain (SBD) [9]. The SBD can be further subdivided into a beta sandwich domain, responsible for binding substrates, and an alpha helical lid that closes over bound substrates [9]. The NBD and SBD are connected by a flexible linker and allosterically link substrate binding to nucleotide hydrolysis [10]. In the ATP bound state, DnaK (DnaK-ATP) has relatively weak affinity for substrates, but, upon ATP hydrolysis, structural changes lead to an increase in substrate affinity by lowering the off-rate [11, 12]. Thus, DnaK is believed to carry out its molecular chaperone activities by repeatedly binding and releasing substrate proteins, a process made possible by coupling substrate affinity to ATP hydrolysis. Whereas DnaK

alone has a very slow intrinsic ATPase rate, as highlighted in Chapter 2, interactions with co-chaperones, DnaJ and GrpE, stimulate ATP turnover. Briefly, DnaJ interacts directly with DnaK via a conserved J-domain, and this interaction stimulates the hydrolysis of ATP [13]. Furthermore, DnaJ is known to bind exposed hydrophobic regions of unfolded proteins [14, 15]. Thus, DnaJ both localizes DnaK to substrate proteins and induces ATP hydrolysis. Meanwhile, GrpE serves as a nucleotide exchange factor, leading to the release of ADP and the re-binding of ATP by DnaK, a process that releases bound substrate proteins and completes the ATPase cycle [14].

3.2.2 Nucleotide-dependent structural changes of DnaK

Defining the structural changes that occur in response to nucleotide cycling is central to understanding the molecular mechanisms by which DnaK functions as a chaperone. Consistent with this idea, a wide variety of biochemical and biophysical methods have been used to characterize the structural and allosteric changes that occur in response to nucleotides. Together, these studies support a model in which the motions of the NBD and SBD are coupled in the ATP bound state (DnaK-ATP), which destabilizes the substrate binding pocket and favors opening of the alpha helical lid [16-19]. Conversely, in the ADP bound state (DnaK-ADP), the NBD and the SBD are observed to move independently, ordering the substrate binding pocket and closing the lid. These insights have benefitted from structural analyses of both isolated domains [20] and two-domain structures. For example, the ATP bound form of DnaK has been modeled based on the X-ray crystal structure of Hsp110, a distant homolog of Hsp70 [21], whereas the two-domain solution structure of DnaK-ADP in complex with a peptide substrate has been

determined by NMR [9]. Together, these structures and others provide insight into the key interfaces involved in nucleotide state-driven changes in structure.

3.2.3 Nucleotide-dependent changes in quaternary structure are not fully understood

Despite advances in our understanding of the interdomain allostery in DnaK, other nucleotide-dependent structural transitions are less clear. For example, multiple groups have noted that, while DnaK-ATP is predominantly monomeric, DnaK-ADP is prone to self-oligomerization [22, 23]. Furthermore, oligomerization has also been observed in human isoforms of Hsp70, suggesting that it is a conserved structural transition [24-27]. To date, these studies suggest that ADP favors Hsp70 self-oligomerization in a concentration- and temperature-dependent manner *in vitro* and that this process is reversed with the addition of ATP, excess peptide substrate, and some co-chaperones, such as GrpE [23, 28, 29]. Finally, oligomeric forms of human Hsp70s may be present in cells [24, 26], and in the case of the ER-resident isoform of Hsp70 called BiP, *in vivo* oligomerization has been shown to be a regulated process that is promoted by post-translational modifications [30]. Yet, it isn't clear whether oligomers represent ordered multimers (i.e. dimers, trimers, etc) or whether they are disordered aggregates. Further, it isn't clear whether the oligomers are inactivated storage forms of the chaperone or whether they play a more active role in the chaperone cycle. The answers to these questions are important in advancing our understanding of Hsp70 structure and function.

3.2.4 Our approach to probing the structure and function of oligomeric DnaK

We hypothesized that oligomerization of DnaK may result in the formation of distinct, higher ordered structures that could have functional relevance in the chaperone cycle. To evaluate this idea, electron microscopy (EM), cross-linking, and biochemical measurements were utilized to explore the architecture and function of DnaK oligomers. Whether these oligomers could be found in cells and if thermal stress could impact their formation was also explored. Together, these studies suggest that DnaK is preferentially assembled into dimers, trimers, and other small oligomers in response to ADP and that these structures are functionally distinct from monomeric DnaK.

3.3 Results

3.3.1 Self-oligomerization of DnaK is influenced by the nucleotide state

As mentioned above, several studies have noted that DnaK and other Hsp70 family members form multimers [22-26]. As a preface for studies into the architecture and function of these assemblies, DnaK was expressed and purified (Appendix 3.1) and performed gel filtration studies on the ATP and ADP bound states. Consistent with previous reports [23], it was observed that DnaK-ATP was primarily monomeric, while DnaK-ADP samples contained higher order oligomers (Figure 3.1A, Appendix 3.1). The apparent molecular weights of these peaks (monomers and oligomers ranging from 110 to 670 kDa) were consistent with previously reported values [23]. Next, to control for any effects of intrinsic ATP hydrolysis, the oligomerization of the T199A mutant of DnaK, which is unable to hydrolyze ATP, was evaluated (Appendix 3.1, Appendix 3.2) [16]. As

expected, DnaK-T199A in the ATP bound state was primarily monomeric by gel filtration, supporting the idea that the ATP bound form is largely a monomer.

To further clarify the size distribution of multimers that could isolate by gel filtration, each of the gel filtration fractions was evaluated by both denaturing and native gel electrophoresis. As expected, ADP favored oligomerization based on the abundance of DnaK bands in earlier fractions (Figure 3.1B). Furthermore, monomer and dimer bands were observed, even in early fractions of our DnaK-ADP sample, suggesting that these structures are in a dynamic equilibrium, as previously described [23] (Figure 3.1B). Notably, a small amount of dimeric DnaK was also observed in the presence of saturating concentrations of ATP (Figure 3.1B). Together, these results suggest that DnaK reversibly forms oligomers, including dimers, and that this balance is influenced by nucleotide.

3.3.2 DnaK oligomerization occurs within cells and is increased in response to heat and elevated expression

Having confirmed that DnaK forms oligomers *in vitro*, next this study aimed to understand whether this process could occur within *E. coli* cells. Towards this goal, *E. coli* cellular lysates were seperated by gel filtration and evaluated fractions by western blot analysis for DnaK in both denaturing and native gel electrophoresis. In cells grown to mid-log phase at 30°C, bands consistent with the molecular mass of monomeric and dimeric forms of DnaK were observed (Figure 3.1C). These results suggest that DnaK

homo-oligomerizes *in vivo*. Next, this study assessed if cellular stresses might impact the

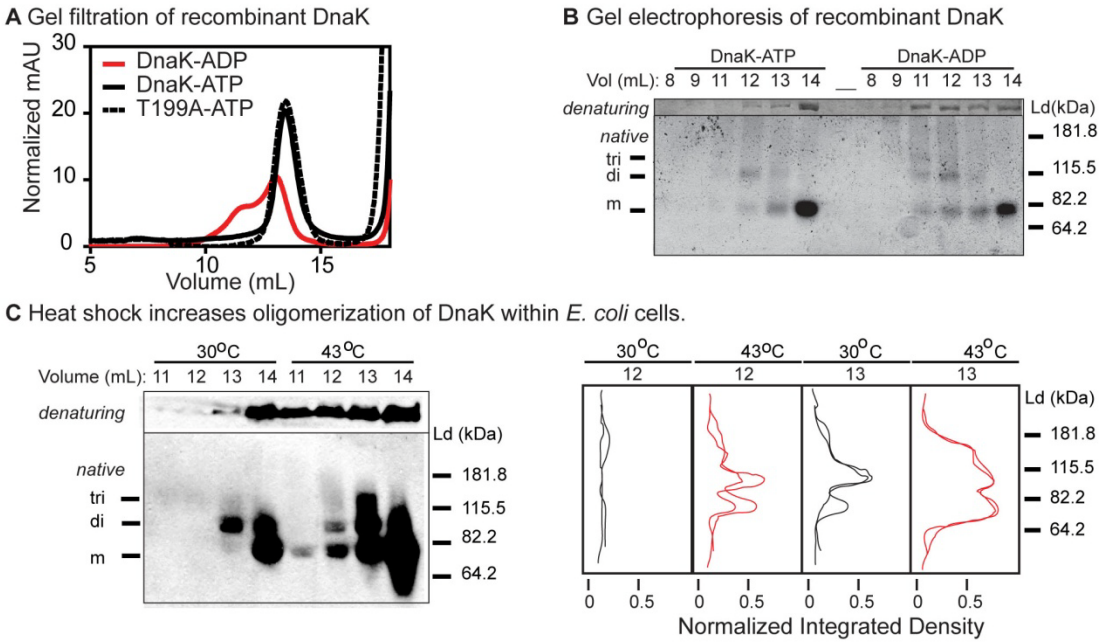

Figure 3.1. DnaK self-oligomerization occurs *in vitro* and *in vivo*.
(A) DnaK in the presence of ATP (DnaK-ATP) is primarily monomeric by gel filtration (black, solid line). The addition of ADP (DnaK-ADP) leads to an increase in higher molecular weight species (red, solid line). A mutant of DnaK that is unable to hydrolyze ATP (T199A-ATP) is also primarily monomeric by gel filtration (black, dotted line). (B) Fractions collected from gel filtration are subject to both denaturing and native gel electrophoresis. Bands consistent with the molecular weight of trimeric (tri), dimeric (di), and monomeric (m) DnaK were observed. These species are increased in the presence of ADP. (C) *E. coli* cells were grown at either 30 °C or 43 °C, the lysates were separated by gel filtration and subject to native and denaturing gel electrophoresis (as in a and b). By western blot, trimeric (tri), dimeric (di), and monomeric (m) DnaK were observed. The experiment was performed in independent duplicates and both histograms of the resulting band intensities for fractions 12 and 13 mL are shown in the right panel.

relative abundance of oligomeric DnaK. Consistent with previous findings, the total amount of DnaK was significantly elevated in response to heat shock (Appendix 3.3) [5, 31, 32]. In addition, it was observed that DnaK eluted in earlier fractions under these conditions (Figure 3.1C), suggesting that it may also be forming higher ordered structures. When these fractions were analyzed by native gel electrophoresis, DnaK was found to be assembled into a discrete series of bands with molecular weights consistent with the trimeric, dimeric, and monomeric forms (Figure 3.1C). Although it is not yet possible to ascribe these changes in oligomerization to a specific mechanism, these findings suggest that DnaK forms oligomers in cells under normal growth conditions and

that these structures are favored in response to heat stress. Next, we evaluated if this response also occurred in cells facing hydrogen peroxide-induced oxidative stress or stress arising from the stationary phase of cellular growth. Consistent with previous reports [6, 33-35], these stresses elevated total DnaK levels, but, interestingly, they did not appreciably alter the extent of oligomerization (Appendix 3.3). This result suggests that an increase in DnaK oligomerization is not a general response to cellular stressors. Finally, whether increasing the levels of DnaK, in the absence of heat stress, would be sufficient to induce oligomerization in cells was tested. To test this idea, DnaK was overexpressed, under an inducible promoter, in a Δ*dnak E. coli* strain and found that high DnaK levels were sufficient to increase the oligomerization of DnaK (Appendix 3.3), suggesting that the amount of oligomeric DnaK within cells is sensitive to its expression level.

3.3.3 DnaK oligomerization is dependent on its concentration, substrate, and co-chaperones

Given the presence of DnaK oligomers within cells, we wanted to better understand the requirements for forming these complexes. Previous work has demonstrated that DnaK self-oligomerization in the ADP bound state occurs in a concentration dependent manner and that ATP, excess peptide substrate, or GrpE led to monomerization [23, 28]. In our hands, very similar results were observed (Appendix 3.4). Furthermore, the J-domain of DnaJ also led to the monomerization of DnaK-ADP (Appendix 3.4D) [36]. Thus, all the components of the active DnaK molecular chaperone cycle (i.e., substrate, J-domain, and GrpE) promoted monomerization.

3.3.4 Oligomers of DnaK retain ATPase and "holdase" activities but have reduced "foldase" activity

These findings lead us to wonder if oligomeric DnaK may represent an enzymatically or functionally inactive pool that might be rapidly monomerized by interaction with other components of the DnaK chaperone system. However, this model seems to be in conflict with the observation of increased oligomerization in response to heat stress (see Figure 3.1C), a condition that actively requires DnaK for viability [5]. Therefore, this study wanted to directly test whether DnaK oligomers have normal or attenuated chaperone activities *in vitro*. The technical challenge in addressing this issue is the dynamic equilibrium between monomeric and oligomeric DnaK, which makes it difficult to specifically evaluate their individual biochemical properties. To circumvent this problem, chemical cross-linking was utilized to stabilize oligomeric DnaK. Because the covalent modification of a protein using a chemical cross-linker can sometimes result in deleterious effects, it was essential to control for changes attributable to the cross-linking reaction. First, DnaK-ATP and DnaK-ADP samples were treated with the quenching reagents prior to adding the cross-linker (0.025% gluteraldehyde; see "Experimental Procedures" for details). As expected, this treatment left DnaK largely monomeric in both the ATP and ADP bound states (Figure 3.2A). Thus, these samples served as controls for the buffer conditions and handling steps that occur during the reactions. Next, cross-linking was performed on both DnaK-ADP and DnaK-ATP samples using 0.025% glutaraldehyde for 20 minutes. It was expected that higher order structures might be stabilized in both samples but that the ADP sample may be enriched for oligomers. When the samples were visualized by gel electrophoresis, bands consistent with oligomers and monomer were indeed observed in both ATP and ADP samples, and there was an

increase in oligomers (57 ± 5 %) in the presence of ADP as compared to ATP (40 ± 4 %) (Figure 3.2A). Oligomers larger than dimers were especially enriched in the ADP sample (33 ± 5 % vs. 16 ± 4%). Next, the intrinsic ATP hydrolysis activity of these crude mixtures was tested. We reasoned that an inactivated pool of oligomeric DnaK might have attenuated ATPase activity, reducing the apparent activity of the mixture. On the contrary, it was observed that cross-linked DnaK-ADP had a 1.5-fold faster rate (0.33 min^{-1}) than the equivalent DnaK-ATP sample (0.22 min^{-1}; Figure 3.2B, Table 3.1). Also, the cross-linked DnaK-ATP sample retained an intrinsic ATPase rate similar to the other control samples (0.20 and 0.18 min^{-1}). Thus, ADP-promoted oligomers of DnaK appear to retain enzymatic activity, and moreover, they may have a slightly higher intrinsic ATPase rate.

Table 3.1 Biochemical analysis of oligomeric DnaK

	ATPase[e]						Luciferase Holdase[e]				Luciferase Binding[e]			
	kcat	SEM	$K_{d,DnaJ}$	SEM	$B_{max,DnaJ}$	SEM	$K_{d,DnaK}$	SEM	$B_{max,DnaK}$	SEM	$K_{d,DnaK}$	SEM	$B_{max,DnaK}$	SEM
	(min^{-1})		μM		pmol Pi/K/m[a]		μM		lumin.		μM		% Binding[d]	
K-ATP[b]	0.20	0.02	0.20	0.08	33	3	0.22	0.05	9200	400	0.19	0.09	88	9
K-ADP	0.18	0.02	0.21	0.07	27	2	0.21	0.04	7300	300	0.11	0.06	80	9
K-ATP cx[c]	0.22	0.02	0.28	0.07	31	2	0.27	0.06	7900	400	0.21	0.07	88	7
K-ADP cx	0.33	0.02	0.39	0.08	19	1	0.17	0.04	7300	400	0.13	0.02	78	3

[a]pmol Pi/ μg DnaK/min,[b]DnaK-ATP and DnaK-ADP respectively,[c]cx represents samples cross-linked using 0.025% gluteraldehyde for 20 minutes,[d]100% Binding is defined by the maximum OD450 in the K-ATP sample,[e]values were obtained from global fitting of all available data.

Alone, DnaK has a low ATPase rate, and it depends on the co-chaperone DnaJ to greatly increase its ATPase activity. Furthermore, DnaJ is required for active refolding of denatured proteins [14, 37, 38]. Thus, whether the cross-linked, oligomeric DnaK could participate in DnaJ-dependent processes was evaluated. By measuring ATPase activity in the presence of increasing DnaJ levels, we observed that DnaK oligomers (K-ADP cx) had significantly reduced ability to respond to this co-chaperone (Figure 3.2C), with a

decrease in the apparent V_{max} for DnaJ (19 pmol Pi/μg DnaK/min) (Table 3.1). Conversely, the control samples (K-ATP and K-ADP) and the cross-linked DnaK-ATP sample (K-ATP cx) had Vmax values (33, 27, and 31 pmol Pi/ μg DnaK/min, respectively), similar to unmodified chaperone. Additionally, the DnaK oligomers demonstrated a mildly increased apparent K_m (0.39 μM), compared to control samples (0.20, 0.21, and 0.28 μM respectively). Similar results were seen with samples that were further enriched for oligomeric DnaK by gel filtration following cross-linking (Figure 3.2E and F). Together, these results suggest that oligomeric DnaK is deficient in DnaJ-mediated ATPase stimulation. It was also probed if the ATPase rate of oligomeric DnaK was deficient in stimulation by either peptide substrate or GrpE. In fact, oligomeric DnaK had a decreased ability to be stimulated by the NRLLLTG peptide (Appendix 3.5C), but no change in its ability to be stimulated by GrpE was observed (Appendix 3.5D).

Based on these results, it was hypothesized that oligomeric DnaK may also be unable to refold luciferase from a denatured state because this is a DnaJ-dependent process that is commonly termed “foldase” activity [37, 38]. To test this hypothesis, we evaluated whether DnaJ could restore active luciferase in combination with either the control or cross-linked DnaK samples. The cross-linked DnaK-ADP was found to have a much lower refolding activity compared to the controls or cross-linked DnaK-ATP (Figure 3.2D). Thus, oligomeric DnaK did not respond normally to DnaJ-mediated stimulation of either ATPase or luciferase refolding activity.

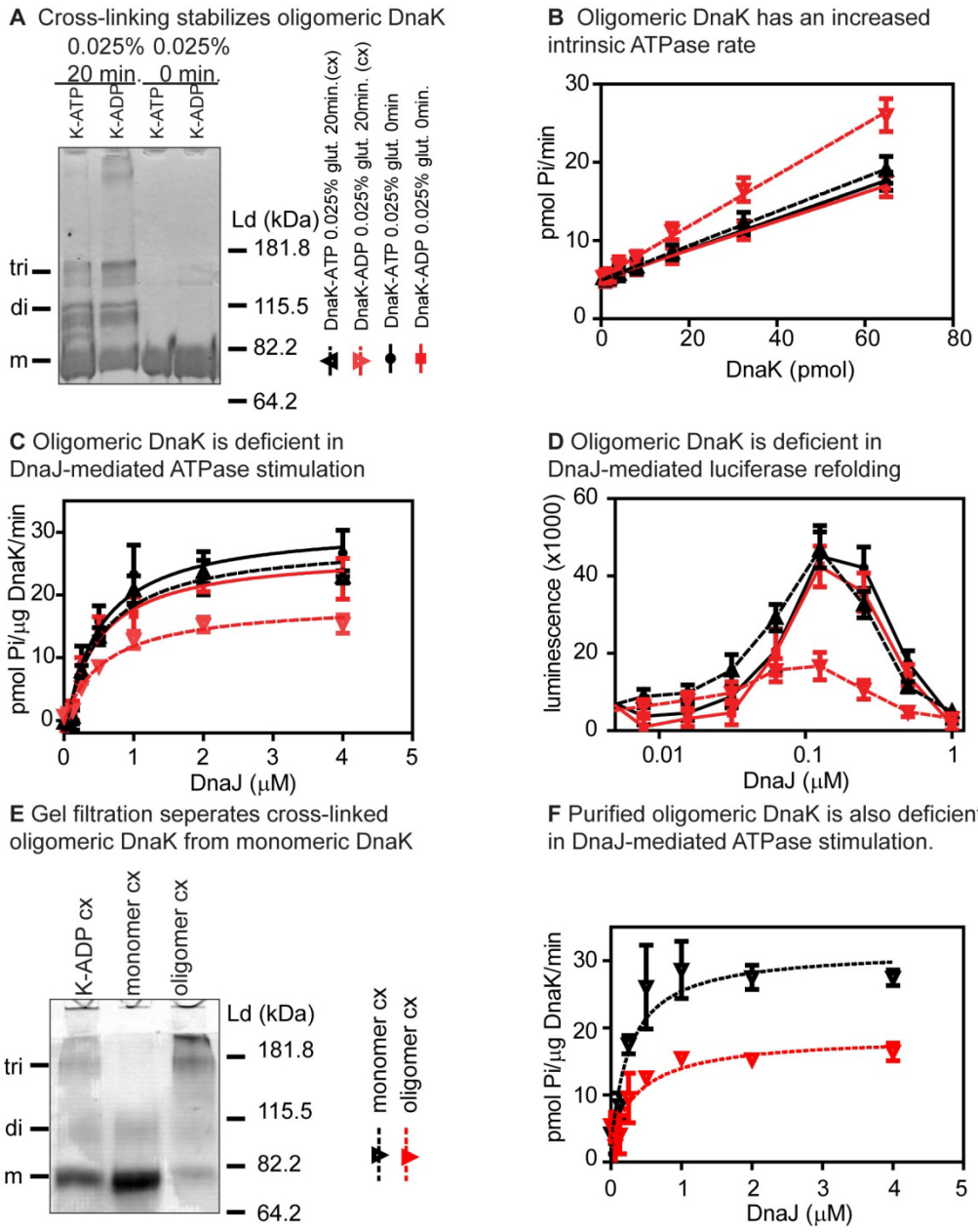

Figure 3.2. Oligomeric DnaK is deficient in "foldase" activity.
(A) Stabilization of DnaK oligomers by chemical cross-linking. DnaK (K) was pre-incubated with either ATP or ADP and treated with 0.025% glutaraldehyde (glut.). Samples were either incubated for 20 min to allow cross-linking (cx) or quenched (0 min) immediately. Bands consistent with monomeric (m), dimeric (di) and trimeric (tri) DnaK were observed, as well as higher-order structures. The gel shown is representative. This cross-linking reaction was performed nine times and quantification of the distribution of total DnaK in all conditions is reported (Appendix 3.5, text). The cross-linked samples were then compared in a variety of assays: (B) intrinsic ATPase rate, (C) DnaJ-mediated ATPase stimulation, and (D) luciferase refolding. A negative control, lacking DnaK, was tested for each experiment and subtracted. The results shown are from a single experiment performed in triplicate and the error bars represent the standard error of the mean. (E) Finally, to asses the validity of performing experiments on complexed mixtures containing monomers, dimers, and higher order oligomers we purified a K-ADP cx sample using gel filtration. Samples were obtained with >80% cx monomer and >80% cx oligomer. (F) We tested these samples for their DnaJ-mediated ATPase stimulation and found results consistent with the results obtained when testing the complexed mixtures.

This study next evaluated whether oligomeric DnaK could still bind a substrate protein, using the well-studied firefly luciferase as a model substrate [29, 37]. In these studies, denatured luciferase was immobilized in microtiter plates and measured the equilibrium binding of DnaK using an anti-DnaK antibody. In the presence of excess ADP, non-cross-linked DnaK binds substrate with an almost ten-fold lower apparent K_D than in the presence of ATP (Appendix 3.6), consistent with the known allosteric link between nucleotide state and substrate affinity. However, in our study, an excess of ATP was utilized in the assay buffer of all tested samples; thus, pre-incubating DnaK with either ATP or ADP during the cross-linking reaction did not greatly affect the apparent affinity

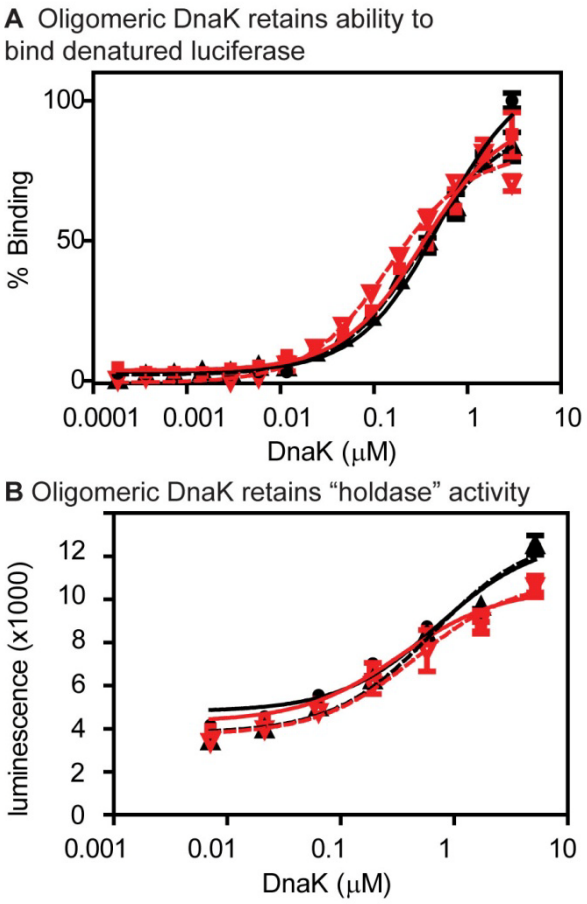

Figure 3.3. Oligomeric DnaK retains "holdase" activity. The same samples and color scheme as described in figure 3.2 were used to evaluate the ability of oligomeric DnaK to bind the model substrate luciferase using two independent assays. (A) An ELISA-like platform to probe the binding of DnaK to denatured luciferase and (B) "holdase" activity to probe the binding of DnaK to unfolding intermediates of luciferase. A negative control, lacking luciferase, was tested for each experiment and subtracted. All of the experiments were performed in triplicate and the error bars represent the standard error of the mean.

(Figure 3.3A, Table 3.1). To our surprise, this method revealed that oligomeric DnaK retained full binding to luciferase (Figure 3.3A, Table 3.1), suggesting that oligomeric DnaK is able to bind substrate proteins. To confirm this conclusion and test whether binding might arise from non-specific interactions that can sometimes be induced by cross-linking, we also tested the substrate-binding activity of the truncated nucleotide-binding domain of DnaK (NBDL). It was found that the untreated NBDL had only a weak non-specific binding (apparent K_D >3 μM) and that this interaction was not changed after cross-linking with 0.025% glutaraldehyde for 20 min (Appendix 3.6). This result supports the conclusion that oligomeric DnaK retains its ability to bind substrate proteins via its SBD.

To confirm this interaction in a different experimental platform, we evaluated the ability of stabilized DnaK oligomers to protect native luciferase from terminal heat denaturation, which is a chaperone function that is commonly called “holdase” activity. In this assay, native luciferase was exposed to elevated temperatures, a process that is sufficient to heat inactivate the enzyme in the absence of chaperone. DnaK is known to limit this terminal denaturation, allowing luciferase to spontaneously reactivate when returned to room temperature. We found that both cross-linked DnaK-ATP and DnaK-ADP retained full “holdase” activity (Figure 3.3B, Table 3.1). Again, cross-linked NBDL was tested under the same conditions and found that it lacked this activity (Appendix 3.6). Furthermore, the DnaK substrate (NRLLLTG) inhibited the “holdase” activity of both cross-linked DnaK-ATP and DnaK-ADP samples (Appendix 3.7). Together, these results suggest that oligomeric DnaK retains the ability to bind substrate proteins through its substrate-

binding domain. Further, these biochemical findings suggest that oligomeric DnaK retains many chaperone functions, including “holdase” ability but that it is functionally distinct from monomeric DnaK because it partially loses some J-stimulated functions.

3.3.5 Multimeric DnaK-ADP is visualized by electron microscopy

In theory, oligomerization of DnaK could result from unfolded monomers being bound as substrates, resulting in relatively disordered multimers. Conversely, these structures could result from the ordered assembly of intact monomers. To better differentiate between these possibilities, DnaK-ADP samples were visualized by electron microscopy (EM) (Appendix 3.8). In doing so, we were able to make several important observations. First, it was observed that monomeric DnaK was readily visible and its two-domain architecture could be resolved, despite its relatively small size (70-kDa). Secondly, numerous structures that appeared to be small, oligomeric forms of DnaK were observed (Appendix 3.8). Importantly, these oligomeric forms were not disordered aggregates; rather, they seemed to represent an ensemble of structurally defined multimers, with sizes roughly corresponding to dimers, trimers, and other small oligomers.

To better understand the protein architectures present in the DnaK-ADP samples, reference-free alignment and classification of 6,090 particle projections into 150 classes was performed (Appendix 3.8). Representative class averages are shown, and these clearly demonstrate the presence of monomeric, dimeric, and small multimeric forms of DnaK (Figure 3.4B). For reference, a ribbon representation of the homology model of DnaK-ATP, based on the yeast Hsp110 (Sse1) crystal structure (PDB: 2QXL) [21], and

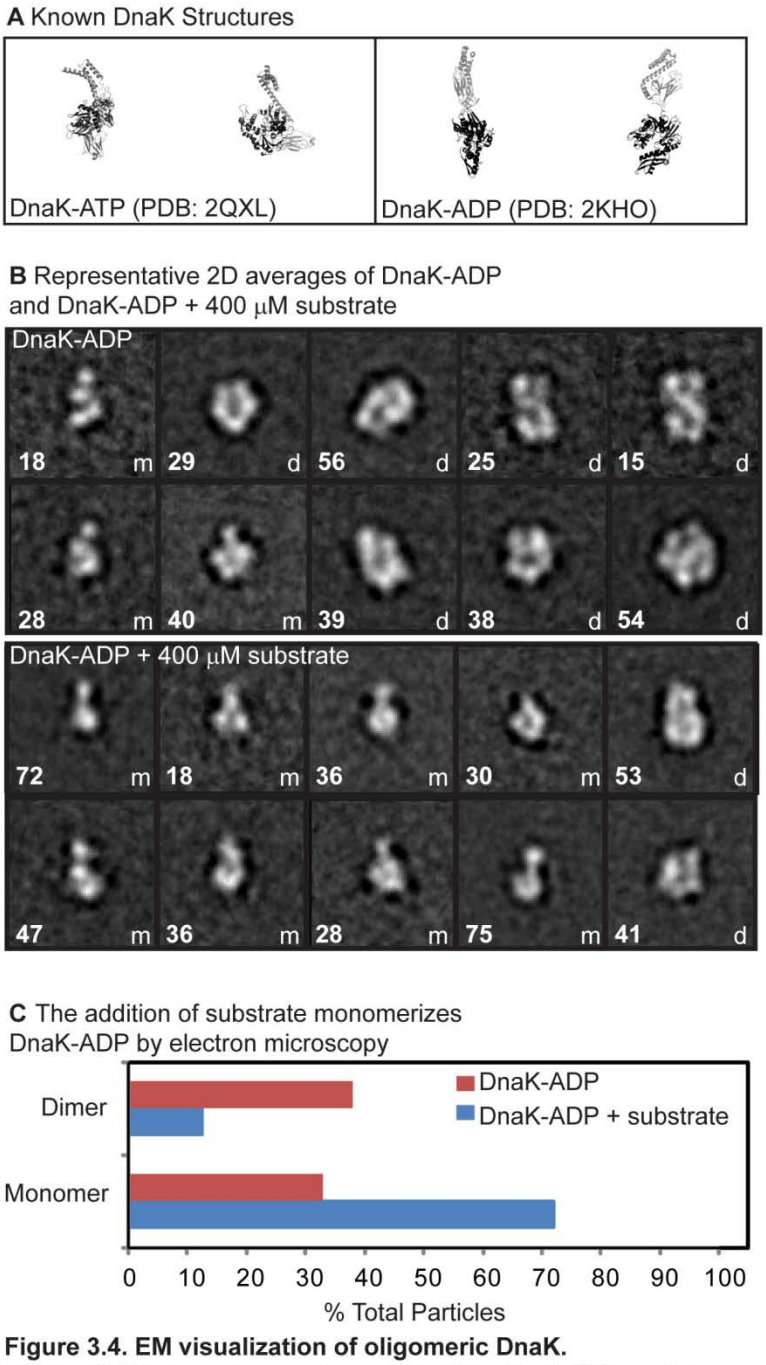

Figure 3.4. EM visualization of oligomeric DnaK.
(A) DnaK-ATP homology model based off the Sse1-ATP crystal structure (PDB: 2QXL) and the DnaK-ADP + substrate NMR structure (PDB: 2KHO) serve as a reference for the EM images. (B) Representative 2D class averages of DnaK-ADP and DnaK-ADP + substrate. The box size is ~27 nm by 27 nm. The number of particles in each class average is shown in the bottom-left of the box, while in the bottom-right we indicate whether the class average was interpreted as monomeric (m), dimeric (d), or oligomeric DnaK greater than dimer (>d). (C) Quantification of the number of dimeric and monomeric DnaK particles reveals that addition of substrate leads to monomerization. Some class averages could not be clearly classified and were therefore left unassigned (see Appendix 3.8 and 3.9 for details).

the monomeric DnaK-ADP structure (PDB: 2KHO) [9] are shown (Figure 3.4A). If the dimeric and oligomeric forms of DnaK that were visualized by EM were similar to those seen in the previous biochemical studies (e.g., gel filtration), one would expected that they would monomerize in the presence of excess peptide substrate. To test this idea, the NRLLLTG peptide substrate (400 μM) was added, 6,098 particles were collected, and, as previously described, reference-free alignment and classification into 150 classes was applied (Appendix 3.9). As expected, a dramatic increase in the number of particles classified as monomers was observed as well as a corresponding decrease in those classified as dimers (Figure 3.4B and C, Appendix 3.8, and Appendix 3.9). Thus, we conclude that reversible multimers of DnaK are assembled from individual, folded monomers.

3.4 Discussion

Oligomerization of DnaK and other Hsp70s has been observed *in vitro* and in cellular studies [23, 24, 26, 30, 39]. However, the possible roles of these oligomers have not been clear. One hypothesis is that oligomeric DnaK may represent an inactive pool that can be rapidly monomerized and activated when needed. However, this model had not been directly tested. Furthermore, the structure of these oligomers was not clear, and so it was not certain if they were assembled from folded or unfolded monomers. Herein, we aimed to better understand nucleotide-dependent changes in DnaK oligomerization to clarify the possible roles of these structures within the chaperone cycle.

3.4.1 DnaK oligomerization *in vivo*

One of our questions was whether DnaK oligomers are present in cells and whether any common stresses might influence their relative abundance. Using gel filtration and native gel electrophoresis on *E. coli* lysates, bands consistent with monomeric, dimeric, and trimeric forms of DnaK were observed under resting conditions (Figure 3.1C). It is possible that these bands could represent DnaK–substrate complexes, but the repeating separation values of 70 kDa suggest that these bands are homo-multimers. Interestingly, oligomeric DnaK levels increased in response to heat stress (Figure 3.1C). This result is consistent with previous work on human cells, where the stress inducible Hsp70 isoform (Hsp72) and the constitutively active isoform (Hsc70) have been found to form oligomeric structures in response to heat stress [24]. Thus, we conclude that DnaK, like other Hsp70s, samples both monomeric and oligomeric forms *in vivo*.

A variety of mechanisms could explain the increase in oligomeric DnaK in response to heat stress. For example, heat stress is known to increase expression of this chaperone [31]; thus, a simple model is that increases in protein concentration lead to enhanced oligomerization. Consistent with this idea, overexpression of DnaK increases oligomerization (Appendix 3.3). Another explanation is that heat stress might change the ratio of ATP and ADP bound DnaK. At high temperatures, the co-chaperone GrpE is known to be partially unfolded and become less active [40-42]. Because GrpE normally catalyzes ADP release, its inactivation might be expected to favor accumulation of the ADP bound state. In what could be a related finding, it has also been shown that the human ER resident Hsp70, BiP, self-oligomerizes in response to glucose deprivation

[30]. Glucose deprivation depletes cellular ATP, and thus, these conditions might also be expected to promote the ADP bound (or nucleotide free) conformation. However, an increase in DnaK oligomerization was not observed under hydrogen peroxide-induced oxidative stress or during stationary phase (Appendix 3.3). Much like glucose deprivation, both of these stress conditions increase the expression of DnaK and deplete cellular ATP [4, 6, 34, 35, 43, 44]. Clearly, further work is required to fully understand the mechanism by which oligomeric DnaK increases in response to heat stress.

It is important to note that DnaK oligomerization in response to specific types of oxidative stress has been well characterized by Jakob and colleagues [6, 45, 46]. In response to a combination of heat stress and hypochlorous acid, they found that DnaK becomes oligomeric and inactivated in a reversible fashion. At the same time, Hsp33 is activated, and this chaperone becomes responsible for cellular protection. Thus, in response to these stress conditions, *E. coli* clearly inactivates DnaK and transitions to an Hsp33- based protection mechanism. This study focused instead on different stress conditions, namely, heat stress alone or hydrogen peroxide treatment under normal growth temperatures, which are known to activate the DnaK chaperone system and, moreover, rely on its molecular chaperone activity to maintain viability [4, 6]. This approach was utilized in an effort to understand potential differences in the way that DnaK responds to stresses that have distinct requirements for its activity. Combined with the findings of the Jakob group, the results suggest that DnaK may be able to form multiple types of oligomers, some of which have partial activity while others do not. Taking this conclusion further, the increase in oligomerization observed during heat

shock may confer a selective advantage (under some conditions) by creating an active form possessing distinct chaperone activities from the monomer.

3.4.2 DnaK oligomers are small, defined multimers

A major goal of this effort was to determine whether oligomeric DnaK was a product of non-specific interactions or whether these higher molecular weight structures represented oligomeric states assembled from well-behaved and properly folded monomers. Electron microscopy has recently been applied to the study of other Hsp70-related processes [47-49]. Therefore, it seemed possible that this method could be used to explore DnaK oligomer structures, despite their small size. In these experiments, it was found that, for most of the monomeric DnaK particles, the two-domain architecture is clearly present. Moreover, DnaK-ADP samples contained small, defined oligomers (see Figure 3.4). It was also found that monomers could be released from the oligomers by substrate, suggesting a dynamic exchange between monomers and discrete multimers. Together, these findings are supportive of multimers being composed of individual folded monomers. In further support of this idea, cross-linked DnaK-ADP samples retained ATPase and "holdase" activity, which is expected of functional monomers assembled into multimers.

3.4.3 DnaK oligomers are functional "holdases" but inactive "foldases"

Another major question is whether DnaK oligomers retain any of the chaperone functions of the well-studied monomer. This question is important because the current models for ATPase cycling and chaperone activity do not take into account any change in DnaK's

oligomerization, yet it appears to form in cells. In fact, it was assumed that the oligomers may serve as a reservoir of inactive chaperone. To test this idea, a number of chaperone functions were evaluated *in vitro* and it was found that DnaJ could not stimulate DnaK oligomers in either ATPase assays (see Figure 3.2C) or luciferase refolding experiments (see Figure 3.2D). However, DnaK oligomers retained many other chaperone functions, such as stimulation by GrpE. Furthermore, it retained the ability to bind luciferase and protect it from terminal heat denaturation ("holdase" activity). Consistent with this finding, oligomeric DnaK is known to bind lambda P [22], and oligomeric BiP still binds its peptide substrates [39]. Furthermore, while studying pre-steady state kinetics, Farr and Witt [50] observed results consistent with the formation of an oligomeric DnaK–peptide complex. Although one can never fully exclude the possibility of cross-linking artifacts, our results and these previous studies [22, 39, 50] support the idea that oligomeric DnaK is capable of binding to substrate proteins. Thus, we hypothesize that oligomerization largely converts DnaK from a co-chaperone dependent "foldase" to a co-chaperone independent "holdase" (Figure 3.5).

This finding could have an important impact on the field's understanding of DnaK biology because, under heat stress conditions, the enzyme might be required to predominately act in a "holdase" capacity until conditions improve. Such a model would be consistent with oligomerization providing a selective advantage under conditions of heat stress.

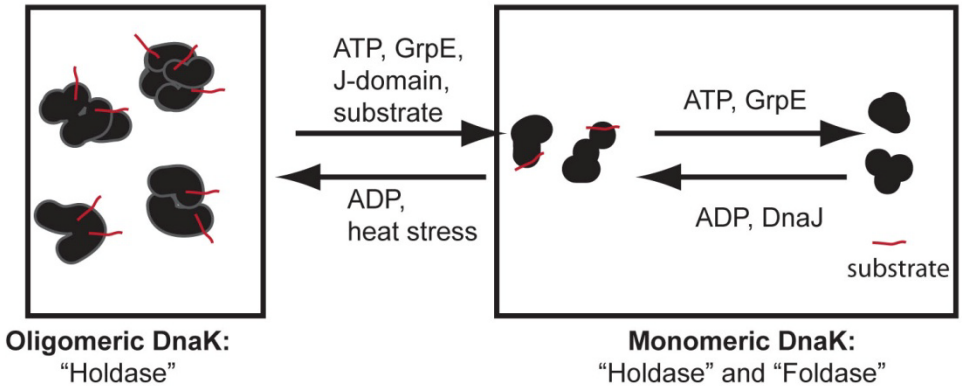

Figure 3.5. Proposed model of the DnaK chaperone cycle.
Oscillation of DnaK between its ATP- and ADP-bound states, in collaboration with DnaJ and GrpE, has been shown to be required for iterative substrate binding and refolding. In addition to this well-known cycling, our data shows that DnaK-ADP additionally samples multimeric structures, discussed in detail within the text. These oligomers are biochemically distinct from monomers because they have a limited "foldase" activity while maintaining "holdase" activity. We speculate that DnaK oligomers are an active part of the chaperone cycle.

3.4.4 DnaK is structurally heterogeneous

Recent NMR studies have suggested that the NBD and SBD of DnaK sample a number of relative orientations in the ADP + peptide state [9]. Consistent with this idea, the two domain structure of DnaK was successfully visualized by EM (Figure 3.4B) and the domains are present in a variety of relative orientations (e.g. some DnaK molecules were elongated, whereas others were compact and more reminiscent of the Hsp110 crystal structure [21]). Although some of this diversity could certainly be attributed to stain drying artifacts or deformations on the carbon support of the EM grid, recent studies using EPR and FRET have also observed multiple inter-domain conformations of Hsp70s in both the ATP and ADP bound state [51, 52]. Moreover, the work of Schlecht *et al.* [52] further highlights the functional importance of this conformational heterogeneity. They found that DnaK adopts a variety of open and closed forms that permit flexibility during binding to substrate proteins with different topologies. Thus, a recurring theme is that Hsp70-class chaperones sample a variety of possible conformations. Although their

substrates, co-chaperones, and nucleotide ligands can shift this balance, they rarely trap the chaperone in a uniform state. For DnaK, our results suggest that this structural heterogeneity should further include allowances for formation of higher ordered multimers.

3.4.5 DnaK oligomerization interface and its potential for small molecule modulation

The EM work has clearly demonstrated that oligomeric DnaK has a defined architecture made up of intact monomers. Furthermore, these oligomers retain some chaperone activities, including substrate binding, while losing the ability to refold substrates or be stimulated by the co-chaperone DnaJ. Thus, we postulate that oligomeric DnaK is formed via a definable interaction surface that could potentially be exploited to regulate chaperone activity. For example, promoting oligomerization of human Hsp70s might block some chaperone functions, perhaps rendering cancer cells more susceptible to apoptosis [53].

However, what is the nature of this interface for oligomerization? Although molecular structures have remained elusive, previous work and our studies provide some clues. For example, Ladjimi and colleagues found that the SBD, but not the NBD, of a human Hsp70 retains the ability to oligomerize [28, 54]. Other evidence also points to the SBD being the major site of inter-monomer contacts in BiP [55]. Interestingly, deletion of the 10-kDa C-terminus of Hsp70 does not affect oligomerization [56], suggesting that the entire SBD is not required. The fact that oligomerization seems to be primarily mediated through the SBD, along with the observation that many of the factors that promote

monomerization also promote peptide release, has appropriately lead to the hypothesis that DnaK oligomerization may be mediated through the substrate binding pocket [28, 54]. However, several groups have demonstrated that oligomeric DnaK can still bind substrates [22, 39, 50], suggesting that any SBD-mediated interface must leave a free substrate-binding region available in at least one DnaK molecule within the oligomer. In support of this model, our results again demonstrate that oligomeric DnaK is still able to bind substrate (see Figure 3.3). This result suggests that some of the substrate-binding pockets within DnaK oligomer are left unoccupied. Further work is required to define the interface(s), but these results suggest that this contact surface might be a good place to target with chemical probes. Recent success by other members of the Gestwicki laboratory in targeting protein–protein interfaces in the chaperone complex support this idea [57, 58].

3.5 Experimental procedures

3.5.1 Materials

Reagents utilized throughout this study were obtained as follows: ATP-agarose column (Sigma, St. Louis, MO, USA), NRLLLTG peptide (University of Michigan Peptide Core) [59], luciferase, and Steady-Glo Reagent (Promega, Madison, WI, USA). The optical density and luminescence measurements were performed using a SpectraMax M5 multimode plate reader (Molecular Devices, Sunnyvale, CA, USA).

3.5.2 Plasmids and protein purification

Wild-type *E. coli* DnaK, the DnaK mutant T199A, *E. coli* DnaJ and *E. coli* GrpE were purified as previously described [60]. When eluting DnaK from the ATP-agarose column,

samples to be tested in the ADP bound state were eluted using ADP. All proteins were concentrated and exchanged into EM buffer [25 mM HEPES buffer pH 7.4, 20 mM KCl (150 mM KCl for DnaJ), 5 mM $MgCl_2$] and stored at −80°C until use. DnaK to be used for EM was never frozen and further purified by Superdex 200 gel filtration column (GE Healthcare, Piscataway, NJ, USA). DnaK NBDL (residues 1–392) was purified by the same approach. The nucleotide state of DnaK was established by pre-incubating with either 1 mM ATP or ADP for 30 min at 4°C, which gave the expected change in tryptophan fluorescence (Appendix 3.1).

3.5.3 Gel filtration

Samples were prepared with 14 μM DnaK (unless otherwise indicated), 1 mM nucleotide, and the indicated amount of NRLLTG (NR) peptide, J-domain, or GrpE in EM buffer. Samples were allowed to equilibrate at 4°C for >30 min. A sample of 300 μL was separated into fractions (1 mL) using a Superdex 200 gel filtration column (GE Healthcare, Piscataway, NJ, USA) in EM buffer at a flow rate of 0.6 mL/min. Absorbance at 285 nm was monitored and normalized according to the nucleotide peak to control for variations in injection volumes. Gel electrophoresis For denaturing gel electrophoresis, samples were denatured with 3× sodium dodecyl sulfate (SDS) denaturing loading dye (1×: 80 mM Tris–HCl pH 6.8, 10% v/v glycerol, 5.3% v/v β-mercaptoethanol, 2% w/v SDS, 0.01% w/v bromophenol blue) and heating to 95 °C for 2 min. Samples were then separated for 1 h at 200 V using a 10% SDS-PAGE gel. For native gel electrophoresis, samples were prepared by adding 3× native loading dye (1×: 80 mM Tris–HCl pH 6.8, 10% v/v glycerol, 0.01% w/v bromophenol blue). Samples

were separated for 4–6 h at 120 V and 4°C using a 4–20% Tris–HCl native gel (Biorad, Hercules, CA, USA) in Tris–acetate running buffer (30 mM Tris–HCl pH 8.0, 0.1% v/v acetic acid, 1 mM EDTA).

3.5.4 Monitoring DnaK oligomerization in lysates

W3110 cells were grown to mid-log phase at 30 °C in Luria–Bertani (LB). Cells were then either left at 30 °C in LB or subject to a specific stress for 1 h. Heat stress conditions were achieved by moving the mid-log phase culture to 43°C [5]. Oxidative stress was applied with the addition of 4 mM H_2O_2 [4, 6]. To probe the effect of DnaK over-expression, Δ*dnak* (DE3) cells transfected with wild-type DnaK under a T7- promoter were utilized [57]. Cells were grown to mid-log phase at 30°C, and DnaK expression was induced by isopropyl β-D-1-thiogalactopyranoside for 1 h. Following growth, cultures were immediately moved to an ice-water bath (4°C) and diluted to have an absorbance at 600 nM (A_{600}) of 0.4 and pelleted. Cells were lysed by resuspending the pellet in 500 µL of lysozyme reaction buffer [1 mg/mL lysozyme in 50 mM Tris–HCl pH 8.0, 2 mM EDTA, 200 µM phenylmethanesulfonylfluoride (PMSF)] for 30 min at 4°C, followed by the addition of 500 µL of 2× DNAase I reaction buffer (60 µg/mL DNAse I, 50 mM Tris–HCl pH 8.0, 4 mM $MgCl_2$, 12 mM $CaCl_2$, 200 µM PMSF). After 10 min, cells were sonicated using a microtip (ThermoFisher Waltham, MA, USA) at 60% for 20 s. Cell debris was pelleted by centrifugation at 13.2 rpm for 15 min, and the resulting supernatant was passed through a 20-µm filter. Lysates were subsequently analyzed as described above. For the Western blots, gels were transferred to 0.2 µm Protran nitrocellulose (Whatman, Piscataway, NJ, USA). The membrane was blocked with 5%

w/v milk in TBS-T (25 mM Tris–HCl pH 7.4, 140 mM NaCl, 0.1% Tween 20) and probed with 1:500 mouse monoclonal anti-DnaK antibody (Assay Designs/Enzo Life Sciences, SPA-880F, Plymouth Meeting, PA, USA) followed by an horseradish peroxidase (HRP)-conjugated goat anti-mouse IgG (Anaspec, 28173, Fremont, CA, USA). Western blots were developed using the Western Lightning Plus-ECL kit according to the manufacturer's protocol (PerkinElmer, Waltham, MA, USA).

3.5.5 Cross-linking

Samples were prepared with 14 μM DnaK (or DnaK NBDL) and 1 mM nucleotide in EM buffer and allowed to equilibrate at 4°C for >30 min. Samples were then moved to room temperature and 0.025% v/v glutaraldehyde in EM buffer was added to each. The reactions were quenched by addition of 100 mM glycine (pH 8.0). This quenching step was either performed immediately (for the control samples) or after incubating the solutions for 20 min at room temperature. To evaluate the cross-linking efficiency, 10 μL of each sample was evaluated by denaturing gel electrophoresis as described above. Furthermore, cross-linked samples were consistently tested for activity in DnaJ-mediated ATPase stimulation as a quality control measure. When testing these samples in the biochemical assays, they were diluted into assay buffer containing 1 mM nucleotide. Each biochemical assay was carried out on at least two independently cross-linked samples. The results depicted in Figures 3.2 and 3.3 are from a single, representative experiment performed in triplicate. The values reported in Table 3.1 were obtained by fitting the results from all replicates.

3.5.6 ATPase activity

This procedure was adapted from a previously described protocol [61]. Briefly, the final concentration of DnaK was 0.5 μM, unless otherwise noted. In each experiment, the signal from non-specific ATP hydrolysis in a control lacking DnaK was subtracted. In testing GrpE stimulation, 0.5 μM DnaK was tested in the presence of 0.5 μM DnaJ and 200 μM NRLLLTG peptide. DnaJ, NRLLLTG, and GrpE stimulation curves were evaluated by fitting the data using a hyperbolic fit with a non-zero intercept. The non-linear fit was performed using GraphPad Prism version 5.0 for Windows (GraphPad Software San Diego, CA, USA). For clarity, graphs in Appendix 3.5 were transformed to obtain a zero y-intercept for all samples.

3.5.7 Luciferase binding

The procedure for DnaK binding to luciferase was adapted from a previous report [62]. Briefly, firefly luciferase (61.3 μM) was denatured by incubation with 6 M GuHCl for 1 h at room temperature and diluted to 100 nM for storage. Aliquots (50 μL) were added to each well of 96-well plates (Thermo Fisher, clear, nonsterile, flat bottom, Waltham, MA, USA), and these plates were then incubated for 2 h at 37°C. The wells were washed with 150 μL of TBS-T (3×3 min, rocking). To these wells, 50μL of a DnaK or DnaK NBDL solution (at indicated concentrations) in binding buffer (25 mM HEPES pH 7.2, 150 mM NaCl, 20 mM KCl, 5 mM $MgCl_2$) with 1 mM ATP was added to each well and allowed to bind at room temperature while rocking overnight. After washing (3×3 min, rocking) with TBS-T, 5% w/v milk in 100 μL of TBS-T was added to each well for 5 min. Next, the primary antibody was added (1:5,000 dilution of rabbit anti-DnaK (Abcam, ab80161,

Cambridge, MA, USA) in TBS-T, 50 μL/well), and the plates were incubated for 1 h at room temperature. Wells were again washed with TBS-T, followed by addition of the secondary antibody [1:5,000 dilution HRPconjugated goat anti-rabbit (Anaspec, 28177, Fremount, CA) in TBS-T, 50 μL/well], and the plates were incubated for 1 h at room temperature. Finally, wells were washed one last time with TBS-T (3×3 min, rocking) and developed for 2 min using a TMB substrate kit (Cell Signaling Technology, Danvers, MA, USA). The absorbance was measured at 450 nM. In each experiment, the signal from non-specific binding of DnaK to empty control wells was subtracted. Binding curves were fit using hyperbolic fit with a non-zero intercept with GraphPad Prism version 5.0 for Windows (GraphPad Software, San Diego, CA, USA).

3.5.8 Luciferase "holdase" assay

"Holdase" activity was evaluated as described with minor changes [60]. The final concentrations per well were 0.016 μM luciferase and 1 mM ADP. After the reaction mixture was heated to 39.5°C for 8 min, 10 μL of the samples were transferred into 96-well, opaque white assay plate (Thermofisher, Waltham, MA, USA) and then 10 μL of 5% v/v SteadyGlo reagent in 50 mM glycine buffer (30 mM MgSO4, 10 mM ATP, and 4 mM dithiothreitol, pH 7.8) was added into each well. Results were again fit using a hyperbolic fit with a non-zero intercept.

3.5.9 Luciferase refolding assay

Luciferase refolding activity was evaluated as described with minor changes [38]. The final concentrations were 1 μM DnaK, 100 nM denatured luciferase, and 1 mM ATP.

After 1 h of incubation at 37°C, 14 μL of 2% v/v SteadyGlo reagent was added into each well, and the luminescence was measured. For each experiment, the signal from a negative control containing everything, but DnaK was subtracted.

3.5.10 Electron microscopy

Samples were prepared containing 14 μM DnaK, 1 mM ADP, with/without 400 μM NRLLTG peptide (substrate), and allowed to equilibrate at 4°C for >30 min. Samples were then separated using a Superdex200 gel filtration column in EM buffer as described above. A fraction from between 13.8 and 14.0 mL was collected and immediately prepared for EM using a conventional negative staining protocol [63]. Briefly, eluted fractions were diluted 100× into EM buffer containing 1 mM ADP or 1 mM ADP + 400 μM substrate, as indicated, and 2 μL of the sample was adsorbed to a glow discharged carbon-coated copper grid (Electron Microscopy Sciences, Hatfield, PA, USA) and stained with 0.75% uranyl formate (Polysciences Inc, Warrington, PA, USA) solution. Samples (see Figure 3.4, Appendix 3.8, and Appendix 3.9) were imaged at room temperature with a Tecnai T12 electron microscope equipped with a LaB6 filament and operated at an acceleration voltage of 120 kV. Images were recorded on a Gatan 4×4 k pixel charge-coupled device camera using low-dose procedures at a magnification of ×52,000 and a defocus value of about–1.5 μm. The images were binned (2×2 pixels) to obtain a pixel size of 4.16 Å on the specimen level, and particles were manually excised using Boxer (part of the EMAN 1.9 software suite;[64]. 2D analysis of DnaK-ADP and DnaK-ADP + 400 μM substrate were carried out using the SPIDER image processing suite [65]. For the 2D analysis of DnaK-ADP, were interactively selected particles

windowed into 64×64 pixel images. A total of 6,313 particles from 49 images were subjected to ten cycles of reference-free alignment specifying 150 classes. Based on the first classification, a heterogeneous sample was observed containing monomeric two-lobe particles of DnaK, small more compact monomeric particles, dimeric assembles of DnaK, and some higher ordered assembles of DnaK (Appendix 3.8). Next, only the particles that were well resolved were selected, removing 223 particles. The remaining 6,090 particles were subjected to a second reference-free alignment to improve their classification (Figure 3.4, Appendix 3.9). For the 2D analysis of DnaK-ADP + 400 μM substrate, the same procedure was followed. A total of 6,689 particles were selected from 84 images, excluding underrepresented large oligomers (Appendix 3.9, arrow) and initially subjected to ten cycles of reference-free alignment specifying 150 classes. Based on this first classification, an increase in monomeric DnaK species was observed as compared to the DnaK-ADP sample (Appendix 3.9). Poorly resolved particles or larger (Appendix 3.9, arrow) underrepresented species (591 particles in total) were removed. The remaining 6,098 particles were subjected to a second multi-reference alignment to improve their classification (Figure 3.4, Appendix 3.9). The number of particles belonging to each class as well as whether that class was interpreted as a monomer (m), dimer (d), assembly larger than a dimer (>d), or ambiguous (−) is recorded in Appendix 3.8 and 3.9.

Notes

This work has been published as “Visualization and functional analysis of the oligomeric states of Escherichia coli heat shock protein 70 (Hsp70/DnaK).” **2012** *Cell Stress and Chaperones.* 17:313-327 doi: 10.1007/s12192-011-0307-1. The original publication is

available at www.springerlink.com. Andrea D. Thompson and Jason E. Gestwicki designed the experiments. Andrea D. Thompson conducted the experiments. Steffan M. Bernard assisted with some of the gel filtration experiments. Georgios Skiniotis provided guidance and expertise in electron microscopy and structural analysis. Min Su provided training in electron microscopy and Brinae Bain assisted in the “holdase” assay. We would also like to thank Erik Zuiderweg and Ursula Jacob for helpful comments.

3.6 Appendix

3.6.1 Protein purification and nucleotide state validation.

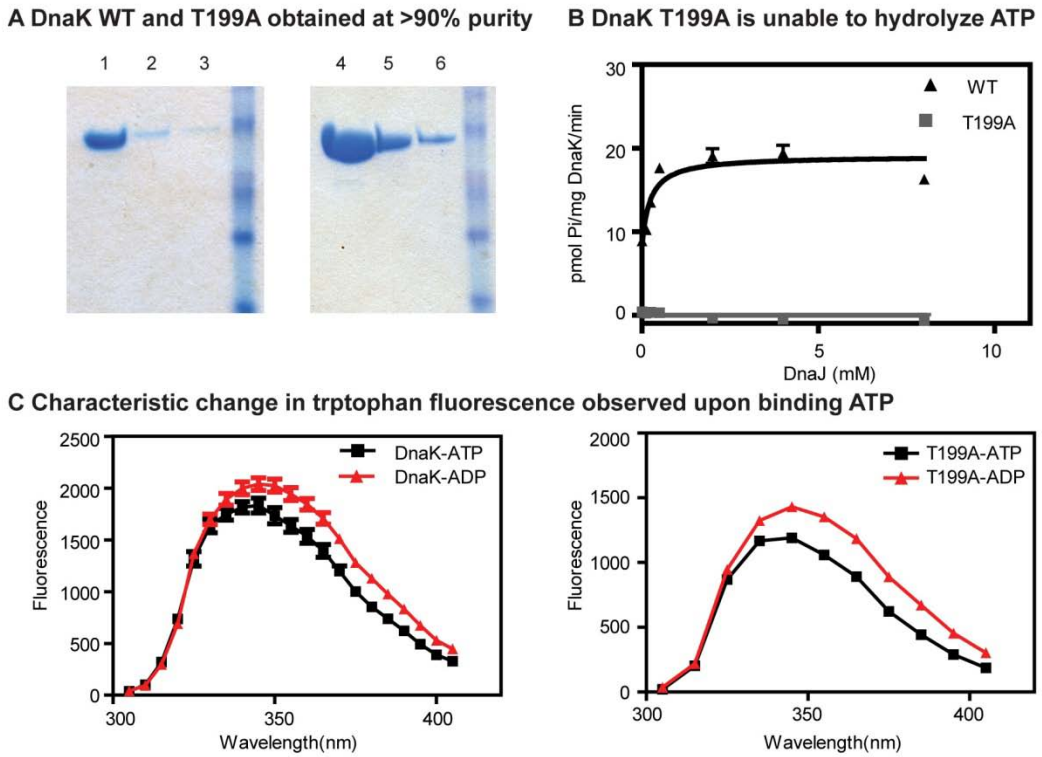

Appendix 3.1 Protein Purification and nucleotide state validation (A) A representative preparation of DnaK wild type is shown; lanes 1, 2, and 3 contain 1, 0.2, and 0.1 μg of DnaK respectively, and demonstrate > 90% purity. Likewise,lanes 4,5, and 6 contain 7, 3.5, and 0.7 μg of DnaK T199A respectively, and demonstrate >90% purity. (B) The DnaJ-mediated stimulation of DnaK's ATPase activity is shown for wild-type DnaK (WT) and a mutant DnaK (T199A), unable to hydrolyze ATP. (C) By tryptophan fluorescence, treatment of either DnaK WT or T199A with 1mM ATP or ADP for 30 minutes on ice resulted in the characteristic quenching of tryptophan fluoresence expected for the ATP-bound state.

3.6.2 Reproducibility of gel filtration (GF) and native gels characterizing nucleotide dependent changes in DnaK homo-oligomerization.

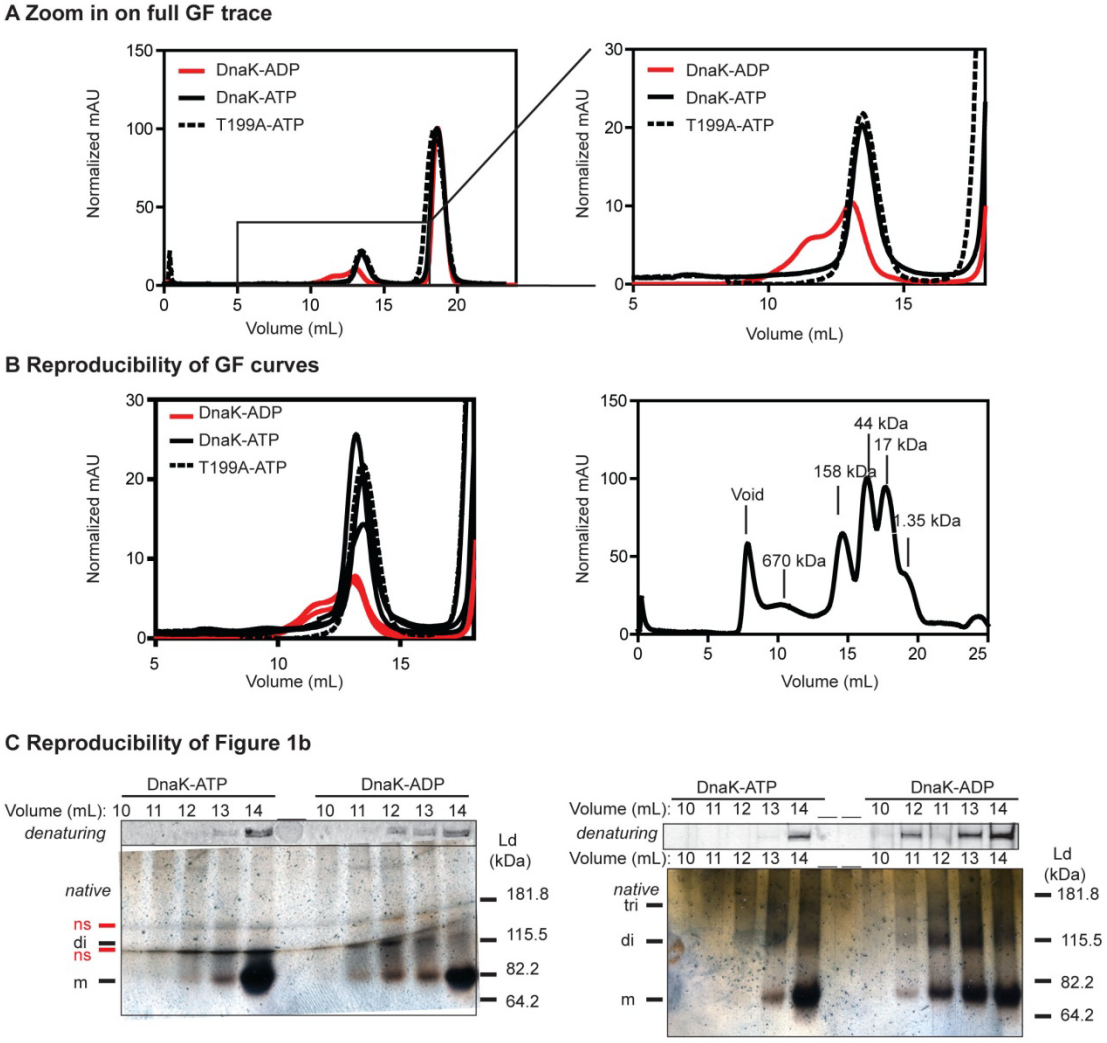

Appendix 3.2 Reproducibility of gel filtration (GF) and native gels characterizing nucleotide dependent changes in DnaK homo-oligomerization.

(A) A view of the full gel filtration (GF) trace from the experiment depicted in Figure 3.1 is provided. The box indicates the zoomed-in portion that is represented to the right and in Figure 3.1. Just to the right of the zoomed-in portion is the major peak created by elution of nucleotide. This peak was used to normalize the mAU and control for any variations in the amount of sample injected onto the column. (B) Gel filtration (GF) curves of DnaK-ADP, DnaK-ATP were performed in triplicate. Samples were prepared using 14μM DnaK and 1mM nucleotide in EM buffer and equilibrated for greater than thirty minutes. Gel filtration was performed on a Superdex 200 column (standard curve shown) using a flow rate of 0.6 ml/min. (C) Gel electrophoresis analysis of the GF fractions was performed in triplicate (see Figure 3.1). Denaturing and native gel electrophoresis was performed on one mL fractions,collected as they eluted from the Superdex 200 gel filtration column. Denaturing and native gels were visulaized by coomassie blue and silver stain respectively. Monomeric (m), dimeric (di), trimer (tri) DnaK is indicated for each native gel. Further in one experiment nonspecific (ns) bands from silver staining contaminated our gel.

3.6.3 Reproducibility of changes in observed DnaK-oligomerization within *E. coli*

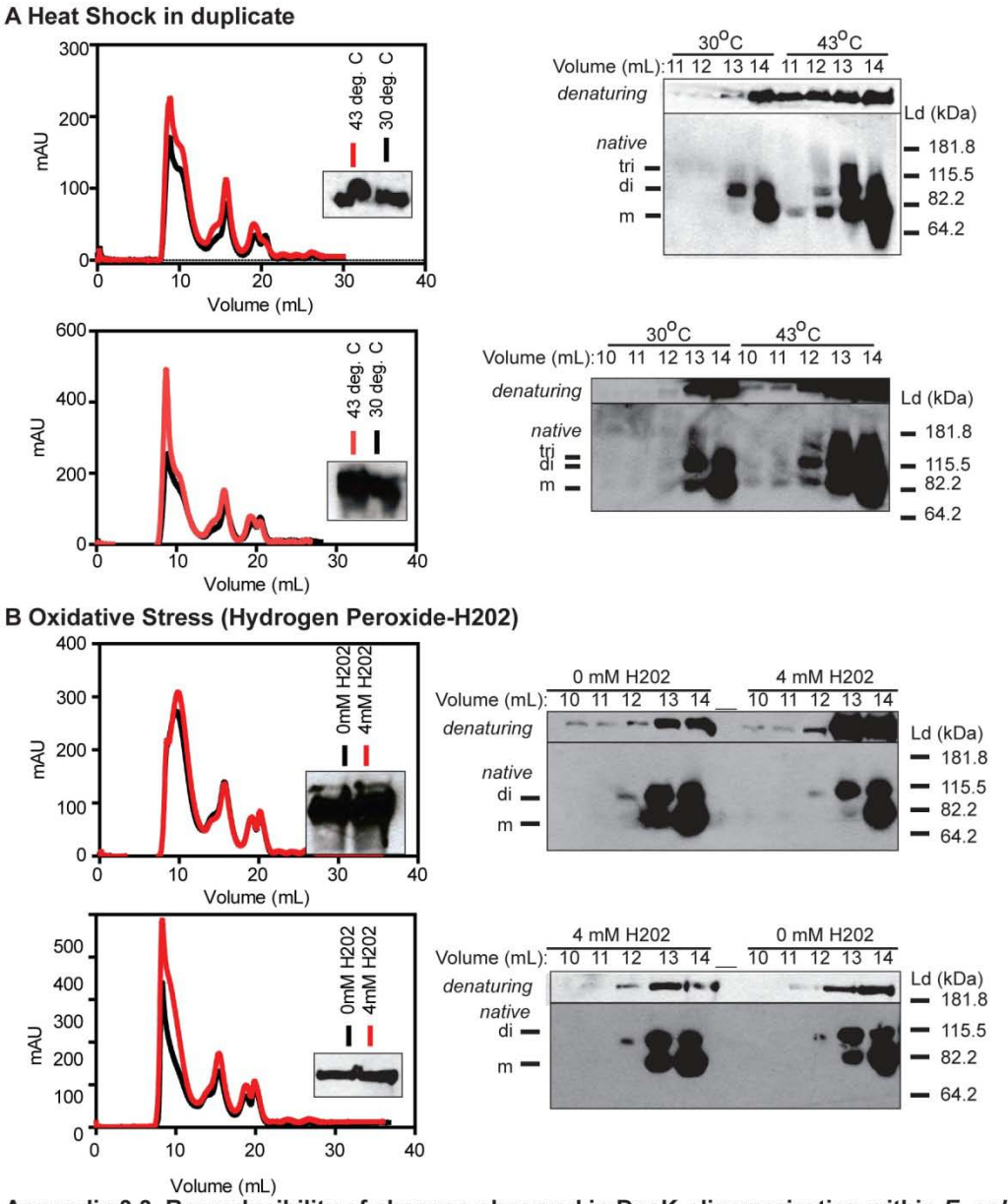

Appendix 3.3 Reproducibility of changes observed in DnaK-oligomerization within *E. coli*. (A) Gel filtration curves of cellular lysates are shown to represent the total protein present in the cellular lysate tested. The gel insert depicts western blot analysis of the amount of DnaK present within total cell lysate by denaturing gel electrophoresis. Both denaturing and native gel electrophoresis were performed on fractions collected from gel filtration (as in Figure 3.1). DnaK was probed by western blot. Heat shock resulted in an increase in DnaK present in earlier fractions. Further bands consistent with the molecular weight of trimeric (tri), dimeric (di), and monomeric (m) DnaK were observed by native gel. The top sample depicts the experiment shown in Figure 3.1, and the bottom sample depicts a duplicate experiment. (B) Likewise the effect of oxidative stress, using hydrogen peroxide (H202), on DnaK self-oligomerization was tested. No change in oligomerization was observed under these condtions.

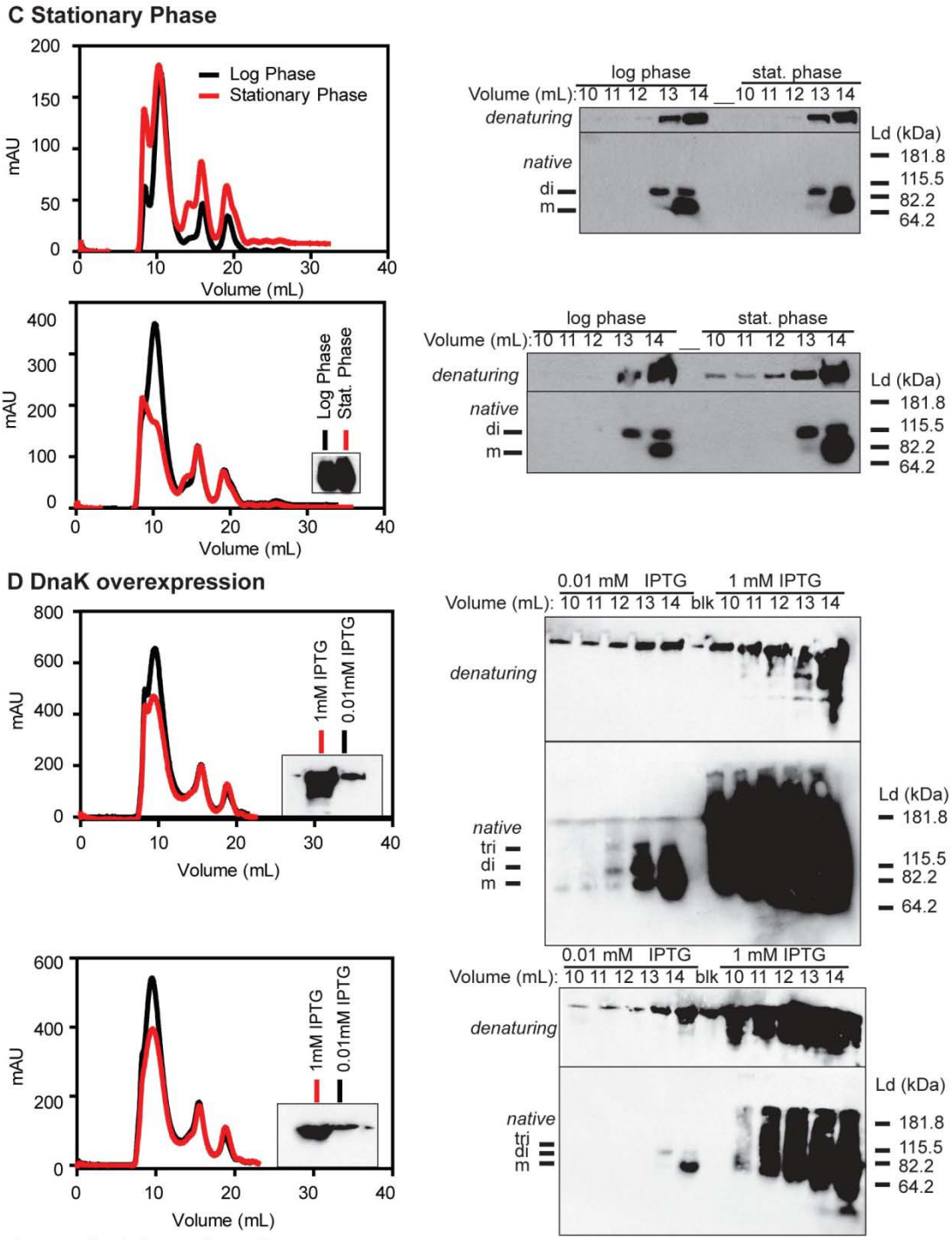

Appendix 3.3 continued

Simular experiments were performed to probe the effect on stationary phase (C) and over-expression of DnaK (D) on DnaK self-oligomerization. In (D) an Δ*dnaK* (DE3) cell line was utilized. 0.01 mM IPTG was used to be representative of natural levels of DnaK and 1 mM IPTG was utilized to probe the effects of over-expression of DnaK on self-oligomerization. No increase in self-oligomerization was observed as a result of stationary phase. However, a dramatic increase in DnaK present in early fractions was observed when DnaK was over-expressed. This is suggestive of increased oligomerization.

3.6.4 Co-chaperones and substrate monomerize DnaK-ADP.

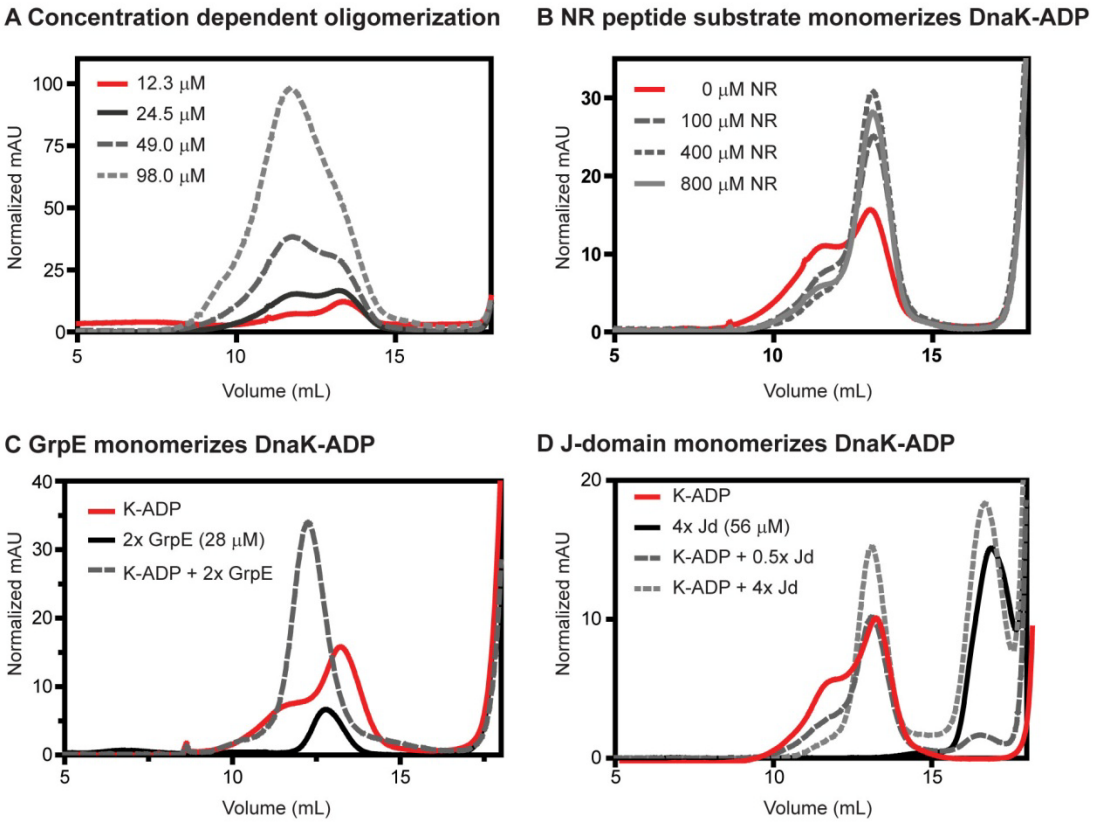

Appendix 3.4 Co-chaperones and substrate monomerize DnaK-ADP
(A) DnaK oligomerization is concentration dependent. Gel filtration was performed using increasing concentrations of purified DnaK with 1 mM ADP. Addition of either NRLLLTG peptide substrate (B), GrpE (C), or the J-domain of DnaJ (Jd) (D) lead to monomerization of 14 μM DnaK-ADP (K-ADP). In the case of GrpE, DnaK forms a complex with the dimeric GrpE, giving a single symmetrical peak. It is interesting to note that full length Ydj1, a yeast DnaJ homolog, has been shown to induce DnaK oligomerization in the presence of ATP but not ADP (36). However, this oligomerization resulted in higher order species than observed in the ADP bound state of DnaK. Thus, King et al. proposed that Ydj1 promoted DnaK self-assembly by utilizing the substrate binding capabilities of Ydj1 to present one DnaK to another, as DnaJ typically presents another client protein to DnaK. Our data shows that the J-domain of DnaJ promotes the monomerization of K-ADP (D). This result supports the proposed model of King et al. and suggests that the self-oligomerization promoted by the ADP bound state is distinct from the self-oligomerization promoted by DnaJ in the presence of ATP.

3.6.5 Examining the ability of co-chaperones to stimulate the ATPase rate of oligomeric DnaK.

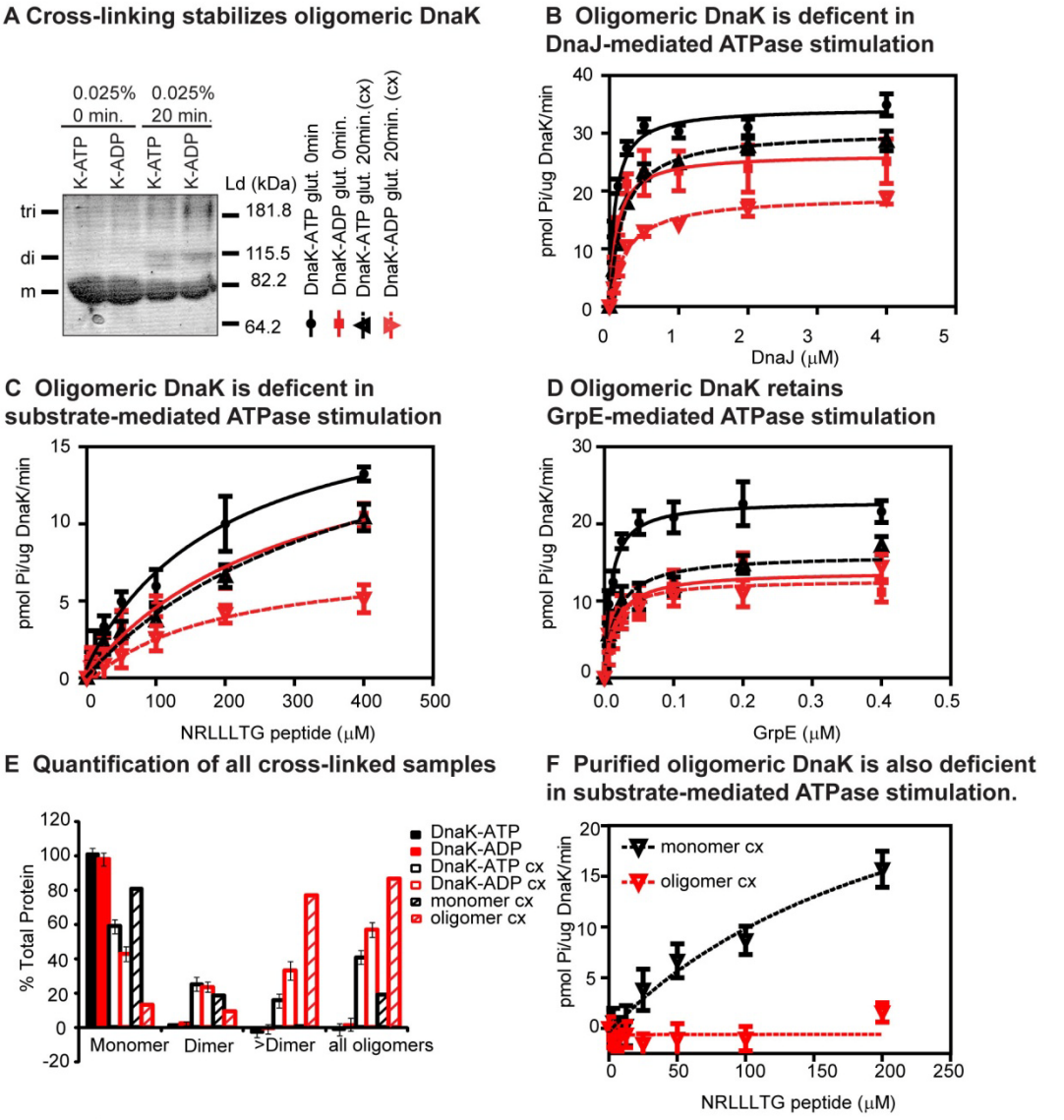

Appendix 3.5 Examing the ability of co-chaperones to stimulate the ATPase rate of oligomeric DnaK
(A) Stabilization of DnaK oligomers by chemical cross-linking. DnaK (K) was pre-incubated with either ATP or ADP and treated with 0.025% glutaraldehyde (glut.). Samples were either incubated for 20 min (cx) or quenched (0 min) immediately. Bands consistent with monomeric (m), dimeric (di) and trimeric (tri) DnaK were observed, as well as higher-order structures, The ATPase rate of these samples was then tested in the presence of DnaJ (B), NRLLTG peptide substrate (C), and GrpE in the presence of DnaJ 0.5 μM and NRLLLTG substrate 100μM (D). All of the experiments were performed in triplicate and the error bars represent the standard error of the mean. A negative control lacking DnaK was also tested and subtracted in each experiment. All curves are baseline normalized so all samples started at zeo. We observe that cross-linked DnaK-ADP has a decreased ability to be stimualted by DnaJ, consistent with the results observed in Figure 3.2. Further we observe that oligomeric DnaK (K-ADP cx) also has a decreased ability to be stimulated by peptide substrate. However, GrpE-mediated stimulation seems to be unaffected under the given cross-linking conditions. (E) The gels shown in Figure 3.2 and (A) are representative of nine cross-linking reactions performed. Quantification of bands from all cross-linked samples revealed that the cross-linked DnaK-ADP sample has more oligomeric species than the DnaK-ATP sample. To ensure that the differences in activity observed between the cross-linked DnaK-ATP sample and cross-linked DnaK-ADP sample were in fact due to the increase in oligomeric species we purified oligomeric DnaK from monomeric DnaK from a cross-linked DnaK-ADP sample via gel filtration (see Figure 3.2E for the gel). We demonstrated that the oligomeric sample was deficient in DnaJ-mediated ATPase stimulation (Figure 3.2F) and substrate-mediated ATPase stimulation (F).

3.6.6 Luciferase binding and "holdase" activity is mediated through the substrate binding domain in both cross-linked and non-cross-linked samples of DnaK.

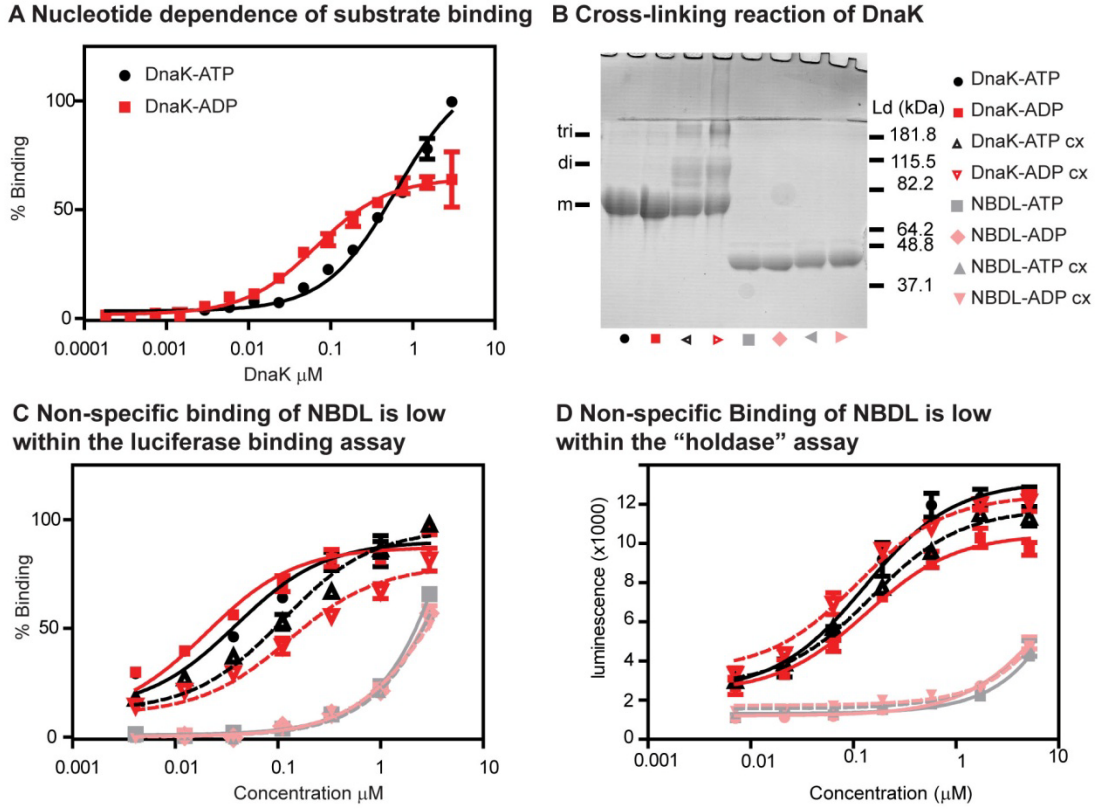

Appendix 3.6 Luciferase binding and "holdase" activity is mediated through the substrate binding domain in both cross-linked and non-crosslinked samples of DnaK

(A) In the ELISA-based susbtrate binding platform, DnaK-ATP binds with a Kd,app of 0.7 +/- 0.1 μM and DnaK-ADP binds with a Kd,app of 0.07 +/- 0.01 μM. When testing cross-linked samples, all samples were diluted in the presenceof 1 mM ATP to minimize effects of pre-incuptation with ADP or ATP. (B) We cross-linked the nucleotide binding domain with linker of DnaK (NBDL) under the same cross-linking conditions used for DnaK. The gel shows that under these condtions NBDL is primarily monomeric and cross-linking does not stabilize oligomeric forms of NBDL. (C) We tested the ability of these samples to bind luciferase, we found that NBDL interacts with luciferase non-specifically with a Kd,app > 3 μM. Our results also show that the cross-linking reaction does not increase this non-specific binding interaction appreciably. (D) Similar results were obtained in the "holdase" assay.

3.6.7 NRLLLTG peptide can inhibit DnaK mediated “holdase” activity.

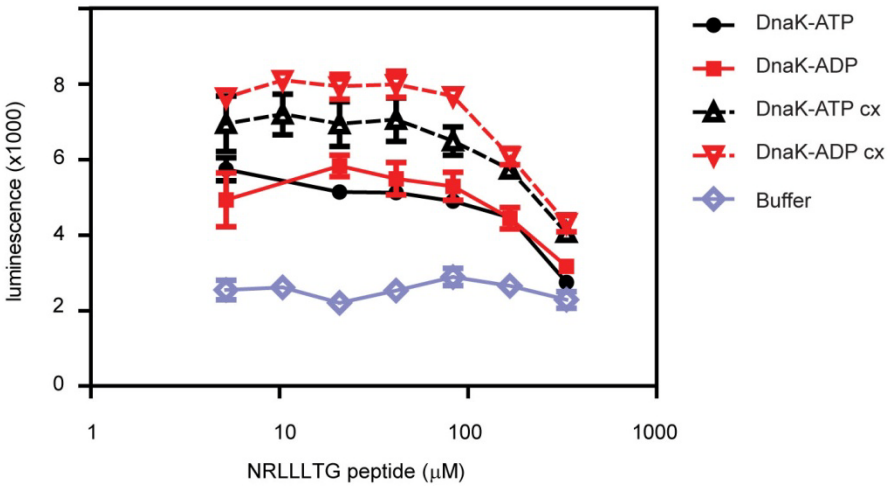

Appendix 3.7 NRLLLTG peptide can inhibit DnaK mediated “holdase” activity
The NRLLLTG peptide is known to interact in the substrate binding pocket of DnaK and we observe that it can inhibit the holdase activity of DnaK to an equal extent in both crosslinked and non-crosslinked samples. This result further supports the idea that the crosslinked samples bind substrate via the substrate binding domain.

3.6.8 2D projection analysis of DnaK-ADP.

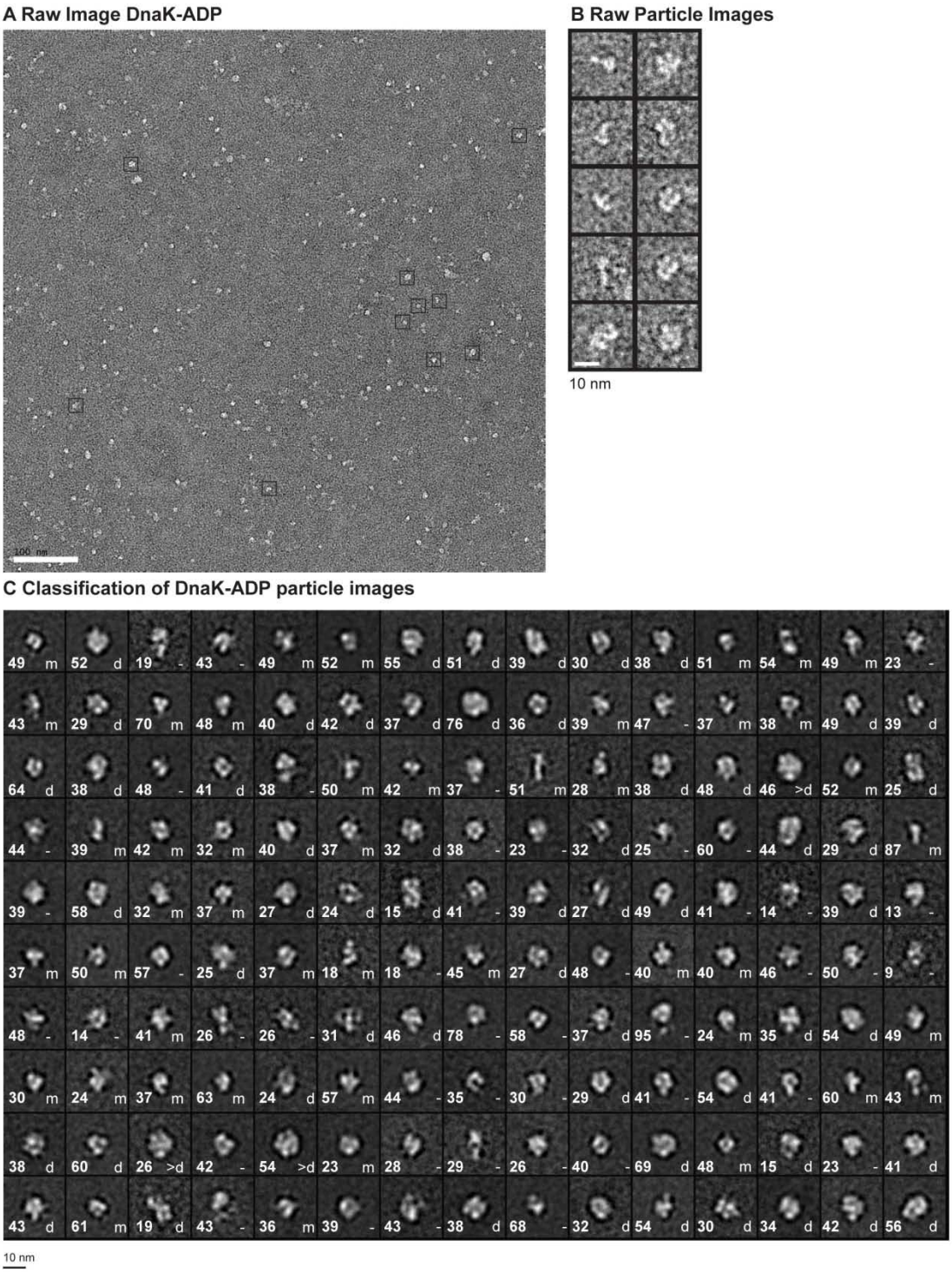

Appendix 3.8 2D projection analysis of DnaK-ADP (A) A raw image of DnaK-ADP embedded in negative stain is shown. Boxes are meant to higlight some of the particles selected for 2D averaging. (B) Examples of raw particle images used for 2D classification are shown. (C) Classification of DnaK-ADP particle images. 6,090 particle images were classified into 150 classes. The numbers in each box indicate the number of particles making up each class average and (m), (d), (>d), (-) indicate the designation assigned by the authors as monomer, dimer, greater than dimer, and unassigned, respectively.

3.6.9 2D projection analysis of DnaK-ADP with peptide (NRLLLTG) substrate.

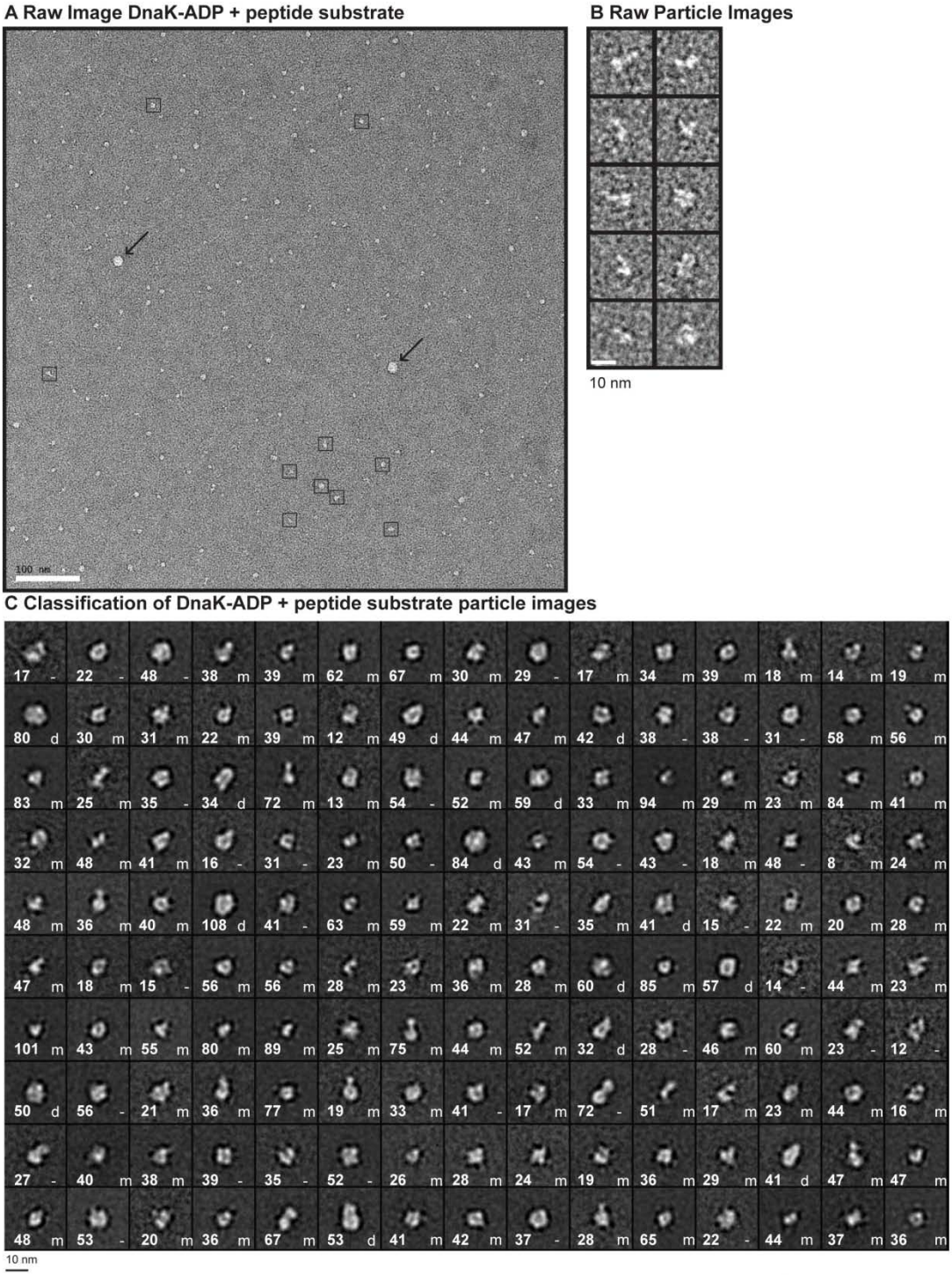

Appendix 3.9 2D projection analysis of DnaK-ADP with peptide (NRLLLTG) substrate (A) A raw image of DnaK-ADP + peptide substrate embedded in negative stain is shown. Boxes are meant to higlight some of the particles selected for 2D averaging. Arrows indicate rare particles excluded from our analysis. (B) Examples of raw particle images used for 2D classification are shown. (C) Classification of DnaK-ADP with peptide substrate particle images. 6,090 particle images were classified into 150 classes. The numbers in each box indicate the number of particles making up each class average and (m), (d), (>d), (-) indicate the designation assigned by the authors as monomer, dimer, greater than dimer, and unassigned, respectively.

3.7 References

1. Hesterkamp, T. and B. Bukau, *Role of the DnaK and HscA homologs of Hsp70 chaperones in protein folding in E.coli.* EMBO J, 1998. **17**(16): p. 4818-28.
2. Parsell, D.A. and S. Lindquist, *The function of heat-shock proteins in stress tolerance: degradation and reactivation of damaged proteins.* Annu Rev Genet, 1993. **27**: p. 437-96.
3. Young, J.C., J.M. Barral, and F. Ulrich Hartl, *More than folding: localized functions of cytosolic chaperones.* Trends Biochem Sci, 2003. **28**(10): p. 541-7.
4. Delaney, J.M., *Requirement of the Escherichia coli dnaK gene for thermotolerance and protection against H2O2.* J Gen Microbiol, 1990. **136**(10): p. 2113-8.
5. Paek, K.H. and G.C. Walker, *Escherichia coli dnaK null mutants are inviable at high temperature.* J Bacteriol, 1987. **169**(1): p. 283-90.
6. Winter, J., et al., *Severe oxidative stress causes inactivation of DnaK and activation of the redox-regulated chaperone Hsp33.* Mol Cell, 2005. **17**(3): p. 381-92.
7. Evans, C.G., L. Chang, and J.E. Gestwicki, *Heat shock protein 70 (hsp70) as an emerging drug target.* J Med Chem, 2010. **53**(12): p. 4585-602.
8. Patury, S., Y. Miyata, and J.E. Gestwicki, *Pharmacological targeting of the Hsp70 chaperone.* Curr Top Med Chem, 2009. **9**(15): p. 1337-51.
9. Bertelsen, E.B., et al., *Solution conformation of wild-type E. coli Hsp70 (DnaK) chaperone complexed with ADP and substrate.* Proc Natl Acad Sci U S A, 2009. **106**(21): p. 8471-6.
10. Slepenkov, S.V. and S.N. Witt, *Peptide-induced conformational changes in the molecular chaperone DnaK.* Biochemistry, 1998. **37**(47): p. 16749-56.
11. Palleros, D.R., et al., *ATP-induced protein-Hsp70 complex dissociation requires K+ but not ATP hydrolysis.* Nature, 1993. **365**(6447): p. 664-6.
12. Palleros, D.R., et al., *hsp70-protein complexes. Complex stability and conformation of bound substrate protein.* J Biol Chem, 1994. **269**(18): p. 13107-14.
13. Wittung-Stafshede, P., et al., *The J-domain of Hsp40 couples ATP hydrolysis to substrate capture in Hsp70.* Biochemistry, 2003. **42**(17): p. 4937-44.
14. Liberek, K., et al., *Escherichia coli DnaJ and GrpE heat shock proteins jointly stimulate ATPase activity of DnaK.* Proc Natl Acad Sci U S A, 1991. **88**(7): p. 2874-8.
15. Szabo, A., et al., *A zinc finger-like domain of the molecular chaperone DnaJ is involved in binding to denatured protein substrates.* EMBO J, 1996. **15**(2): p. 408-17.
16. Buchberger, A., et al., *Nucleotide-induced conformational changes in the ATPase and substrate binding domains of the DnaK chaperone provide evidence for interdomain communication.* J Biol Chem, 1995. **270**(28): p. 16903-10.
17. Rist, W., et al., *Amide hydrogen exchange reveals conformational changes in hsp70 chaperones important for allosteric regulation.* J Biol Chem, 2006. **281**(24): p. 16493-501.
18. Shi, L., M. Kataoka, and A.L. Fink, *Conformational characterization of DnaK and its complexes by small-angle X-ray scattering.* Biochemistry, 1996. **35**(10): p. 3297-308.
19. Swain, J.F., et al., *Hsp70 chaperone ligands control domain association via an allosteric mechanism mediated by the interdomain linker.* Mol Cell, 2007. **26**(1): p. 27-39.
20. Mayer, M.P. and B. Bukau, *Hsp70 chaperones: cellular functions and molecular mechanism.* Cell Mol Life Sci, 2005. **62**(6): p. 670-84.
21. Liu, Q. and W.A. Hendrickson, *Insights into Hsp70 chaperone activity from a crystal structure of the yeast Hsp110 Sse1.* Cell, 2007. **131**(1): p. 106-20.

22. Osipiuk, J., C. Georgopoulos, and M. Zylicz, *Initiation of lambda DNA replication. The Escherichia coli small heat shock proteins, DnaJ and GrpE, increase DnaK's affinity for the lambda P protein.* J Biol Chem, 1993. **268**(7): p. 4821-7.
23. Schonfeld, H.J., et al., *The DnaK chaperone system of Escherichia coli: quaternary structures and interactions of the DnaK and GrpE components.* J Biol Chem, 1995. **270**(5): p. 2183-9.
24. Angelidis, C.E., I. Lazaridis, and G.N. Pagoulatos, *Aggregation of hsp70 and hsc70 in vivo is distinct and temperature-dependent and their chaperone function is directly related to non-aggregated forms.* Eur J Biochem, 1999. **259**(1-2): p. 505-12.
25. Benaroudj, N., et al., *Self-association of the molecular chaperone HSC70.* Biochemistry, 1995. **34**(46): p. 15282-90.
26. Carlino, A., et al., *Interactions of liver Grp78 and Escherichia coli recombinant Grp78 with ATP: multiple species and disaggregation.* Proc Natl Acad Sci U S A, 1992. **89**(6): p. 2081-5.
27. Toledo, H., et al., *Dissociation of glucose-regulated protein Grp78 and Grp78-IgE Fc complexes by ATP.* Proc Natl Acad Sci U S A, 1993. **90**(6): p. 2505-8.
28. Benaroudj, N., F. Triniolles, and M.M. Ladjimi, *Effect of nucleotides, peptides, and unfolded proteins on the self-association of the molecular chaperone HSC70.* J Biol Chem, 1996. **271**(31): p. 18471-6.
29. Schroder, H., et al., *DnaK, DnaJ and GrpE form a cellular chaperone machinery capable of repairing heat-induced protein damage.* EMBO J, 1993. **12**(11): p. 4137-44.
30. Freiden, P.J., J.R. Gaut, and L.M. Hendershot, *Interconversion of three differentially modified and assembled forms of BiP.* EMBO J, 1992. **11**(1): p. 63-70.
31. Cowing, D.W., et al., *Consensus sequence for Escherichia coli heat shock gene promoters.* Proc Natl Acad Sci U S A, 1985. **82**(9): p. 2679-83.
32. Tilly, K., et al., *The dnaK protein modulates the heat-shock response of Escherichia coli.* Cell, 1983. **34**(2): p. 641-6.
33. Delaney, J.M., *A grpE mutant of Escherichia coli is more resistant to heat than the wild-type.* J Gen Microbiol, 1990. **136**(5): p. 797-801.
34. Dukan, S. and T. Nystrom, *Bacterial senescence: stasis results in increased and differential oxidation of cytoplasmic proteins leading to developmental induction of the heat shock regulon.* Genes Dev, 1998. **12**(21): p. 3431-41.
35. Spence, J., A. Cegielska, and C. Georgopoulos, *Role of Escherichia coli heat shock proteins DnaK and HtpG (C62.5) in response to nutritional deprivation.* J Bacteriol, 1990. **172**(12): p. 7157-66.
36. King, C., E. Eisenberg, and L. Greene, *Polymerization of 70-kDa heat shock protein by yeast DnaJ in ATP.* J Biol Chem, 1995. **270**(38): p. 22535-40.
37. Szabo, A., et al., *The ATP hydrolysis-dependent reaction cycle of the Escherichia coli Hsp70 system DnaK, DnaJ, and GrpE.* Proc Natl Acad Sci U S A, 1994. **91**(22): p. 10345-9.
38. Wisen, S. and J.E. Gestwicki, *Identification of small molecules that modify the protein folding activity of heat shock protein 70.* Anal Biochem, 2008. **374**(2): p. 371-7.
39. Blond-Elguindi, S., et al., *Peptide-dependent stimulation of the ATPase activity of the molecular chaperone BiP is the result of conversion of oligomers to active monomers.* J Biol Chem, 1993. **268**(17): p. 12730-5.
40. Grimshaw, J.P., et al., *Thermosensor action of GrpE. The DnaK chaperone system at heat shock temperatures.* J Biol Chem, 2003. **278**(21): p. 19048-53.
41. Grimshaw, J.P., et al., *The heat-sensitive Escherichia coli grpE280 phenotype: impaired interaction of GrpE(G122D) with DnaK.* J Mol Biol, 2005. **353**(4): p. 888-96.

42. Siegenthaler, R.K. and P. Christen, *Tuning of DnaK chaperone action by nonnative protein sensor DnaJ and thermosensor GrpE.* J Biol Chem, 2006. **281**(45): p. 34448-56.
43. Osorio, H., et al., *H2O2, but not menadione, provokes a decrease in the ATP and an increase in the inosine levels in Saccharomyces cerevisiae. An experimental and theoretical approach.* Eur J Biochem, 2003. **270**(7): p. 1578-89.
44. Tran, Q.H. and G. Unden, *Changes in the proton potential and the cellular energetics of Escherichia coli during growth by aerobic and anaerobic respiration or by fermentation.* Eur J Biochem, 1998. **251**(1-2): p. 538-43.
45. Hoffmann, J.H., et al., *Identification of a redox-regulated chaperone network.* EMBO J, 2004. **23**(1): p. 160-8.
46. Winter, J., et al., *Bleach activates a redox-regulated chaperone by oxidative protein unfolding.* Cell, 2008. **135**(4): p. 691-701.
47. Moreno-del Alamo, M., et al., *Structural Analysis of the Interactions Between Hsp70 Chaperones and the Yeast DNA Replication Protein Orc4p.* Journal of Molecular Biology, 2010. **403**(1): p. 24-39.
48. Schuermann, J.P., et al., *Structure of the Hsp110 : Hsc70 nucleotide exchange machine.* Molecular Cell, 2008. **31**(2): p. 232-243.
49. Xing, Y., et al., *Structure of clathrin coat with bound Hsc70 and auxilin: mechanism of Hsc70-facilitated disassembly.* EMBO J, 2010. **29**(3): p. 655-65.
50. Farr, C.D. and S.N. Witt, *Kinetic evidence for peptide-induced oligomerization of the molecular chaperone DnaK at heat shock temperatures.* Biochemistry, 1997. **36**(35): p. 10793-800.
51. Marcinowski, M., et al., *Substrate discrimination of the chaperone BiP by autonomous and cochaperone-regulated conformational transitions.* Nat Struct Mol Biol, 2011. **18**(2): p. 150-8.
52. Schlecht, R., et al., *Mechanics of Hsp70 chaperones enables differential interaction with client proteins.* Nat Struct Mol Biol, 2011. **18**(3): p. 345-51.
53. Powers, M.V., P.A. Clarke, and P. Workman, *Death by chaperone: HSP90, HSP70 or both?* Cell Cycle, 2009. **8**(4): p. 518-26.
54. Benaroudj, N., B. Fouchaq, and M.M. Ladjimi, *The COOH-terminal peptide binding domain is essential for self-association of the molecular chaperone HSC70.* J Biol Chem, 1997. **272**(13): p. 8744-51.
55. Gaut, J.R., *In vivo threonine phosphorylation of immunoglobulin binding protein (BiP) maps to its protein binding domain.* Cell Stress Chaperones, 1997. **2**(4): p. 252-62.
56. Fouchaq, B., et al., *Oligomerization of the 17-kDa peptide-binding domain of the molecular chaperone HSC70.* Eur J Biochem, 1999. **259**(1-2): p. 379-84.
57. Chang, L., et al., *Chemical Screens against a Reconstituted Multiprotein Complex: Myricetin Blocks DnaJ Regulation of DnaK through an Allosteric Mechanism.* Chem Biol, 2011. **18**(2): p. 210-21.
58. Wisen, S., et al., *Binding of a small molecule at a protein-protein interface regulates the chaperone activity of hsp70-hsp40.* ACS Chem Biol, 2010. **5**(6): p. 611-22.
59. Buczynski, G., et al., *Characterization of a lidless form of the molecular chaperone DnaK: deletion of the lid increases peptide on- and off-rate constants.* J Biol Chem, 2001. **276**(29): p. 27231-6.
60. Chang, L., et al., *Mutagenesis reveals the complex relationships between ATPase rate and the chaperone activities of Escherichia coli heat shock protein 70 (Hsp70/DnaK).* J Biol Chem, 2010. **285**(28): p. 21282-91.

61. Chang, L., et al., *High-throughput screen for small molecules that modulate the ATPase activity of the molecular chaperone DnaK.* Anal Biochem, 2008. **372**(2): p. 167-76.
62. Miyata, Y., et al., *High-throughput screen for Escherichia coli heat shock protein 70 (Hsp70/DnaK): ATPase assay in low volume by exploiting energy transfer.* J Biomol Screen, 2010. **15**(10): p. 1211-9.
63. Ohi, M., et al., *Negative Staining and Image Classification - Powerful Tools in Modern Electron Microscopy.* Biol Proced Online, 2004. **6**: p. 23-34.
64. Ludtke, S.J., P.R. Baldwin, and W. Chiu, *EMAN: semiautomated software for high-resolution single-particle reconstructions.* J Struct Biol, 1999. **128**(1): p. 82-97.
65. Frank, J., et al., *SPIDER and WEB: processing and visualization of images in 3D electron microscopy and related fields.* J Struct Biol, 1996. **116**(1): p. 190-9.

Chapter 4

Analysis of the tau-associated proteome reveals that exchange of Hsp70 for Hsp90 targets to tau for degradation.

4.1 Abstract

The microtubule associated protein tau (MAPT/tau) aberrantly accumulates in fifteen neurodegenerative diseases, termed tauopathies. One way to treat tauopathies may be to accelerate tau clearance; however, the molecular mechanisms that govern tau stability are not yet clear. The Gestwicki and Dickey laboratories had recently identified Hsp70-dependent chemical probes that dramatically accelerate the clearance of tau in cellular and animal models. In this chapter, we used one of these probes in combination with immunoprecipitation and mass spectrometry to identify 48 proteins that change in their association with tau during the first 10 minutes after treatment. These proteins included known modifiers of tau proteotoxicity, such as ILF-2 (NFAT), ILF-3, and ataxin-2. One of the most striking observations from the dataset was that tau binding to heat shock protein 70 (Hsp70) decreased while binding to Hsp90 significantly increased. These chaperones have been linked to tau homeostasis, but their mechanisms hadn't been clear. Using peptide microarrays and binding assays, Hsp70 and Hsp90 appeared to compete for binding to shared sites on tau. Further, the Hsp90-bound complex was important in initiating tau clearance in cells. These results suggest that the relative levels of Hsp70 and Hsp90 may help determine whether tau is retained or degraded. Consistent with this model, analysis of reported microarray expression data from Alzheimer's disease patients

and age-matched controls showed that the levels of Hsp90 are reduced in the diseased hippocampus. These studies suggest that Hsp70 and Hsp90 work together to coordinate tau homeostasis.

4.2 Introduction

4.2.1 Tau protein homeostasis in disease

Tau is primarily expressed in neurons, where it plays a central role in stabilizing microtubules within axons [1-3]. Tau protein homeostasis is regulated by its expression, phosphorylation and, turnover [4]. Within tauopathies, including Alzheimer's disease (AD), frontotemporal dementia (FTLD), progressive supranuclear palsy (PSP), and corticobasal degeneration (CBD), tau homeostasis is disrupted, leading to hyperphosphorylation and accumulation of intracellular aggregates [5-7]. Genetic depletion of tau restores cognitive defects in several mouse models [8-12], suggesting that reducing tau levels may be an effective way to re-balance its homeostasis. Indeed, recent studies using compounds that reduce tau levels by increasing proteosomal and/or autophagic clearance [13] have shown that this strategy is able to partially recover cognitive defects in cellular and mouse models [14, 15]. Together, these findings have focused attention on understanding which cellular pathways protect tau and which proteins are important for its degradation.

4.2.2 Molecular chaperones regulate tau homeostasis

As discussed in Chapter 1, important regulators of tau homeostasis include the molecular chaperones, heat shock protein 70 (Hsp70). Hsp70 and its constitutively-expressed

isoform, Hsc70, bind directly to tau in a region near the microtubule-binding domains upon release from the microtubule [16]. Through these interactions, Hsp70s can facilitate the rebinding of tau to microtubules and have also been implicated in blocking tau aggregation and promoting its degradation [17-19]. Similarly, Hsp90 and a number of other co-chaperones have been implicated in regulating tau phosphorylation, aggregation, and degradation [16, 17, 20-22]. Thus, Hsp70 and Hsp90 appear to play roles during multiple processes involved in establishing tau homeostasis. However, these studies have not yet revealed the molecular mechanisms involved and it is unclear how these chaperones ultimately control tau stability.

4.2.3 A chemical biology approach to understand tau homeostasis

Here, we have used a small molecule to acutely disrupt tau equilibrium and favor a switch to a degradation fate. A key feature of this approach is that the molecule reduces tau levels rapidly (within ~ 15 minutes in HeLa cells), allowing identification of proteins that change in their association with tau during the first few minutes of triage. Using mass spectrometry and quantitative spectral analysis, it was determined that only 48 tau-associated proteins are either released or enriched on tau during the switch to a degradation fate. Interestingly, Hsp70 is released during the early stages of tau degradation and is replaced by Hsp90. Knock-down analysis revealed that Hsp90 is required for degradation, suggesting that the switch to Hsp90 is an important step on the path to degradation. Further, Hsp70 competes with Hsp90 for binding to tau, suggesting that the levels of Hsp70 and Hsp90, in some cases, may dictate tau stability, a result supported by analysis of expression data from AD patients and age matched controls.

These studies reveal possible new strategies for the development of therapeutics that target tau for clearance.

4.3 Results

4.3.1 Identification of proteins involved in tau homeostasis

Tau is an intrinsically disordered protein [23] that is thought to engage in protein-protein interactions that govern its localization, activity, and stability. Thus, we reasoned that there are likely tau-associated proteins that stabilize tau within the cell, whereas other complexes may be critical for its clearance. Further, a better understanding of these tau-binding factors might reveal potential new drug targets and provide insights into the mechanisms of chaperone-mediated tau triage. Towards these goals, an important advance is the recent discovery of molecules that acutely disrupt tau equilibrium and favor a rapid and dramatic change in tau stability. One such molecule, methylene blue (MB), has been shown to reduce tau levels in a variety of cellular and animal models of tauopathies [13-15].

To test whether this compound could be used to explore changes in the tau-associated proteome, we first confirmed that MB reduces total tau levels by ~80% in HeLa (C3) cells, which stably express V5-4RON tau (Appendix 4.1A). Loss of tau in this model is dose-dependent, with an effective concentration (EC_{50}) of 8 +/- 1 μM, and rapid with a new equilibrium reached within ~10 to 20 minutes (Appendix 4.1B). The speed of this switch is important because it allows insights into the acute changes that occur in the tau-associated protein complexes, while avoiding complications originating from global

cellular responses to MB. Finally, given our interested in chaperone-mediated tau degradation pathways it is particularly interesting to note that MB has been found to alter the ATPase activity of Hsp70 [13]. Further, it was observed that Hsp70 overexpression enhanced the ability of MB to clear tau from the cell [13]. Finally, a series of very recent experiments have clearly established the direct role of Hsp70 in MB-mediated clearance of tau. It was determined that MB inhibits the ATPase activity of Hsp70 via oxidization of specific cysteines on Hsp70. When these cysteines were mutated to serine, so that they could no longer be oxidized, not only was MB no longer able to inhibit the ATPase activity of Hsp70, but it was also no longer able to induce tau clearance within the cellular model utilized in our studies [Miyata and Rauch, unpublished data]. Thus, we conclude that MB would be an excellent chemical tool to induce the rapid and robust formation of pro-degradation tau protein complexes in an Hsp70-dependent manner.

To identify proteins that change in their association with tau during the compound-initiated switch to a degradation fate, cells were pre-treated with the proteasome inhibitor, bortezomib (bortez.), for 4 hours, followed by MB treatment (50 μM) or treatment with a vehicle control. Bortezomib was used to trap complexes destined for the proteasome, facilitating their subsequent identification by mass spectrometry (Appendix 4.1C). Immunoprecipitations with a V5 antibody were performed 10 minutes after MB/vehicle treatment and the precipitated material was subject to analysis by LC-MS/MS to identify the tau-associated proteome (Figure 4.1A). These experiments were performed in two independent, biological replicates and each replicate was analyzed by mass spectrometry in triplicate. Similar levels of tau (MAPT) were immunoprecipitated in each sample

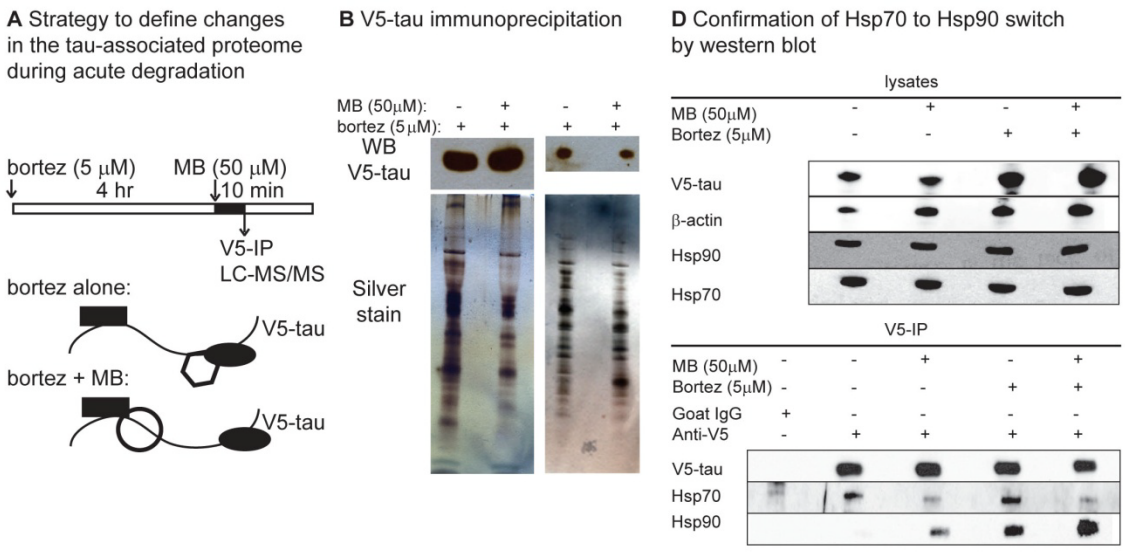

C 48 proteins differentially associated with tau

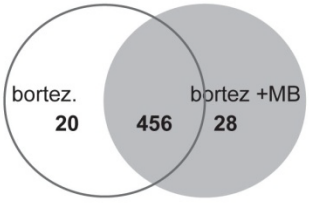

Increased tau binding			Decreased tau binding		
Bayes Factor	Fold Change	Gene Name	Bayes Factor	Fold Change	Gene Name
8.37 E+ 04	2.27	EPPK1	1.65 E+ 06	3.29	KHSRP
5.22 E+ 03	2.85	HNRNPUL1	7.42 E+ 05	15.94	ATXN2
1.91 E+ 03	2.38	SEC16A	2.00 E+ 04	6.03	SNRPD1
1.90 E+ 03	2.83	HIST1H1D	1.14 E+ 03	7.99	ATXN2L
1.43 E+ 03	2.82	CAD	281.18	4.49	ILF2
777.16	2.38	NCL	99.47	3.27	NHP2L1
363.17	8.86	VIM	93.31	2.98	LSM12
304.15	5.73	AHCY	**68.63**	**2.22**	**HSPA1B**
261.25	5.42	KRT17	57.03	2.59	FAM98B
244.74	**2.42**	**HSP90AB1**	50.93	3.95	SMARCE1
100.75	9.15	RPS4X	30.57	2.12	SMARCA4
91.64	5.12	RPL7	24.08	2.41	ILF3
86.70	4.51	RPS24	22.42	2.89	TNRC6B
68.23	3.23	NUDT21	18.07	3.92	HNRNPAB
49.20	4.06	S100A8	15.78	3.38	GSTM3
47.63	3.56	RPL34	15.08	2.62	HLA-DRA
29.67	2.22	DST	13.02	4.17	CD59
29.03	3.00	RPS8	12.07	3.35	GRPEL1
26.95	3.80	KRT79	12.07	3.35	COTL1
25.14	2.82	G3BP1	10.32	2.81	SLC3A2
22.09	3.19	MRPS28			
19.77	2.55	HRNR			
19.48	3.54	FASN			
18.09	2.44	RPL32			
16.82	2.95	RPL7A			
14.83	5.23	RPL10A			
14.19	3.50	S100A9			
10.23	3.52	TIA1			

Figure 4.1. Proteomic analysis of the proteins associated with tau during the acute switch to a degradation fate in response to MB treatment. (A) Schematic of the experimental strategy for identifying tau-associated proteins. (B) A silver stained gel of the anti-V5 immunoprecipitated samples is shown, highlighting interacting proteins. Also, a western blot for V5-tau is also shown to demonstrate that similar amounts of tau were obtained. (C) Using spectral counting, 456 tau-associated proteins did not change in their association with tau in response to MB treatment. However, 20 proteins decreased their association with tau and 28 preferentially bound. (D) Western blots on freshly immunoprecipitated samples confirmed that MB causes Hsp70 to be released from tau, while Hsp90 binding increases, in the presence and absence of proteasome inhibition.

(Figure 4.1B) and a total of 504 interacting proteins were identified, including tubulin, TARDBP (TDP-43), vimentin, Hsp70, and Hsp90 (Appendix 4.2).

Next, quantitative spectral counting was utilized to detect proteins that change in their association with tau in response to MB. To be considered differentially associated with tau, proteins with greater than a two-fold change in abundance and a Bayes factor greater than ten were identified. Whereas the vast majority of interacting proteins, including tubulin, did not change their association with tau upon compound treatment, this criteria identified 48 differentially associated proteins, 20 of which decreased their binding to tau and 28 that increased their binding (Figure 4.1C). Interestingly, this list includes a number of factors previously identified as modifiers of tau toxicity, such as ataxin-2, IL-2, and IL-3 [24, 25], suggesting that some of these factors might, in part, alter tau proteotoxicity by influencing its turnover. This list also included a number of proteins involved in gene regulation, such as the SWI-SNF components SMARCE1 (BAF57) and SMARCA4 (BRG1), and ribosome-associated proteins, such as RPS4X.

4.3.2 Hsp90 is an important factor in tau degradation

One of the most striking observations from the tau interactome analysis was that the association with stress-inducible Hsp70 (HSPA1B) in response to MB was significantly reduced, while binding to Hsp90 (HSP90AB1) was increased (Figure 4.1C). To confirm this finding, the V5-immunoprecipitations were repeated on freshly treated HeLa (C3) cells and western blots for Hsp70 and Hsp90 were performed. Consistent with the mass spectrometry findings, Hsp70 decreased while Hsp90 increased its association with tau after MB treatment (Figure 4.1D). This switch also occurred in the absence of a proteasome inhibitor (Figure 4.1D).

These results suggest that interplay between Hsp70 and Hsp90 may be involved in targeting tau for clearance. Consistent with this result, as discussed above, it had been previously shown that over-expression of Hsp70 enhances MB-mediated clearance of tau [13]. This result is significant because it highlights that MB is not playing a purely inhibitory role on Hsp70, release tau from the stabilizing influence of Hsp70. Rather, Hsp70 seems to be actively involved in initiating MB-mediated clearance of tau, either through acute release or active transfer of tau to pro-degradation complexes.

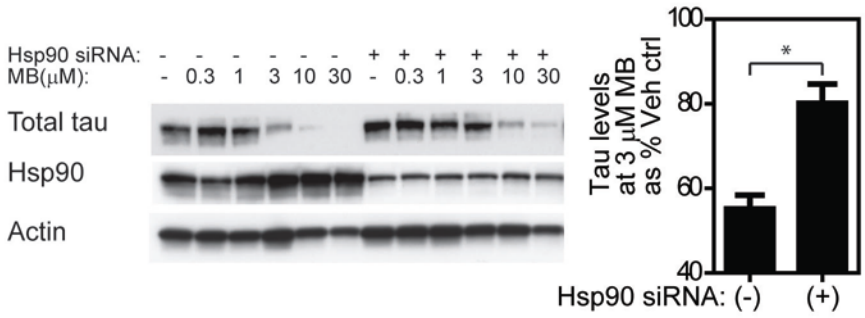

Figure 4.2. MB-initiated tau degradation is dependent on Hsp90.
Hsp90 siRNA does not cause a significant change in total tau levels in untreated cells, but it attenuates tau clearance in response to MB. Quantifications of band intensities from two independent experiments were performed using Image J. (* Student's two-tailed unpaired t-test, p-value <0.05)

To better understand the specific role of Hsp90 in this system, examined whether it is required for MB-initiated tau degradation. Hsp90 is best known for its ability to stabilize many substrates, such as nuclear hormone receptors and kinases, protecting them from degradation [26, 27]. However, Hsp90 also promotes the degradation of other substrates, such as von Hippal Lindau factor and high-density lipoprotein [28, 29]. To explore which role might predominate in the tau system, siRNA knock-down was utilized to reduce the levels of Hsp90 in the cell. Consistent with previous reports [17, 20, 30, 31], knock-down of Hsp90 did not significantly change the levels of total tau, however it did suppress the

ability of MB to clear tau (Figure 4.2). This result supports a model in which Hsp90 is actively involved in targeting tau for degradation, at least in response to MB.

4.3.3 The biochemistry which initiates an Hsp70 to Hsp90 switch

To better understand this chaperone-dependent tau degradation pathway, we first explored how compound modulation of Hsp70 would lead to a decrease in Hsp70 binding. It has previously been shown that MB decreases the ability of Hsp40 co-chaperones to stimulate the ATPase rate of Hsp70 or stimulate Hsp70-dependent refolding of luciferase (Miyata and Rauch unpublished data, Appendix 4.3). Hsp40s promote the binding of Hsp70 to client proteins [32, 33]. Thus, one mechanism by which MB may disrupt the binding Hsp70 to tau could be by decoupling Hsp70 from Hsp40s within the cell, causing a passive release of tau from Hsp70. The effect of compound treatment on direct binding of Hsp70 to tau was also evaluated and no change in affinity was observed upon compound treatment (Appendix 4.4). Finally, another mechanism by which an Hsp70 to Hsp90 switch could occur is through a more active hand-off facilitated by the co-chaperone Hop, which binds both Hsp70 and Hsp90 to promote substrate transfer [34, 35]. However, no change in the affinity of Hsp70 for Hop was observed in response to compound treatment (Appendix 4.5). Further, knock-down of Hop had no effect on compound-mediated tau clearance. Interestingly, overexpression of Hop does enhance compound-induced tau clearance. These results suggest that in the presence of high levels of Hop the hand-off of tau from Hsp70 to Hsp90 is more efficient, promoting clearance. However, at endogenous levels of Hop, Hsp70 may instead

passively releases tau to initiate this degradation pathway, potentially due to being decoupled from J-proteins.

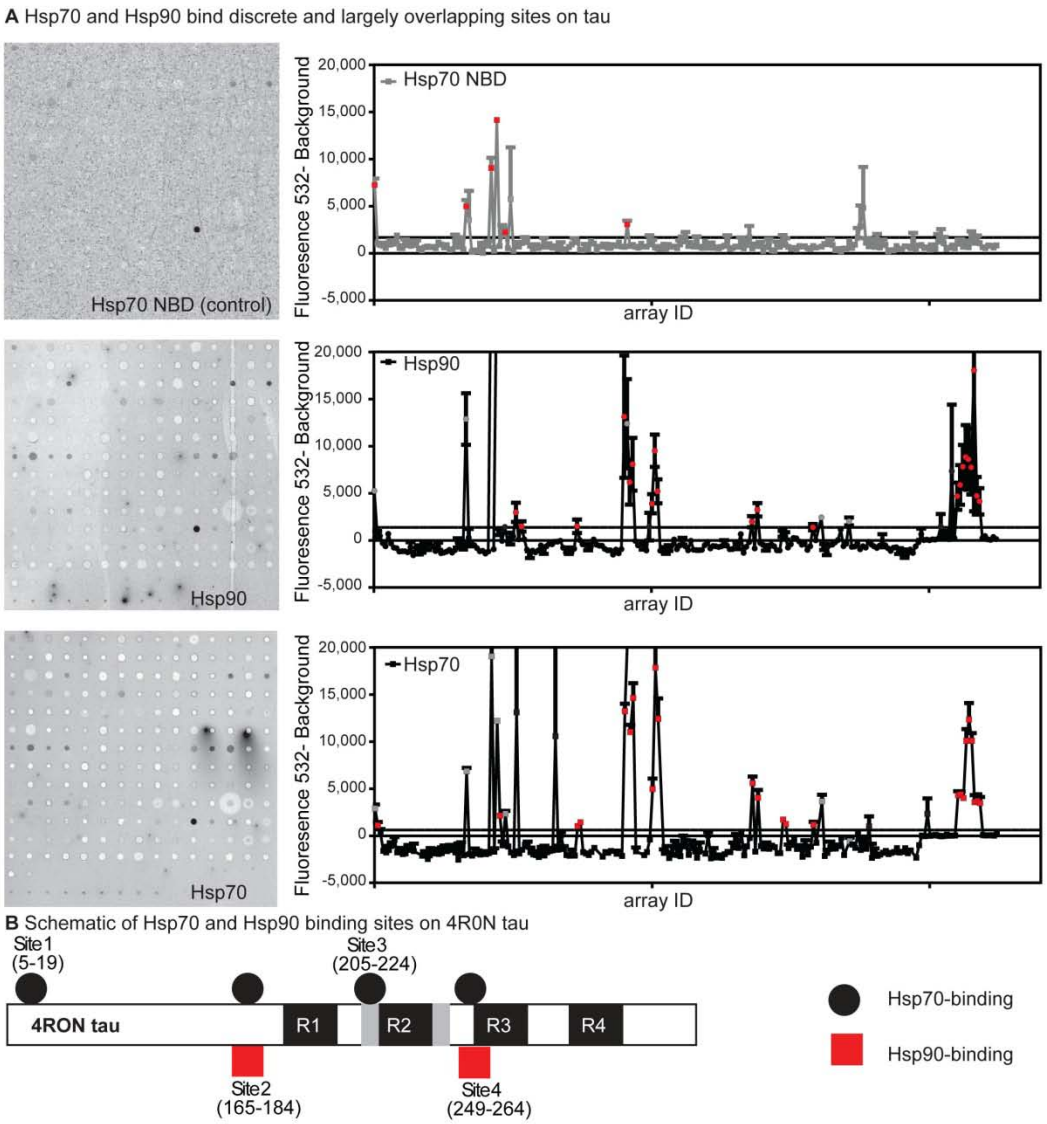

Figure 4.3. Hsp70 and Hsp90 bind discrete and largely overlapping sites on tau, as measured by peptide microarrays. (A) Representative array results using Hsp70 NBD, Hsp90, and Hsp70 (all 10 μM) are shown, along with the histogram of the fluorescence intensities from the triplicate experiments. Peptides with intensities 3 standard errors of the mean above the mean of the total dataset are colored in red. Peptides that bound either Hsp70 NBD or antibody alone are shown in gray. One false-positive spot (array ID: 161 was removed for clarity). (B) Schematic of the Hsp70 and Hsp90 binding sites mapped onto 4RON tau, highlighting the proximity to the four microtubule-binding repeats (R1-4).

4.3.4 Hsp90 competes with Hsp70 for binding to tau

Based on these results, we hypothesized that exchange of Hsp70 for Hsp90 on tau might occur via competition for shared binding sites. At least two binding sites for Hsp70 have

been identified on tau [36], but the binding sites for Hsp90 have not yet been described. To study this question, we developed a peptide microarray composed of 15-mer peptides covering the peripheral nervous system tau sequence with 4 amino acid overlap (194 total spots in triplicate). Binding to Hsp70-His and Hsp90-His was measured using fluorescent anti-His antibodies and the controls were antibody alone and the nucleotide-binding domain (NBD) of Hsp70, which should not bind peptide substrates. As expected, the NBD bound non-specifically to only a few peptides, which were excluded from subsequent analyses (Figure 4.3A, Appendix 4.6). In contrast, Hsp70 and Hsp90 were bound to a number of tau-derived peptides (Figure 4.3A, Appendix 4.6). Restricting the analysis of these binding sites to one of the central nervous system tau isoforms (4R0N), which was utilized in the cellular studies, four sites were identified for Hsp70 and two for Hsp90 (Figure 4.3B). Strikingly, both of the Hsp90 binding sites were shared by Hsp70.

Table 4.1 Testing competition between Hsp70 and Hsp90 for binding to tau

	Hsp70-tau binding		Hsp90α-tau binding	
Protein	**IC_{50} μM**	**SEM**	**IC_{50} μM**	**SEM**
Hsp70 (HSPA1B)	8	4	4	2
Hsc70 (HSPA8)	17	9	1.9	0.5
Hsp90α (HSP90AA1)	>100	NA	4	2
Hsp90β (HSP90AB1)	59	42	3	1
buffer	>100	NA	>100	NA
Hsp70 NBD	>100	NA	NA	NA

Previous work has determined that deletion of residues I219, I220 and I250, V251 reduces Hsp70 binding to tau [36]. Consistent with this result, these residues were present in the third and fourth Hsp70 binding sites, as measured by peptide microarray. These Hsp70 binding sites were further validated using a software program [37] developed to

predict binding sites for the prokaryotic Hsp70, DnaK. Using this approach, sites 2, 3, and 4 were positively identified.

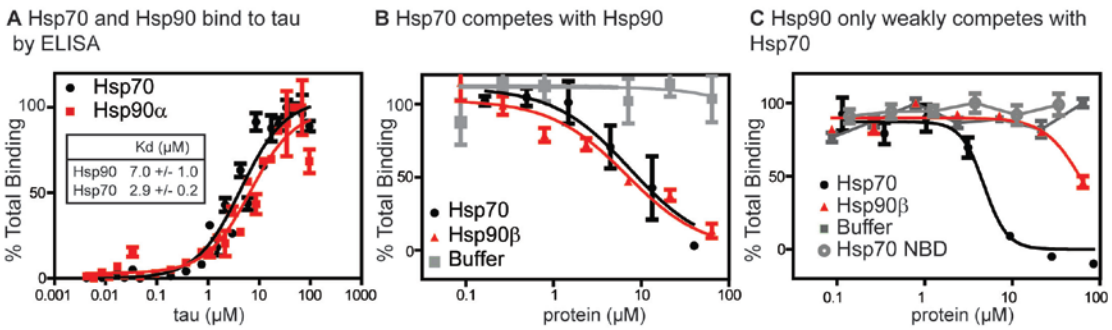

Figure 4.4. Hsp70 competes with Hsp90 for binding to tau.
(A) Immobilized Hsp70 and Hsp90 bind 4RON tau. (B) Soluble Hsp70 can inhibit binding of tau to immobilized Hsp90α with an IC_{50} value of 4 μM. As a control, free Hsp90β also competes with this interaction. (C) Soluble Hsp90β only weakly competes with immobilized Hsp70 for binding to tau with an IC_{50} value greater than 50 μM. As a control, free Hsp70 inhibits binding with an IC_{50} of 8 μM. Similar values were seen using different Hsp70 and Hsp90 isoforms (see Table 4.1). All experiments were performed in triplicate. Results are shown as the average and standard error of the mean.

These findings suggest that Hsp90 binding sites are shared by Hsp70 and, thus, that these chaperones might compete for binding to tau. To test this model, we first synthesized peptides, smaller than 15 amino acids in length, corresponding to the binding sites predicted by the microarray. However, these peptides showed weak (>100 μM) binding, which was difficult to accurately measure. However, these peptides showed weak (>100 μM) binding, which was difficult to accurately measure. Therefore, we switched to studying binding in the context of full-length 4RON tau in an ELISA-like platform. Using this method, immobilized Hsp70 bound tau with an affinity of 2.9 ± 0.2 μM and Hsp90 bound with a slightly weaker affinity of 7.0 ± 1.0 μM (Figure 4.4A). As predicted by the peptide microarray results, Hsp70 competed for binding with Hsp90 (IC_{50} ~ 4 μM) (Figure 4.4B). Conversely, Hsp90 was less effectively at competing with Hsp70 (IC_{50} > 50 μM), perhaps because of the two unique Hsp70 binding sites (Figure 4.4C). These same relationships were observed with the major stress-inducible (Hsp70, Hsp90α) and

the constitutively expressed (Hsc70, Hsp90β) isoforms (Table 1). Based on these results, it was concluded that the MB-initiated increase in Hsp90 binding observed by mass spectrometry may be the result of exchange of Hsp70 for Hsp90 on shared binding sites within tau.

4.3.5 Hsp90 is decreased in human brains with Alzheimer's disease

These results suggest that tau degradation may be sensitive to the relative levels of Hsp70 and Hsp90. More specifically, reduced Hsp90 levels might favor net retention of tau, perhaps unbalancing tau homeostasis. To explore this idea, we examined the GDS810 dataset, which collected microarray expression data from the hippocampal tissue of patients with incipient, moderate, and severe Alzheimer's disease (AD) and age matched controls [38]. Similarly, the GSE5281 dataset that includes expression results from

Table 4.2 Gene expression level changes for Hsp70 and Hsp90 in Alzheimer's disease.

		GSE5281	GDS810		
Gene	Array ID*	AD p-value	Incipient AD p-value	Moderate AD p-value	Severe AD p-value
HSP90AA1	210211_s_at, 211968_s_at, 214328_s_at	d0.088	d0.031	d0.236	d0.088
HSP90AB1	200064_at, 214359_s_at for both and 1557910_at GSE5281	d0.017	d0.114	d0.046	d0.008
HSPA1B	200799_at, 200800_s_at, 202581_at	0.438	d0.252	0.743	0.272
HSPA8	208687_x_at, 210338_s_at, 221891_x_at for both and 224187_x_at for GSE5281	d0.028	d0.211	d0.236	d0.066
HSPA2	211538_s_at	0.227	d0.470	0.370	u0.224
HSPA4	208815_x_at, 211015_s_at, 211016_x_at	0.515	1.000	0.321	0.864
HSPA6	117_at, 213418_at	u0.032	d0.252	0.321	0.181
HSPA14	219212_at for both and 226887_at, 227650_at for GSE5281	0.687	0.711	d0.167	d0.114
NUP37	218622_at	0.403	0.837	0.321	0.776

*Unless otherwise noted the Array IDs given were present in both datasets. Abbreviations are used to indicate the direction of change in gene expression; **d** denotes a decrease in gene expression in AD patients and **u** denotes an increase. Grey denotes gene expression changes with a Mann Whitney U test p-value of <0.05.

micro-dissected, histopathologically normal, hippocampal neurons from AD patients and age matched controls was also queried [39, 40]. Previous analyses of these datasets had already noted AD-related changes in gene expression within protein folding genes, such as chaperones. However, we wanted to specifically ask how the relative levels of cytosolic Hsp70 and Hsp90 might change as a function of disease. Accordingly, both datasets were analyzed (Appendix 4.7) and observed statistically significant changes and trends that indicated an AD-associated decrease in Hsp90 (Figure 4.5). Conversely, no consistent changes in stress-inducible Hsp70 levels were observed (HSPA1B, HSPA2,

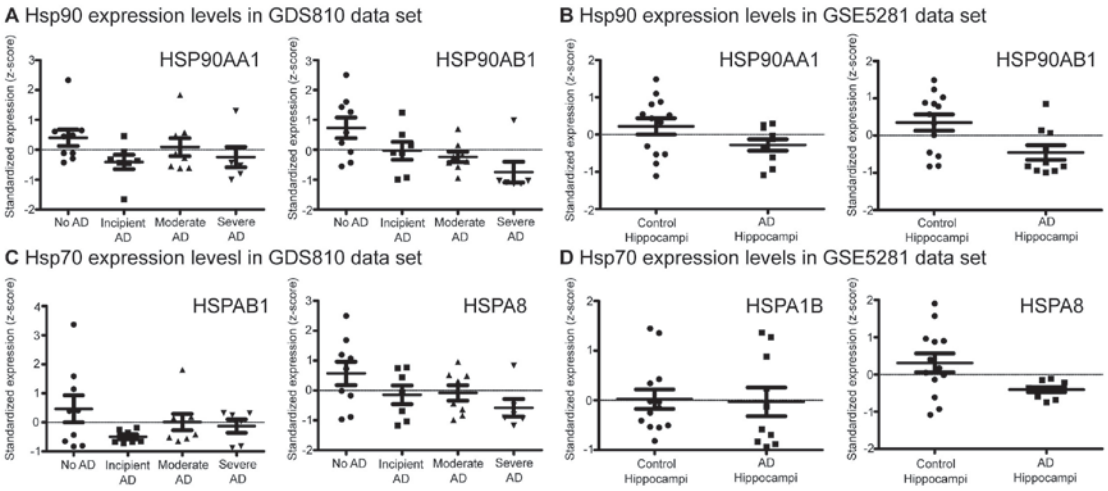

Figure 4.5. Hsp90 expression levels are decreased in hippocampal samples from Alzheimer's disease patients. Analysis of the (A) GDS810 and (B) GSE5281 datasets reveals a decrease in the mRNA levels of both isoforms of Hsp90 (HSP90AA1 and HSP90AB1) in Alzheimer's disease (AD) samples. There were no statistically significant changes in the levels of stress-inducible Hsp70s, such as HSPA1B (C and D), HSPA2, HSPA4, and HSPA14 (See Table 4.2 and Appendix 4.6). However, the levels of Hsc70 (HSPA8) were decreased in AD patient samples (C and D).

HSPA6, HSPA14) but the constitutively expressed Hsc70 (HSPA8) was decreased in both datasets (Table 4.2). Importantly for the current study, the ratio of stress-inducible Hsp70s and Hsp90s was significantly changed in AD, suggesting that imbalance in the chaperone ratio might contribute to the accumulation of tau. Interestingly, these finding are consistent with an observation made in an AD mouse model in which Hsp90 protein levels were found to be inversely correlated with tau levels [17]. Taken together, a model emerges in which Hsp90 levels and the Hsp70:Hsp90 ratio help determine tau stability.

4.4 Discussion

4.4.1 Insights into proteins potentially involved in regulating tau homeostasis

Tau homeostasis is important in neurodegenerative tauopathies and enhancing tau degradation may be a promising therapeutic strategy [10, 13-16]. Thus, it is important to understand the pathways that stabilize tau and those that favor its turnover. Using a chemical biology approach, we specifically studied the early changes in the tau-associated proteome that occur during the acute switch to a degradation fate. The resulting list of proteins included a number of factors previously linked to tau proteotoxicity, including ILF-2 (NFAT), ILF-3 and ataxin 2 [24, 25]. The results with ataxin-2 (ATXN2) and ataxin-2-like protein (ATXN2L) were particularly striking, with ~16- and 8-fold reductions in binding to tau during degradation, respectively. These observations are interesting because ataxin-2 is linked to spinocerebellar ataxia type 2 (SCA2), a polyglutamine expansion neurodegenerative disorder [41], so direct contacts between these disease-associated proteins might be contribute to their pathophysiology.

4.4.2 The role of Hsp70 in tau homeostasis

From the list of tau-associated proteins, one of the most striking observations was a loss of Hsp70 (HSPA1B) binding, coupled with an increase in Hsp90 (HSP90AB1). What role is Hsp70 playing in this process? Previous findings suggest that Hsp70 is important in stabilizing tau. For example, Hsc70 is required to recycle tau on microtubules, perhaps restricting its availability to the degradation pathways [19]. However, it is also clear that Hsp70s are not exclusively devoted to stabilizing tau. For example, if this were the case, then Hsp70 knock-down should reduce tau levels, phenocopying MB treatment. Instead,

only mild changes in tau levels are typically observed upon knock-down or over-expression of myc-Hsp70 [17]. One possible way to account for these observations is that Hsp70 could play an active role in "hand-off" of tau to the degradation pathway. This process might be initiated by MB in these studies, because, although MB is certainly not a selective Hsp70 inhibitor [42, 43], over-expression of Hsp70 enhances compound-induced degradation of tau [13]. Thus, MB might be leading to conversion of Hsp70, such that it links the chaperone to the degradation pathway. Such a mechanism could involve co-chaperones, however our data suggests that, if so, this mechanism is not driven by the co-chaperone Hop (Appendix 4.5). Alternatively, an acute release of tau from Hsp70 may be important to enable Hsp90 binding. In this model, the activity of Hsp70 that is favored by chemical inhibitors might not produce the same phenotype as knock-down or over-expression, which removes the entire protein. Rather, the transition might require a chemical trigger, such as MB or other Hsp70 inhibitors, which alter Hsp70's nucleotide state, substrate affinity, or conformation [16, 44].

4.4.3 Hsp90-dependent degradation of tau

What role is Hsp90 playing in this process? Many of our observations point to an unexpected role of Hsp90 in the degradation of tau. For example, knock-down of Hsp90 attenuated MB-induced clearance (see Figure 4.2). This finding is unexpected, in part, because Hsp90 is best known for its ability to stabilize ~200 "client" proteins, such as the glucocorticoid receptor (GR) [27]. In those systems, Hsp90 is normally found in the final, high affinity complex that protects the active protein fold [26, 45-47]. Accordingly, inhibitors of Hsp90 relieve the protective effect and favor degradation of the clients,

usually through a process involving Hsp70. Thus, Hsp90 is typically considered a protective chaperone, while Hsp70 is considered a triage chaperone. However, there are clear examples of clients in the literature that don't follow this paradigm. For example, Hsp90 promotes the degradation of the von Hippel-Lindau tumor-suppressor protein and high-density lipoprotein [28, 29] and, in those systems, Hsp70 appears to play an upstream role in folding. Our results suggest that tau might fall into this latter category of atypical chaperone clients, those in which Hsp90 can assume the task of promoting turnover. However, tau seems to be different in some important ways. For example, Hsp90 inhibitors block the degradation of Von Hippel-Lindau tumor-suppressor protein and high-density lipoprotein, whereas these same compounds reduce mutant and phosphorylated forms of tau in a pathway dependent on CHIP, but not HSF-1 or Hsp70 [20]. These findings point to a model in which Hsp90 stabilizes some forms of tau, protecting them from clearance [20, 30, 48], while also being involved in the clearance of tau when Hsp70 is inhibited by MB. Clearly, the roles played by Hsp90 in tau homeostasis are complex.

One compelling way to rationalize these observations is to invoke different "pools" of Hsp90. Hsp90 engages in protein-protein interactions with many different co-chaperones and recent work has elegantly shown that distinct Hsp90 complexes exist in the cytosol [49]. We can speculate that some of these Hsp90 complexes may be involved in stabilizing tau while others, such as the ones apparently favored by MB treatment, might target it for degradation. Indeed, some Hsp90 co-chaperones are known to promote tau stabilization, such as cdc37 and FKBP51, while others accelerate degradation, such as

FKBP52 and CHIP [16]. Further, the acetylation state of Hsp90 may also influence whether it targets tau for degradation [50, 51]. Unfortunately, there was no obvious change in co-chaperone levels in the tau mass spectrometry studies (Appendix 4.2), but these proteins may not have been abundant enough or might bind too weakly to be detected. Further work, perhaps using small molecules that target individual Hsp90 complexes, will likely be required to better understand the mechanism by which co-chaperones affect the fate of tau.

4.4.4 Summary and future directions

Some of the unresolved issues in understanding tau degradation are what happens during the handoff of tau from Hsp70 to Hsp90 and what happens after formation of the Hsp90-tau complex? One key observation is that Hsp70 efficiently competes with Hsp90 for binding tau, but not the inverse (see Figure 4.4 and Table 4.1). Thus, Hsp90-mediated degradation might depend on a prior signal to release Hsp70. Moreover, this signal might induce a conformation of Hsp70 that actively recruits Hsp90, although we know it does not directly change the binding of Hop or tau to Hsp70 (Appendix 4.4 and 4.5). Despite these speculations and open questions, the use of a chemical probe allowed us to uncover changes in chaperone-tau complexes, which may be transiently present at low levels, during the initiation of degradation. In doing so, we gained unexpected insight into how Hsp90 is involved in degrading tau in response to MB. These findings suggest that exchange of Hsp70 for Hsp90 is one key aspect of the mechanism. This model is supported by the decreased gene expression levels of Hsp90 within Alzheimer's disease patients (Figure 4.5, Table 4.2). Further, within a mouse model [17], it has been observed

that decreased Hsp90 levels is linked to tau accumulation. Additional insights into mechanisms of tau clearance will likely accelerate drug discovery in tauopathies, perhaps by suggesting ways of using Hsp70 and Hsp90 inhibitors to maximize the restoration of tau homeostasis.

4.5 Experimental procedures

4.5.1 Reagents, cell lines, and general methods

Tetramethylthionine (methylene blue) was purchased from Sigma (St. Louis, MO). siRNAs (Qiagen, Valencia, CA) were transfected at 20 nM. Antibodies utilized are as follows: V5 (Sigma, V8137), β-actin (Anaspec, 54591, Fremont, CA), tau-WB/ELISA (Santa Cruz Biotech, sc5587, Santa Cruz, CA), pTau (p396/404, provided by Dr. Peter Davies, Albert Einstein College of Medicine, Bronx, NY), Hsp70 (Assay Designs, Plymouth Meeting, PA), Hsp90 (Santa Cruz Biotech, sc7947), goat anti-rabbit HRP (Anaspec, 28177), and goat anti-mouse HRP (Anaspec 28173). All cells were maintained according to ATCC guidelines. Stably transfected HeLa (C3) cells overexpressing wild-type 4RON human tau were previously generated by clonal selection with G418 (Invitrogen, Grand Island, NY) [13]. The absorbance and luminescence measurements were performed using a SpectraMax M5 multimode plate reader (Molecular Devices, Sunnyvale, CA, USA).

4.5.2 Western blot analysis

Samples were separated under reducing and denaturing conditions using 10-20% Tris-Tricine gels (Invitrogen). After transfering to nitrocellulose membrane (Whatman,

Piscataway, NJ, USA), the membranes were blocked with 5% milk in TBS-T (25 mM Tris–HCl, 140 mM NaCl, 0.1% Tween 20) for at least 3 hours. Protein levels were detected by incubating the membrane overnight at 4 ^{o}C with primary antibodies diluted 1:1,000, unless otherwise noted, in TBS-T containing 2% bovine serum albumin (BSA, Sigma). Finally, the membrane was incubated for 1 hour with the appropriate HRP-conjugated secondary antibody diluted 1:10,000 in TBS-T with 5% BSA. Membranes were washed three times for 5 minutes with TBS-T at each step. Membranes were developed using Supersignal West Pico chemiluminescence kit (Thermo Scientific, Waltham, MA).

4.5.3 Immunoprecipitation of V5-tau

HeLa cells stably transfected with V5-4RON tau[13] were grown to 90 % confluence and subsequently treated with 5 mM bortezimib for four hours, followed by a ten minute treatment with either 50 mM MB or DMSO control (1%). Cells were lysed with M-Per lysis buffer[19] and 5 mg of lysate was immunoprecipitated by incubating with 75 μL of goat anti-V5 conjugated to agarose beads (Bethyl Laboratories, S190-119, Montgomery, TX) at 4 ^{o}C overnight in the dark. Beads were subsequently washed with 100 μL of PBS + 0.1% Tween 20, followed by washes with 100 μL and then 200 μL of PBS. Finally proteins associated were eluted using 45 μL of 0.1 M glycine (pH 2.7) and neutralized by adding 5 μL 1M Tris-HCl (pH 8.0). 25 μL of these samples were separated on 10-20% Tris-Tricine gel (Invitrogen).

4.5.4 Mass spectrometry

Gels were submitted for mass spectrometry analysis at the University of Michigan's Department of Pathology Proteomics Facility. Immunoprecipitations were performed on two independent biological samples and each sample was subject to in-gel digestion with trypsin. Proteins were identified by liquid chromatography-tandem MS (MS/MS) as previously described[52]. Mass spectrometric analysis was performed in technical triplicates on each sample, providing a total of six datasets. Identified peptides were searched against the human IPI database developed by the Global Proteome Machine (www.thegpm.org). Tau interacting proteins were defined as proteins with at least 1 peptide fulfilling a ProteinProphet [53, 54] probability score of > 0.97. This method gave a false-discovery-rate (FDR) of 0.05 and identified 504 tau-interacting proteins (Appendix 4.2).

4.5.5 Quantitative spectral analysis

Quantitative spectral analysis was performed as previously described [55, 56]. Briefly, a protein was considered to be differentially associated with tau if it had a Bayes factor greater than ten and exhibited a fold change greater than two. Using this definition, 48 of the 504 interacting proteins were found to be differentially associated upon MB treatment (Figure 4.1C, Appendix 4.2).

4.5.6 Protein purification

Human Hsp70 (HSPA1B), Hsc70 (HSPA8), Hsp70 NBD (HSPA1B 1-383), and Hsp70 mutants were purified as previously described for DnaK using a His column, including

cleavage of the His tag via TEV protease, and final purification on an ATP-agarose column [57, 58]. Mutants were made using QuikChange site-directed mutagenesis kit (Stratagene, La Jolla, CA) according to the manufacture's protocol [59]. Human Hsp90β (HSP90AB1) and Hsp90α (HSP90AA1) were purified as previously described [60]. Finally, N-terminal His-tagged Human 4RON tau and Hop were purified according to the previously developed protocols [61] [62].

4.5.7 Tau peptide microarray

Tau peptides were designed as 15-mers containing 4 amino acid overhangs, spanning the full sequence of PNS-tau (P10636-9). In addition, full-length proteins expected to bind Hsp70 and Hsp90 were printed as positive controls, including human and mouse IgG and tau. Empty spots were used as negative controls. The microarrays were printed on single microscope slides in triplicate (JPT Peptide Technologies, Berlin, Germany). Binding was tested per the manufacturer's protocol using 10 μM Hsp70-His, Hsp90-His, or Hsp70 nucleotide binding domain (NBD) in binding buffer (25 mM HEPES pH 7.2, 150 mM NaCl, 20 mM KCl, 5 mM $MgCl_2$, 0.01% Tween 20). Binding was detected using 1:1,000 titer of HiLyte555 anti-His antibody (Anaspec) in TBS-T with 1% bovine serum albumin (Sigma) and scanning the microarrays at a fluorescence emission of 532 nM using a GenePix 4100A Microarray Scanner (Molecular Devices, Sunnyvale, CA). A standard local background subtraction was performed for all experiments. Binding was defined as peptides giving fluorescence signals greater than 3 standard errors above the mean and those that did not appear as positive in the Hsp70 NBD or antibody alone tests.

4.5.8 ELISA-based tau binding

The procedure for chaperone binding to luciferase was adapted from a previous report [63]. Briefly, 0.1 mg/mL of either human Hsp70 or Hsp90 (30 μL) in 50 mM MES buffer (pH 5.5) was added to each well of 96-well plates (Thermo Fisher, clear, nonsterile, flat bottom) and these plates incubated for 6 hrs at 37 °C. The wells were then washed with 100 μL of TBS-T (3×3 min, rocking). To these wells, 50 μL of 4RON tau solution (at indicated concentrations) in binding buffer (25 mM HEPES pH 7.2, 150 mM NaCl, 20 mM KCl, 5 mM $MgCl_2$, 0.01% Tween20) with 1 mM ATP, unless otherwise noted, was added and the plates were incubated at room temperature with gentle rocking overnight. Plates were developed using the rabbit anti-tau primary antibody (Santa Cruz, sc5587) (1:2,000 dilution, in TBS-T, 50 μL/well) and the goat anti-rabbit HRP conjugated secondary antibody (Anaspec, 28177) (1:2,000 dilution in TBS-T, 50 μL/well). The TMB substrate kit (Cell Signaling Technology, Danvers, MA) was used to detect binding. In each experiment, the signal from non-specific binding of 4RON to empty control wells was used as a negative control and subtracted, but this signal was minimal. Binding curves were fit using hyperbolic fits with a non-zero intercept in GraphPad Prism version 5.0 for Windows (GraphPad Software, San Diego, CA). MB treatment *in vitro* was performed by incubating 10 μM Hsp70 with 5 mM MB at 37 ^{o}C for 1 hour. Treated protein samples were subsequently dialyzed in 4 liters of dialysis buffer (25 mM HEPES, pH 7.4, 20 mM KCl, 6 mM $MgCl_2$) at 4 ^{o}C changing dialysis buffer twice. Thus, only the irreversibly oxidized Hsp70 was evaluated in this *in vitro* binding assay and all other *in vitro* biochemical assays discussed.

4.5.9 ATPase assay

ATPase activity was measured according to the previously published method [58]. Briefly, malachite green-based assays were used to measure phosphate release from purified Hsp70s (1 μM). Reactions were initiated with 1 mM ATP, performed for 60 minutes and quenched before measuring absorbance. Absorbance readings were converted to pmol of ATP using a phosphate standard curve.

4.5.10 Luciferase refolding assay

The luciferase refolding activity of DnaK WT and mutants was evaluated as described with minor changes [64]. Briefly, Gu-HCl denatured firefly luciferase (100 nM) was incubated with an enzyme mix containing Hsp70, MB treated Hsp70, or Hsp70 mutants (1 μM), and increasing concentrations of human J-protein DJA2. Refolding was initiated with the addition of 1 mM ATP. After 1 h of incubation at 37 °C, refolding was detected using a 2% (v/v) SteadyGlo (Promega, Madison, WI) reagent followed by measurement of luminescence. As a negative control, the signal from samples containing everything but Hsp70 was evaluated.

4.5.11 Surface plasmon resonance experiments

A streptavidin chip (SA; GE Healthcare) was docked and equilibrated with HBS modified buffer (25 mM HEPES pH 7.4, 150 mM NaCl, 20 mM KCl, 5 mM $MgCl_2$, 0.005% Tween-20) overnight at 5 uL/min. Proteins were biotinylated using Sulfo-NHS-LC-Biotin (Invitrogen, B-6353) following the protocol provided by Invitrogen (MP00143). The chip was washed twice with two 10 μl pulses of 1M NaCl in 50mM

NaOH. Then, the indicated Hsp70's were immobilized in MES buffer (50 mM MES pH 5.5, 150 mM NaCl, 0.01% Tween-20) at 5 µl/min. Average immobilization responses for the various Hsp70 truncations were approximately 1,000 RUs. Hsp70 NBD was immobilized as a negative control, and signal from this lane was subtracted from that of the test lanes. After immobilization of all biotinylated proteins, the chip was equilibrated for at least 4 hours at 5 µL/min. Varying concentrations of HOP were prepared in HBS modified buffer and 30 µL was injected at 20 µL/min. For competition experiments, HOP (3 µM) and increasing concentrations of unlabeled Hsp70 were combined in HBS modified buffer greater than 30 min prior to injection. For both direct and competition binding, the binding surface was recovered with regeneration buffer (50 mM NaOH, 1M NaCl), using 2 pulse injections of 10 µL. Equilibrium data were fit using the RU values 5 seconds prior to the end of the association phase, followed by non-linear regression analysis using GraphPad Prism software.

4.5.11 Analysis of Hsp70 and Hsp90 expression levels in AD samples

The GDS810 [38] and GSE5281 [39] gene expression microarray datasets were downloaded from the NCBI Gene Expression Omnibus. Normalized data for relevant microarray probes in all samples were extracted for the genes listed in Table 4.2. The sample GSM21206 was excluded from the GDS810 dataset due to artifact rendering which made this sample incomparable to the rest. Probe expression values were standardized as a z-score (z = (value – mean)/(standard deviation)) for all cytosolic isoforms of Hsp70 and Hsp90. Individual probe z-scores were averaged for a given gene and compared across sample groups (control patients versus patients with disease).

Statistical significance (p-value <0.05) for gene expression changes between two sample groups was determined with a Mann-Whitney U test (see Appendix 4.7).

Notes

This work will in part be submitted for publication as "Analysis of the Tau-Associated Proteome Reveals that Exchange of Hsp70 for Hsp90 Targets Tau for Degradation." Andrea Thompson and Jason Gestwicki designed the experiments. Andrea Thompson, Umesh K. Jinwal performed the experiments. John Prensner analyzed the gene expression data from the AD patient samples. Anne T. Gillies developed the peptide microarray binding platform. Jennifer Rauch performed the ATPase assay and luciferase refolding assay on *in vitro* treated methylene blue and the cysteine to aspartic acid mutations of Hsp70. Finally, for intellectual contributions we recognize Matthew Scaglione, Arul Chinnaiyan, Henry L. Paulson, and Chad A. Dickey. The authors would to thank William B. Pratt, Andrew Lieberman, and Yoichi Osawa for helpful discussions. We would also like to acknowledge Daniel R. Southworth for help in purifying Hsp90. The University of Michigan's Department of Pathology Proteomics Core performed the mass spectrometry studies. A.D.T. was supported by a pre-doctoral fellowship from the National Institute of Health (F30AG035464). This work was additionally supported by NIH R01NS059690 and an anonymous gift from the Michigan Alzheimer's Research Center (MADC).

4.6 Appendix

4.6.1 Methylene Blue (MB) causes robust, rapid clearance of tau.

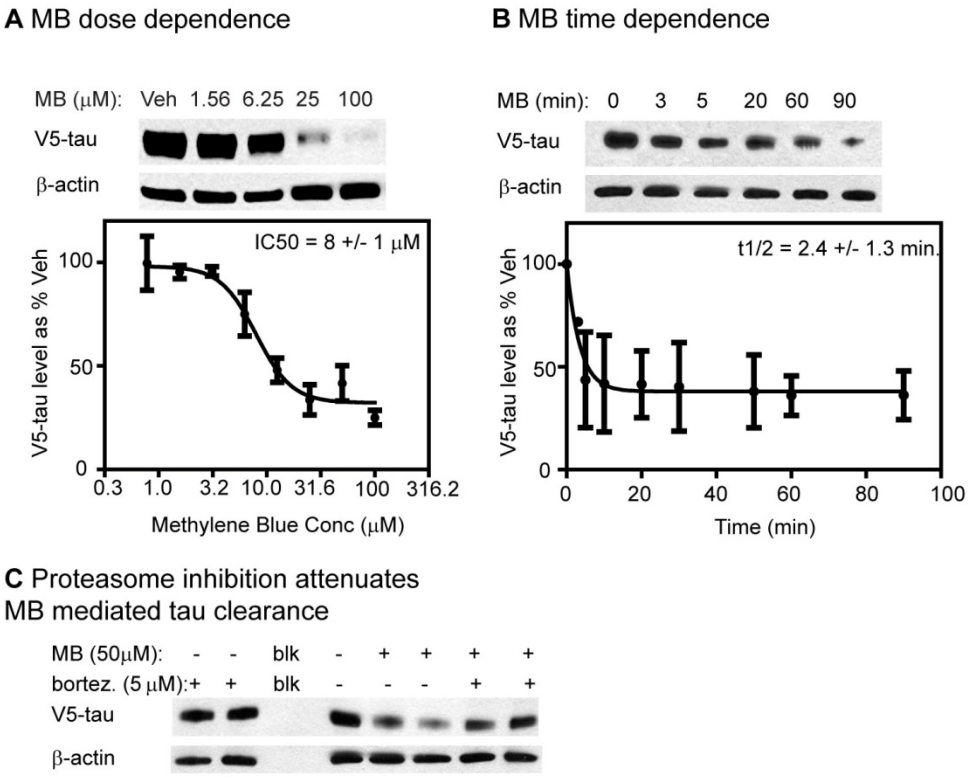

Appendix 4.1. Methylene Blue (MB) causes robust, rapid clearance of tau. (A) HeLa (C3) cells, stably transfected with V5-4RON tau, were treated with MB. A representative western blot and quantification of four independent experiments is shown. (B) HeLa (C3) cells, stably transfected with V5-4R0N tau, were treated with 50 μM MB and lysates were prepared at the indicated times. A representative western blot and quantification of three independent experiments is shown. (C) Pre-treatment with bortezomib (bortez.) for 4 hours attenuates the loss of tau in response to MB (50 μM) for 1hr. Quantification of tau levels in (A and B) was performed using Image J as percentage of the vehicle (veh.) control and error bars indicate the standard error of the mean.

4.6.2 Full results of mass spectrometry and quantitative spectral analysis

Tau-association increased by MB treatment

Protein	Bayes Factor	Fold Change	Direction	FLAG	description
P58107	8.37E+04	2.27	1		ID=|EPIPL_HUMAN| GeneName=|EPPK1|
sp|TRYP_PIG|	5.79E+04	1.18	1	FLAG	COMMON CONTAMINANT!
Q9UG75	5.22E+03	2.85	1		ID=|HNRL1_HUMAN| GeneName=|HNRNPUL1|
O15027	1.91E+03	2.38	1		ID=|SC16A_HUMAN| GeneName=|SEC16A|
P16402	1.90E+03	2.83	1		ID=|H13_HUMAN| GeneName=|HIST1H1D|
P27708	1.43E+03	2.82	1		ID=|PYR1_HUMAN| GeneName=|CAD|
P19338	777.16	2.38	1		ID=|NUCL_HUMAN| GeneName=|NCL|
Q96ML2	363.17	8.86	1		ID=|VIME_HUMAN| GeneName=|VIM|
P23526	304.15	5.73	1		ID=|SAHH_HUMAN| GeneName=|AHCY|
Q8N1P6	261.25	5.42	1		ID=|K1C17_HUMAN| GeneName=|KRT17|
P08238	**244.74**	**2.42**	**1**		**ID=|HS90B_HUMAN| GeneName=|HSP90AB1|**
P30050	142.86	1.50	1	FLAG	ID=|RL12_HUMAN| GeneName=|RPL12|
P62701	100.75	9.15	1		ID=|RS4X_HUMAN| GeneName=|RPS4X|
P08729	95.25	1.96	1	FLAG	ID=|K2C7_HUMAN| GeneName=|KRT7|
P18124	91.64	5.12	1		ID=|RL7_HUMAN| GeneName=|RPL7|
P62847	86.70	4.51	1		ID=|RS24_HUMAN| GeneName=|RPS24|
Q14444	84.36	1.78	1	FLAG	ID=|CAPR1_HUMAN| GeneName=|CAPRIN1|
O43809	68.23	3.23	1		ID=|CPSF5_HUMAN| GeneName=|NUDT21|
P05109	49.20	4.06	1		ID=|S10A8_HUMAN| GeneName=|S100A8|
P49207	47.63	3.56	1		ID=|RL34_HUMAN| GeneName=|RPL34|
Q96QT5	29.67	2.22	1		ID=|BPA1_HUMAN| GeneName=|DST|
P62241	29.03	3.00	1		ID=|RS8_HUMAN| GeneName=|RPS8|
P62081	28.53	1.99	1	FLAG	ID=|RS7_HUMAN| GeneName=|RPS7|
Q5XKE5	26.95	3.80	1		ID=|K2C79_HUMAN| GeneName=|KRT79|
Q13283	25.14	2.82	1		ID=|G3BP1_HUMAN| GeneName=|G3BP1|
Q9Y2Q9	22.09	3.19	1		ID=|RT28_HUMAN| GeneName=|MRPS28|
Q86YZ3	19.77	2.55	1		ID=|HORN_HUMAN| GeneName=|HRNR|
Q96IT0	19.48	3.54	1		ID=|FAS_HUMAN| GeneName=|FASN|
P62269	18.15	1.75	1	FLAG	ID=|RS18_HUMAN| GeneName=|RPS18|
P62910	18.09	2.44	1		ID=|RL32_HUMAN| GeneName=|RPL32|
P62424	16.82	2.95	1		ID=|RL7A_HUMAN| GeneName=|RPL7A|
Q92841	15.50	1.47	1	FLAG	ID=|DDX17_HUMAN| GeneName=|DDX17|
P62906	14.83	5.23	1		ID=|RL10A_HUMAN| GeneName=|RPL10A|
P06702	14.19	3.50	1		ID=|S10A9_HUMAN| GeneName=|S100A9|
Q08211	12.78	1.47	1	FLAG	ID=|DHX9_HUMAN| GeneName=|DHX9|
P31483	10.23	3.52	1		ID=|TIA1_HUMAN| GeneName=|TIA1|

Tau-association decreased by MB treatment

Protein	Bayes Factor	Fold Change	Direction	FLAG	description
sp|K22E_ HUMAN|	5.08E+10	2.87	-1		COMMON CONTAMINANT!
Q92945	1.65E+06	3.29	-1		ID=|FUBP2_HUMAN| GeneName=|KHSRP|
P13645	1.31E+06	1.73	-1	FLAG	ID=|K1C10_HUMAN| GeneName=|KRT10|
Q99700	7.42E+05	15.94	-1		ID=|ATX2_HUMAN| GeneName=|ATXN2|
P62314	2.00E+04	6.03	-1		ID=|SMD1_HUMAN| GeneName=|SNRPD1|
P62316	4.15E+03	1.80	-1	FLAG	ID=|SMD2_HUMAN| GeneName=|SNRPD2|
Q8WWM4	1.14E+03	7.99	-1		ID=|ATX2L_HUMAN| GeneName=|ATXN2L|
Q9Y224	573.74	1.56	-1	FLAG	ID=|CN166_HUMAN| GeneName=|C14orf166|
Q12905	281.18	4.49	-1		ID=|ILF2_HUMAN| GeneName=|ILF2|
P55769	99.47	3.27	-1		ID=|NH2L1_HUMAN| GeneName=|NHP2L1|

Tau-association decreased by MB treatment					
Protein	**Bayes Factor**	**Fold Change**	**Direction**	**FLAG**	**description**
Q3MHD2	93.31	2.98	-1		ID=|LSM12_HUMAN| GeneName=|LSM12|
P08107	**68.63**	**2.22**	**-1**		**ID=|HSP71_HUMAN| GeneName=|HSPA1B|**
Q52LJ0	57.03	2.59	-1		ID=|FA98B_HUMAN| GeneName=|FAM98B|
Q969G3	50.93	3.95	-1		ID=|SMCE1_HUMAN| GeneName=|SMARCE1|
Q86TJ0	35.16	1.36	-1	FLAG	ID=|SC31A_HUMAN| GeneName=|SEC31A|
P51532	30.57	2.12	-1		ID=|SMCA4_HUMAN| GeneName=|SMARCA4|
P63261	26.19	1.61	-1	FLAG	ID=|ACTG_HUMAN| GeneName=|ACTG1|
Q9NQA2	24.08	2.41	-1		ID=|ILF3_HUMAN| GeneName=|ILF3|
Q9UPQ9	22.42	2.89	-1		ID=|TNR6B_HUMAN| GeneName=|TNRC6B|
Q99729	18.07	3.92	-1		ID=|ROAA_HUMAN| GeneName=|HNRNPAB|
P21266	15.78	3.38	-1		ID=|GSTM3_HUMAN| GeneName=|GSTM3|
P01903	15.08	2.62	-1		ID=|DRA_HUMAN| GeneName=|HLA-DRA|
Q9Y367	14.56	1.98	-1	FLAG	ID=|PAIRB_HUMAN| GeneName=|SERBP1|
P13987	13.02	4.17	-1		ID=|CD59_HUMAN| GeneName=|CD59|
Q9HAV7	12.07	3.35	-1		ID=|GRPE1_HUMAN| GeneName=|GRPEL1|
Q14019	12.07	3.35	-1		ID=|COTL1_HUMAN| GeneName=|COTL1|
P08195	10.32	2.81	-1		ID=|4F2_HUMAN| GeneName=|SLC3A2|

Tau-association unchanged by MB treatment (Bayes Factor < 10)					
Protein	**Bayes Factor**	**Fold Change**	**Direction**	**FLAG**	**description**
P46777	9.45	3.75	1		ID=|RL5_HUMAN| GeneName=|RPL5|
P61313	9.33	3.16	1		ID=|RL15_HUMAN| GeneName=|RPL15|
P12268	9.24	2.55	1		ID=|IMDH2_HUMAN| GeneName=|IMPDH2|
O43390	9.20	1.64	-1	FLAG	ID=|HNRPR_HUMAN| GeneName=|HNRNPR|
Q7Z794	7.93	3.10	-1		ID=|K2C1B_HUMAN| GeneName=|KRT77|
O75340	7.76	1.36	1	FLAG	ID=|PDCD6_HUMAN| GeneName=|PDCD6|
P27635	7.53	3.34	1		ID=|RL10_HUMAN| GeneName=|RPL10|
P32969	7.50	3.53	1		ID=|RL9_HUMAN| GeneName=|RPL9P9|
P15880	7.43	2.98	1		ID=|RS2_HUMAN| GeneName=|RPS2|
P99999	7.35	3.30	-1		ID=|CYC_HUMAN| GeneName=|CYCS|
P61513	6.86	4.72	1		ID=|RL37A_HUMAN| GeneName=|RPL37A|
Q07020	6.83	2.94	1		ID=|RL18_HUMAN| GeneName=|RPL18|
Q8NCA5	6.63	3.43	-1		ID=|FA98A_HUMAN| GeneName=|FAM98A|
P62244	6.29	2.08	1		ID=|RS15A_HUMAN| GeneName=|RPS15A|
P26373	6.12	2.11	1		ID=|RL13_HUMAN| GeneName=|RPL13|
P62306	6.05	2.24	-1		ID=|RUXF_HUMAN| GeneName=|SNRPF|
P05388	6.01	3.61	1		ID=|RLA0_HUMAN| GeneName=|RPLP0|
P09382	5.66	3.30	1		ID=|LEG1_HUMAN| GeneName=|LGALS1|
Q13442	5.52	2.28	-1		ID=|HAP28_HUMAN| GeneName=|PDAP1|
P35637	5.29	1.60	1		ID=|FUS_HUMAN| GeneName=|FUS|
Q9Y4L1	5.15	2.23	-1		ID=|HYOU1_HUMAN| GeneName=|HYOU1|
P62913	5.11	1.92	1		ID=|RL11_HUMAN| GeneName=|RPL11|
Q6S381	5.07	2.81	1		ID=|PLEC_HUMAN| GeneName=|PLEC|
P02647	4.95	2.87	1		ID=|APOA1_HUMAN| GeneName=|APOA1|
P04843	4.88	3.05	-1		ID=|RPN1_HUMAN| GeneName=|RPN1|
P08779	4.85	2.41	1		ID=|K1C16_HUMAN| GeneName=|KRT16|
P32322	4.76	2.81	-1		ID=|P5CR1_HUMAN| GeneName=|PYCR1|
P37837	4.74	2.68	1		ID=|TALDO_HUMAN| GeneName=|TALDO1|
Q96RN5	4.71	2.16	-1		ID=|MED15_HUMAN| GeneName=|MED15|
P39019	4.67	1.37	1		ID=|RS19_HUMAN| GeneName=|RPS19|
P23246	4.67	3.06	-1		ID=|SFPQ_HUMAN| GeneName=|SFPQ|

Tau-association unchanged by MB treatment (Bayes Factor < 10)

Protein	Bayes Factor	Fold Change	Direction	FLAG	description
Q15819	4.63	2.57	-1		ID=|UB2V2_HUMAN| GeneName=|UBE2V2|
P63167	4.63	2.75	-1		ID=|DYL1_HUMAN| GeneName=|DYNLL1|
P05783	4.60	2.56	1		ID=|K1C18_HUMAN| GeneName=|KRT18|
P25398	4.57	1.40	1		ID=|RS12_HUMAN| GeneName=|RPS12|
O96019	4.52	3.04	-1		ID=|ACL6A_HUMAN| GeneName=|ACTL6A|
P04264	4.43	1.19	-1		ID=|K2C1_HUMAN| GeneName=|KRT1|
P62841	4.38	1.97	1		ID=|RS15_HUMAN| GeneName=|RPS15|
Q01650	4.27	2.81	-1		ID=|LAT1_HUMAN| GeneName=|SLC7A5|
P17096	4.24	3.06	-1		ID=|HMGA1_HUMAN| GeneName=|HMGA1|
Q9H3K6	4.16	2.55	-1		ID=|BOLA2_HUMAN| GeneName=|BOLA2B|
Q00839	4.11	1.02	-1		ID=|HNRPU_HUMAN| GeneName=|HNRNPU|
P35527	4.03	1.45	-1		ID=|K1C9_HUMAN| GeneName=|KRT9|
P50748	3.97	3.36	1		ID=|KNTC1_HUMAN| GeneName=|KNTC1|
P08708	3.87	1.60	1		ID=|RS17_HUMAN| GeneName=|RPS17|
P01040	3.75	2.09	-1		ID=|CYTA_HUMAN| GeneName=|CSTA|
P46782	3.65	1.61	1		ID=|RS5_HUMAN| GeneName=|RPS5|
P27482	3.60	2.23	1		ID=|CALL3_HUMAN| GeneName=|CALML3|
P46781	3.48	3.17	1		ID=|RS9_HUMAN| GeneName=|RPS9|
P46779	3.44	1.97	1		ID=|RL28_HUMAN| GeneName=|RPL28|
P06576	3.40	2.34	-1		ID=|ATPB_HUMAN| GeneName=|ATP5B|
Q9P157	3.33	2.24	-1		ID=|ALBU_HUMAN| GeneName=|ALB|
P98160	3.24	1.67	-1		ID=|PGBM_HUMAN| GeneName=|HSPG2|
P18621	3.22	1.48	1		ID=|RL17_HUMAN| GeneName=|RPL17|
Q96HK3	3.10	2.40	1		ID=|CALM_HUMAN| GeneName=|CALM3|
Q96SI9	3.03	2.75	1		ID=|STRBP_HUMAN| GeneName=|STRBP|
P60174	2.95	1.50	1		ID=|TPIS_HUMAN| GeneName=|TPI1|
Q99584	2.90	2.54	-1		ID=|S10AD_HUMAN| GeneName=|S100A13|
P40259	2.89	2.08	-1		ID=|CD79B_HUMAN| GeneName=|CD79B|
P82932	2.89	3.72	1		ID=|RT06_HUMAN| GeneName=|MRPS6|
P07900	2.89	2.10	1		ID=|HS90A_HUMAN| GeneName=|HSP90AA1|
P35268	2.87	1.29	-1		ID=|RL22_HUMAN| GeneName=|RPL22|
P62633	2.85	2.26	1		ID=|CNBP_HUMAN| GeneName=|CNBP|
Q13765	2.81	1.82	1		ID=|NACA_HUMAN| GeneName=|NACA|
P82650	2.80	2.14	1		ID=|RT22_HUMAN| GeneName=|MRPS22|
P11021	2.79	1.44	-1		ID=|GRP78_HUMAN| GeneName=|HSPA5|
P62899	2.74	1.44	-1		ID=|RL31_HUMAN| GeneName=|RPL31|
P07437	2.70	1.18	1		ID=|TBB5_HUMAN| GeneName=|TUBB|
P26196	2.69	2.12	-1		ID=|DDX6_HUMAN| GeneName=|DDX6|
O75347	2.64	1.89	-1		ID=|TBCA_HUMAN| GeneName=|TBCA|
Q8TAQ2	2.64	1.97	-1		ID=|SMRC2_HUMAN| GeneName=|SMARCC2|
P00558	2.61	1.14	-1		ID=|PGK1_HUMAN| GeneName=|PGK1|
Q9P225	2.59	2.34	1		ID=|DYH2_HUMAN| GeneName=|DNAH2|
P62753	2.57	2.34	1		ID=|RS6_HUMAN| GeneName=|RPS6|
Q86V69	2.52	1.82	-1		ID=|F120A_HUMAN| GeneName=|FAM120A|
P30048	2.51	2.30	1		ID=|PRDX3_HUMAN| GeneName=|PRDX3|
Q15233	2.48	1.75	-1		ID=|NONO_HUMAN| GeneName=|NONO|
Q96EP5	2.48	2.29	1		ID=|DAZP1_HUMAN| GeneName=|DAZAP1|
P62273	2.45	2.13	-1		ID=|RS29_HUMAN| GeneName=|RPS29|
P84098	2.44	2.62	1		ID=|RL19_HUMAN| GeneName=|RPL19|
P78332	2.39	2.69	-1		ID=|RBM6_HUMAN| GeneName=|RBM6|
Q14157	2.37	1.31	1		ID=|UBP2L_HUMAN| GeneName=|UBAP2L|
Q5D862	2.37	2.32	-1		ID=|FILA2_HUMAN| GeneName=|FLG2|
Q9UBQ5	2.36	2.10	-1		ID=|EIF3K_HUMAN| GeneName=|EIF3K|

Tau-association unchanged by MB treatment (Bayes Factor < 10)					
Protein	Bayes Factor	Fold Change	Direction	FLAG	description
P52597	2.36	1.45	1		ID=|HNRPF_HUMAN| GeneName=|HNRNPF|
P63220	2.35	2.72	-1		ID=|RS21_HUMAN| GeneName=|RPS21|
P62917	2.30	1.82	1		ID=|RL8_HUMAN| GeneName=|RPL8|
Q9NR22	2.26	2.27	1		ID=|ANM8_HUMAN| GeneName=|PRMT8|
P61254	2.24	1.38	1		ID=|RL26_HUMAN| GeneName=|RPL26|
Q96Q81	2.23	2.02	1		ID=|DUT_HUMAN| GeneName=|DUT|
Q02809	2.23	1.88	-1		ID=|PLOD1_HUMAN| GeneName=|PLOD1|
Q6GMP2	2.22	1.39	-1		ID=|ENOA_HUMAN| GeneName=|ENO1|
P08575	2.20	2.19	-1		ID=|PTPRC_HUMAN| GeneName=|PTPRC|
P14678	2.19	1.34	-1		ID=|RSMB_HUMAN| GeneName=|SNRPB|
P52292	2.16	2.62	-1		ID=|IMA2_HUMAN| GeneName=|KPNA2|
O15042	2.14	1.54	-1		ID=|SR140_HUMAN| GeneName=|SR140|
Q9UQ80	2.09	2.69	1		ID=|PA2G4_HUMAN| GeneName=|PA2G4|
P61978	2.08	1.99	1		ID=|HNRPK_HUMAN| GeneName=|HNRNPK|
Q13148	2.05	1.71	-1		ID=|TADBP_HUMAN| GeneName=|TARDBP|
O00425	2.03	2.10	-1		ID=|IF2B3_HUMAN| GeneName=|IGF2BP3|
Q9Y3I0	2.02	1.40	-1		ID=|CV028_HUMAN| GeneName=|C22orf28|
Q9UPA5	2.01	1.44	-1		ID=|BSN_HUMAN| GeneName=|BSN|
O43684	1.99	1.65	1		ID=|BUB3_HUMAN| GeneName=|BUB3|
Q9Y237	1.99	1.81	-1		ID=|PIN4_HUMAN| GeneName=|PIN4|
Q15185	1.98	1.43	1		ID=|TEBP_HUMAN| GeneName=|PTGES3|
Q99377	1.98	1.51	-1		ID=|RU17_HUMAN| GeneName=|SNRNP70|
P11940	1.98	1.59	1		ID=|PABP1_HUMAN| GeneName=|PABPC1|
P01912	1.98	2.15	-1		ID=|2B13_HUMAN| GeneName=|HLA-DRB1|
Q5SRE5	1.96	2.52	-1		ID=|NU188_HUMAN| GeneName=|NUP188|
Q00610	1.92	1.09	1		ID=|CLH1_HUMAN| GeneName=|CLTC|
Q14671	1.91	1.37	-1		ID=|PUM1_HUMAN| GeneName=|PUM1|
P39023	1.91	2.06	1		ID=|RL3_HUMAN| GeneName=|RPL3|
Q9Y293	1.89	2.29	1		ID=|RTN4_HUMAN| GeneName=|RTN4|
P00441	1.89	1.99	1		ID=|SODC_HUMAN| GeneName=|SOD1|
P24534	1.86	1.86	1		ID=|EF1B_HUMAN| GeneName=|EEF1B2|
P68363	1.84	1.35	1		ID=|TBA1B_HUMAN| GeneName=|TUBA1B|
P00492	1.83	1.85	-1		ID=|HPRT_HUMAN| GeneName=|HPRT1|
P13671	1.83	1.85	-1		ID=|CO6_HUMAN| GeneName=|C6|
P35030	1.82	2.59	1		ID=|TRY3_HUMAN| GeneName=|PRSS3|
Q06323	1.81	2.05	1		ID=|PSME1_HUMAN| GeneName=|PSME1|
P29558	1.81	2.61	-1		ID=|RBMS1_HUMAN| GeneName=|RBMS1|
P36873	1.72	1.93	1		ID=|PP1G_HUMAN| GeneName=|PPP1CC|
Q01469	1.70	1.66	-1		ID=|FABP5_HUMAN| GeneName=|FABP5|
Q9BWG4	1.70	2.29	-1		ID=|SSBP4_HUMAN| GeneName=|SSBP4|
P63241	1.69	1.26	1		ID=|IF5A1_HUMAN| GeneName=|EIF5A|
P81605	1.68	1.92	-1		ID=|DCD_HUMAN| GeneName=|DCD|
O14737	1.64	1.92	-1		ID=|PDCD5_HUMAN| GeneName=|PDCD5|
Q96DT0	1.63	1.79	1		ID=|LEG12_HUMAN| GeneName=|LGALS12|
Q6IBQ6	1.63	2.08	-1		ID=|SAP_HUMAN| GeneName=|PSAP|
P26447	1.61	1.60	-1		ID=|S10A4_HUMAN| GeneName=|S100A4|
Q96PK6	1.61	1.54	-1		ID=|RBM14_HUMAN| GeneName=|RBM14|
Q14974	1.60	1.09	1		ID=|IMB1_HUMAN| GeneName=|KPNB1|
Q66GS9	1.60	1.30	1		ID=|CP135_HUMAN| GeneName=|CEP135|
P09497	1.60	1.25	1		ID=|CLCB_HUMAN| GeneName=|CLTB|
P63244	1.59	1.42	1		ID=|GBLP_HUMAN| GeneName=|GNB2L1|
Q92973	1.57	1.45	-1		ID=|TNPO1_HUMAN| GeneName=|TNPO1|
Q562E7	1.54	1.75	1		ID=|WDR81_HUMAN| GeneName=|WDR81|

Tau-association unchanged by MB treatment (Bayes Factor < 10)					
Protein	Bayes Factor	Fold Change	Direction	FLAG	description
P84103	1.54	2.64	-1		ID=|SFRS3_HUMAN| GeneName=|SFRS3|
Q15365	1.54	1.30	1		ID=|PCBP1_HUMAN| GeneName=|PCBP1|
P38159	1.54	1.99	-1		ID=|HNRPG_HUMAN| GeneName=|RBMX|
P01700	1.52	1.73	-1		ID=|LV102_HUMAN| GeneName=|LUZP6|
Q9UN86	1.52	1.52	1		ID=|G3BP2_HUMAN| GeneName=|G3BP2|
P02545	1.51	1.60	-1		ID=|LMNA_HUMAN| GeneName=|LMNA|
P01871	1.50	1.57	-1		ID=|IGHM_HUMAN| GeneName=|IGHM|
Q02878	1.50	1.66	1		ID=|RL6_HUMAN| GeneName=|RPL6|
Q02543	1.49	1.74	1		ID=|RL18A_HUMAN| GeneName=|RPL18A|
P31946	1.49	1.32	1		ID=|1433B_HUMAN| GeneName=|YWHAB|
P30040	1.49	1.52	-1		ID=|ERP29_HUMAN| GeneName=|ERP29|
O60869	1.47	1.40	1		ID=|EDF1_HUMAN| GeneName=|EDF1|
Q9BW65	1.47	1.95	1		ID=|RL14_HUMAN| GeneName=|RPL14|
P07355	1.46	1.09	-1		ID=|ANXA2_HUMAN| GeneName=|ANXA2|
Q07666	1.46	1.34	-1		ID=|KHDR1_HUMAN| GeneName=|KHDRBS1|
P61604	1.46	2.16	-1		ID=|CH10_HUMAN| GeneName=|HSPE1|
Q13435	1.45	1.79	-1		ID=|SF3B2_HUMAN| GeneName=|SF3B2|
P15531	1.44	1.60	-1		ID=|NDKA_HUMAN| GeneName=|NME1|
P04220	1.44	1.52	-1		ID=|MUCB_HUMAN| GeneName=|MUC7| |
Q9UJ07	1.44	1.14	-1		ID=|SYNE1_HUMAN| GeneName=|SYNE1|
P62854	1.43	1.71	-1		ID=|RS26_HUMAN| GeneName=|RPS26|
Q92600	1.43	1.57	-1		ID=|RCD1_HUMAN| GeneName=|RQCD1|
O95486	1.39	2.62	1		ID=|SC24A_HUMAN| GeneName=|SEC24A|
P68032	1.39	1.77	-1		ID=|ACTC_HUMAN| GeneName=|ACTC1|
Q9Y3F4	1.36	1.20	-1		ID=|STRAP_HUMAN| GeneName=|STRAP| |
Q86V81	1.35	1.68	1		ID=|THOC4_HUMAN| GeneName=|THOC4|
P55327	1.34	1.76	1		ID=|TPD52_HUMAN| GeneName=|TPD52|
Q9HA92	1.34	1.76	1		ID=|RSAD1_HUMAN| GeneName=|RSAD1|
P35579	1.33	1.30	-1		ID=|MYH9_HUMAN| GeneName=|MYH9|
P02786	1.33	1.46	-1		ID=|TFR1_HUMAN| GeneName=|TFRC|
O96005	1.33	1.46	-1		ID=|CLPT1_HUMAN| GeneName=|CLPTM1|
Q15717	1.32	1.73	-1		ID=|ELAV1_HUMAN| GeneName=|ELAVL1|
P05387	1.32	1.13	1		ID=|RLA2_HUMAN| GeneName=|RPLP2|
Q9Y583	1.31	1.79	1		ID=|HNRPQ_HUMAN| GeneName=|SYNCRIP|
Q9P0T4	1.31	1.77	1		ID=|ZN581_HUMAN| GeneName=|ZNF581|
O00233	1.29	1.86	-1		ID=|PSMD9_HUMAN| GeneName=|PSMD9|
Q70E73	1.29	1.86	-1		ID=|RAPH1_HUMAN| GeneName=|RAPH1|
P42126	1.29	1.86	-1		ID=|D3D2_HUMAN| GeneName=|DCI|
P43243	1.29	1.36	-1		ID=|MATR3_HUMAN| GeneName=|MATR3|
P23396	1.25	1.14	1		ID=|RS3_HUMAN| GeneName=|RPS3|
P47914	1.25	1.28	1		ID=|RL29_HUMAN| GeneName=|RPL29|
P51398	1.24	1.52	1		ID=|RT29_HUMAN| GeneName=|DAP3|
P62249	1.24	1.26	1		ID=|RS16_HUMAN| GeneName=|RPS16|
Q9NUJ1	1.24	1.63	1		ID=|ABHDA_HUMAN| GeneName=|ABHD10|
P40429	1.24	1.65	1		ID=|RL13A_HUMAN| GeneName=|RPL13A|
Q9Y3D9	1.24	1.47	1		ID=|RT23_HUMAN| GeneName=|MRPS23|
Q9BWW4	1.23	1.55	-1		ID=|SSBP3_HUMAN| GeneName=|SSBP3|
Q92922	1.23	1.57	-1		ID=|SMRC1_HUMAN| GeneName=|SMARCC1|
P35613	1.23	1.57	-1		ID=|BASI_HUMAN| GeneName=|BSG|
Q15181	1.23	1.60	-1		ID=|IPYR_HUMAN| GeneName=|PPA1|
P49321	1.23	1.45	-1		ID=|NASP_HUMAN| GeneName=|NASP|
P32970	1.23	1.51	-1		ID=|CD70_HUMAN| GeneName=|CD70|
Q9UKK9	1.21	1.80	-1		ID=|NUDT5_HUMAN| GeneName=|NUDT5|

Tau-association unchanged by MB treatment (Bayes Factor < 10)					
Protein	Bayes Factor	Fold Change	Direction	FLAG	description
P52434	1.21	1.39	1		ID=|RPAB3_HUMAN| GeneName=|POLR2H|
P30043	1.21	1.39	1		ID=|BLVRB_HUMAN| GeneName=|BLVRB|
P56703	1.21	1.39	1		ID=|WNT3_HUMAN| GeneName=|WNT3|
P56537	1.20	1.11	1		ID=|IF6_HUMAN| GeneName=|EIF6|
Q15691	1.19	1.61	-1		ID=|MARE1_HUMAN| GeneName=|MAPRE1|
P62263	1.19	1.20	1		ID=|RS14_HUMAN| GeneName=|RPS14|
P22626	1.19	1.45	1		ID=|ROA2_HUMAN|
P51149	1.18	1.83	-1		ID=|RAB7A_HUMAN| GeneName=|RAB7A|
P16949	1.17	1.45	1		ID=|STMN1_HUMAN| GeneName=|STMN1|
Q09666	1.17	1.24	1		ID=|AHNK_HUMAN| GeneName=|AHNAK|
Q9GZT3	1.16	1.50	-1		ID=|SLIRP_HUMAN| GeneName=|SLIRP|
P62891	1.15	1.69	1		ID=|RL39_HUMAN| GeneName=|RPL39|
Q14307	1.15	1.48	1		ID=|FGFR1_HUMAN| GeneName=|FGFR1|
P62851	1.14	1.27	1		ID=|RS25_HUMAN| GeneName=|RPS25|
P62820	1.14	1.10	1		ID=|RAB1A_HUMAN| GeneName=|RAB1A|
P27348	1.14	1.08	1		ID=|1433T_HUMAN| GeneName=|YWHAQ|
Q07955	1.14	1.25	-1		ID=|SFRS1_HUMAN| GeneName=|SFRS1|
O76031	1.14	1.55	1		ID=|CLPX_HUMAN| GeneName=|CLPX|
Q9P246	1.13	1.53	1		ID=|STIM2_HUMAN| GeneName=|STIM2|
P08758	1.11	1.15	1		ID=|ANXA5_HUMAN| GeneName=|ANXA5|
P49368	1.11	1.35	-1		ID=|TCPG_HUMAN| GeneName=|CCT3|
Q9Y6E2	1.11	1.35	-1		ID=|BZW2_HUMAN| GeneName=|BZW2|
Q8IY67	1.11	1.35	-1		ID=|RAVR1_HUMAN| GeneName=|RAVER1|
Q9UBC3	1.11	1.35	-1		ID=|DNM3B_HUMAN| GeneName=|DNMT3B|
P13928	1.11	1.35	-1		ID=|ANXA8_HUMAN| GeneName=|ANXA8|
P04075	1.10	1.21	1		ID=|ALDOA_HUMAN| GeneName=|ALDOA|
Q96I24	1.10	1.16	-1		ID=|FUBP3_HUMAN| GeneName=|FUBP3|
Q14011	1.09	1.73	-1		ID=|CIRBP_HUMAN| GeneName=|CIRBP|
Q9BY44	1.09	1.48	-1		ID=|EIF2A_HUMAN| GeneName=|EIF2A|
Q15056	1.09	1.16	-1		ID=|IF4H_HUMAN| GeneName=|EIF4H|
Q9H668	1.08	1.70	-1		ID=|STN1_HUMAN| GeneName=|OBFC1|
P35080	1.07	2.00	-1		ID=|PROF2_HUMAN| GeneName=|PFN2|
P61204	1.07	1.45	1		ID=|ARF3_HUMAN| GeneName=|ARF3|
P61224	1.06	1.01	-1		ID=|RAP1B_HUMAN| GeneName=|RAP1B|
Q9UC36	1.06	1.21	1		ID=|HSPB1_HUMAN| GeneName=|HSPB1|
Q04837	1.06	2.09	1		ID=|SSBP_HUMAN| GeneName=|SSBP1|
P06703	1.06	2.11	-1		ID=|S10A6_HUMAN| GeneName=|S100A6|
Q9Y687	1.05	1.80	-1		ID=|ZFR_HUMAN| GeneName=|ZFR|
P02538	1.05	1.48	1		ID=|K2C6A_HUMAN| GeneName=|KRT6A|
Q9H910	1.05	2.08	-1		ID=|HN1L_HUMAN| GeneName=|HN1L|
P78417	1.05	1.46	-1		ID=|GSTO1_HUMAN| GeneName=|GSTO1|
O14733	1.04	1.83	-1		ID=|MP2K7_HUMAN| GeneName=|MAP2K7|
P09496	1.04	1.17	1		ID=|CLCA_HUMAN| GeneName=|CLTA|
Q92817	1.04	1.06	1		ID=|EVPL_HUMAN| GeneName=|EVPL|
Q9Y6Y8	1.04	1.52	-1		ID=|S23IP_HUMAN| GeneName=|SEC23IP|
O95622	1.03	1.38	-1		ID=|ADCY5_HUMAN| GeneName=|ADCY5|
Q6ZW31	1.03	1.38	-1		ID=|SYDE1_HUMAN| GeneName=|SYDE1|
Q14697	1.03	1.38	-1		ID=|GANAB_HUMAN| GeneName=|GANAB|
Q9NTI5	1.03	1.38	-1		ID=|PDS5B_HUMAN| GeneName=|PDS5B|
Q07021	1.02	1.52	-1		ID=|C1QBP_HUMAN| GeneName=|C1QBP|
P31327	1.02	1.45	1		ID=|CPSM_HUMAN| GeneName=|CPS1|
O14818	1.02	1.25	1		ID=|PSA7_HUMAN| GeneName=|PSMA7|
Q8N1F7	1.01	1.34	1		ID=|NUP93_HUMAN| GeneName=|NUP93|

Tau-association unchanged by MB treatment (Bayes Factor < 10)

Protein	Bayes Factor	Fold Change	Direction	FLAG	description
P01621	1.01	1.34	1		ID=|KV303_HUMAN| GeneName=|IGKV1-5|
Q9P1Z9	1.01	1.21	-1		ID=|K1529_HUMAN| GeneName=|KIAA1529|
P14923	1.00	1.39	1		ID=|PLAK_HUMAN| GeneName=|JUP|
O95429	1.00	1.39	1		ID=|BAG4_HUMAN| GeneName=|BAG4|
Q5VT18	1.00	1.39	1		ID=|CSKP_HUMAN| GeneName=|CASK|
O75223	1.00	1.05	-1		ID=|GGCT_HUMAN| GeneName=|GGCT|
Q9CWI7	0.99	1.36	1		ID=|RAN_HUMAN| GeneName=|RAN|
P21108	0.99	1.31	1		ID=|PRPS3_HUMAN| GeneName=|PRPS1L1|
P09661	0.97	1.07	1		ID=|RU2A_HUMAN| GeneName=|SNRPA1|
O43813	0.97	1.27	1		ID=|LANC1_HUMAN| GeneName=|LANCL1| |
P01622	0.97	2.16	1		ID=|KV304_HUMAN| GeneName=|IGKV1-5|
Q92626	0.97	1.65	1		ID=|PXDN_HUMAN| GeneName=|PXDN|
P31943	0.96	1.38	1		ID=|HNRH1_HUMAN| GeneName=|HNRNPH1|
O43399	0.95	1.57	1		ID=|TPD54_HUMAN| GeneName=|TPD52L2|
Q6P4C7	0.94	1.38	1		ID=|K2C8_HUMAN| GeneName=|KRT8|
P28907	0.94	1.52	-1		ID=|CD38_HUMAN| GeneName=|CD38|
P69849	0.94	1.52	-1		ID=|NOMO3_HUMAN| GeneName=|NOMO3|
P26641	0.94	1.52	-1		ID=|EF1G_HUMAN| GeneName=|EEF1G|
O75533	0.94	1.34	-1		ID=|SF3B1_HUMAN| GeneName=|SF3B1|
P25705	0.94	1.34	-1		ID=|ATPA_HUMAN| GeneName=|ATP5A1|
Q6P161	0.94	1.34	-1		ID=|RM54_HUMAN| GeneName=|MRPL54|
Q9BUE0	0.94	1.34	-1		ID=|MED18_HUMAN| GeneName=|MED18|
P50990	0.92	1.38	1		ID=|TCPQ_HUMAN| GeneName=|CCT8|
P20339	0.92	1.38	1		ID=|RAB5A_HUMAN| GeneName=|RAB5A|
sp|CAS2_BOVIN|	0.92	1.38	1		COMMON CONTAMINANT!
O00299	0.92	1.09	-1		ID=|CLIC1_HUMAN| GeneName=|CLIC1|
Q13740	0.92	1.49	-1		ID=|CD166_HUMAN| GeneName=|ALCAM|
P13639	0.92	1.75	1		ID=|EF2_HUMAN| GeneName=|EEF2|
P54920	0.92	1.28	1		ID=|SNAA_HUMAN| GeneName=|NAPA|
Q9BWB5	0.92	1.80	1		ID=|KPYM_HUMAN| GeneName=|PKM2|
P23528	0.91	1.15	1		ID=|COF1_HUMAN| GeneName=|CFL1|
P49458	0.89	1.07	1		ID=|SRP09_HUMAN| GeneName=|SRP9|
P04080	0.89	1.06	1		ID=|CYTB_HUMAN| GeneName=|CSTB|
Q6PKG0	0.88	1.23	1		ID=|LARP1_HUMAN| GeneName=|LARP1| |
O14907	0.88	1.41	1		ID=|TX1B3_HUMAN| GeneName=|TAX1BP3| |
Q92560	0.88	1.45	-1		ID=|BAP1_HUMAN| GeneName=|BAP1|
Q6P179	0.87	1.49	-1		ID=|ERAP2_HUMAN| GeneName=|ERAP2|
Q9UML6	0.87	1.60	1		ID=|CO1A1_HUMAN| GeneName=|COL1A1|
P32119	0.87	1.21	1		ID=|PRDX2_HUMAN| GeneName=|PRDX2|
Q13151	0.87	1.07	-1		ID=|ROA0_HUMAN| GeneName=|HNRNPA0|
P29966	0.87	1.37	-1		ID=|MARCS_HUMAN| GeneName=|MARCKS|
O43143	0.87	1.22	-1		ID=|DHX15_HUMAN| GeneName=|DHX15|
Q01518	0.87	1.20	-1		ID=|CAP1_HUMAN| GeneName=|CAP1|
P78396	0.87	1.41	-1		ID=|CCNA1_HUMAN| GeneName=|CCNA1|
Q86X55	0.87	1.32	1		ID=|CARM1_HUMAN| GeneName=|CARM1|
P28066	0.86	1.21	-1		ID=|PSA5_HUMAN| GeneName=|PSMA5|
Q86VC0	0.86	1.03	1		ID=|RSSA_HUMAN| GeneName=|RPSA|
Q9UKV8	0.86	1.19	1		ID=|AGO2_HUMAN| GeneName=|EIF2C2|
P52565	0.86	1.13	1		ID=|GDIR1_HUMAN| GeneName=|ARHGDIA|
Q9UKM9	0.86	1.44	-1		ID=|RALY_HUMAN| GeneName=|RALY|
P13010	0.85	1.86	1		ID=|XRCC5_HUMAN| GeneName=|XRCC5|
P10809	0.85	1.33	-1		ID=|CH60_HUMAN| GeneName=|HSPD1|
P13647	0.85	1.26	1		ID=|K2C5_HUMAN| GeneName=|KRT5|

Tau-association unchanged by MB treatment (Bayes Factor < 10)					
Protein	Bayes Factor	Fold Change	Direction	FLAG	description
Q4VC05	0.84	1.46	-1		ID=|BCL7A_HUMAN| GeneName=|BCL7A|
P63173	0.84	1.41	-1		ID=|RL38_HUMAN| GeneName=|RPL38|
P10599	0.84	1.07	1		ID=|THIO_HUMAN| GeneName=|TXN| Def=|Surface-associated sulphydryl protein|
P49755	0.84	1.19	-1		ID=|TMEDA_HUMAN| GeneName=|TMED10|
O75368	0.83	1.18	1		ID=|SH3L1_HUMAN| GeneName=|SH3BGRL|
P84243	0.83	1.48	1		ID=|H33_HUMAN| GeneName=|H3F3B|
P55854	0.82	1.36	1		ID=|SUMO3_HUMAN| GeneName=|SUMO3|
P09972	0.82	1.30	-1		ID=|ALDOC_HUMAN| GeneName=|ALDOC|
Q9BW01	0.82	1.48	-1		ID=|SF01_HUMAN| GeneName=|SF1| Def=|Mammalian branch point-binding protein|
P30086	0.82	1.12	-1		ID=|PEBP1_HUMAN| GeneName=|PEBP1|
Q06830	0.81	1.17	1		ID=|PRDX1_HUMAN| GeneName=|PRDX1|
P42766	0.81	1.10	1		ID=|RL35_HUMAN| GeneName=|RPL35|
P06744	0.80	1.19	1		ID=|G6PI_HUMAN| GeneName=|GPI|
P46776	0.80	1.54	1		ID=|RL27A_HUMAN| GeneName=|RPL27A|
Q9UBV8	0.79	1.34	-1		ID=|PEF1_HUMAN| GeneName=|PEF1|
P46778	0.79	1.82	1		ID=|RL21_HUMAN| GeneName=|RPL21|
P30041	0.79	1.11	1		ID=|PRDX6_HUMAN| GeneName=|PRDX6|
Q9Y315	0.79	1.49	-1		ID=|DEOC_HUMAN| GeneName=|DERA|
Q9Y3S5	0.78	1.40	1		ID=|TTC28_HUMAN| GeneName=|TTC28|
O75821	0.78	1.40	1		ID=|EIF3G_HUMAN| GeneName=|EIF3G|
P68104	0.78	1.13	-1		ID=|EF1A1_HUMAN| GeneName=|EEF1A1|
Q9UBD9	0.77	1.16	1		ID=|CLCF1_HUMAN| GeneName=|CLCF1|
P04632	0.77	1.02	1		ID=|CPNS1_HUMAN| GeneName=|CAPNS1|
Q96AE4	0.77	2.26	-1		ID=|FUBP1_HUMAN| GeneName=|FUBP1| |
Q9UFU4	0.77	1.21	1		ID=|HNRH3_HUMAN| GeneName=|HNRNPH3|
Q9H7N4	0.77	1.67	-1		ID=|SFR19_HUMAN| GeneName=|SCAF1|
O00764	0.77	1.67	-1		ID=|PDXK_HUMAN| GeneName=|PDXK|
P14866	0.74	1.42	-1		ID=|HNRPL_HUMAN| GeneName=|HNRNPL|
Q9UL46	0.74	1.18	-1		ID=|PSME2_HUMAN| GeneName=|PSME2|
P21291	0.74	1.28	1		ID=|CSRP1_HUMAN| GeneName=|CSRP1|
P40925	0.74	1.00	1		ID=|MDHC_HUMAN| GeneName=|MDH1|
P62258	0.73	1.26	-1		ID=|1433E_HUMAN| GeneName=|YWHAE|
P20073	0.73	1.04	1		ID=|ANXA7_HUMAN| GeneName=|ANXA7|
O43707	0.73	1.10	1		ID=|ACTN4_HUMAN| GeneName=|ACTN4|
P42677	0.73	1.38	-1		ID=|RS27_HUMAN| GeneName=|RPS27|
Q96HM4	0.73	2.01	-1		ID=|HNRPC_HUMAN| GeneName=|HNRNPC|
P55735	0.73	1.18	1		ID=|SEC13_HUMAN| GeneName=|SEC13|
P07737	0.72	1.00	1		ID=|PROF1_HUMAN| GeneName=|PFN1|
Q9Y4F4	0.72	1.28	-1		ID=|F179B_HUMAN| GeneName=|FAM179B|
P62861	0.71	2.59	1		ID=|RS30_HUMAN| GeneName=|FAU|
Q92804	0.70	1.96	1		ID=|RBP56_HUMAN| GeneName=|TAF15| |
Q8WW12	0.70	1.08	-1		ID=|PCNP_HUMAN| GeneName=|PCNP|
P52952	0.70	1.10	1		ID=|NKX25_HUMAN| GeneName=|NKX2-5|
P09429	0.70	1.38	-1		ID=|HMGB1_HUMAN| GeneName=|HMGB1|
P62829	0.70	1.09	1		ID=|RL23_HUMAN| GeneName=|RPL23|
P40926	0.69	1.76	1		ID=|MDHM_HUMAN| GeneName=|MDH2|
Q86W34	0.69	1.35	-1		ID=|AMZ2_HUMAN| GeneName=|AMZ2|
Q99625	0.69	1.35	-1		ID=|PIMT_HUMAN| GeneName=|PCMT1|
Q5HYW2	0.69	1.35	-1		ID=|NHSL2_HUMAN| GeneName=|NHSL2|
P26599	0.69	1.03	1		ID=|PTBP1_HUMAN| GeneName=|PTBP1|
Q15437	0.69	1.07	-1		ID=|SC23B_HUMAN| GeneName=|SEC23B|
P15311	0.69	1.17	1		ID=|EZRI_HUMAN| GeneName=|EZR|

Tau-association unchanged by MB treatment (Bayes Factor < 10)

Protein	Bayes Factor	Fold Change	Direction	FLAG	description
P12429	0.69	1.44	1		ID=|ANXA3_HUMAN| GeneName=|ANXA3|
sp|CAS1_BOVIN|	0.68	1.16	1		COMMON CONTAMINANT!
O15347	0.68	1.19	-1		ID=|HMGB3_HUMAN| GeneName=|HMGB3|
P50995	0.68	1.08	-1		ID=|ANX11_HUMAN| GeneName=|ANXA11|
A5PL33	0.68	1.16	-1		ID=|KRBA1_HUMAN| GeneName=|KRBA1|
Q9UC56	0.67	1.46	1		ID=|GRP75_HUMAN| GeneName=|HSPA9|
P62277	0.66	1.21	1		ID=|RS13_HUMAN| GeneName=|RPS13|
P62318	0.66	2.88	-1		ID=|SMD3_HUMAN| GeneName=|SNRPD3|
P62266	0.65	1.33	-1		ID=|RS23_HUMAN| GeneName=|RPS23|
P37108	0.65	1.02	1		ID=|SRP14_HUMAN| GeneName=|SRP14|
O60814	0.64	1.13	-1		ID=|H2B1K_HUMAN| GeneName=|HIST1H2BK|
P55145	0.64	1.03	-1		ID=|MANF_HUMAN| GeneName=|MANF|
P18085	0.64	1.10	-1		ID=|ARF4_HUMAN| GeneName=|ARF4|
A8MWD9	0.64	1.92	-1		ID=|RUXGL_HUMAN| GeneName=|SNRPF|
Q9BZC7	0.64	1.11	-1		Def=|ATP-binding cassette transporter 2|
Q9UNX3	0.64	1.30	-1		ID=|RL26L_HUMAN| GeneName=|RPL26L1|
Q8N9B5	0.64	1.22	-1		ID=|JMY_HUMAN| GeneName=|JMY|
Q99497	0.64	1.11	1		ID=|PARK7_HUMAN| GeneName=|PARK7|
P37802	0.63	1.00	1		ID=|TAGL2_HUMAN| GeneName=|TAGLN2|
Q96AT6	0.63	1.09	1		ID=|NPM_HUMAN| GeneName=|NPM1|
P09012	0.63	1.07	-1		ID=|SNRPA_HUMAN| GeneName=|SNRPA|
P02533	0.63	1.54	1		ID=|K1C14_HUMAN| GeneName=|KRT14|
Q7Z2W4	0.62	1.38	-1		ID=|ZCCHV_HUMAN| GeneName=|ZC3HAV1|
Q1KMD3	0.61	1.61	-1		ID=|HNRL2_HUMAN| GeneName=|HNRNPUL2|
Q7L576	0.61	1.14	-1		ID=|CYFP1_HUMAN| GeneName=|CYFIP1| O
P60866	0.60	1.14	-1		ID=|RS20_HUMAN| GeneName=|RPS20|
P30626	0.60	1.01	-1		ID=|SORCN_HUMAN| GeneName=|SRI| |
P58546	0.60	1.06	1		ID=|MTPN_HUMAN| GeneName=|MTPN|
Q8TEM1	0.59	1.55	-1		ID=|PO210_HUMAN| GeneName=|NUP210|
Q861H8	0.59	1.55	-1		ID=|2B1C_HUMAN| GeneName=|HLA-DRB1|
P62937	0.59	1.51	1		ID=|PPIA_HUMAN| GeneName=|PPIA|
P21333	0.58	1.16	1		ID=|FLNA_HUMAN| GeneName=|FLNA|
P23284	0.58	1.22	1		ID=|PPIB_HUMAN| GeneName=|PPIB|
P0C0S8	0.57	1.01	1		ID=|H2A1_HUMAN| GeneName=|HIST1H2AM|
P11142	0.57	1.00	-1		ID=|HSP7C_HUMAN| GeneName=|HSPA8|
P80723	0.57	1.42	-1		ID=|BASP1_HUMAN| GeneName=|BASP1|
P62280	0.57	1.32	-1		ID=|RS11_HUMAN| GeneName=|RPS11|
P61353	0.56	1.41	1		ID=|RL27_HUMAN| GeneName=|RPL27|
P16989	0.56	1.03	-1		ID=|DBPA_HUMAN| GeneName=|CSDA|
Q15532	0.56	1.29	1		ID=|SSXT_HUMAN| GeneName=|SS18|
Q16650	0.56	1.18	1		ID=|TBR1_HUMAN| GeneName=|TBR1|
Q15366	0.56	1.20	1		ID=|PCBP2_HUMAN| GeneName=|PCBP2|
P09211	0.55	1.45	1		ID=|GSTP1_HUMAN| GeneName=|GSTP1|
P83731	0.55	1.09	1		ID=|RL24_HUMAN| GeneName=|RPL24|
P61981	0.55	1.35	1		ID=|1433G_HUMAN| GeneName=|YWHAG|
P02765	0.55	1.34	1		ID=|FETUA_HUMAN| GeneName=|AHSG|
Q01085	0.55	1.34	-1		ID=|TIAR_HUMAN| GeneName=|TIAL1|
O14979	0.54	1.56	1		ID=|HNRDL_HUMAN| GeneName=|HNRPDL|
P62304	0.54	1.02	-1		ID=|RUXE_HUMAN| GeneName=|SNRPE|
Q92734	0.54	2.16	1		ID=|TFG_HUMAN| GeneName=|TFG|
P98179	0.53	1.01	1		ID=|RBM3_HUMAN| GeneName=|RBM3|

Tau-association unchanged by MB treatment (Bayes Factor < 10)					
Protein	**Bayes Factor**	**Fold Change**	**Direction**	**FLAG**	**description**
P46783	0.53	1.05	-1		ID=|RS10_HUMAN| GeneName=|RPS10|
Q92499	0.53	1.46	1		ID=|DDX1_HUMAN| GeneName=|DDX1|
P62805	0.52	1.04	-1		ID=|H4_HUMAN| GeneName=|HIST4H4|
Q9UEG1	0.49	1.04	-1		ID=|RS27A_HUMAN| GeneName=|RPS27A|
Q16629	0.49	1.31	1		ID=|SFRS7_HUMAN| GeneName=|SFRS7|
O95487	0.49	1.01	-1		ID=|SC24B_HUMAN| GeneName=|SEC24B|
P55795	0.48	1.09	1		ID=|HNRH2_HUMAN| GeneName=|HNRNPH2|
Q01844	0.47	1.02	1		ID=|EWS_HUMAN| GeneName=|EWSR1|
P14625	0.47	1.78	-1		ID=|ENPL_HUMAN| GeneName=|HSP90B1|
Q01105	0.46	1.34	-1		ID=|SET_HUMAN| GeneName=|SET|
P29401	0.45	1.01	-1		ID=|TKT_HUMAN| GeneName=|TKT|
P13797	0.45	1.13	-1		ID=|PLST_HUMAN| GeneName=|PLS3|
P62888	0.44	1.07	-1		ID=|RL30_HUMAN| GeneName=|RPL30|
P09651	0.41	1.14	-1		ID=|ROA1_HUMAN| GeneName=|HNRNPA1|
P26583	0.41	1.09	-1		ID=|HMGB2_HUMAN| GeneName=|HMGB2|
P04406	0.40	1.03	1		ID=|G3P_HUMAN| GeneName=|GAPDH|
P53999	0.40	1.49	-1		ID=|TCP4_HUMAN| GeneName=|SUB1|
Q14847	0.39	1.07	1		ID=|LASP1_HUMAN| GeneName=|LASP1|
P04275	0.37	1.49	-1		ID=|VWF_HUMAN| GeneName=|VWF|
P78371	0.36	1.59	-1		ID=|TCPB_HUMAN| GeneName=|CCT2|
P49773	0.35	1.67	1		ID=|HINT1_HUMAN| GeneName=|HINT1|
P67809	0.34	1.20	-1		ID=|YBOX1_HUMAN| GeneName=|YBX1|
P04083	0.33	1.22	-1		ID=|ANXA1_HUMAN| GeneName=|ANXA1|
Q9UPA0	0.32	1.45	-1		ID=|XPO2_HUMAN| GeneName=|CSE1L|
P15559	0.32	1.36	-1		ID=|NQO1_HUMAN| GeneName=|NQO1|
P22314	0.32	1.36	-1		ID=|UBA1_HUMAN| GeneName=|UBA1|
Q9UCE8	0.27	1.44	-1		ID=|HNRPD_HUMAN| GeneName=|HNRNPD|
Q6NUR9	0.27	1.02	-1		ID=|1433Z_HUMAN| GeneName=|YWHAZ|
P53992	0.27	1.36	1		ID=|SC24C_HUMAN| GeneName=|SEC24C|
P61289	0.27	1.53	1		ID=|PSME3_HUMAN| GeneName=|PSME3|
Q5CZI7	**0.25**	**1.15**	**1**		**ID=|TAU_HUMAN| GeneName=|MAPT|**
sp|ALBU_BOVIN|	0.24	1.13	1		COMMON CONTAMINANT!
P51991	0.20	1.08	-1		ID=|ROA3_HUMAN| GeneName=|HNRNPA3|
P62750	0.20	1.32	-1		ID=|RL23A_HUMAN| GeneName=|RPL23A|
Q13242	0.19	1.12	-1		ID=|SFRS9_HUMAN| GeneName=|SFRS9|
P07195	0.19	2.43	1		ID=|LDHB_HUMAN| GeneName=|LDHB|
Q9HCM4	0.18	1.68	1		ID=|E41L5_HUMAN| GeneName=|EPB41L5|
P61247	0.18	1.93	-1		ID=|RS3A_HUMAN| GeneName=|RPS3A|
P09234	0.17	1.32	1		ID=|RU1C_HUMAN| GeneName=|SNRPC| C|
P62857	0.14	1.57	-1		ID=|RS28_HUMAN| GeneName=|RPS28|
P18669	0.11	1.15	-1		ID=|PGAM1_HUMAN| GeneName=|PGAM1|
O00571	0.08	2.60	1		ID=|DDX3X_HUMAN| GeneName=|DDX3X|
P00338	0.06	1.93	1		ID=|LDHA_HUMAN| GeneName=|LDHA|
Q15436	0.05	2.81	1		ID=|SC23A_HUMAN| GeneName=|SEC23A|
P17844	0.01	4.45	1		ID=|DDX5_HUMAN| GeneName=|DDX5|

4.6.3 MB treatment inhibits J-mediated stimulation of Hsp70.

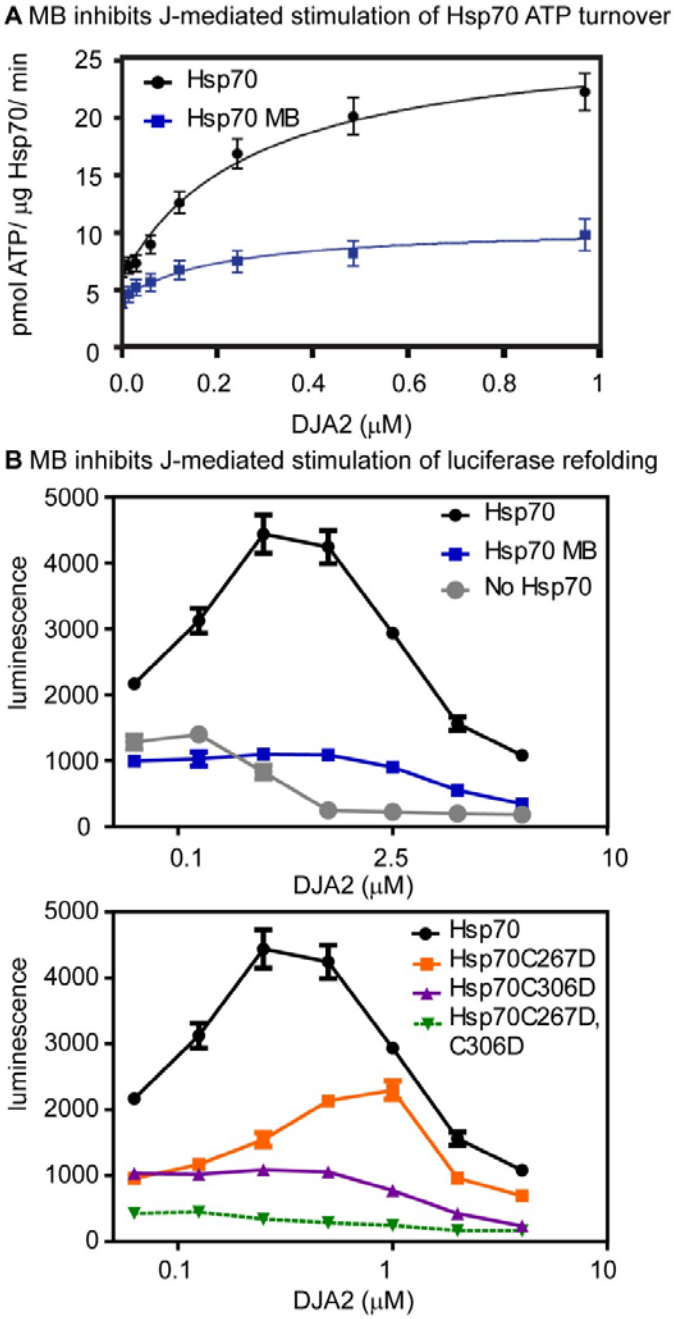

Appendix 4.3. MB treatment inhibits J-mediated stimulation of Hsp70. (A) MB treated Hsp70 has a significantly reduced response to J-protein (DJA2) mediated stimulation of ATP turnover. (B) MB treated Hsp70 also has significantly reduced J-protein (DJA2) stimulation of luciferase refolding as compared to WT Hsp70. These results sugges that MB decouples Hsp70 for J-protein co-chaperone regulation and may be one mechanism by which MB induces a decrease in Hsp70 binding. Interestingly, as noted previously MB has been found to function via oxidation of specific cysteines on Hsp70. Mutantions of these cysteines to aspartic acid found to phenocopy MB effects on tau levels in cells also exhibit impaired J-protein (DJA2) stimulated luciferase refolding.

4.6.4 MB treatment does not change tau binding to Hsp70.

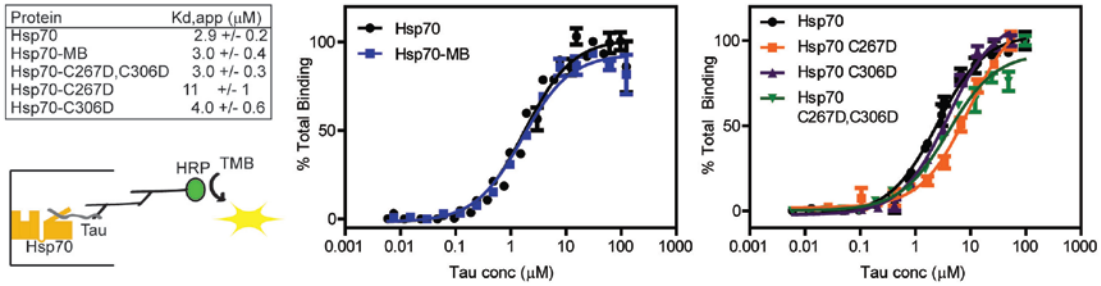

Appendix 4.4. MB does not significantly affect direct binding to tau.
MB treated Hsp70 shows no appreciable affect on Hsp70 binding to tau. Further, cysteine to aspartic acid mutants shown to phenocopy MB treatment within cells also did not exhibit a decreased ability to bind tau, with the exception of C267D which showed a mild decrease in affinity. This experiment was perfromed in triplicate. The graphs show a representative experiment reporting the mean and standard error of the mean. These experiments were perfromed on two or more independently prepared protein preparations and the Kd,app from fitting all replicates is reported to the right.

4.6.5 MB treatment does not promote Hop binding, although Hop can improve efficiency of degradation.

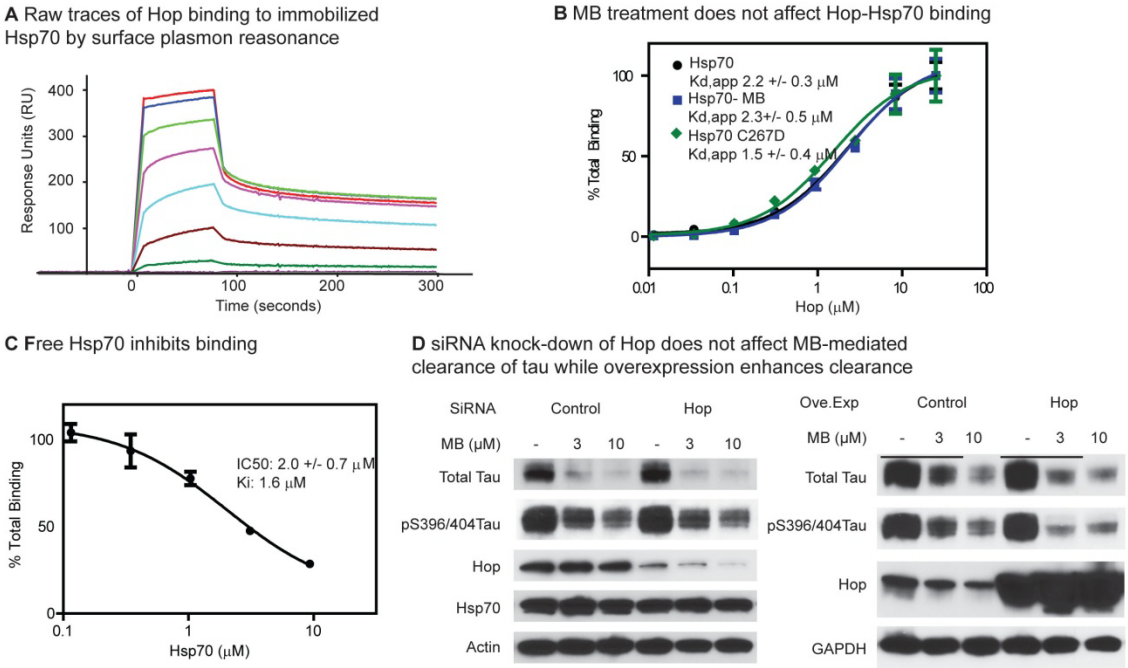

Appendix 4.5. MB treatment does not promote Hop binding, although Hop can improve efficiency of degradation.
(A) Hop binding to immobilized Hsp70 was measured using surface plasmon reasonance (SPR). Raw traces for one concentration series is shown. The experiment was performed in duplicate. (B) Binding was tested for Hsp70, MB treated Hsp70 (MB-Hsp70), and Hsp70 C267D. All samples demonstrated Kd,app binding of ~ 2 μM. (C) free Hsp70 was effectively able to compete away Hop binding to immobilized Hsp70 with an IC_{50} of 2 μM. (D) Although siRNA knock-down does not affect MB-mediated clearance of tau, overexpression (Ove. Exp.) improved tau clearance.

4.6.6 Results from peptide microarray experiments.

Appendix 4.6 Results from peptide microarray experiments.

array ID	residue #	Hsp90α 10 μM	Hsp72 10 μM	Hsp72 NBD 10 μM	antibody only	antibody only
	PNS-tau	Name	Name	Name	Name	Name
1	1	MAEPRQEFEV MEDHA	MAEPRQEFEV MEDHA	MAEPRQEFEV MEDHA	MAEPRQEFEV MEDHA	MAEPRQEFEV MEDHA
2	5	RQEFEVMEDH AGTYG	RQEFEVMEDH AGTYG	RQEFEVMEDH AGTYG	RQEFEVMEDH AGTYG	RQEFEVMEDHA GTYG
3	9	EVMEDHAGTY GLGDR	EVMEDHAGTY GLGDR	EVMEDHAGTY GLGDR	EVMEDHAGTY GLGDR	EVMEDHAGTY GLGDR
4	13	DHAGTYGLGD RKDQG	DHAGTYGLGD RKDQG	DHAGTYGLGD RKDQG	DHAGTYGLGD RKDQG	DHAGTYGLGDR KDQG
5	17	TYGLGDRKDQ GGYTM	TYGLGDRKDQ GGYTM	TYGLGDRKDQ GGYTM	TYGLGDRKDQ GGYTM	TYGLGDRKDQ GGYTM
6	21	GDRKDQGGYT MHQDQ	GDRKDQGGYT MHQDQ	GDRKDQGGYT MHQDQ	GDRKDQGGYT MHQDQ	GDRKDQGGYT MHQDQ
7	25	DQGGYTMHQD QEGDT	DQGGYTMHQD QEGDT	DQGGYTMHQD QEGDT	DQGGYTMHQD QEGDT	DQGGYTMHQD QEGDT
8	29	YTMHQDQEGD TDAGL	YTMHQDQEGD TDAGL	YTMHQDQEGD TDAGL	YTMHQDQEGD TDAGL	YTMHQDQEGD TDAGL
9	33	QDQEGDTDAG LKESP	QDQEGDTDAG LKESP	QDQEGDTDAG LKESP	QDQEGDTDAG LKESP	QDQEGDTDAG LKESP
10	37	GDTDAGLKESP LQTP	GDTDAGLKESP LQTP	GDTDAGLKESP LQTP	GDTDAGLKESP LQTP	GDTDAGLKESP LQTP
11	41	AGLKESPLQTP TEDG	AGLKESPLQTP TEDG	AGLKESPLQTP TEDG	AGLKESPLQTP TEDG	AGLKESPLQTP TEDG
12	45	ESPLQTPTEDG SEEP	ESPLQTPTEDG SEEP	ESPLQTPTEDG SEEP	ESPLQTPTEDG SEEP	ESPLQTPTEDG SEEP
13	49	QTPTEDGSEEP GSET	QTPTEDGSEEP GSET	QTPTEDGSEEP GSET	QTPTEDGSEEP GSET	QTPTEDGSEEP GSET
14	53	EDGSEEPGSET SDAK	EDGSEEPGSET SDAK	EDGSEEPGSET SDAK	EDGSEEPGSET SDAK	EDGSEEPGSET SDAK
15	57	EEPGSETSDAK STPT	EEPGSETSDAK STPT	EEPGSETSDAK STPT	EEPGSETSDAK STPT	EEPGSETSDAK STPT
16	61	SETSDAKSTPT AEDV	SETSDAKSTPT AEDV	SETSDAKSTPT AEDV	SETSDAKSTPT AEDV	SETSDAKSTPT AEDV
17	65	DAKSTPTAEDV TAPL	DAKSTPTAEDV TAPL	DAKSTPTAEDV TAPL	DAKSTPTAEDV TAPL	DAKSTPTAEDV TAPL
18	69	TPTAEDVTAPL VDEG	TPTAEDVTAPL VDEG	TPTAEDVTAPL VDEG	TPTAEDVTAPL VDEG	TPTAEDVTAPL VDEG
19	73	EDVTAPLVDEG APGK	EDVTAPLVDEG APGK	EDVTAPLVDEG APGK	EDVTAPLVDEG APGK	EDVTAPLVDEG APGK
20	77	APLVDEGAPGK QAAA	APLVDEGAPGK QAAA	APLVDEGAPGK QAAA	APLVDEGAPGK QAAA	APLVDEGAPGK QAAA
21	81	DEGAPGKQAA AQPHT	DEGAPGKQAA AQPHT	DEGAPGKQAA AQPHT	DEGAPGKQAA AQPHT	DEGAPGKQAAA QPHT
22	85	PGKQAAAQPH TEIPE	PGKQAAAQPH TEIPE	PGKQAAAQPH TEIPE	PGKQAAAQPH TEIPE	PGKQAAAQPHT EIPE
23	89	AAAQPHTEIPE GTTA	AAAQPHTEIPE GTTA	AAAQPHTEIPE GTTA	AAAQPHTEIPE GTTA	AAAQPHTEIPE GTTA
24	93	PHTEIPEGTTAE EAG	PHTEIPEGTTAE EAG	PHTEIPEGTTAE EAG	PHTEIPEGTTAE EAG	PHTEIPEGTTAE EAG
25	97	IPEGTTAEEAGI GDT	IPEGTTAEEAGI GDT	IPEGTTAEEAGI GDT	IPEGTTAEEAGI GDT	IPEGTTAEEAGI GDT
26	101	TTAEEAGIGDT PSLE	TTAEEAGIGDT PSLE	TTAEEAGIGDT PSLE	TTAEEAGIGDT PSLE	TTAEEAGIGDTP SLE
27	105	EAGIGDTPSLE DEAA	EAGIGDTPSLE DEAA	EAGIGDTPSLE DEAA	EAGIGDTPSLE DEAA	EAGIGDTPSLE DEAA
28	109	GDTPSLEDEAA GHVT	GDTPSLEDEAA GHVT	GDTPSLEDEAA GHVT	GDTPSLEDEAA GHVT	GDTPSLEDEAA GHVT
29	113	SLEDEAAGHVT QEPE	SLEDEAAGHVT QEPE	SLEDEAAGHVT QEPE	SLEDEAAGHVT QEPE	SLEDEAAGHVT QEPE
30	117	EAAGHVTQEPE SGKV	EAAGHVTQEPE SGKV	EAAGHVTQEPE SGKV	EAAGHVTQEPE SGKV	EAAGHVTQEPE SGKV
31	121	HVTQEPESGKV	HVTQEPESGKV	HVTQEPESGKV	HVTQEPESGKV	HVTQEPESGKV

		VQEG	VQEG	VQEG	VQEG	VQEG
32	125	EPESGKVVQE GFLRE	EPESGKVVQE GFLRE	EPESGKVVQE GFLRE	EPESGKVVQE GFLRE	EPESGKVVQEG FLRE
33	129	GKVVQEGFLRE PGPP	GKVVQEGFLRE PGPP	GKVVQEGFLRE PGPP	GKVVQEGFLRE PGPP	GKVVQEGFLRE PGPP
34	133	**QEGFLREPGPP GLSH**	**QEGFLREPGPP GLSH**	**QEGFLREPGPP GLSH**	**QEGFLREPGPP GLSH**	**QEGFLREPGPP GLSH**
35	137	LREPGPPGLSH QLMS	LREPGPPGLSH QLMS	LREPGPPGLSH QLMS	LREPGPPGLSH QLMS	LREPGPPGLSH QLMS
36	141	GPPGLSHQLM SGMPG	GPPGLSHQLM SGMPG	GPPGLSHQLM SGMPG	GPPGLSHQLM SGMPG	GPPGLSHQLMS GMPG
37	145	LSHQLMSGMP GAPLL	LSHQLMSGMP GAPLL	LSHQLMSGMP GAPLL	LSHQLMSGMP GAPLL	LSHQLMSGMP GAPLL
38	149	LMSGMPGAPLL PEGP	LMSGMPGAPLL PEGP	LMSGMPGAPLL PEGP	LMSGMPGAPLL PEGP	LMSGMPGAPLL PEGP
39	153	MPGAPLLPEGP REAT	MPGAPLLPEGP REAT	MPGAPLLPEGP REAT	MPGAPLLPEGP REAT	MPGAPLLPEGP REAT
40	157	PLLPEGPREAT RQPS	PLLPEGPREAT RQPS	PLLPEGPREAT RQPS	PLLPEGPREAT RQPS	PLLPEGPREAT RQPS
41	161	EGPREATRQPS GTGP	EGPREATRQPS GTGP	EGPREATRQPS GTGP	EGPREATRQPS GTGP	EGPREATRQPS GTGP
42	165	EATRQPSGTGP EDTE	EATRQPSGTGP EDTE	EATRQPSGTGP EDTE	EATRQPSGTGP EDTE	EATRQPSGTGP EDTE
43	169	**QPSGTGPEDTE GGRH**	**QPSGTGPEDTE GGRH**	**QPSGTGPEDTE GGRH**	**QPSGTGPEDTE GGRH**	**QPSGTGPEDTE GGRH**
44	173	TGPEDTEGGR HAPEL	TGPEDTEGGR HAPEL	TGPEDTEGGR HAPEL	TGPEDTEGGR HAPEL	TGPEDTEGGRH APEL
45	177	**DTEGGRHAPE LLKHQ**	**DTEGGRHAPE LLKHQ**	**DTEGGRHAPE LLKHQ**	**DTEGGRHAPE LLKHQ**	**DTEGGRHAPEL LKHQ**
46	NA	AA	**AA**	AA	AA	AA
47	181	GRHAPELLKHQ LLGD	GRHAPELLKHQ LLGD	GRHAPELLKHQ LLGD	GRHAPELLKHQ LLGD	GRHAPELLKHQ LLGD
48	185	PELLKHQLLGD LHQE	**PELLKHQLLGD LHQE**	**PELLKHQLLGD LHQE**	**PELLKHQLLGD LHQE**	**PELLKHQLLGD LHQE**
49	189	KHQLLGDLHQE GPPL	KHQLLGDLHQE GPPL	KHQLLGDLHQE GPPL	KHQLLGDLHQE GPPL	**KHQLLGDLHQE GPPL**
50	193	LGDLHQEGPPL KGAG	LGDLHQEGPPL KGAG	LGDLHQEGPPL KGAG	LGDLHQEGPPL KGAG	LGDLHQEGPPL KGAG
51	197	HQEGPPLKGA GGKER	HQEGPPLKGA GGKER	HQEGPPLKGA GGKER	HQEGPPLKGA GGKER	HQEGPPLKGAG GKER
52	201	**PPLKGAGGKE RPGSK**	PPLKGAGGKER PGSK	PPLKGAGGKER PGSK	PPLKGAGGKER PGSK	PPLKGAGGKER PGSK
53	205	GAGGKERPGS KEEVD	GAGGKERPGS KEEVD	GAGGKERPGS KEEVD	GAGGKERPGS KEEVD	GAGGKERPGS KEEVD
54	209	KERPGSKEEVD EDRD	KERPGSKEEVD EDRD	KERPGSKEEVD EDRD	KERPGSKEEVD EDRD	KERPGSKEEVD EDRD
55	213	GSKEEVDEDR DVDES	GSKEEVDEDR DVDES	GSKEEVDEDR DVDES	GSKEEVDEDR DVDES	GSKEEVDEDRD VDES
56	217	EVDEDRDVDES SPQD	EVDEDRDVDES SPQD	EVDEDRDVDES SPQD	EVDEDRDVDES SPQD	EVDEDRDVDES SPQD
57	221	DRDVDESSPQ DSPPS	DRDVDESSPQ DSPPS	DRDVDESSPQ DSPPS	DRDVDESSPQ DSPPS	DRDVDESSPQD SPPS
58	225	DESSPQDSPPS KASP	DESSPQDSPPS KASP	DESSPQDSPPS KASP	DESSPQDSPPS KASP	DESSPQDSPPS KASP
59	229	PQDSPPSKASP AQDG	PQDSPPSKASP AQDG	PQDSPPSKASP AQDG	PQDSPPSKASP AQDG	PQDSPPSKASP AQDG
60	233	PPSKASPAQDG RPPQ	PPSKASPAQDG RPPQ	PPSKASPAQDG RPPQ	PPSKASPAQDG RPPQ	PPSKASPAQDG RPPQ
61	237	ASPAQDGRPP QTAAR	ASPAQDGRPP QTAAR	ASPAQDGRPP QTAAR	ASPAQDGRPP QTAAR	ASPAQDGRPP QTAAR
62	241	QDGRPPQTAA REATS	QDGRPPQTAA REATS	QDGRPPQTAA REATS	QDGRPPQTAA REATS	QDGRPPQTAA REATS
63	245	PPQTAAREATS IPGF	PPQTAAREATS IPGF	PPQTAAREATS IPGF	PPQTAAREATS IPGF	PPQTAAREATSI PGF
64	249	AAREATSIPGF PAEG	AAREATSIPGF PAEG	AAREATSIPGF PAEG	AAREATSIPGF PAEG	AAREATSIPGFP AEG
65	253	ATSIPGFPAEG AIPL	ATSIPGFPAEG AIPL	ATSIPGFPAEG AIPL	ATSIPGFPAEG AIPL	ATSIPGFPAEGA IPL

66	257	PGFPAEGAIPL PVDF	PGFPAEGAIPL PVDF	PGFPAEGAIPL PVDF	PGFPAEGAIPL PVDF	PGFPAEGAIPLP VDF
67	261	AEGAIPLPVDFL SKV	AEGAIPLPVDFL SKV	AEGAIPLPVDFL SKV	AEGAIPLPVDFL SKV	AEGAIPLPVDFL SKV
68	265	IPLPVDFLSKVS TEI	IPLPVDFLSKVS TEI	IPLPVDFLSKVS TEI	IPLPVDFLSKVS TEI	IPLPVDFLSKVS TEI
69	269	VDFLSKVSTEIP ASE	VDFLSKVSTEIP ASE	VDFLSKVSTEIP ASE	VDFLSKVSTEIP ASE	VDFLSKVSTEIP ASE
70	273	SKVSTEIPASEP DGP	SKVSTEIPASEP DGP	SKVSTEIPASEP DGP	SKVSTEIPASEP DGP	SKVSTEIPASEP DGP
71	277	TEIPASEPDGP SVGR	TEIPASEPDGP SVGR	TEIPASEPDGP SVGR	TEIPASEPDGP SVGR	TEIPASEPDGPS VGR
72	281	ASEPDGPSVG RAKGQ	ASEPDGPSVG RAKGQ	ASEPDGPSVG RAKGQ	ASEPDGPSVG RAKGQ	ASEPDGPSVGR AKGQ
73	285	DGPSVGRAKG QDAPL	DGPSVGRAKG QDAPL	DGPSVGRAKG QDAPL	DGPSVGRAKG QDAPL	DGPSVGRAKG QDAPL
74	289	**VGRAKGQDAP LEFTF**	**VGRAKGQDAP LEFTF**	VGRAKGQDAP LEFTF	VGRAKGQDAP LEFTF	VGRAKGQDAPL EFTF
75	293	KGQDAPLEFTF HVEI	**KGQDAPLEFTF HVEI**	KGQDAPLEFTF HVEI	KGQDAPLEFTF HVEI	KGQDAPLEFTF HVEI
76	297	APLEFTFHVEIT PNV	APLEFTFHVEIT PNV	APLEFTFHVEIT PNV	APLEFTFHVEIT PNV	APLEFTFHVEIT PNV
77	301	FTFHVEITPNVQ KEQ	FTFHVEITPNVQ KEQ	FTFHVEITPNVQ KEQ	FTFHVEITPNVQ KEQ	FTFHVEITPNVQ KEQ
78	305	VEITPNVQKEQ AHSE	VEITPNVQKEQ AHSE	VEITPNVQKEQ AHSE	VEITPNVQKEQ AHSE	VEITPNVQKEQ AHSE
79	309	PNVQKEQAHS EEHLG	PNVQKEQAHS EEHLG	PNVQKEQAHS EEHLG	PNVQKEQAHS EEHLG	PNVQKEQAHSE EHLG
80	313	KEQAHSEEHLG RAAF	KEQAHSEEHLG RAAF	KEQAHSEEHLG RAAF	KEQAHSEEHLG RAAF	KEQAHSEEHLG RAAF
81	317	HSEEHLGRAAF PGAP	HSEEHLGRAAF PGAP	HSEEHLGRAAF PGAP	HSEEHLGRAAF PGAP	HSEEHLGRAAF PGAP
82	321	HLGRAAFPGAP GEGP	HLGRAAFPGAP GEGP	HLGRAAFPGAP GEGP	HLGRAAFPGAP GEGP	HLGRAAFPGAP GEGP
83	325	AAFPGAPGEGP EARG	AAFPGAPGEGP EARG	AAFPGAPGEGP EARG	AAFPGAPGEGP EARG	AAFPGAPGEGP EARG
84	329	GAPGEGPEAR GPSLG	GAPGEGPEAR GPSLG	GAPGEGPEAR GPSLG	GAPGEGPEAR GPSLG	GAPGEGPEAR GPSLG
85	333	EGPEARGPSLG EDTK	EGPEARGPSLG EDTK	EGPEARGPSLG EDTK	EGPEARGPSLG EDTK	EGPEARGPSLG EDTK
86	337	ARGPSLGEDTK EADL	ARGPSLGEDTK EADL	ARGPSLGEDTK EADL	ARGPSLGEDTK EADL	ARGPSLGEDTK EADL
87	341	SLGEDTKEADL PEPS	SLGEDTKEADL PEPS	SLGEDTKEADL PEPS	SLGEDTKEADL PEPS	SLGEDTKEADL PEPS
88	345	DTKEADLPEPS EKQP	DTKEADLPEPS EKQP	DTKEADLPEPS EKQP	DTKEADLPEPS EKQP	DTKEADLPEPS EKQP
89	349	ADLPEPSEKQP AAAP	ADLPEPSEKQP AAAP	ADLPEPSEKQP AAAP	ADLPEPSEKQP AAAP	ADLPEPSEKQP AAAP
90	353	EPSEKQPAAAP RGKP	EPSEKQPAAAP RGKP	EPSEKQPAAAP RGKP	EPSEKQPAAAP RGKP	EPSEKQPAAAP RGKP
91	357	**KQPAAAPRGK PVSRV**	**KQPAAAPRGK PVSRV**	KQPAAAPRGKP VSRV	KQPAAAPRGKP VSRV	KQPAAAPRGKP VSRV
92	361	**AAPRGKPVSR VPQLK**	**AAPRGKPVSR VPQLK**	**AAPRGKPVSR VPQLK**	**AAPRGKPVSR VPQLK**	**AAPRGKPVSRV PQLK**
93	365	**GKPVSRVPQL KARMV**	**GKPVSRVPQL KARMV**	GKPVSRVPQLK ARMV	GKPVSRVPQLK ARMV	GKPVSRVPQLK ARMV
94	369	**SRVPQLKARM VSKSK**	**SRVPQLKARM VSKSK**	SRVPQLKARMV SKSK	SRVPQLKARMV SKSK	SRVPQLKARMV SKSK
95	373	QLKARMVSKSK DGTG	QLKARMVSKSK DGTG	QLKARMVSKSK DGTG	QLKARMVSKSK DGTG	QLKARMVSKSK DGTG
96	377	RMVSKSKDGT GSDDK	RMVSKSKDGT GSDDK	RMVSKSKDGT GSDDK	RMVSKSKDGT GSDDK	RMVSKSKDGT GSDDK
97	381	KSKDGTGSDD KKAKT	KSKDGTGSDD KKAKT	KSKDGTGSDD KKAKT	KSKDGTGSDD KKAKT	KSKDGTGSDDK KAKT
98	385	GTGSDDKKAKT STRS	GTGSDDKKAKT STRS	GTGSDDKKAKT STRS	GTGSDDKKAKT STRS	GTGSDDKKAKT STRS
99	389	DDKKAKTSTRS SAKT	DDKKAKTSTRS SAKT	DDKKAKTSTRS SAKT	DDKKAKTSTRS SAKT	DDKKAKTSTRS SAKT
100	393	AKTSTRSSAKT LKNR	AKTSTRSSAKT LKNR	AKTSTRSSAKT LKNR	AKTSTRSSAKT LKNR	AKTSTRSSAKT LKNR

101	397	**TRSSAKTLKNR PCLS**	**TRSSAKTLKNR PCLS**	TRSSAKTLKNR PCLS	TRSSAKTLKNR PCLS	TRSSAKTLKNR PCLS
102	401	**AKTLKNRPCLS PKLP**	**AKTLKNRPCLS PKLP**	AKTLKNRPCLS PKLP	AKTLKNRPCLS PKLP	AKTLKNRPCLS PKLP
103	405	**KNRPCLSPKLP TPGS**	**KNRPCLSPKLP TPGS**	KNRPCLSPKLP TPGS	KNRPCLSPKLP TPGS	KNRPCLSPKLP TPGS
104	409	CLSPKLPTPGS SDPL	CLSPKLPTPGS SDPL	CLSPKLPTPGS SDPL	CLSPKLPTPGS SDPL	CLSPKLPTPGS SDPL
105	413	KLPTPGSSDPLI QPS	KLPTPGSSDPLI QPS	KLPTPGSSDPLI QPS	KLPTPGSSDPLI QPS	KLPTPGSSDPLI QPS
106	417	PGSSDPLIQPS SPAV	PGSSDPLIQPS SPAV	PGSSDPLIQPS SPAV	PGSSDPLIQPS SPAV	PGSSDPLIQPS SPAV
107	421	DPLIQPSSPAV CPEP	DPLIQPSSPAV CPEP	DPLIQPSSPAV CPEP	DPLIQPSSPAV CPEP	DPLIQPSSPAVC PEP
108	425	QPSSPAVCPEP PSSP	QPSSPAVCPEP PSSP	QPSSPAVCPEP PSSP	QPSSPAVCPEP PSSP	QPSSPAVCPEP PSSP
109	429	PAVCPEPPSSP KHVS	PAVCPEPPSSP KHVS	PAVCPEPPSSP KHVS	PAVCPEPPSSP KHVS	PAVCPEPPSSP KHVS
110	433	PEPPSSPKHVS SVTS	PEPPSSPKHVS SVTS	PEPPSSPKHVS SVTS	PEPPSSPKHVS SVTS	PEPPSSPKHVS SVTS
111	437	SSPKHVSSVTS RTGS	SSPKHVSSVTS RTGS	SSPKHVSSVTS RTGS	SSPKHVSSVTS RTGS	SSPKHVSSVTS RTGS
112	441	HVSSVTSRTGS SGAK	HVSSVTSRTGS SGAK	HVSSVTSRTGS SGAK	HVSSVTSRTGS SGAK	HVSSVTSRTGS SGAK
113	445	VTSRTGSSGAK EMKL	VTSRTGSSGAK EMKL	VTSRTGSSGAK EMKL	VTSRTGSSGAK EMKL	VTSRTGSSGAK EMKL
114	449	TGSSGAKEMKL KGAD	TGSSGAKEMKL KGAD	TGSSGAKEMKL KGAD	TGSSGAKEMKL KGAD	TGSSGAKEMKL KGAD
115	453	GAKEMKLKGA DGKTK	GAKEMKLKGA DGKTK	GAKEMKLKGA DGKTK	GAKEMKLKGA DGKTK	GAKEMKLKGAD GKTK
116	457	MKLKGADGKTK IATP	MKLKGADGKTK IATP	MKLKGADGKTK IATP	MKLKGADGKTK IATP	MKLKGADGKTK IATP
117	461	GADGKTKIATP RGAA	GADGKTKIATP RGAA	GADGKTKIATP RGAA	GADGKTKIATP RGAA	GADGKTKIATP RGAA
118	465	KTKIATPRGAA PPGQ	KTKIATPRGAA PPGQ	KTKIATPRGAA PPGQ	KTKIATPRGAA PPGQ	KTKIATPRGAAP PGQ
119	469	ATPRGAAPPG QKGQA	ATPRGAAPPG QKGQA	ATPRGAAPPG QKGQA	ATPRGAAPPG QKGQA	ATPRGAAPPGQ KGQA
120	473	GAAPPGQKGQ ANATR	GAAPPGQKGQ ANATR	GAAPPGQKGQ ANATR	GAAPPGQKGQ ANATR	GAAPPGQKGQ ANATR
121	477	PGQKGQANAT RIPAK	PGQKGQANAT RIPAK	PGQKGQANAT RIPAK	PGQKGQANAT RIPAK	PGQKGQANAT RIPAK
122	481	GQANATRIPAK TPPA	GQANATRIPAK TPPA	GQANATRIPAK TPPA	GQANATRIPAK TPPA	GQANATRIPAK TPPA
123	485	ATRIPAKTPPAP KTP	ATRIPAKTPPAP KTP	ATRIPAKTPPAP KTP	ATRIPAKTPPAP KTP	ATRIPAKTPPAP KTP
124	489	PAKTPPAPKTP PSSG	PAKTPPAPKTP PSSG	PAKTPPAPKTP PSSG	PAKTPPAPKTP PSSG	PAKTPPAPKTP PSSG
125	493	PPAPKTPPSSG EPPK	PPAPKTPPSSG EPPK	PPAPKTPPSSG EPPK	PPAPKTPPSSG EPPK	PPAPKTPPSSG EPPK
126	497	KTPPSSGEPPK SGDR	KTPPSSGEPPK SGDR	KTPPSSGEPPK SGDR	KTPPSSGEPPK SGDR	KTPPSSGEPPK SGDR
127	501	SSGEPPKSGD RSGYS	SSGEPPKSGD RSGYS	SSGEPPKSGD RSGYS	SSGEPPKSGD RSGYS	SSGEPPKSGDR SGYS
128	505	PPKSGDRSGY SSPGS	PPKSGDRSGY SSPGS	PPKSGDRSGY SSPGS	PPKSGDRSGY SSPGS	PPKSGDRSGYS SPGS
129	509	GDRSGYSSPG SPGTP	GDRSGYSSPG SPGTP	GDRSGYSSPG SPGTP	GDRSGYSSPG SPGTP	GDRSGYSSPG SPGTP
130	513	GYSSPGSPGTP GSRS	GYSSPGSPGTP GSRS	GYSSPGSPGTP GSRS	GYSSPGSPGTP GSRS	GYSSPGSPGTP GSRS
131	517	PGSPGTPGSR SRTPS	PGSPGTPGSR SRTPS	PGSPGTPGSR SRTPS	PGSPGTPGSR SRTPS	PGSPGTPGSRS RTPS
132	521	GTPGSRSRTPS LPTP	GTPGSRSRTPS LPTP	GTPGSRSRTPS LPTP	GTPGSRSRTPS LPTP	GTPGSRSRTPS LPTP
133	525	SRSRTPSLPTP PTRE	SRSRTPSLPTP PTRE	SRSRTPSLPTP PTRE	SRSRTPSLPTP PTRE	SRSRTPSLPTP PTRE
134	529	TPSLPTPPTRE PKKV	TPSLPTPPTRE PKKV	TPSLPTPPTRE PKKV	TPSLPTPPTRE PKKV	TPSLPTPPTRE PKKV
135	533	PTPPTREPKKV AVVR	PTPPTREPKKV AVVR	PTPPTREPKKV AVVR	PTPPTREPKKV AVVR	PTPPTREPKKV AVVR

136	537	TREPKKVAVVR TPPK	TREPKKVAVVR TPPK	TREPKKVAVVR TPPK	TREPKKVAVVR TPPK	TREPKKVAVVR TPPK
137	541	**KKVAVVRTPPK SPSS**	**KKVAVVRTPPK SPSS**	KKVAVVRTPPK SPSS	KKVAVVRTPPK SPSS	KKVAVVRTPPK SPSS
138	NA	AA	AA	AA	AA	AA
139	545	**VVRTPPKSPSS AKSR**	**VVRTPPKSPSS AKSR**	VVRTPPKSPSS AKSR	VVRTPPKSPSS AKSR	VVRTPPKSPSS AKSR
140	549	PPKSPSSAKSR LQTA	PPKSPSSAKSR LQTA	PPKSPSSAKSR LQTA	PPKSPSSAKSR LQTA	PPKSPSSAKSR LQTA
141	553	PSSAKSRLQTA PVPM	PSSAKSRLQTA PVPM	PSSAKSRLQTA PVPM	PSSAKSRLQTA PVPM	PSSAKSRLQTA PVPM
142	557	KSRLQTAPVPM PDLK	KSRLQTAPVPM PDLK	KSRLQTAPVPM PDLK	KSRLQTAPVPM PDLK	KSRLQTAPVPM PDLK
143	561	QTAPVPMPDLK NVKS	QTAPVPMPDLK NVKS	QTAPVPMPDLK NVKS	QTAPVPMPDLK NVKS	QTAPVPMPDLK NVKS
144	565	VPMPDLKNVKS KIGS	VPMPDLKNVKS KIGS	VPMPDLKNVKS KIGS	VPMPDLKNVKS KIGS	VPMPDLKNVKS KIGS
145	569	DLKNVKSKIGS TENL	DLKNVKSKIGS TENL	DLKNVKSKIGS TENL	DLKNVKSKIGS TENL	DLKNVKSKIGST ENL
146	573	VKSKIGSTENLK HQP	VKSKIGSTENLK HQP	VKSKIGSTENLK HQP	VKSKIGSTENLK HQP	VKSKIGSTENLK HQP
147	577	IGSTENLKHQP GGGK	IGSTENLKHQP GGGK	IGSTENLKHQP GGGK	IGSTENLKHQP GGGK	IGSTENLKHQP GGGK
148	581	ENLKHQPGGG KVQII	**ENLKHQPGGG KVQII**	ENLKHQPGGG KVQII	ENLKHQPGGG KVQII	ENLKHQPGGG KVQII
149	585	HQPGGGKVQII NKKL	HQPGGGKVQII NKKL	HQPGGGKVQII NKKL	HQPGGGKVQII NKKL	HQPGGGKVQII NKKL
150	589	GGKVQIINKKLD LSN	GGKVQIINKKLD LSN	GGKVQIINKKLD LSN	GGKVQIINKKLD LSN	GGKVQIINKKLD LSN
151	593	QIINKKLDLSNV QSK	QIINKKLDLSNV QSK	QIINKKLDLSNV QSK	QIINKKLDLSNV QSK	QIINKKLDLSNV QSK
152	597	KKLDLSNVQSK CGSK	KKLDLSNVQSK CGSK	KKLDLSNVQSK CGSK	KKLDLSNVQSK CGSK	KKLDLSNVQSK CGSK
153	601	LSNVQSKCGSK DNIK	LSNVQSKCGSK DNIK	LSNVQSKCGSK DNIK	LSNVQSKCGSK DNIK	LSNVQSKCGSK DNIK
154	605	QSKCGSKDNIK HVPG	QSKCGSKDNIK HVPG	QSKCGSKDNIK HVPG	QSKCGSKDNIK HVPG	QSKCGSKDNIK HVPG
155	609	GSKDNIKHVPG GGSV	GSKDNIKHVPG GGSV	GSKDNIKHVPG GGSV	GSKDNIKHVPG GGSV	GSKDNIKHVPG GGSV
156	613	NIKHVPGGGSV QIVY	NIKHVPGGGSV QIVY	NIKHVPGGGSV QIVY	NIKHVPGGGSV QIVY	NIKHVPGGGSV QIVY
157	617	VPGGGSVQIVY KPVD	VPGGGSVQIVY KPVD	VPGGGSVQIVY KPVD	VPGGGSVQIVY KPVD	VPGGGSVQIVY KPVD
158	621	GSVQIVYKPVD LSKV	GSVQIVYKPVD LSKV	GSVQIVYKPVD LSKV	GSVQIVYKPVD LSKV	GSVQIVYKPVD LSKV
159	625	**IVYKPVDLSKV TSKC**	**IVYKPVDLSKV TSKC**	IVYKPVDLSKVT SKC	IVYKPVDLSKVT SKC	IVYKPVDLSKVT SKC
160	629	PVDLSKVTSKC GSLG	PVDLSKVTSKC GSLG	PVDLSKVTSKC GSLG	PVDLSKVTSKC GSLG	PVDLSKVTSKC GSLG
161	633	**SKVTSKCGSLG NIHH**	**SKVTSKCGSLG NIHH**	**SKVTSKCGSLG NIHH**	**SKVTSKCGSLG NIHH**	**SKVTSKCGSLG NIHH**
162	637	**SKCGSLGNIHH KPGG**	**SKCGSLGNIHH KPGG**	SKCGSLGNIHH KPGG	**SKCGSLGNIHH KPGG**	**SKCGSLGNIHH KPGG**
163	641	SLGNIHHKPGG GQVE	SLGNIHHKPGG GQVE	SLGNIHHKPGG GQVE	SLGNIHHKPGG GQVE	SLGNIHHKPGG GQVE
164	645	IHHKPGGGQVE VKSE	IHHKPGGGQVE VKSE	IHHKPGGGQVE VKSE	IHHKPGGGQVE VKSE	IHHKPGGGQVE VKSE
165	649	PGGGQVEVKS EKLDF	PGGGQVEVKS EKLDF	PGGGQVEVKS EKLDF	PGGGQVEVKS EKLDF	PGGGQVEVKS EKLDF
166	653	QVEVKSEKLDF KDRV	QVEVKSEKLDF KDRV	QVEVKSEKLDF KDRV	QVEVKSEKLDF KDRV	QVEVKSEKLDF KDRV
167	657	KSEKLDFKDRV QSKI	KSEKLDFKDRV QSKI	KSEKLDFKDRV QSKI	KSEKLDFKDRV QSKI	KSEKLDFKDRV QSKI
168	661	LDFKDRVQSKI GSLD	LDFKDRVQSKI GSLD	LDFKDRVQSKI GSLD	LDFKDRVQSKI GSLD	LDFKDRVQSKI GSLD
169	665	DRVQSKIGSLD NITH	DRVQSKIGSLD NITH	DRVQSKIGSLD NITH	DRVQSKIGSLD NITH	DRVQSKIGSLD NITH
170	669	SKIGSLDNITHV PGG	SKIGSLDNITHV PGG	SKIGSLDNITHV PGG	SKIGSLDNITHV PGG	SKIGSLDNITHV PGG

171	673	SLDNITHVPGGGNKK	SLDNITHVPGGGNKK	SLDNITHVPGGGNKK	SLDNITHVPGGGNKK	SLDNITHVPGGGNKK
172	677	**ITHVPGGGNKKIETH**	ITHVPGGGNKKIETH	ITHVPGGGNKKIETH	ITHVPGGGNKKIETH	**ITHVPGGGNKKIETH**
173	681	PGGGNKKIETHKLTF	PGGGNKKIETHKLTF	PGGGNKKIETHKLTF	PGGGNKKIETHKLTF	PGGGNKKIETHKLTF
174	685	NKKIETHKLTFRENA	NKKIETHKLTFRENA	NKKIETHKLTFRENA	NKKIETHKLTFRENA	NKKIETHKLTFRENA
175	689	ETHKLTFRENAKAKT	ETHKLTFRENAKAKT	ETHKLTFRENAKAKT	ETHKLTFRENAKAKT	ETHKLTFRENAKAKT
176	693	LTFRENAKAKTDHGA	LTFRENAKAKTDHGA	LTFRENAKAKTDHGA	LTFRENAKAKTDHGA	LTFRENAKAKTDHGA
177	697	ENAKAKTDHGAEIVY	ENAKAKTDHGAEIVY	ENAKAKTDHGAEIVY	ENAKAKTDHGAEIVY	ENAKAKTDHGAEIVY
178	701	AKTDHGAEIVYKSPV	AKTDHGAEIVYKSPV	AKTDHGAEIVYKSPV	AKTDHGAEIVYKSPV	AKTDHGAEIVYKSPV
179	705	HGAEIVYKSPVVSGD	HGAEIVYKSPVVSGD	HGAEIVYKSPVVSGD	HGAEIVYKSPVVSGD	HGAEIVYKSPVVSGD
180	709	IVYKSPVVSGDTSPR	IVYKSPVVSGDTSPR	IVYKSPVVSGDTSPR	IVYKSPVVSGDTSPR	IVYKSPVVSGDTSPR
181	713	SPVVSGDTSPRHLSN	SPVVSGDTSPRHLSN	SPVVSGDTSPRHLSN	SPVVSGDTSPRHLSN	SPVVSGDTSPRHLSN
182	717	SGDTSPRHLSNVSST	SGDTSPRHLSNVSST	SGDTSPRHLSNVSST	SGDTSPRHLSNVSST	SGDTSPRHLSNVSST
183	721	SPRHLSNVSSTGSID	SPRHLSNVSSTGSID	SPRHLSNVSSTGSID	SPRHLSNVSSTGSID	SPRHLSNVSSTGSID
184	725	LSNVSSTGSIDMVDS	LSNVSSTGSIDMVDS	LSNVSSTGSIDMVDS	LSNVSSTGSIDMVDS	LSNVSSTGSIDMVDS
185	729	SSTGSIDMVDSPQLA	SSTGSIDMVDSPQLA	SSTGSIDMVDSPQLA	SSTGSIDMVDSPQLA	SSTGSIDMVDSPQLA
186	733	SIDMVDSPQLATLAD	SIDMVDSPQLATLAD	SIDMVDSPQLATLAD	SIDMVDSPQLATLAD	SIDMVDSPQLATLAD
187	737	VDSPQLATLADEVSA	VDSPQLATLADEVSA	VDSPQLATLADEVSA	VDSPQLATLADEVSA	VDSPQLATLADEVSA
188	741	QLATLADEVSASLAK	QLATLADEVSASLAK	QLATLADEVSASLAK	QLATLADEVSASLAK	QLATLADEVSASLAK
189	745	TLADEVSASLAKQGL	TLADEVSASLAKQGL	TLADEVSASLAKQGL	TLADEVSASLAKQGL	TLADEVSASLAKQGL
190	749	GYSSPGEPGEPGSRS	GYSSPGEPGEPGSRS	GYSSPGEPGEPGSRS	GYSSPGEPGEPGSRS	GYSSPGEPGEPGSRS
191	753	GYSSPGEPGTPGSRS	GYSSPGEPGTPGSRS	GYSSPGEPGTPGSRS	GYSSPGEPGTPGSRS	GYSSPGEPGTPGSRS
192	757	PGSPGEPGSRSRTPS	PGSPGEPGSRSRTPS	PGSPGEPGSRSRTPS	PGSPGEPGSRSRTPS	PGSPGEPGSRSRTPS
193	761	VKSKIGETENLKHQP	VKSKIGETENLKHQP	VKSKIGETENLKHQP	VKSKIGETENLKHQP	VKSKIGETENLKHQP
194	765	DRVQSKIGELDNITH	DRVQSKIGELDNITH	DRVQSKIGELDNITH	DRVQSKIGELDNITH	DRVQSKIGELDNITH
195	769	HGAEIVYKEPVVSGD	HGAEIVYKEPVVSGD	HGAEIVYKEPVVSGD	HGAEIVYKEPVVSGD	HGAEIVYKEPVVSGD
196	773	SPVVSGDTEPRHLSN	SPVVSGDTEPRHLSN	SPVVSGDTEPRHLSN	SPVVSGDTEPRHLSN	SPVVSGDTEPRHLSN
197	NA	AA	AA	AA	AA	AA
198		empty	empty	empty	empty	empty
199		empty	empty	empty	empty	empty
200		empty	empty	empty	empty	empty
201		empty	empty	empty	empty	empty
202		empty	empty	empty	empty	empty
203		empty	empty	empty	empty	empty
204		empty	empty	empty	empty	empty
205		**empty**	empty	empty	empty	empty
206		empty	empty	empty	empty	empty
207		empty	empty	empty	empty	empty

208	empty	empty	empty	empty	empty
209	empty	empty	empty	empty	empty
210	empty	empty	empty	empty	empty
211	**Human IgG**	**Human IgG**	Human IgG	Human IgG	Human IgG
212	**Human IgG**	**Human IgG**	Human IgG	Human IgG	Human IgG
213	**Human IgG**	**Human IgG**	Human IgG	Human IgG	Human IgG
214	**mouse IgG**	**mouse IgG**	mouse IgG	mouse IgG	mouse IgG
215	**mouse IgG**	**mouse IgG**	mouse IgG	mouse IgG	mouse IgG
216	**mouse IgG**	**mouse IgG**	mouse IgG	mouse IgG	mouse IgG
217	**TAU**	**TAU**	TAU	TAU	TAU
218	**TAU**	**TAU**	TAU	TAU	TAU
219	**TAU**	**TAU**	TAU	TAU	TAU
220	empty	empty	empty	empty	empty
221	empty	empty	empty	empty	empty
222	empty	empty	empty	empty	empty
223	empty	empty	empty	empty	empty
224	empty	empty	empty	empty	empty
225	empty	empty	empty	empty	empty

BOLD indicates peptides which met the cut-off: 3 standard errors above the mean
Grey indicates peptide that were positive for binding in the antibody controls and NBD experiments and were thus excluded from later analysis
Green indicates peptides which met the cut-off and were not positive in any control experiments

4.6.7 Analysis of Hsp70 and Hsp90 mRNA levels in Alzheimer's disease human hippocampus.

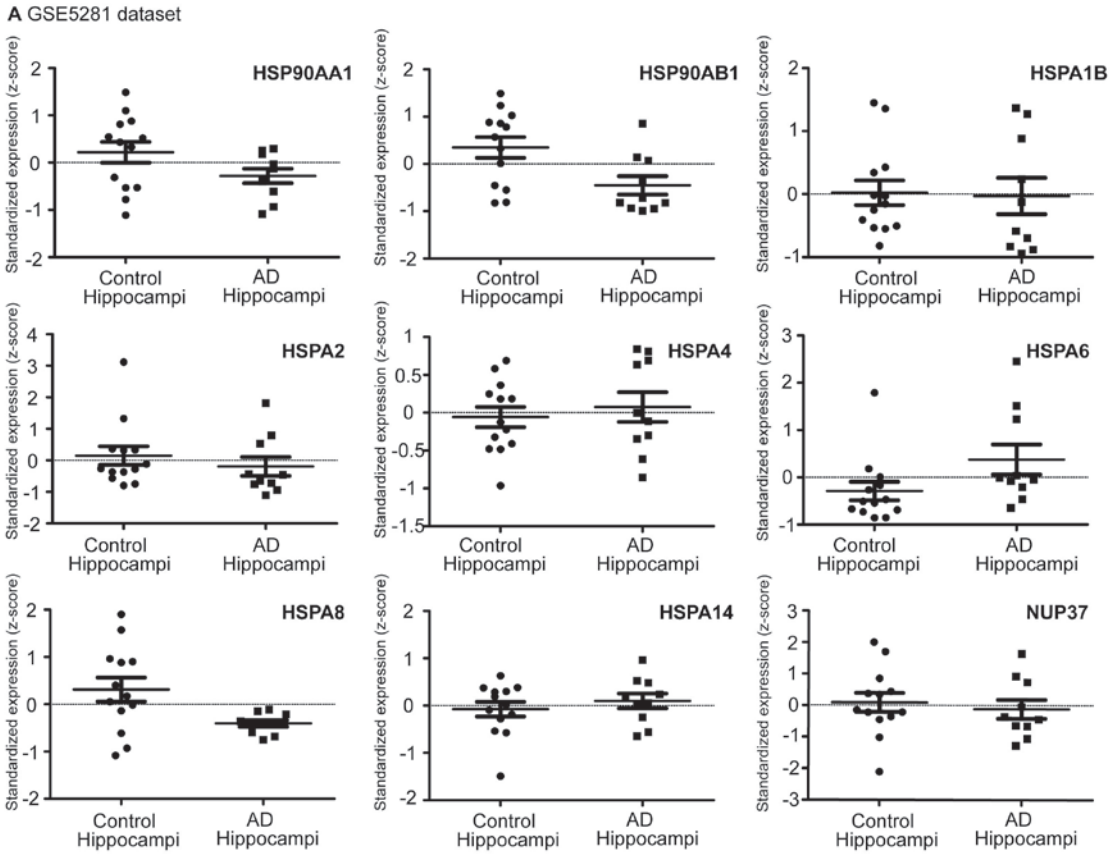

Appendix 4.7. Analysis of Hsp70 and Hsp90 mRNA levels in Alzheimer's disease human hippocampus. Dataset GSE5281 originates from expression microarray data on microdissected, histopathologically normal neurons from the hippocampus of Alzheimer's disease (AD) patients and age matched controls at autopsy. NUP37 was used as an unrelated control.

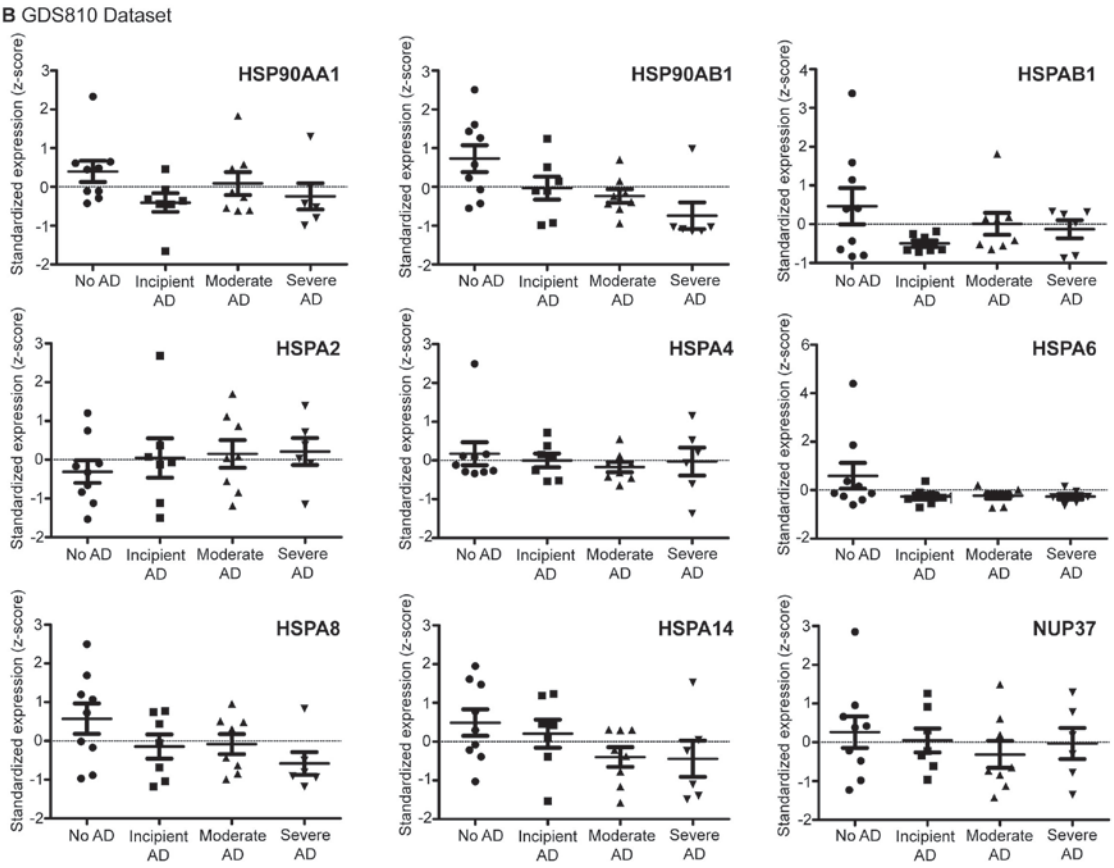

Appendix 4.7 continued. Dataset GDS810 compared the expression levels by microarray analysis from the autopsy of hippocampal samples of AD at various stages of severity compared to age-matched controls.

4.7 References

1. Drechsel, D.N., et al., *Modulation of the dynamic instability of tubulin assembly by the microtubule-associated protein tau.* Mol Biol Cell, 1992. **3**(10): p. 1141-54.
2. Drubin, D.G., et al., *Nerve growth factor-induced neurite outgrowth in PC12 cells involves the coordinate induction of microtubule assembly and assembly-promoting factors.* J Cell Biol, 1985. **101**(5 Pt 1): p. 1799-807.
3. Kempf, M., et al., *Tau binds to the distal axon early in development of polarity in a microtubule- and microfilament-dependent manner.* J Neurosci, 1996. **16**(18): p. 5583-92.
4. Drewes, G., et al., *MARK, a novel family of protein kinases that phosphorylate microtubule-associated proteins and trigger microtubule disruption.* Cell, 1997. **89**(2): p. 297-308.
5. Spillantini, M.G. and M. Goedert, *Tau protein pathology in neurodegenerative diseases.* Trends Neurosci, 1998. **21**(10): p. 428-33.
6. Williams, D.R., *Tauopathies: classification and clinical update on neurodegenerative diseases associated with microtubule-associated protein tau.* Intern Med J, 2006. **36**(10): p. 652-60.
7. Kidd, M., *Paired helical filaments in electron microscopy of Alzheimer's disease.* Nature, 1963. **197**: p. 192-3.
8. Santacruz, K., et al., *Tau suppression in a neurodegenerative mouse model improves memory function.* Science, 2005. **309**(5733): p. 476-81.
9. Sydow, A., et al., *Tau-induced defects in synaptic plasticity, learning, and memory are reversible in transgenic mice after switching off the toxic Tau mutant.* J Neurosci, 2011. **31**(7): p. 2511-25.
10. Roberson, E.D., et al., *Amyloid-beta/Fyn-induced synaptic, network, and cognitive impairments depend on tau levels in multiple mouse models of Alzheimer's disease.* J Neurosci, 2011. **31**(2): p. 700-11.
11. Roberson, E.D., et al., *Reducing endogenous tau ameliorates amyloid beta-induced deficits in an Alzheimer's disease mouse model.* Science, 2007. **316**(5825): p. 750-4.
12. Vossel, K.A., et al., *Tau reduction prevents Abeta-induced defects in axonal transport.* Science, 2010. **330**(6001): p. 198.
13. Jinwal, U.K., et al., *Chemical manipulation of hsp70 ATPase activity regulates tau stability.* J Neurosci, 2009. **29**(39): p. 12079-88.
14. Congdon, E.E., et al., *Methylthioninium chloride (methylene blue) induces autophagy and attenuates tauopathy in vitro and in vivo.* Autophagy, 2012. **8**(4).
15. O'Leary, J.C., 3rd, et al., *Phenothiazine-mediated rescue of cognition in tau transgenic mice requires neuroprotection and reduced soluble tau burden.* Mol Neurodegener, 2010. **5**: p. 45.
16. Miyata, Y., et al., *Molecular chaperones and regulation of tau quality control: strategies for drug discovery in tauopathies.* Future Med Chem, 2011. **3**(12): p. 1523-37.
17. Dou, F., et al., *Chaperones increase association of tau protein with microtubules.* Proc Natl Acad Sci U S A, 2003. **100**(2): p. 721-6.
18. Petrucelli, L., et al., *CHIP and Hsp70 regulate tau ubiquitination, degradation and aggregation.* Hum Mol Genet, 2004. **13**(7): p. 703-14.
19. Jinwal, U.K., et al., *Hsc70 rapidly engages tau after microtubule destabilization.* J Biol Chem, 2010. **285**(22): p. 16798-805.

20. Dickey, C.A., et al., *The high-affinity HSP90-CHIP complex recognizes and selectively degrades phosphorylated tau client proteins.* J Clin Invest, 2007. **117**(3): p. 648-58.
21. Jinwal, U.K., et al., *The Hsp90 cochaperone, FKBP51, increases Tau stability and polymerizes microtubules.* J Neurosci, 2010. **30**(2): p. 591-9.
22. Shimura, H., Y. Miura-Shimura, and K.S. Kosik, *Binding of tau to heat shock protein 27 leads to decreased concentration of hyperphosphorylated tau and enhanced cell survival.* J Biol Chem, 2004. **279**(17): p. 17957-62.
23. Uversky, V.N., C.J. Oldfield, and A.K. Dunker, *Intrinsically disordered proteins in human diseases: introducing the D2 concept.* Annu Rev Biophys, 2008. **37**: p. 215-46.
24. Bilen, J. and N.M. Bonini, *Genome-wide screen for modifiers of ataxin-3 neurodegeneration in Drosophila.* PLoS Genet, 2007. **3**(10): p. 1950-64.
25. Shulman, J.M. and M.B. Feany, *Genetic modifiers of tauopathy in Drosophila.* Genetics, 2003. **165**(3): p. 1233-42.
26. Caplan, A.J., A.K. Mandal, and M.A. Theodoraki, *Molecular chaperones and protein kinase quality control.* Trends Cell Biol, 2007. **17**(2): p. 87-92.
27. Pratt, W.B., et al., *Chaperoning of glucocorticoid receptors.* Handb Exp Pharmacol, 2006(172): p. 111-38.
28. McClellan, A.J., M.D. Scott, and J. Frydman, *Folding and quality control of the VHL tumor suppressor proceed through distinct chaperone pathways.* Cell, 2005. **121**(5): p. 739-48.
29. Gusarova, V., et al., *Apoprotein B degradation is promoted by the molecular chaperones hsp90 and hsp70.* J Biol Chem, 2001. **276**(27): p. 24891-900.
30. Luo, W., et al., *Roles of heat-shock protein 90 in maintaining and facilitating the neurodegenerative phenotype in tauopathies.* Proc Natl Acad Sci U S A, 2007. **104**(22): p. 9511-6.
31. Sahara, N., et al., *Molecular chaperone-mediated tau protein metabolism counteracts the formation of granular tau oligomers in human brain.* J Neurosci Res, 2007. **85**(14): p. 3098-108.
32. Langer, T., et al., *Successive action of DnaK, DnaJ and GroEL along the pathway of chaperone-mediated protein folding.* Nature, 1992. **356**(6371): p. 683-9.
33. Szabo, A., et al., *The ATP hydrolysis-dependent reaction cycle of the Escherichia coli Hsp70 system DnaK, DnaJ, and GrpE.* Proc Natl Acad Sci U S A, 1994. **91**(22): p. 10345-9.
34. Chen, S. and D.F. Smith, *Hop as an adaptor in the heat shock protein 70 (Hsp70) and hsp90 chaperone machinery.* J Biol Chem, 1998. **273**(52): p. 35194-200.
35. Southworth, D.R. and D.A. Agard, *Client-loading conformation of the Hsp90 molecular chaperone revealed in the cryo-EM structure of the human Hsp90:Hop complex.* Mol Cell, 2011. **42**(6): p. 771-81.
36. Sarkar, M., J. Kuret, and G. Lee, *Two motifs within the tau microtubule-binding domain mediate its association with the hsc70 molecular chaperone.* J Neurosci Res, 2008. **86**(12): p. 2763-73.
37. Rudiger, S., et al., *Substrate specificity of the DnaK chaperone determined by screening cellulose-bound peptide libraries.* EMBO J, 1997. **16**(7): p. 1501-7.
38. Blalock, E.M., et al., *Incipient Alzheimer's disease: microarray correlation analyses reveal major transcriptional and tumor suppressor responses.* Proc Natl Acad Sci U S A, 2004. **101**(7): p. 2173-8.
39. Liang, W.S., et al., *Alzheimer's disease is associated with reduced expression of energy metabolism genes in posterior cingulate neurons.* Proc Natl Acad Sci U S A, 2008. **105**(11): p. 4441-6.

40. Liang, W.S., et al., *Gene expression profiles in anatomically and functionally distinct regions of the normal aged human brain.* Physiol Genomics, 2007. **28**(3): p. 311-22.
41. Lastres-Becker, I., U. Rub, and G. Auburger, *Spinocerebellar ataxia 2 (SCA2).* Cerebellum, 2008. **7**(2): p. 115-24.
42. Oz, M., D.E. Lorke, and G.A. Petroianu, *Methylene blue and Alzheimer's disease.* Biochem Pharmacol, 2009. **78**(8): p. 927-32.
43. Schirmer, R.H., et al., *"Lest we forget you--methylene blue...".* Neurobiol Aging, 2011. **32**(12): p. 2325 e7-16.
44. Rousaki, A., et al., *Allosteric drugs: the interaction of antitumor compound MKT-077 with human Hsp70 chaperones.* J Mol Biol, 2011. **411**(3): p. 614-32.
45. Morishima, Y., et al., *Stepwise assembly of a glucocorticoid receptor.hsp90 heterocomplex resolves two sequential ATP-dependent events involving first hsp70 and then hsp90 in opening of the steroid binding pocket.* J Biol Chem, 2000. **275**(24): p. 18054-60.
46. Billecke, S.S., et al., *The role of hsp90 in heme-dependent activation of apo-neuronal nitric-oxide synthase.* J Biol Chem, 2004. **279**(29): p. 30252-8.
47. Schumacher, R.J., et al., *ATP-dependent chaperoning activity of reticulocyte lysate.* J Biol Chem, 1994. **269**(13): p. 9493-9.
48. Dickey, C.A., et al., *HSP induction mediates selective clearance of tau phosphorylated at proline-directed Ser/Thr sites but not KXGS (MARK) sites.* FASEB J, 2006. **20**(6): p. 753-5.
49. Moulick, K., et al., *Affinity-based proteomics reveal cancer-specific networks coordinated by Hsp90.* Nat Chem Biol, 2011. **7**(11): p. 818-26.
50. Cook, C., et al., *Loss of HDAC6, a novel CHIP substrate, alleviates abnormal tau accumulation.* Hum Mol Genet, 2012.
51. Kovacs, J.J., et al., *HDAC6 regulates Hsp90 acetylation and chaperone-dependent activation of glucocorticoid receptor.* Mol Cell, 2005. **18**(5): p. 601-7.
52. Brady, G.F., et al., *Regulation of the copper chaperone CCS by XIAP-mediated ubiquitination.* Mol Cell Biol, 2010. **30**(8): p. 1923-36.
53. Keller, A., et al., *Empirical statistical model to estimate the accuracy of peptide identifications made by MS/MS and database search.* Anal Chem, 2002. **74**(20): p. 5383-92.
54. Nesvizhskii, A.I., et al., *A statistical model for identifying proteins by tandem mass spectrometry.* Anal Chem, 2003. **75**(17): p. 4646-58.
55. Choi, H., D. Fermin, and A.I. Nesvizhskii, *Significance analysis of spectral count data in label-free shotgun proteomics.* Mol Cell Proteomics, 2008. **7**(12): p. 2373-85.
56. Zhang, Y., et al., *Refinements to label free proteome quantitation: how to deal with peptides shared by multiple proteins.* Anal Chem, 2010. **82**(6): p. 2272-81.
57. Chang, L., et al., *Mutagenesis reveals the complex relationships between ATPase rate and the chaperone activities of Escherichia coli heat shock protein 70 (Hsp70/DnaK).* J Biol Chem, 2010. **285**(28): p. 21282-91.
58. Chang, L., et al., *High-throughput screen for small molecules that modulate the ATPase activity of the molecular chaperone DnaK.* Anal Biochem, 2008. **372**(2): p. 167-76.
59. Zheng, L., U. Baumann, and J.L. Reymond, *An efficient one-step site-directed and site-saturation mutagenesis protocol.* Nucleic Acids Res, 2004. **32**(14): p. e115.
60. Southworth, D.R. and D.A. Agard, *Species-dependent ensembles of conserved conformational states define the Hsp90 chaperone ATPase cycle.* Mol Cell, 2008. **32**(5): p. 631-40.

61. Barghorn, S., J. Biernat, and E. Mandelkow, *Purification of recombinant tau protein and preparation of Alzheimer-paired helical filaments in vitro.* Methods Mol Biol, 2005. **299**: p. 35-51.
62. Buchner, J., et al., *Purification of Hsp90 partner proteins Hop/p60, p23, and FKBP52.* Methods Enzymol, 1998. **290**: p. 418-29.
63. Miyata, Y., et al., *High-throughput screen for Escherichia coli heat shock protein 70 (Hsp70/DnaK): ATPase assay in low volume by exploiting energy transfer.* J Biomol Screen, 2010. **15**(10): p. 1211-9.
64. Wisen, S. and J.E. Gestwicki, *Identification of small molecules that modify the protein folding activity of heat shock protein 70.* Anal Biochem, 2008. **374**(2): p. 371-7.

Chapter 5

Conclusions and future directions: Progress towards understanding molecular decision making within the Hsp70 chaperone system.

5.1 Abstract

In the previous chapters, the effects of discrete variables such as ATPase rate, oligomerization, and substrate binding on the chaperone activities of Hsp70 were evaluated. These studies have improved the field's understanding of the Hsp70 chaperone system, especially in linking its *in vitro* biochemical activities to cellular functions. However, there is still much to learn. For example, the mechanism(s) by which Hsp70 and Hsp90 target substrates, such as tau, for degradation is not yet fully understood. The relative contributions of ATP turnover and co-chaperone interactions towards various chaperone functions, such as tau stability, are also unknown. This chapter discusses potential future directions towards answering these questions. In addition, this chapter highlights how this thesis work might predict novel therapeutic strategies. One of the major conclusions made herein is that a suite of small molecules and single point mutations could be combined to illuminate factors which drive molecular decision making in the Hsp70 complex.

5.2 Conclusions

A major goal of this thesis was to utilize a variety of technical approaches to probe what factors within the Hsp70 chaperone system direct the fate of its substrates. Hsp70 is

considered a major triage chaperone, which can promote either the degradation or stabilization of a substrate protein. As such, Hsp70 is central to normal protein homeostasis and its function may be disrupted in a variety of protein misfolding diseases. By understanding how Hsp70 makes "decisions" about whether to fold or degrade a substrate, I hoped to gain insight into how Hsp70 might be targeted therapeutically, especially in tauopathies.

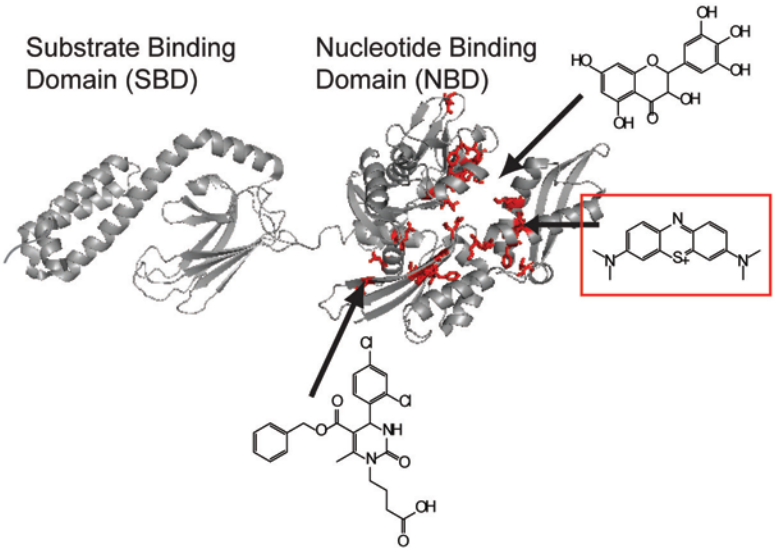

Figure 5.1. Tools to perturb the Hsp70 chaperone system. Point mutations within Hsp70 and Hsp70 chemical modulators, made by myself and others in the Gestwicki lab, are available to perturb this system and aid in our quest to better understand chaperone functions. In red are the mutations and small molecule utilized within this thesis.

When I joined the Gestwicki laboratory in 2008 the first high-throughput screens on both the *E.coli* and human isoforms of Hsp70 had recently been carried out [1, 2]. Whereas Hsp70 alone has a very low ATPase rate, adding J-proteins permitted sufficient nucleotide turnover to give a usable signal. The Gestwicki lab had used this approach to identify a number of compounds that inhibited this Hsp70-J protein system, including methylene blue (MB). At the same time, dihydropyrimidines that stimulate the ATPase activity of Hsp70 were being described by Susan Wisén [3]. Combined, these efforts resulted in

several first-generation chemical tools that could be use to perturb the Hsp70 system and understand its function (Figure 5.1). Further, in collaboration with Chad Dickey's laboratory at the University of South Florida, the Gestwicki lab had learned that Hsp70 ATPase stimulators of the dihydropyrimidine class increased cellular tau levels, while inhibitors, belonging to the phenothiazine and flavonoid chemical classes, reduced tau levels in several cellular models of tauopathies [1].

Based on these exciting developments, I wanted to further explore the logic of Hsp70 chaperone system. In particular, the aim of this thesis was to understand how various variables within the Hsp70 chaperone system contribute to chaperone function. First, we explored whether ATPase activity linked to the fate of Hsp70-bound substrates. To probe this question, in Chapter 2, a series of point mutants within the prokaryotic Hsp70, DnaK, was generated (Figure 5.1). These point mutations provided DnaK variants with a wide range of ATPase activities and different responsiveness to co-chaperones. Using these mutants, it was found that ATPase rate is not directly related to classic chaperone activities, specifically refolding and the protection from heat stress (Figure 5.2B). Thus, one of the major results of Chapter 2 was that variables other than ATPase rate combine to determine molecular chaperone activities. Moving forward, point mutations may allow one to catalog the effect of these alterations on multiple variables of the Hsp70 chaperone system, which include ATPase rate, nucleotide state, co-chaperone interactions, and substrate binding (Figure 5.2A). This is important because these variables are inter-dependent. For example, co-chaperone interactions influence ATPase rate and *vice versa*. By using a suite of mutant proteins and fully characterizing their biochemical and

chaperone activities, one may begin to tease apart the major variables which control a given function.

Next, in Chapter 3, we focused on another variable with the Hsp70 chaperone system. Specifically, how nucleotide state dependent oligomerization of Hsp70 may influence chaperone functions. Specifically, the architecture and function of oligomeric DnaK was explored. This work showed that ADP-bound DnaK formed small, defined multimers that retained some chaperone functions, such as substrate binding. However, these oligomers had reduced refolding activity and they were poorly stimulated by the co-chaperone, DnaJ (Figure 5.2B). These studies imply that oligomerization might be an important step in Hsp70 chaperone cycling. Further, these studies suggest that there may be insight to be gained by monitoring the effects of Hsp70 chemical modulators on oligomerization, as this might be a viable mechanism by which small molecules alter Hsp70 function.

Another major goal of my thesis work was to utilize the new chemical tools developed by the Gestwicki lab to understand molecular decision making within the Hsp70 chaperone system. In particular, these molecules seemed particularly well suited for probing tau stability and homeostasis, given the observed changes in tau homeostasis upon treatment [1]. Thus, in Chapter 4, changes in tau associated protein complexes during an acute, small molecule-induced, switch to a degradation fate were monitored. For this study methylene blue (MB) was utilized (Figure 5.1, red box), because it resulted in the most robust reductions in tau levels. Further, another key feature of MB is that it reduces tau levels rapidly (within ~ 15 minutes in HeLa cells). Thus, performing

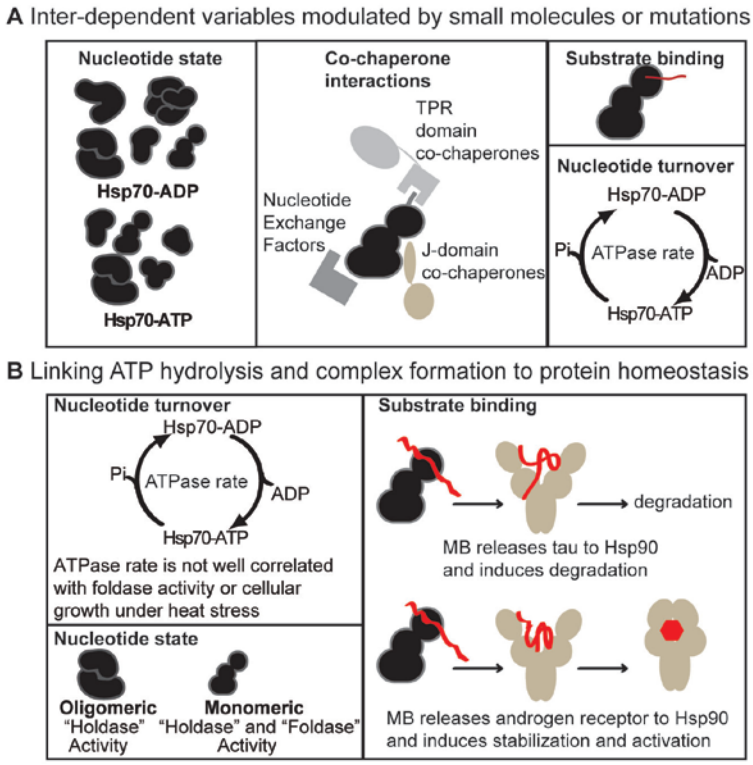

Figure 5.2 Understanding the influence of discrete variables on Hsp70 chaperone activities. (A) The variables which may influence chaperone activity within the Hsp70 system are defined. Specifically nucleotide state, co-chaperone interactions, substrate binding, and nucleotide turnover rate are all variables which may regulate Hsp70 chaperone activities. (B) Using the tools described in Figure 5.1, my work contributed insight into how nucleotide turnover, nucleotide state, and substrate binding may influence chaperone activities. Specifically, in chapter 2, we found that ATPase rate was poorly coorelated with discrete chaperone activites of Hsp70. In chapter 3,we found that the oligomeric ADP-bound form of Hsp70 switches Hsp70 from a "foldase" to a "holdase." Finally, in chapter 4,using methylene blue (MB, red box Figure 5.1) we were able to transiently induce tau degradation and uncover an Hsp90-dependent degradation pathway for tau.

immunoprecipitation of tau with and without MB treatment allowed for the identification of proteins that change in their association with tau during the first few minutes of triage. Using mass spectrometry and quantitative spectral analysis, 48 tau-associated proteins were identified which either release or enrich their binding to tau during the switch to a degradation fate. Interestingly, this work discovered a rapid switch from an Hsp70-bound complex to an Hsp90-bound complex during tau degradation (Figure 5.2B). Further, Hsp70 and Hsp90 seemed to compete for binding to similar regions of tau, suggesting that relative levels of these chaperones might influence tau stability. Finally, these

studies, taken in the context of known literature, highlight some interesting insights into how the substrate itself may influence whether the Hsp70-Hsp90 system favors stabilization or degradation. One striking example of this idea is that two substrates, tau and androgen receptor, were handled in an opposing manner after MB treatment (Figure 5.2B) [4]. This observation is very interesting and, in the remainder of this chapter, I will discuss some possible mechanisms and suggest experiments to further this work. Finally, I will suggest how this work might predict unanticipated therapeutic strategies to rebalance protein homeostasis.

5.3 Future directions

5.3.1 Utilizing mutations in Hsp70 to uncover factors important to chaperone function.

The work in Chapter 2 suggests that alterations in ATP turnover are not predictive of certain chaperone functions, specifically refolding and cellular protection from heat shock [5]. However, it remains unclear whether ATPase rate may be directly linked to other chaperone functions, such as tau turnover and other aspects of proteostasis. Towards this goal, a series of point mutants in human consitutively active (Hsc70) and stress-induced (Hsp70) Hsp70s were chosen based on the results in Chapter 2 (Figure 5.1). Currently other members of the laboratory are actively pursuing this area of research and preliminary findings suggest that ATP turnover does not directly predict the extent of tau stabilization. If this result is confirmed, it would further support a model in which nucleotide state, conformation, or some other combination of variables dictates Hsp70's chaperone functions (Figure 5.2A). For example, molecules that stabilize the ADP-bound conformation of Hsp70 seem to be potent at destabilizing tau, despite their weak effect on

steady-state ATP turnover [6]. This result suggests that the structure of Hsp70, or possibly its affinity for substrates, may be a better predictor of chaperone function than ATPase rate. Understanding this issue will be important because it will lead to more informed high throughput screens for molecules that destabilize tau and, ultimately, restore tau homeostasis in tauopathy.

5.3.2 Expanding the identification of chaperone-dependent tau degradation pathways using a chemical biology approach.

The results in Chapter 4 suggest that Hsp70 and Hsp90 work together to coordinate tau degradation. However, there are still many questions to be addressed before this mechanism is fully understood. I am particularly interested in the logic of this pathway as well as its generality. The work in Chapter 4 showed that chemical probes might be particularly powerful reagents to use in these inquiries, because they allow rapid and transient perturbations in tau homeostasis in an Hsp70-dependent manner. The speed with which these molecules act is important because it reduces the likelihood of activation of compensatory pathways. Ultimately, a full suite of small molecule modulators, which target different aspects of Hsp70 and/or Hsp90 structure and function, may be the best way of understanding the determinants of tau homeostasis within these chaperone systems.

To enable these studies, a diverse array of Hsp70 and Hsp90 modulators able to acutely alter tau levels [1, 6-9], have been identified. These modulators interact with Hsp70 and Hsp90 via different molecular mechanisms (Figure 5.3A) [1, 6, 8-11]. Moreover, recent work by other members of the Gestwicki lab has further expanded the list of available

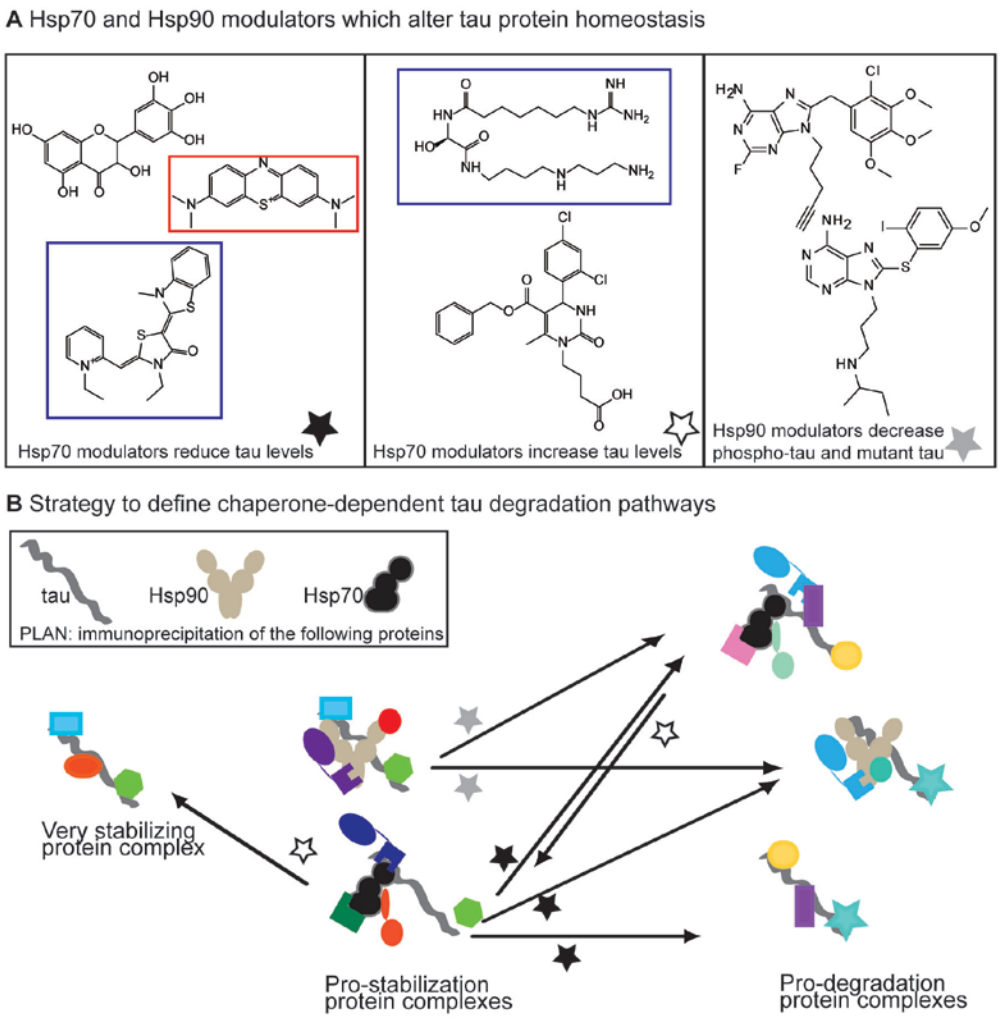

Figure 5.3. A chemical biology approach to uncover chaperone-dependent pathways which maintain tau protein homeostasis.
(A) Multiple small molecule modulators of Hsp70 and Hsp90 are able to alter tau homeostasis. Specifically, there are Hsp70 modulators which lead to tau clearance (solid black star), tau accumulation (open black star). Also, Hsp90 inhibitors can lead to clearance of phosphorylated and mutant forms of tau (grey stars). The compound used in chapter 4 is highlighted in the red box. Newly developed modulators are highlighted in the blue boxes. (B) Using this suite of small molecules and IP-M experiments we monitor for changes in tau-chaperone protein complexes in response to acute changes in tau homeostasis. This may allow us to appreciate the diversity of available chaperone -dependent degradation pathways as well as identify common signals that are important for the "decision" to degrade.

probes (Figure 5.2A, blue boxes) [Matt Smith, unpublished data] [6]. These compounds bind to new sites on Hsp70, suggesting that they might use mechanisms that are not currently accessed by other molecules. Based on what was found in Chapter 4, I suggest that, using this suite of Hsp70 and Hsp90 small molecules, one could expand on the

chemoproteomics approach to understand the breadth of protein complexes important in tau homeostasis [12]. Immunoprecipitation of tau coupled with MS could probe whether these distinct chemicals target tau for degradation by similar or unique changes in tau associated protein complexes (Figure 5.2B). Further, by also immunoprecipitating Hsp70 and Hsp90, one may be able to capture changes in co-chaperone interactions (Figure 5.2B). In addition to Chapter 4, the utility of the proposed approach is highlighted in work by Dickey and colleagues which have shown that an Hsp90 inhibitor causes the degradation of phosphorylated but not total tau via a process dependent on Hsp90 [7]. Thus, both an Hsp90 inhibitor and MB target tau for degradation via Hsp90, suggesting that the Hsp90-depenent degradation observed in Chapter 4 may represent a general pathway by which the cell clears tau. Expanding this approach to new Hsp70 and Hsp90 modulators, may have the potential to uncover several chaperone-dependent tau degradation pathways and improve the field's understanding of the principles that drive tau clearance.

5.3.3 Understanding substrate-dependent behavior

Another exciting use of the available chemical tools would be to study multiple chaperone substrates. This approach may provide a better understanding of how the substrates itself may influence which chaperone pathway is initiated. Interestingly, recent findings have uncovered that different substrates may access different chaperone pathways. For example, Gladis Walter and other members of the Gestwicki laboratory recently used the Hsp70 stimulator, 115-7c, and mass spectrometry to show that soluble (Q25) and aggregation-prone polyQ (Q103) interacts with the molecular chaperones

Hsp26, Hsp70, Hsp90 and Hsp104 in a specific order [8]. Further, work by Yoshi Miyata in collaboration with Andrew Lieberman's lab, at the University of Michigan, demonstrated that MKT-077 targets polyglutamine-expanded androgen receptor (polyQ-AR) for ubiqutin-dependent degradation by increasing Hsp70 binding [13]. These examples highlight how Hsp70 might be involved in different stages in the degradation of tau and other substrates, such as polyglutamines. More examples will likely further clarify the scope of Hsp70's activities and mass spectrometry-based proteomics may be a particularly powerful method for rapidly examining many substrates. For example, if one compound leads two substrates to opposing fates in a single cellular system, one could utilize these substrates to understand the mechanisms which drive this divergent outcome. Two substrates well suited for this analysis are the androgen receptor and tau. MB binding was previously found to increase Hsp90 binding for the androgen receptor. Yet, instead of leading to clearance as observed for tau in Chapter 4, androgen receptor was stabilized by compound treatment [4]. Thus, in this example the same change in Hsp70 and Hsp90 binding led to two different cellular outcomes. It would be interesting to improve to know which co-chaperones are in complex with Hsp90 under these conditions. Further, coupling these studies with structural and kinetic characterization of substrate binding may help to reveal insights into the molecular mechanisms by which the structure and/or identity of the substrate protein may influence its cellular fate.

5.3.4 New therapeutic strategies for the Hsp70 chaperone systems

Another major goal of this work was to better to enable improved screening and therapeutic strategies for the Hsp70 system. Although previous screening efforts have

focused on ATPase activity, my studies suggest that complementary approaches should include screens that focus on different chaperone activities, such as substrate binding or co-chaperone interactions. For example, decreased Hsp70 binding to tau was shown in Chapter 4 to induce tau clearance. Therefore, fluorescence polarization, using a model peptide substrate, might be used to monitor substrate binding to Hsp70 [14, 15] and identify molecules that block this interaction. Further, the work in Chapter 3 has pointed to the functional role that nucleotide state plays in chaperone functions [16]. Thus, screens that specifically examine nucleotide state might also be good platforms for the discovery of useful compounds. One suitable method might be Förster resonance energy transfer (FRET). A recent study used FRET pairs to visualize ternary structural changes in Hsp70, especially those that are dependent on nucleotide [17, 18]. Together these new screening strategies have the potential to uncover novel scaffolds, which may modulate the activity of Hsp70 in different ways and with greater mechanistic specificity.

This work has also provided insights into potential therapeutic strategies for the treatment of tauopathies (Figure 5.4). Specifically, Chapter 4 showed that tau is degraded through an Hsp90-dependent pathway. Interestingly, as mentioned above, Hsp90 inhibitors also reduce tau levels [7] via an Hsp90 and CHIP depedent degradation complex. Further, Hsp90 inhibitors also elevate Hsp70 levels through the induction of HSF1. Thus, combining Hsp90 inhibitors and MB might have synergistic effects on tau degradation because they utilize parallel mechanisms that converge on a common Hsp90-dependent degradation pathway [7, 19] (Figure 5.4). This approach might access multiple “pools” of

tau. Further, the elevated Hsp70 levels induced by Hsp90 inhibitors typically counteracts tau clearance [10]. However, elevated Hsp70 levels enhance MB-mediated clearance of tau [1]. Thus, combining Hsp70 and Hsp90 treatments may turn what use to be a limitation of Hsp90 inhibition into an asset.

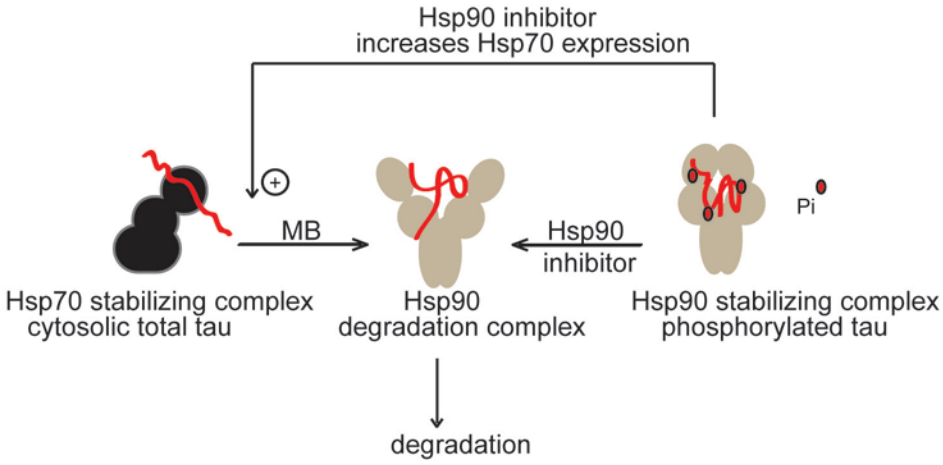

Figure 5.4 An Hsp70 and Hsp90 co-treatment strategy.
Methylene blue (MB) targets tau for degradation via an Hsp90-dependent pathway (chapter 4). Likewise, we know that Hsp90 inhibitors target certain phosphorylated and mutant forms of tau for degradation via a pathway dependent on Hsp90 and not Hsp70. Finally, Hsp90 inhibitors increase Hsp70 levels which may counteract tau clearance. Treatment with both MB and an Hsp90 inhibitor would allow us to target both the tau bound to Hsp70 and Hsp90 for clearance. Further, increased Hsp70 levels, which can be induced by Hsp90 inhibition, have been shown to enhance MB-mediated clearance of tau. Thus, a co-treatment strategy could potentially improve tau clearance and therapeutic otucomes.

5.4 Final thoughts

Herein I have summarized the progress made towards understanding Hsp70 chaperone functions and outlined future studies to exploit Hsp70 as a therapeutic target. The major theme of this work is that combining mutants with chemical probes is a powerful way to perturb and learn about chaperone functions. One major conclusion is that no single Hsp70 function (e.g. ATPase rate, oligomerization, *etc.*) seems directly linked to functional outcomes. Also, this thesis uncovered an unexpected Hsp90-dependent

degradation pathway for the pathologically important client protein tau. Put together, this work shows how mutants and chemical tools can be used to probe chaperone function in neurodegenerative disease. In the future, it will be important to look at multiple chaperone systems, in multiple models and with new chemical probes because no one principle will likely be universal. Rather, a broad interdisciplinary approach, driven by collaborations, will reveal the factors governing the cellular fate of Hsp70 substrates.

5.5 References

1. Jinwal, U.K., et al., *Chemical manipulation of hsp70 ATPase activity regulates tau stability.* J Neurosci, 2009. **29**(39): p. 12079-88.
2. Chang, L., et al., *High-throughput screen for small molecules that modulate the ATPase activity of the molecular chaperone DnaK.* Anal Biochem, 2008. **372**(2): p. 167-76.
3. Wisen, S., et al., *Binding of a small molecule at a protein-protein interface regulates the chaperone activity of hsp70-hsp40.* ACS Chem Biol, 2010. **5**(6): p. 611-22.
4. Wang, A.M., et al., *Inhibition of hsp70 by methylene blue affects signaling protein function and ubiquitination and modulates polyglutamine protein degradation.* J Biol Chem, 2010. **285**(21): p. 15714-23.
5. Chang, L., et al., *Mutagenesis reveals the complex relationships between ATPase rate and the chaperone activities of Escherichia coli heat shock protein 70 (Hsp70/DnaK).* J Biol Chem, 2010. **285**(28): p. 21282-91.
6. Rousaki, A., et al., *Allosteric drugs: the interaction of antitumor compound MKT-077 with human Hsp70 chaperones.* J Mol Biol, 2011. **411**(3): p. 614-32.
7. Dickey, C.A., et al., *The high-affinity HSP90-CHIP complex recognizes and selectively degrades phosphorylated tau client proteins.* J Clin Invest, 2007. **117**(3): p. 648-58.
8. Evans, C.G., et al., *Improved synthesis of 15-deoxyspergualin analogs using the Ugi multi-component reaction.* Bioorg Med Chem Lett, 2011. **21**(9): p. 2587-90.
9. Luo, W., et al., *Roles of heat-shock protein 90 in maintaining and facilitating the neurodegenerative phenotype in tauopathies.* Proc Natl Acad Sci U S A, 2007. **104**(22): p. 9511-6.
10. Brunden, K.R., J.Q. Trojanowski, and V.M. Lee, *Advances in tau-focused drug discovery for Alzheimer's disease and related tauopathies.* Nat Rev Drug Discov, 2009. **8**(10): p. 783-93.
11. Evans, C.G., L. Chang, and J.E. Gestwicki, *Heat shock protein 70 (hsp70) as an emerging drug target.* J Med Chem, 2010. **53**(12): p. 4585-602.
12. Schirle, M., M. Bantscheff, and B. Kuster, *Mass spectrometry-based proteomics in preclinical drug discovery.* Chem Biol, 2012. **19**(1): p. 72-84.
13. Wang, A.M.M.Y.P., H.-M.; Chua J.C.; Komiyama,T.; Pratt, W.B.; Osawa Y.; Collins C.A.;Gestwicki J.E.;Lieberman, A.P. , *Allosteric activation of Hsp70 binding promotes polyglutamine androgen receptor clearance and rescues toxicity in a Drosophila model of SBMA.* 2012.
14. Ricci, L. and K.P. Williams, *Development of fluorescence polarization assays for the molecular chaperone Hsp70 family members: Hsp72 and DnaK.* Curr Chem Genomics, 2008. **2**: p. 90-5.
15. Xu, X., et al., *Unique peptide substrate binding properties of 110-kDa heat-shock protein (Hsp110) determine its distinct chaperone activity.* J Biol Chem, 2012. **287**(8): p. 5661-72.
16. Thompson, A.D., et al., *Visualization and functional analysis of the oligomeric states of Escherichia coli heat shock protein 70 (Hsp70/DnaK).* Cell Stress Chaperones, 2012. **17**(3): p. 313-27.
17. Mapa, K., et al., *The conformational dynamics of the mitochondrial Hsp70 chaperone.* Mol Cell, 2010. **38**(1): p. 89-100.
18. Marcinowski, M., et al., *Substrate discrimination of the chaperone BiP by autonomous and cochaperone-regulated conformational transitions.* Nat Struct Mol Biol, 2011. **18**(2): p. 150-8.

19. Luo, Y., et al., *Homocysteine induces tau hyperphosphorylation in rats.* Neuroreport, 2007. **18**(18): p. 2005-8.

Appendix A

Chaperones preferentially bind fibril forming peptides.

A.1 Abstract

Molecular chaperones maintain protein homeostasis within the cell in a variety of ways, which include promoting protein folding, inhibiting aggregation, facilitating disaggregation, and targeting proteins for clearance. The ability of molecular chaperones to regulate protein aggregation plays a central role in the pathophysiology of diseases caused by the terminal aggregation of proteins into amyloid fibrils. Aggregation assays have consistently demonstrated that a variety of chaperones inhibit amyloid formation, however the mechanisms are not completely understood. Perhaps chaperones recognize the distinct signature of amyloid-prone peptides, thus protecting the cell from exposure to sequences that are particularly susceptible to aggregation. Recent work has shown that amyloid-prone sequences interdigitate their side chains into "steric zippers," which stabilize the aggregated form. Using peptide microarrays and a suite of different chaperones, it was observed that some chaperones can discriminate between amyloid- and non-amyloid-forming sequences. Further, these chaperones contain cognate regions of high amyloid propensity in their binding sites, suggesting that chaperones might use hetero-amyloid recognition motifs to seek out problematic sequences. These results have important implications for how chaperones combat protein misfolding diseases, such as tauopathies.

A.2 Introduction

A.2.1 Amyloid fibrils are linked to disease

Amyloid fibers are rich in β sheets and they represent a characteristic fold in terminally aggregated proteins [1, 2]. In approximately 25 protein misfolding diseases, different proteins form amyloid fibrils [2], with perhaps the best known example being those formed by amyloid-β peptide (Aβ) within Alzheimer's disease (AD) [3]. These amyloids are linked to gain-of-function toxicity and there is great interest in understanding how amyloids form and how they are removed.

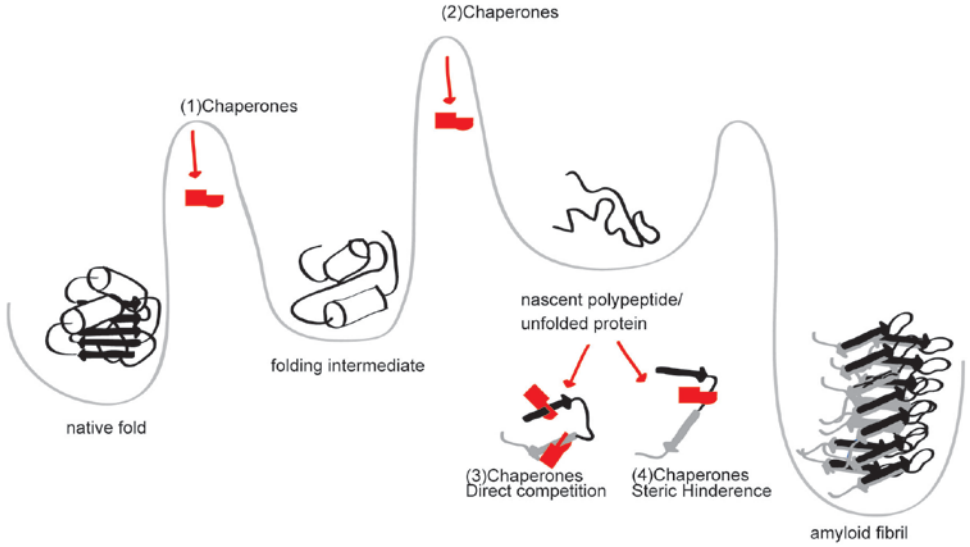

Figure A.1 Schematic of potential mechanisms by which molecular chaperones can inhibit aggregation.

A.2.2 Molecular chaperones inhibit protein aggregation and amyloid formation

Molecular chaperones play a central role in regulating protein folding and homeostasis within the cell [4]. Molecular chaperones are a structurally non-homologous class proteins that either promote protein folding or prevent misfolding and aggregation. Several molecular chaperones are heat shock proteins that are named by their apparent molecular weights (e.g. Hsp70, Hsp90, Hsp100, etc). *In vitro* and *in vivo* studies have consistently shown that molecular chaperones inhibit amyloid formation [5-11], yet the

mechanisms by which chaperones inhibit aggregation are not yet characterized (Figure A.1). Molecular chaperones likely inhibit aggregation, in part, by promoting proper protein folding. In addition, they may bind directly to amyloid-prone proteins and block aberrant interactions.

A.2.3 "Steric zippers" stabilize amyloid fibrils.

Recently, the atomic level structures of amyloids have been determined, providing some insights into how these structures form [1, 12-19]. Interestingly, one key observation is that the side chains in the amyloid-forming sequences are tightly interdigitated, with water excluded from the interface. These motifs are termed "dry steric zippers" [1] and they appear to be a common (and distinguishing) feature of amyloid-prone peptides. The sequences prone to these interactions can vary in their physicochemical properties and side chain identity, being polar or non-polar, with large or small side chains. Rather, what seems to be consistent is that they must fit together to form complementary hydrophobic and/or hydrogen bonding contacts. These "steric zippers" often form from complementary sequences, but they do not need to be self-complementary. For example, there is strong evidence from solid state NMR that in Aβ, some close interactions between β strands with different sequence form what seems to be a "heterosteric zipper." [20, 21]. Consistent with this model, computationally determining the ability of a sequence to form a "dry steric zipper" with favorable interaction energy can reliably predict whether a peptide sequence will form amyloid fibrils [22-24].

A.3 Results

A.3.1 Chaperones recognize fibril forming peptides.

Perhaps the same molecular mechanisms which guide amyloid formation may also guide chaperone binding. Specifically, molecular chaperones may preferentially bind aggregation prone or fibril forming peptides using "heterosteric zippers" formed between the chaperone and the peptide substrate. To test this idea, a peptide microarray was designed containing both fibril and non-fibril forming peptides that were chosen from both disease and non-disease related proteins (Appendix A.1). These 120 peptides come from 33 different proteins, representing both secreted and extracellular proteins as well as cytosolic proteins. Finally, these peptides were chosen such that their average hydrophobicity and other properties were the same between the fibril forming and non fibril forming peptides (Appendix A.2, Figure A.3).

A.3.2 A subset of chaperones and co-chaperones preferentially bind fibril forming peptides.

Using this peptide microarray, printed in triplicate, the binding of a variety of His-tagged chaperones was tested (Figure A.2, Table A.1). Binding was determined using fluorescently labeled anti-His antibodies. For the major chaperones, Hsp70 and Hsp90, significant changes and trends consistent with a preference for binding to fibrils was observed with an odds ratio (OR) of ~1.8 to 2.3. Hsp70s typically bound ~60% of fibril-forming peptides and only ~40% of non-fibril forming peptides. Similarly, Hsp90 demonstrate an ~1.5 to 2-fold preference for binding to fibril forming peptides (Table A.1, Appendix A.3). A significant preference for fibril forming peptides was observed for

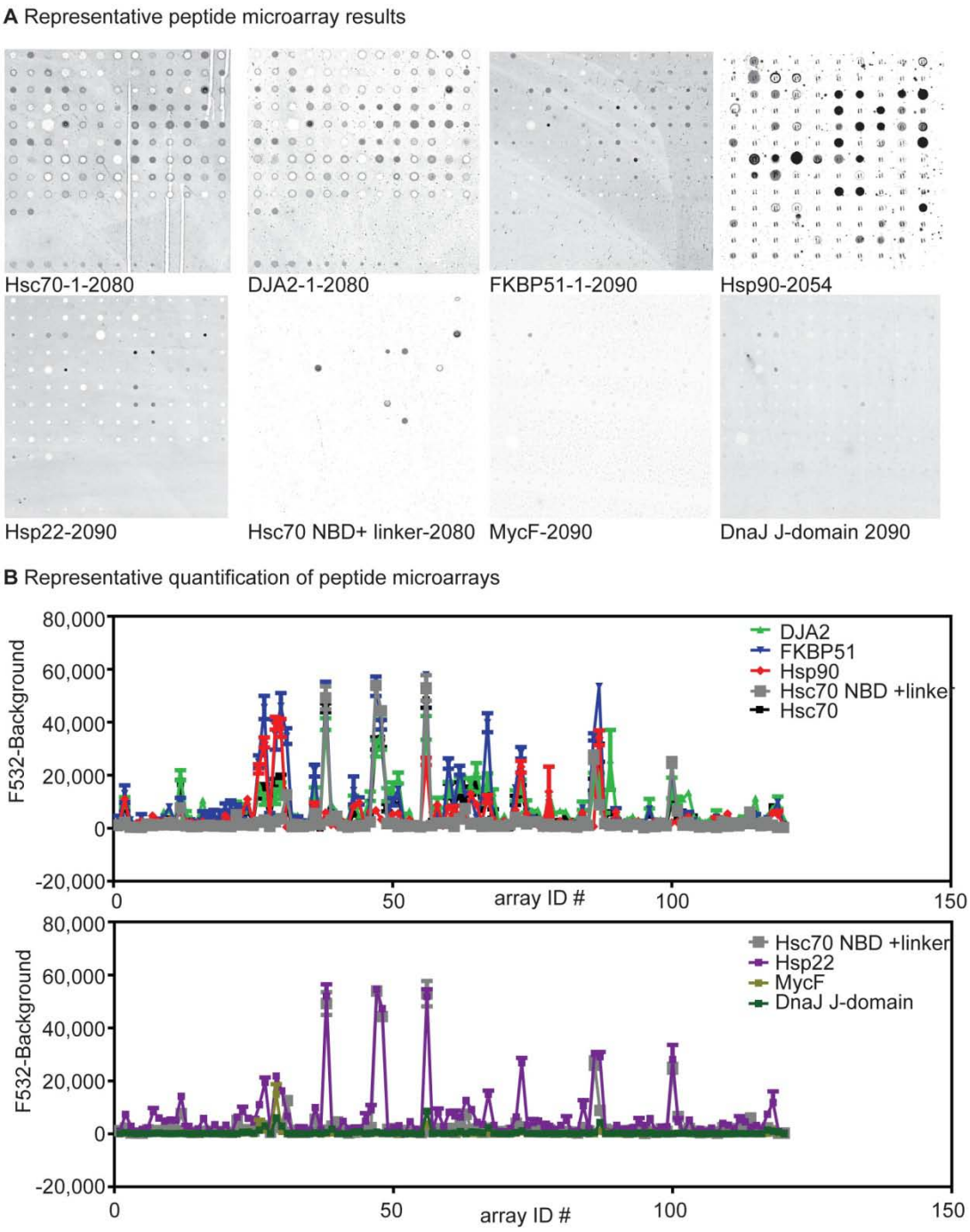

Figure A.2. Representative results from peptide microarray binding experiments.
(A) Representative arrays from experiments are shown for Hsc70, DJA2, FKBP51, Hsp90, Hsp22, Hsc70 NBD+linker, MycF, and DnaJ J-domain. (B) Likewise, quantification of fluorescence at 532 nm (F532) after background subtraction for peptides tested in triplicate is shown. Error represents standard error of the mean.

the J-domain co-chaperones DJA2 and DnaJ with an OR of 2.833 and 4.800, respectively (Table A.1, Appendix A.3). In this case DJA2 and DnaJ bound approximately ~40% of fibril forming peptides and only ~20% of non-fibril forming peptides. Finally, much like Hsp70 and Hsp90, the cis-trans prolyl isomerase, FKBP51 demonstrated trends consistent with ~ 1.5 to 2 fold preference for binding to fibril forming peptides with an OR of 2.489, although the combined result from two experiments was not significant using a 95% confidence interval (Table A.1, Appendix A.3). These preference cannot be explained by a preference for hydrophobic peptides, quantified using a gravy score (Figure A.3). In fact, this subset of chaperones appears to recognize some structural feature of the amyloid-prone peptides that is not obvious from any physicochemical property. In contrast, small heat shock proteins and clusterin bound a significant number of peptides but did not demonstrate a preference for fibrils (Appendix A3 and A4). This result suggests that a preference for fibril forming peptides is a property unique to a subset of chaperones. Further, chaperones disulfide isomerase (PDI) and FKBP12 did not show a preference for fibrils. Rather, PDI and FKBP12 bound very few peptides. Similarly, negative controls were performed by testing antibody alone, the nucleotide binding domain of Hsp70s, and the J-domain of DnaJ. These proteins are not expected to bind peptide substrates and indicate the relative false positive rate that can be expect from this platform. These proteins exhibited a very low signal for binding to peptides on the microarray and, using the same analysis applied all tested proteins, were determined to bind ~10% of fibril and non-fibril forming peptides. Finally, two unrelated proteins; nanobody80 and MycF, were tested which behaved as negative controls binding very few peptides. Thus, it was concluded that preference for fibril forming peptides exhibited by

some chaperones and co-chaperones is not a result of non-specific binding. Rather, together these results demonstrate that a subset of molecular chaperones and co-chaperones show a unique preference for binding to amyloid-prone peptides.

Table A.1 Odds ratio analysis of chaperone binding preference for fibril forming peptides.

Sample type	Human Chaperones	replicates	OR	95% CI
negative-ctrl	NBD	4	0.942	0.308-2.882
Hsp70/Hsp90	Hsc70 (HSPA8)	4	2.063	0.920-4.625
	DnaK	1	1.803	0.767-4.235
	Hsp70 (HSPA1B)	1	1.722	0.783-3.789
	Hsp90 (HSP90AA1)	2	2.150	0.737-6.271
small Hsps	Hsp27 (HSPB1)	1	1.488	0.615-3.600
	Hsp22 (HSPB8)	2	0.939	0.180-0.489
	αB crystallin (HSPB5)	2	0.887	0.304-2.586
co-chaperones	DJA2 combined	3	2.833	1.199-6.694
	DnaJ (E.coli)	1	2.844	1.145-7.066
	J-domain DnaJ (E.coli)	1	0.750	0.234-2.408
	FKBP51 (FKBP5)	2	2.489	0.959-6.461
other	FKBP12 combined	2	no binding	
chaperones	PDI	1	0.404	0.095-1.712
	clusterin	1	1.026	0.473-6.079
more neg ctrls	MycF	1	1.804	0.316-10.314
	nano80	1	1.044	0.348-3.126
	antibody	3	0.461	0.040-5.250

Odds ratio (OR) and 95% confidence interval (CI) werecalculated based on the results obtained from testing the above proteins for binding in our peptide microarray. See Appendix A.3, A.4 and experimental procedures for full details. Dark grey indicates proteins which demonstrated preference for fibril-forming peptides. Light grey indicates proteins which demonstrated a preference for fibril forming peptides but did not reach consistently statistical signifcance using a 95% CI cutt-off.

Within cells a full complement of molecular chaperones, including representatives of all the major families, are likely to be expressed. Thus, whether the molecular chaperones would collectively be able to bind all of the amyloid-prone sequences was of interest. This analysis demonstrated that peptides that bound 3 or more chaperone proteins of different structural classes are two times more likely to be fibril forming and recognize 60% of all fibril forming peptides (Figure A.3). Thus, there seems to be reasonable

coverage as well as redundancy within the molecular chaperone system for binding fibril forming sequences.

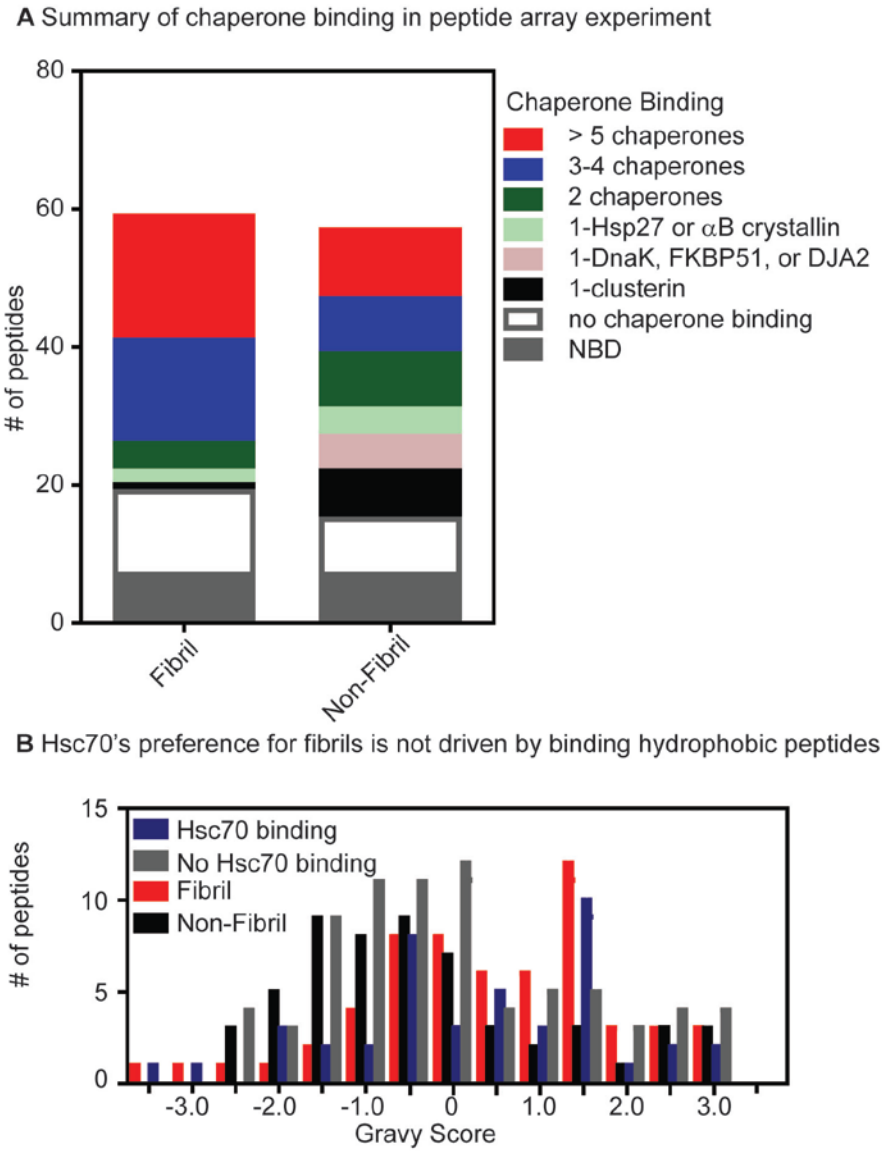

Figure A.3. Chaperone binding to peptide array analyzed.
(A) We see that peptides which bind 3 or more chaperones are ~2 times more likely to be fibril forming. Further, collectively all the chaperones tested bind a large diversity of peptides on our peptide microarray. For a complete summary of the peptides a given chaperone binds please see Appendix A.4. (B) For the chaperones which demonstrate a preference for fibril forming peptides, such as Hsc70 shown here, this binding is not indicative of a general preference for hydrophobic peptides as demonstrated by the overlapping distributions of gravy scores (a measure of hydrophobicity) for both peptides which bind and those which do not bind.

A.3.2 Chaperones which preferentially bind fibril forming peptides have predicted "steric zipper" forming regions within their substrate binding sites.

To further explore the "heterosteric zipper" model, the amino acid sequence of molecular chaperones was computationally evaluated to predict which regions may have a propensity to form "homosteric zippers" [22]. It was observed that the proteins which had a preference for fibril forming peptides (e.g. Hsp70 and DJA2) had regions within their known substrate-binding sites that were predicted to form "homosteric zippers" (Figure A.4) [25, 26]. Further, FKBP51 also had regions near a potential substrate-binding site enriched for "steric zippers." Interestingly this same region in FKBP12 was not enriched for "steric zippers." These observations suggest that chaperones may use heterotypic "steric zippers" to identify particularly problematic regions of target proteins. Further, many of the molecular chaperones are known to bind substrates as molecular clamps, protecting their bound substrate from the cellular environment [27]. Thus, chaperones may use an elegant mechanism for blocking aggregation, by forming complementary interactions with amyloid-prone peptides and blocking their polymerization.

A.4 Future directions

Although exciting, this model has not been rigorously tested. The peptide microarray binding results need to be validated in independent assays and the ability of these chaperones to inhibit aggregation of the fibril forming peptides also must be tested. Additionally, whether the peptides on the microarray are computationally predicted to form "heterostreic zippers" with peptide sequences within the substrate binding sites of

molecular chaperones will be evaluated. It will be particularly informative if computationally determining the ability of complexes between chaperones and peptides

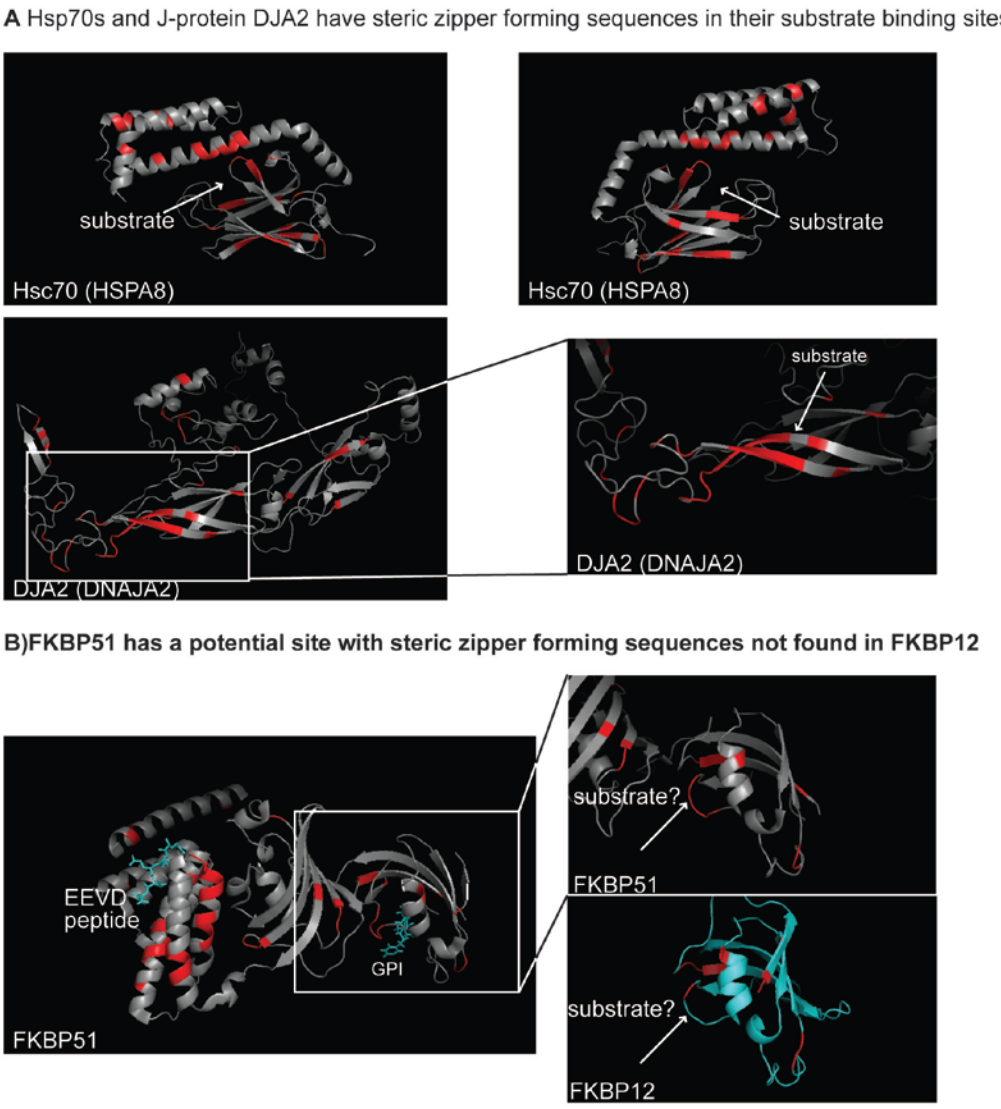

Figure A.4. Predicting "Steric zipper" forming sequences within molecular chaperones. (A) The substrate binding domains from Hsp70 and J-protein DJA2 were determined using homology modeling using the crystal structures of the substrate binding domain of DnaK and Ydj1 as templates [PDB code: 1DKY, 1NLT]. We predicted the ability of regions within a chaperone's amino acid sequence to form "homosteric zippers" using zipperDB. Regions predicted to have a ΔG of less that -22 kcal/mol are shown in red. (B) FKBP51 structure (PDB code:1KTO) is depicted with regions predicted to form homosteric zipper (ΔG <-22kcal/mol) highlighted in red. A loop adjacent to the GPI/FK506 binding site is predicted to form homosteric zippers. The analagous loop is not predicted to form homosteric zippers in FKBP12 (PDB code: 1F40). This may be a potential peptide binding site.

to form "heterosteric zipper" with favorable interaction energy can reliably reproduce the results obtained in the peptide microarray binding experiments. Finally, future work will

directly probe this hypothesis by obtaining co-crystal structures of complexes formed between chaperones and fibril-forming peptides.

A.5 Summary

In summary, this work has demonstrated that certain chaperones and co-chaperones have a preference for fibril forming peptides. Further, it has been shown that the substrate binding sites of chaperones that exhibit this preference have regions predicted to form "steric zippers." Although there is much work left to do, this study has the potential to uncover a mechanistic understanding of how amyloidogenic conformations of proteins are recognized by the cellular protein quality control systems.

A.6 Experimental procedures

A.6.1 Proteins making

Hsp70s (DnaK, Hsc70, Hsp70, NBD constructs; Hsp70 NBD (1-383), Hsc70 NBD (1-383), and Hsc70 NBD+linker (1-394) were purified as previously described [28]. Likewise, Hsp90, J-domain (1-108), and DnaJ were purified as previously described [28, 29], with the addition of a superdex 200 size exclusion column (GE Healthcare, Pittsburg, PA) as the last step of the J-domain purification. N-terminal his tagged DJA1, DJA2 was purified as previously described [30]. Hsp27, Hsp22, αB crystallin, were expressed in Rosetta cells using the pMCSG7 vector with a N-terminal his tag. Cells were lysed by sonication into lysis buffer (20 mM Tris pH 8.0, 100 mM NaCl, 6M urea, 5 mM β-mercaptoethanol, 15 mM imidazole) and purified by standard denaturing his purification using Ni-NTA resin (Novagen, Darmstadt,Germany). Proteins were eluted with 150 mM

imidazole. Following elution EDTA was added to 5 mM and protein was concentrated to ~20 mg/ml. Protein was refolded upon injection on a superdex 200 size exclusion column (GE Healthcare, Pittsburg, PA) with refolding buffer (20 mM NaP_i pH 7.2, 100 mM NaCl). The protein was flash frozen and stored at -80 ^oC. Finally, FKBP51 was purified by using a standard His purification with Ni-NTA resin (Novagen) followed by separation using a superdex 200 size exclusion column in (10mM NaPi, 2mM KPi pH 7.4, 137 mM NaCl, 2.7 mM KCl, 1 mM DTT). The following proteins were purchased as follows; Clusterin (Enzo Life Sciences, 201-335-C050, Farmingdale, NY), PDI (PROSPEC, enz-262-b, East Burnswick, NJ), FKBP12 (PROSPEC, enz-347-c). MycF was a kind gift from Janet Smith (University of Michigan), nanobody80 was gift from Roger Sunahara (University of Michigan).

A.6.2 Peptide microarray

A peptide microarray consisting of a variety of proteins experimentally evaluated for their ability to form fibrils was designed (Appendix A.1). Empty spots and process controls were used as negative controls. The microarrays were printed on single microscope slides in triplicate (JPT peptide technologies, Berlin, Germany). Binding was tested per manufacturer's protocol using 10 μM of His-tagged protein in binding buffer (25 mM HEPES pH 7.2, 150 mM NaCl, 20 mM KCl, 5 mM $MgCl_2$, 0.01% Tween20). Binding was detected using 1:1,000 titer of Hilyte555 anti-His antibody (Anaspec, Fremont, CA) in TBS-T with 1% bovine serum albumin (Sigma) and scanning the microarrays at a fluorescence emission of 532 nM using a GenePix 4100A Microarray Scanner (Molecular Devices, Sunnyvale, CA). Binding was defined using previously

described peptide microarray analysis program, rapmad, which performed the following taskes; a log2 transformation, a control peptide based linear model fit, a mixture model removal of peptides positive in negative control experiment (in this analysis the NBD was consistently utilized as a control experiment for the corresponding lot of microarrays for this purpose), and finally a mixture model signal call to identify peptides which bound compared to the noise from unbound peptides [31]. The optional random forest procedure to remove potentially unreliable peptide spots was excluded from the analysis. Odds ratio (OR) were calculated for each individual experiment using the following equation;

$$(FB*NN)/(NB*FN), \qquad \text{(Equation 1)}$$

where FB indicates fibril forming peptides found to bind the chaperone, FN indicates fibril forming peptides found to not bind, NB indicates non-fibril forming peptides found to bind, and NN indicates non-fibril forming peptides found to not bind. Further, for proteins tested more than once, an OR was calculated for the combined data. In combining the data binding was defined as peptides found to bind in $\geq 2/3$ of experiments for that given chaperone (Appendix A.3 for full results).

A.6.3 ZipperDB analysis of molecular chaperones

Molecular chaperone amino acid sequences were submitted to ZipperDB for analysis [22]. Structures for Hsp70 and DJA2 were obtained using homology models based on the DnaK and Ydj1 structures respectively [25, 26, 32, 33]. Further a structure was available for FKBP51 and FKBP12 [34, 35]. Within these structures, the first amino acid from a 6-

mer sequence which exhibit a binding energy for homosteric zipper formation of less than -22 kcal/mol is indicated in red (Figure A.3).

Notes

This project is a collaboration with David Eisenberg's lab (UCLA). Andrea Thompson, Atta Ahmad, and Jason Gestwicki designed the experiments. Andrea Thompson performed the experiments. We would like to acknowledge Jennifer Rauch, Tomoko Komiyama, Leah Makley, Steffen Bernard, and Brian DeVree for providing proteins used in this study.

A.7 Appendix

Appendix A.1 Peptide microarray design and layout

ID #	Name	Protein	Fibril/Non-Fibril	Control	Location
1	GGVLVN	248PAP286	Fibril [36]		Cytoplasm
2	SLFLIG	AIM1	non-Fibril [23]		membrane
3	VGGAVVTGV	α synuclein	Fibril [17, 24]		Cytoplasm
4	GSIAAT	α synuclein	Fibril [17]		Cytoplasm
5	GVATVA	α synuclein	Fibril [17]		Cytoplasm
6	GGAVVT	α synuclein	predicted Fibril [22]		cytoplasm
7	AEKTKQ	α synuclein	predicted non-fibril [22]		cytoplasm
8	MPVDPD	α synuclein	predicted non-fibril [22]		cytoplasm
9	NFGAIL	amylin	Fibril [19, 22, 24, 37]		secreted/extra
10	FLVHSS	amylin	Fibril [22, 38]		secreted/extra
11	TNVGSNTY	amylin	Fibril [39]		secreted/extra
12	QRLANFLVH	amylin	Fibril [40]		secreted/extra
13	SSTNVG	amylin	Fibril [17]		secreted/extra
14	LIAGFN	amylin	non-Fibril [22]		secreted/extra
15	NLGPVL	amylin	non-Fibril [22]		secreted/extra
16	KLVFFAED	Aβ	Fibril [24, 41]		extra
17	AIIGLMVGGVV	Aβ	Fibril [17]		extra
18	GGVVIA	Aβ	Fibril [17]		extra
19	*MVGGVV*	Aβ	Fibril [17]		extra
20	*DGVVIA*	Aβ	non-fibril FL [42]		extra
21	*LVGGVV*	Aβ	non-fibril FL[20, 42]		extra
22	GFVVIA	Aβ	non-fibril FL [20]		extra
23	FFKRAA	AR	predicted non-fibril [22]		Cytoplasm, Nucleus
24	AVFIIY	ASPM	Fibril [23]		Nucleus, Cytoplasm
25	GRGHGG	ataxin-1 (ATXN1)	predicted non-fibril [22]		Cytoplasm
26	DWSFYLLYYTEFT	b2-microglobulin	Fibril [17, 43]		secreted/extra
27	KDWSFY	b2-microglobulin	Fibril [14]		secreted/extra
28	KIVKWD	b2-microglobulin	Fibril [14]		secreted/extra
29	*FYLLYY*	b2-microglobulin	Fibril [14]		secreted/extra
30	LLYYTE	b2-microglobulin	Fibril [14]		secreted/extra
31	NHVTLS	b2-microglobulin	Fibril [12, 14, 17, 22]		secreted/extra
32	FHPSDIEVDLLK	b2-microglobulin	non-Fibril [43]		secreted/extra
33	IQRTPKIQVYSRHPAE	b2-microglobulin	non-Fibril [43]		secreted/extra
34	LSQPKIVKWDRDM	b2-microglobulin	non-Fibril [43]		secreted/extra
35	NGERIEKVEHSDLSFSKD	b2-microglobulin	non-Fibril [43]		secreted/extra
36	NGKSNFLNCYVSG	b2-microglobulin	non-Fibril [43]		secreted/extra
37	PTGKDEYACRVNHVT	b2-microglobulin	non-Fibril [43]		secreted/extra
38	YVSGFH	b2-microglobulin	non-Fibril [14, 22]		secreted/extra
39	VYSRHP	b2-microglobulin	non-Fibril [14, 22]		secreted/extra
40	KSNFLN	b2-microglobulin	non-Fibril [14, 22]		secreted/extra
41	RTPKIQ	b2-microglobulin	non-Fibril [14, 22]		secreted/extra
42	VTLSQP	b2-microglobulin	non-Fibril [14, 22]		secreted/extra
43	TEFTPT	b2-microglobulin	non-Fibril [14, 22]		secreted/extra
44	SRHPAE	b2-microglobulin	non-Fibril [14, 22]		secreted/extra
45	GGSGGSGGGSDYKDDDDK		process control		
46	EALYLV	b2-microglobulin	non-Fibril [14, 22]		secreted/extra
47	DFNKFH	Calcitonin	Fibril[17, 44]		secreted

ID #	Name	Protein	Fibril/Non-Fibril	Control	Location
48	NFVNYS	CELR3	Fibril [23]		membrane
49	VTFTIQ	CPNE5	Fibril [23]		Cytoplasm, membrane
50	YLVNFT	ECM1	Fibril [23]		extra membrane
51	NEFIIT	EMBP	non-Fibril [23]		secreted; cytoplasmic vesicles
52	YLVLIM	Fibulin-1	non-Fibril [23]		secreted/extra
53	MIFFIY	GCYB2	non-Fibril [23]		cytoplasm
54	SAILTA	gelsolin (GSN)	predicted Fibril [22]		Cytoplasm, Extra cellular
55	TMSVSL	gelsolin (GSN)	predicted Fibril [22]		Cytoplasm, Extra cellular
56	LYNYRH	gelsolin (GSN)	predicted non-fibril [22]		Cytoplasm, Extra cellular
57	IRDNER	gelsolin (GSN)	predicted non-fibril [22]		Cytoplasm, Extra cellular
58	LYVLIV	GRP21	Fibril [23]		membrane
59	QQSLFQ	HNRPD	Fibril [23]		Nucleus, Cytoplasm
60	EIDFIL	Huntington (HTT)	predicted non-fibril [22]		Cytoplasm
61	QQQQQQ	Huntington, ATXN1, ATXN2, AR	Fibril [17]		Cytoplasm
62	***SLYQLENY***	Insulin	Fibril [13]		extra
63	***LVEALYL****V*	Insulin	Fibril [13]		extra
64	L***VEALY***	Insulin	Fibril [14, 17, 22]		extra
65	***VEALY***L	Insulin	Fibril [14, 17, 22]		extra
66	*LY****QLEN***	Insulin	Fibril [14, 17, 22]		extra
67	***YQLENY***	Insulin	Non-Fibril [14, 22]		extra
68	FVNQHL	Insulin	Non-Fibril [14, 22]		extra
69	*GSH****LVE***	Insulin	Non-Fibril [14, 22]		extra
70	***HLVEAL***	Insulin	Non-Fibril [14, 22]		extra
71	FYTPKT	Insulin	Non-Fibril [14, 22]		extra
72	GERGFF	Insulin	Non-Fibril [14, 22]		extra
73	GVWWFF	Integrin beta-1	Fibril [23]		membrane
74	GIFNIK	LASS2	Fibril [23]		membrane
75	IFQINS	Lysozyme	Fibril [17, 24]		Cytoplasm
76	TFQINS	Lysozyme-Hu	Fibril [17]		Cytoplasm
77	NRLLLTG	model substrate	Unknown	DnaK [26]	NA
78	AGAAAAGA	Prion	Fibril [16, 45]		extra membrane
79	SNQNNF	Prion	Fibril [17]		extra membrane
80	VHDCVNITIK	Prion 180-193	Fibril [24, 46]		extra membrane
81	NITIKQHTVT	Prion 180-193	Non-Fibril [24, 46]		extra membrane
82	QHTVTTTKG	Prion 180-193	Non-Fibril [24, 46]		extra membrane
83	TTTKGENFTE	Prion 180-193	Non-Fibril [24, 46]		extra membrane
84	MIHFGND	Prion(Mu)	Fibril [17]		extra membrane
85	SMVLFSSPPV	Prion141-150	Fibril [24, 46]		extra membrane
86	EDRYYRENMH	Prion144-154	non-Fibril [24, 46]		extra membrane
87	FGSDYEDRYY	Prion144-154	non-Fibril [24, 46]		extra membrane
88	SSEITT	PTMA	predicted Fibril [22]		cytoplasm
89	EVDEEE	PTMA	predicted non-fibril [22]		cytoplasm
90	AA		process control		
91	KRAAED	PTMA	predicted non-fibril [22]		cytoplasm

ID #	Name	Protein	Fibril/Non-Fibril	Control	Location
92	*SSTSAASSSNY*	Rnase	Fibril [47]		Cytoplasm
93	KHIIVA	Rnase	Fibril [47]		Cytoplasm
94	SYSTMS	Rnase	Fibril [47]		Cytoplasm
95	*SSTSAA*	Rnase	Fibril [17]		Cytoplasm
96	*ASSSNY*	Rnase	Fibril [47]		Cytoplasm
97	RNLTKD	Rnase	Non-Fibril [47]		cytoplasm
98	IHKAQN	Rnase, scrambled	Non-Fibril [47]		cytoplasm
99	ISMTTS	Rnase, scrambled	Non-Fibril [47]		cytoplasm
100	FERQHM	Rnase, scrambled	Non-Fibril [47]		cytoplasm
101	GNNQQNY	Sup35	Fibril [17]		Yeast- Fibril control
102	NNQQNY	Sup35	Fibril [17]		Yeast- Fibril Control
103	VQIVYK	Tau (PHF6)	Fibril [17, 48]	Hsc70 [49]	cytoplasm
104	VQIPYK	Tau	Non-Fibril [48]		Cytoplasm
105	VQPVYK	Tau	Non-Fibril [48]		Cytoplasm
106	GQVEVSKE	Tau	Non-Fibril [24]		cytoplasm
107	VQEVYK	Tau	unknown		cytoplasm
108	VQYK	Tau	unknown		cytoplasm
109	VVRTPPKSPSSAKSR	Tau	unknown		cytoplasm
110	VQIINK	Tau	Fibril [50]	Hsc70 [49]	Cytoplasm
111	VDLSKVTSK	Tau	Non-Fibril [24]		cytoplasm
112	PGGGKVQIVYKPV	Tau (K19)	Fibril [24]	Hsc70 [49]	Cytoplasm
113	PGGKVYKPV	Tau (K19d)	Non-Fibril [24]		cytoplasm
114	QTAPVPMPD	Tau (K19Glu78)	Non-Fibril [24]		cytoplasm
115	GISVHI	TDP-43	predicted Fibril [22]		cytoplasm
116	GEVLMV	TDP-43	predicted Fibril [22]		cytoplasm
117	LRYRNP	TDP-43	predicted non-fibril [22]		cytoplasm
118	VFFFIG	TRHDE	non-Fibril [23]		membrane
119	WTVNYS	WDR36	Fibril [23]		Cytoplasm
120	FIVNIV	XRP2	Fibril [23]		membrane

Appendix A.2 Peptide microarray design summary

	Fibril		Non-Fibril		Unknown	
Number of Peptides	59		56		5	
Experimentally validated	54		49		NA	
disease related	39		44		3	
hexamers	43		41		1	
< or > hexamers	16		15		2	
average length peptide	7.22	3.26	6.91	1.58	6.25	0.50
average MW	822.51	351.41	807.69	196.87	775.53	95.89
average pI	5.80	1.37	5.83	1.72	5.83	0.61
average pos charge	0.29	0.56	0.73	1.06	0.25	0.50
average neg charge	0.25	0.54	0.45	0.66	0.25	0.50
average instability index	26.95	42.76	36.36	43.30	21.26	16.23
average aliphatic index	108.06	68.01	88.49	73.19	16.25	32.50
average GRAVY	0.48	1.47	-0.26	1.46	-1.74	1.66

Appendix A.3 Full Odds Ratio (OR) analysis of chaperones binding to peptide microarray

Sample type	array lot #	Chaperones	[F] bound	[F] not bound	total [F]	[NF] bound	[NF] not bound	total [NF]	OR	95% CI
negative-ctrl	2080	Hsp70-NBD-ADP	7	52	59	5	51	56	1.373	0.409-4.609
	2054	Hsp70-NBD-ATP	10	49	59	9	47	56	1.066	0.398-2.855
	2090	Hsc70-NBD+linker-ATP	6	53	59	8	48	56	0.679	0.220-2.099
	2090	Hsc70-NBD-linker-ATP (gain800)	10	49	59	10	46	56	0.939	0.358-2.463
	2090	Hsc70-NBD-ADP	5	54	59	7	49	56	0.648	0.193-2.176
		NBD combined analysis	**7**	**52**	**59**	**7**	**49**	**56**	**0.942**	**0.308-2.882**
	2054	antibody	5	44	49	4	43	47	1.222	0.307-4.857
	2090	antibody-1	10	43	53	10	38	48	0.841	0.316-2.240
	2090	antibody-2	7	52	59	7	49	56	0.906	0.296-2.771
		antibody combined analysis	**1**	**51**	**52**	**2**	**47**	**49**	**0.461**	**0.040-5.250**
Hsp70s	2054	Hsc70 (HSPA8)-ATP	28	21	49	19	38	47	1.965	0.872-4.426
	2080	Hsc70 (HSPA8)-ADP-1	28	24	52	17	34	51	2.333	1.051-5.181
	2080	Hsc70 (HSPA8)-ADP-2	33	18	51	25	24	49	1.760	0.789-3.926
	2090	Hsc70 (HSPA8)-ADP	24	29	53	15	33	48	1.821	0.806-4.115
		Hsc70 combined analysis	**26**	**26**	**52**	**16**	**33**	**49**	**2.063**	**0.920-4.625**
	2080	DnaK (*E. coli*)-ADP	37	13	50	30	19	49	1.803	0.767-4.235

Sample type	array lot #	Chaperones	[F] bound	[F] not bound	total [F]	[NF] bound	[NF] not bound	total [NF]	OR	95% CI
	2090	Hsp70 (HSPA1B)-ADP	27	27	54	18	31	49	1.722	0.7827-3.789
Hsp90	2054	Hsp90 (HSP90AA1)-ATP	26	23	49	16	31	47	2.190	0.961-4.992
	2090	Hsp90 (HSP90AA1)-ATP	18	36	54	12	37	49	1.542	0.651-3.653
		Hsp90 combined	**12**	**40**	**52**	**6**	**43**	**49**	**2.150**	**0.737-6.271**
small Hsps	2054	Hsp27 (HSPB1) (gain600)	20	24	44	14	25	39	1.488	0.615-3.600
	2054	Hsp22 (HSPB8)	12	32	44	9	30	39	1.250	0.461-3.390
	2090	Hsp22 (HSPB8)	13	40	53	8	40	48	1.546	0.478-4.134
		Hsp22 combined	**3**	**49**	**52**	**3**	**46**	**49**	**0.939**	**0.180-0.489**
	2054	αB crystallin (HSPB5)	10	39	49	8	39	47	1.250	0.446-3.502
	2090	αB crystallin (HSPB5)	10	43	53	8	40	48	1.163	0.4174-3.239
		αB crystallin combined	**8**	**44**	**52**	**8**	**41**	**49**	**0.887**	**0.304-2.586**
co-chaperones	2080	DJA2 (DNAJA2)-1	27	25	52	14	37	51	2.854	1.256-6.488
	2080	DJA2 (DNAJA2)-2	22	30	52	11	40	51	2.667	1.123-6.332
	2090	DJA2 (DNAJA2) (gain650)	20	34	54	12	37	49	1.714	0.730-4.025
		DJA2 combined	21	31	52	11	38	49	2.833	1.199-6.694
	2080	DJA1 (DNAJA1)-1	8	44	52	3	48	51	2.909	0.726-11.662
	2080	DJA1 (DNAJA1)-2	12	40	52	3	48	51	4.800	1.266-18.202
		DJA1 combined	2	50	52	0	49	49	NA	
	2090	DnaJ (*E.coli*)	21	32	53	9	39	48	2.844	1.145-7.066
	2090	J-domain DnaJ (*E.coli*) (gain650)	6	48	54	7	42	49	0.750	0.234-2.408
	2090	FKBP51 (FKBP5)-1	34	19	53	20	28	48	2.505	1.123-5.591
	2090	FKBP51 (FKBP5)-2 (gain800)	27	22	49	20	26	46	1.596	0.710-3.589
	2090	**FKBP51 combined**	17	35	52	8	41	49	2.489	0.959-6.461
other chaperones	2080	FKBP12	5	47	52	3	48	51	1.702	0.385-7.528
	2090	FKBP12	2	52	54	2	47	49	0.868	0.118-6.409
		FKBP12 combined	0	52	52	0	49	49	NA	
	2090	PDI	3	51	54	6	43	49	0.404	0.095-1.712
	2090	clusterin	29	25	54	25	24	49	1.026	0.473-6.079
unrealated negatives	2090	MycF	4	50	54	2	47	49	1.804	0.316-10.314
	2090	nano80	8	46	54	7	42	49	1.044	0.348-3.126

[F] and [NF] denote fibril and non-fibril, respectively. Unless otherwise noted, proteins tested were human proteins.
OR and CI denote odds ratio and confidence interval, respectively.

Appendix A.4 Summary of full results of chaperone binding to microarrays

Array ID #	Name	Fibril/Non-Fibril	Chaperone Binding Results
1	GGVLVN	Fibril	
2	SLFLIG	non-Fibril	Hsc70, Hsp70, Hsp90, αB crystallin, Hsp27, Hsp22, DnaK, PDI, Clusterin, DJA2,DnaJ, FKBP51
3	VGGAVVTGV	Fibril	
4	GSIAAT	Fibril	
5	GVATVA	Fibril	clusterin, DnaJ, FKBP51
6	GGAVVT	predicted Fibril	clusterin
7	AEKTKQ	predicted non-fibril	Hsp27, Hsp70, clusterin
8	MPVDPD	predicted non-fibril	FKBP51
9	NFGAIL	Fibril	Hsc70, DnaK, clusterin
10	FLVHSS	Fibril	Hsp27, DnaK,DnaJ
11	TNVGSNTY	Fibril	DnaK, clusterin,FKBP51
12	QRLANFLVH	Fibril	NBD
13	SSTNVG	Fibril	
14	LIAGFN	non-Fibril	Hsc70, Hsp27,DnaK
15	NLGPVL	non-Fibril	Hsp27, DnaK
16	KLVFFAED	Fibril	Hsc70, Hsp27,DnaK, DJA2
17	AIIGLMVGGVV	Fibril	
18	GGVVIA	Fibril	
19	MVGGVV	Fibril	
20	DGVVIA	non-fibril FL, peptide NT	Hsc70, clusterin, FKBP51
21	LVGGVV	non-fibril FL, peptide NT	clusterin
22	GFVVIA	non-fibril FL, peptide NT	
23	FFKRAA	predicted non-fibril	Hsp70, αB crystallin, DnaK, J-domain, clusterin,nanobody80
24	AVFIIY	Fibril	Hsc70, Hsp70, Hsp90, αB crystallin, DnaK, J-domain, MycF,clusterin, nanobody80, DJA2, DnaJ
25	GRGHGG	predicted non-fibril	Hsp27, DnaK
26	DWSFYLLYYTEFT	Fibril	Hsc70, αB crystallin, DnaK, DJA2
27	KDWSFY	Fibril	Hs70, αB crystallin, DnaK, DJA2, DnaJ
28	KIVKWD	Fibril	Hsc70,DnaK, clusterin, DJA2
29	FYLLYY	Fibril	Hsc70, αB crystallin, DnaK, DJA2, DnaJ
30	LLYYTE	Fibril	NBD
31	NHVTLS	Fibril	αB crystallin, antibody
32	FHPSDIEVDLLK	non-Fibril	clusterin
33	IQRTPKIQVYSRHPAE	non-Fibril	clusterin, FKBP51
34	LSQPKIVKWDRDM	non-Fibril	DnaK
35	NGERIEKVEHSDLSFSKD	non-Fibril	

Array ID #	Name	Fibril/Non-Fibril	Chaperone Binding Results
36	NGKSNFLNCYVSG	non-Fibril	Hsc70, Hsp70, Hsp90, αB crystallin, DnaK, PDI, clusterin, nanobody 80, DJA2, antibody
37	PTGKDEYACRVNHVT	non-Fibril	
38	YVSGFH	non-Fibril	NBD
39	VYSRHP	non-Fibril	DJA2, antibody
40	KSNFLN	non-Fibril	
41	RTPKIQ	non-Fibril	Hsp27
42	VTLSQP	non-Fibril	
43	TEFTPT	non-Fibril	Hsc70, Hsp70, Hsp27, DnaK, J-domain, MycF, PDI, clusterin, nanobody 80, DJA2, DnaJ
44	SRHPAE	non-Fibril	Hsp70, Hsp27,DnaK, J-domain, MycF, PDI, clusterin, nanobody80, DnaJ
45	GGSGGSGGGSDYKDDDDK		
46	EALYLV	non-Fibril	Hsc70, Hsp70, Hsp90, αB crystallin, Hsp22, PDI, clusterin, DJA2, DnaJ
47	DFNKFH	Fibril	NBD
48	NFVNYS	Fibril	NBD
49	VTFTIQ	Fibril	Hsc70, DnaK, DJA2, DnaJ
50	YLVNFT	Fibril	Hsc70, Hsp70, Hsp90, DnaK, nanobody80, DJA2, DnaJ, FKBP51
51	NEFIIT	non-Fibril	Hsc70, Hsp70, Hsp90, DnaK, J-domain, clusterin, nanobody80,DJA2, DnaJ, FKBP51
52	YLVLIM	non-Fibril	Hsp27, DnaK
53	MIFFIY	non-Fibril	Hsc70, Hsp27, DnaK
54	SAILTA	predicted Fibril	
55	TMSVSL	predicted Fibril	
56	LYNYRH	predicted non-fibril	NBD
57	IRDNER	predicted non-fibril	clusterin
58	LYVLIV	Fibril	Hsp90, Hsp70, αB crystallin, Hsp27, Hsp22, PDI, clusterin, DJA2, DnaJ,FKBP51
59	QQSLFQ	Fibril	Hsp27
60	EIDFIL	predicted non-fibril	Hsc70, Hsp70, Hsp90, αB crystallin, DnaK, PDI, clusterin,DJA2, DnaJ, FKBP51
61	QQQQQQ	Fibril	Hsc70, Hsp90, Hsp27, Hsp22,DnaK, clusterin, DJA2, FKBP51
62	SLYQLENY	Fibril	Hsc70, Hsp70, Hsp90, DnaK, J-domain,clusterin, nanobody80, DJA2, DnaJ, FKBP51
63	LVEALYLV	Fibril	NBD
64	LVEALY	Fibril	Hsc70, Hsp70, Hsp90, Hsp22, DnaK, J-domain, clusterin,DJA2, DnaJ, FKBP51
65	VEALYL	Fibril	Hsc70, Hsp70, αB crystallin, DnaK, J-domain, PDI, clusterin, nanobody80, DJA2, DJA1, DnaJ, FKBP51

Array ID #	Name	Fibril/Non-Fibril	Chaperone Binding Results
66	LYQLEN	Fibril	Hsc70, DnaK,clusterin,DnaJ, FKBP51
67	YQLENY	Non-Fibril	Hsc70, αB crystallin, DnaK,DJA2, DnaJ
68	FVNQHL	Non-Fibril	Hsc70, DnaK, clusterin, DJA2, DnaJ, FKBP51
69	GSHLVE	Non-Fibril	Hsp27
70	HLVEAL	Non-Fibril	clusterin
71	FYTPKT	Non-Fibril	
72	GERGFF	Non-Fibril	Hsc70, Hsp70, Hsp90, αB crystallin, Hsp27, Hsp22,DnaK, J-domain,clusterin, nanobody80,DJA2,DnaJ, FKBP51
73	GVWWFF	Fibril	Hsc70, Hsp70, Hsp90, αB crystallin,DnaK, J-domain, MycF, PDI,clusterin, nanobody80, DJA2, DnaJ, FKBP51
74	GIFNIK	Fibril	Hsc70, Hsp70, Hsp90, DnaK, clusterin,DJA2,DnaJ, FKBP51
75	IFQINS	Fibril	Hsp27, clusterin
76	TFQINS	Fibril	Hsp27, DnaK
77	NRLLLTG	predicted non-fibril	Hsp27, DnaK
78	AGAAAAGA	Fibril	Hsc70, Hsp70, Hsp90, Hsp27, DnaK, clusterin,DJA2,DnaJ, FKBP51
79	SNQNNF	Fibril	Hsc70, Hsp27,DnaK, clusterin
80	VHDCVNITIK	Fibril	Hsc70, Hsp27, DnaK, clusterin
81	NITIKQHTVT	Non-Fibril	
82	QHTVTTTKG	Non-Fibril	
83	TTTKGENFTE	Non-Fibril	
84	MIHFGND	Fibril	Hsc70, Hsp70, Hsp90, αB crystallin, Hsp27, DnaK, PDI,clusterin, DJA2, DnaJ, FKBP51
85	SMVLFSSPPV	Fibril	
86	EDRYYRENMH	non-Fibril	NBD
87	FGSDYEDRYY	non-Fibril	NBD
88	SSEITT	predicted Fibril	DnaK, MycF, clusterin
89	EVDEEE	predicted non-fibril	Hsc70, DnaK,clusterin, DJA2
90	AA		Hsc70, Hsp70, Hsp90, Hsp27,DnaK, clusterin,DJA2, FKBP51
91	KRAAED	predicted non-fibril	clusterin
92	SSTSAASSSNY	Fibril	NBD
93	KHIIVA	Fibril	Hsc70, DnaK, clusterin
94	SYSTMS	Fibril	Hsp27, DnaK, clusterin
95	SSTSAA	Fibril	Hsp27, DnaK, clusterin
96	ASSSNY	Fibril	Hsc70, Hsp27,DnaK,MycF, clusterin, nanobody80,DJA2,DnaJ
97	RNLTKD	Non-Fibril	DnaK, clusterin
98	IHKAQN	Non-Fibril	DnaK, clusterin

Array ID #	Name	Fibril/Non-Fibril	Chaperone Binding Results
99	ISMTTS	Non-Fibril	clusterin
100	FERQHM	Non-Fibril	NBD
101	GNNQQNY	Fibril	NBD
102	NNQQNY	Fibril	Hsc70, Hsp27,DnaK, DJA2, DJA1, FKBP51
103	VQIVYK	Fibril	Hsc70, Hsp90, Hsp27,DnaK, clusterin, DJA2, FKBP51
104	VQIPYK	Non-Fibril	Hsc70,DnaK
105	VQPVYK	Non-Fibril	DnaK
106	GQVEVSKE	Non-Fibril	clusterin
107	VQEVYK	unknown	Hsp27, DnaK, clusterin
108	VQYK	unknown	DnaK, clusterin, FKBP51
109	VVRTPPKSPSSAKSR	unknown	Hsp27,DnaK, clusterin
110	VQIINK	Fibril	DnaK, Hsp70, clusterin,DnaJ, FKBP51
111	VDLSKVTSK	Non-Fibril	
112	PGGGKVQIVYKPV	Fibril	
113	PGGKVYKPV	Non-Fibril	DnaK
114	QTAPVPMPD	Non-Fibril	Hsp27,DnaK
115	GISVHI	predicted Fibril	Hsc70, Hsp27, DnaK, FKBP51
116	GEVLMV	predicted Fibril	
117	LRYRNP	predicted non-fibril	Hsc70, αB crystallin,DnaK
118	VFFFIG	non-Fibril	Hsc70, αB crystallin, DnaK
119	WTVNYS	Fibril	Hsc70, Hsp70, Hsp90, Hsp27,DnaK, J-domain, nanobody80,DJA2, DnaJ
120	FIVNIV	Fibril	Hsp27, clusterin

A.8 References

1. Eisenberg, D. and M. Jucker, *The amyloid state of proteins in human diseases.* Cell, 2012. **148**(6): p. 1188-203.
2. Chiti, F. and C.M. Dobson, *Protein misfolding, functional amyloid, and human disease.* Annu Rev Biochem, 2006. **75**: p. 333-66.
3. Hardy, J. and D.J. Selkoe, *The amyloid hypothesis of Alzheimer's disease: progress and problems on the road to therapeutics.* Science, 2002. **297**(5580): p. 353-6.
4. Hartl, F.U., A. Bracher, and M. Hayer-Hartl, *Molecular chaperones in protein folding and proteostasis.* Nature, 2011. **475**(7356): p. 324-32.
5. Ahmad, A., *DnaK/DnaJ/GrpE of Hsp70 system have differing effects on alpha-synuclein fibrillation involved in Parkinson's disease.* Int J Biol Macromol, 2010. **46**(2): p. 275-9.
6. Ballet, T., et al., *DnaK prevents human insulin amyloid fiber formation on hydrophobic surfaces.* Biochemistry, 2012. **51**(11): p. 2172-80.
7. Chien, V., et al., *The chaperone proteins HSP70, HSP40/DnaJ and GRP78/BiP suppress misfolding and formation of beta-sheet-containing aggregates by human amylin: a potential role for defective chaperone biology in Type 2 diabetes.* Biochem J, 2010. **432**(1): p. 113-21.
8. Evans, C.G., S. Wisen, and J.E. Gestwicki, *Heat shock proteins 70 and 90 inhibit early stages of amyloid beta-(1-42) aggregation in vitro.* J Biol Chem, 2006. **281**(44): p. 33182-91.
9. Kumita, J.R., et al., *The extracellular chaperone clusterin potently inhibits human lysozyme amyloid formation by interacting with prefibrillar species.* J Mol Biol, 2007. **369**(1): p. 157-67.
10. Muchowski, P.J., et al., *Hsp70 and hsp40 chaperones can inhibit self-assembly of polyglutamine proteins into amyloid-like fibrils.* Proc Natl Acad Sci U S A, 2000. **97**(14): p. 7841-6.
11. Robertson, A.L., et al., *Small heat-shock proteins interact with a flanking domain to suppress polyglutamine aggregation.* Proc Natl Acad Sci U S A, 2010. **107**(23): p. 10424-9.
12. Ivanova, M.I., et al., *An amyloid-forming segment of beta2-microglobulin suggests a molecular model for the fibril.* Proc Natl Acad Sci U S A, 2004. **101**(29): p. 10584-9.
13. Ivanova, M.I., et al., *Molecular basis for insulin fibril assembly.* Proc Natl Acad Sci U S A, 2009. **106**(45): p. 18990-5.
14. Ivanova, M.I., M.J. Thompson, and D. Eisenberg, *A systematic screen of beta(2)-microglobulin and insulin for amyloid-like segments.* Proc Natl Acad Sci U S A, 2006. **103**(11): p. 4079-82.
15. Nelson, R., et al., *Structure of the cross-beta spine of amyloid-like fibrils.* Nature, 2005. **435**(7043): p. 773-8.
16. Sambashivan, S., et al., *Amyloid-like fibrils of ribonuclease A with three-dimensional domain-swapped and native-like structure.* Nature, 2005. **437**(7056): p. 266-9.
17. Sawaya, M.R., et al., *Atomic structures of amyloid cross-beta spines reveal varied steric zippers.* Nature, 2007. **447**(7143): p. 453-7.
18. Teng, P.K., et al., *Ribonuclease A suggests how proteins self-chaperone against amyloid fiber formation.* Protein Sci, 2012. **21**(1): p. 26-37.
19. Tenidis, K., et al., *Identification of a penta- and hexapeptide of islet amyloid polypeptide (IAPP) with amyloidogenic and cytotoxic properties.* J Mol Biol, 2000. **295**(4): p. 1055-71.

20. Luhrs, T., et al., *3D structure of Alzheimer's amyloid-beta(1-42) fibrils.* Proc Natl Acad Sci U S A, 2005. **102**(48): p. 17342-7.
21. Petkova, A.T., et al., *A structural model for Alzheimer's beta -amyloid fibrils based on experimental constraints from solid state NMR.* Proc Natl Acad Sci U S A, 2002. **99**(26): p. 16742-7.
22. Thompson, M.J., et al., *The 3D profile method for identifying fibril-forming segments of proteins.* Proc Natl Acad Sci U S A, 2006. **103**(11): p. 4074-8.
23. Maurer-Stroh, S., et al., *Exploring the sequence determinants of amyloid structure using position-specific scoring matrices.* Nat Methods, 2010. **7**(3): p. 237-42.
24. Fernandez-Escamilla, A.M., et al., *Prediction of sequence-dependent and mutational effects on the aggregation of peptides and proteins.* Nat Biotechnol, 2004. **22**(10): p. 1302-6.
25. Li, J., X. Qian, and B. Sha, *The crystal structure of the yeast Hsp40 Ydj1 complexed with its peptide substrate.* Structure, 2003. **11**(12): p. 1475-83.
26. Zhu, X., et al., *Structural analysis of substrate binding by the molecular chaperone DnaK.* Science, 1996. **272**(5268): p. 1606-14.
27. Stirling, P.C., et al., *Convergent evolution of clamp-like binding sites in diverse chaperones.* Nat Struct Mol Biol, 2006. **13**(10): p. 865-70.
28. Chang, L., et al., *Mutagenesis reveals the complex relationships between ATPase rate and the chaperone activities of Escherichia coli heat shock protein 70 (Hsp70/DnaK).* J Biol Chem, 2010. **285**(28): p. 21282-91.
29. Southworth, D.R. and D.A. Agard, *Species-dependent ensembles of conserved conformational states define the Hsp90 chaperone ATPase cycle.* Mol Cell, 2008. **32**(5): p. 631-40.
30. Tzankov, S., et al., *Functional divergence between co-chaperones of Hsc70.* J Biol Chem, 2008. **283**(40): p. 27100-9.
31. Renard, B.Y., et al., *rapmad: Robust analysis of peptide microarray data.* BMC Bioinformatics, 2011. **12**: p. 324.
32. Roy, A., A. Kucukural, and Y. Zhang, *I-TASSER: a unified platform for automated protein structure and function prediction.* Nat Protoc, 2010. **5**(4): p. 725-38.
33. Zhang, Y., *I-TASSER server for protein 3D structure prediction.* BMC Bioinformatics, 2008. **9**: p. 40.
34. Sich, C., et al., *Solution structure of a neurotrophic ligand bound to FKBP12 and its effects on protein dynamics.* Eur J Biochem, 2000. **267**(17): p. 5342-55.
35. Sinars, C.R., et al., *Structure of the large FK506-binding protein FKBP51, an Hsp90-binding protein and a component of steroid receptor complexes.* Proc Natl Acad Sci U S A, 2003. **100**(3): p. 868-73.
36. Sievers, S.A., et al., *Structure-based design of non-natural amino-acid inhibitors of amyloid fibril formation.* Nature, 2011. **475**(7354): p. 96-100.
37. Azriel, R. and E. Gazit, *Analysis of the minimal amyloid-forming fragment of the islet amyloid polypeptide. An experimental support for the key role of the phenylalanine residue in amyloid formation.* J Biol Chem, 2001. **276**(36): p. 34156-61.
38. Mazor, Y., et al., *Identification and characterization of a novel molecular-recognition and self-assembly domain within the islet amyloid polypeptide.* J Mol Biol, 2002. **322**(5): p. 1013-24.
39. Nilsson, M.R. and D.P. Raleigh, *Analysis of amylin cleavage products provides new insights into the amyloidogenic region of human amylin.* J Mol Biol, 1999. **294**(5): p. 1375-85.

40. Jaikaran, E.T., et al., *Identification of a novel human islet amyloid polypeptide beta-sheet domain and factors influencing fibrillogenesis.* J Mol Biol, 2001. **308**(3): p. 515-25.
41. Landau, M., et al., *Towards a pharmacophore for amyloid.* PLoS Biol, 2011. **9**(6): p. e1001080.
42. Kanski, J., et al., *Role of glycine-33 and methionine-35 in Alzheimer's amyloid beta-peptide 1-42-associated oxidative stress and neurotoxicity.* Biochim Biophys Acta, 2002. **1586**(2): p. 190-8.
43. Jones, S., et al., *Amyloid-forming peptides from beta2-microglobulin-Insights into the mechanism of fibril formation in vitro.* J Mol Biol, 2003. **325**(2): p. 249-57.
44. Reches, M., Y. Porat, and E. Gazit, *Amyloid fibril formation by pentapeptide and tetrapeptide fragments of human calcitonin.* J Biol Chem, 2002. **277**(38): p. 35475-80.
45. Gasset, M., et al., *Predicted alpha-helical regions of the prion protein when synthesized as peptides form amyloid.* Proc Natl Acad Sci U S A, 1992. **89**(22): p. 10940-4.
46. Thompson, A., et al., *Amyloidogenicity and neurotoxicity of peptides corresponding to the helical regions of PrP(C).* J Neurosci Res, 2000. **62**(2): p. 293-301.
47. Goldschmidt, L., et al., *Identifying the amylome, proteins capable of forming amyloid-like fibrils.* Proc Natl Acad Sci U S A, 2010. **107**(8): p. 3487-92.
48. von Bergen, M., et al., *Assembly of tau protein into Alzheimer paired helical filaments depends on a local sequence motif ((306)VQIVYK(311)) forming beta structure.* Proc Natl Acad Sci U S A, 2000. **97**(10): p. 5129-34.
49. Sarkar, M., J. Kuret, and G. Lee, *Two motifs within the tau microtubule-binding domain mediate its association with the hsc70 molecular chaperone.* J Neurosci Res, 2008. **86**(12): p. 2763-73.
50. von Bergen, M., et al., *Mutations of tau protein in frontotemporal dementia promote aggregation of paired helical filaments by enhancing local beta-structure.* J Biol Chem, 2001. **276**(51): p. 48165-74.